Monday Morning, November 4, 2002

Electrochemistry and Fluid-Solid Interfaces Room: C-104 - Session EC+SS-MoM

Fuel Cells and Surface Electrochemical Reactions

Moderator: J.G. Chen, University of Delaware

8:20am **EC+SS-MoM1 Imaging of Water Ionization at Platinum Surfaces in High Electric Fields**, *C. Rothfuss*, *V. Medvedev*, *E.M. Stuve*, University of Washington

The high electric field intrinsic to the electrode/electrolyte interface plays an important role in electrochemical surface chemistry. To study these fields, which are of the order of 1 V/?, we employ a field ionization system in which water and other electrolytic species are adsorbed and ionized on Pt field emitter tips. Ions produced by the applied field are imaged onto microchannel plates and mass resolved with time-of-flight or ExB (Wien filter) mass spectrometers. Water ionization produces hydrated protons with 1-10 water molecules per proton, that are ejected from the tip. Images of ramped field ionization experiments show dramatic differences in ionization of amorphous vs. crystalline water. Below 135 K, where water exists in amorphous form, ionization is random overall, increasing in intensity with increasing field. Above 135 K, where water is crystalline, ionization occurs in long-lived zones that, with increasing field, increase in intensity and number and redistribute themselves about the surface so as to be as far apart as possible. Temperature dependent studies over the range of 80-300 K follow the energetic details of water ionization. Below 170 K the field required for dissociative ionization decreases linearly with increasing temperature. In a ramped field desorption experiment, ionization produces hydrated proton clusters with 2-7 water molecules per cluster. Above 170 K protonated clusters desorb sequentially beginning with the 6-water cluster and followed by progressively smaller clusters as the field increases. The disappearance of an n-water ion cluster results from loss of a water molecule to form cluster n - 1. The respective energies for water removal from clusters of n = 5, 4, and 3 were found to be 0.55, 0.76, and 0.85 eV. These numbers are in excellent agreement with previous measurements of water attachment energies. This work is supported by the Office of Naval Research.

8:40am EC+SS-MoM2 A Specular He Scattering Study of Water Adsorption, Desorption, and Clustering on Pt(111), J.L. Daschbach, B.M. Peden, R.S. Smith, B.D. Kay, Pacific Northwest National Laboratory

Specular He atom scattering is used to probe the adsorption, desorption, and clustering kinetics of sub-monolayer H₂O on Pt(111) over the temperature range 22 K to 185 K. Water deposited on clean Pt at low temperatures is shown to be arranged random ly on the Pt substrate. Over a narrow temperature range, as the clean substrate temperature is raised, the deposited water transforms to a 2-D condensed phase. Rearrangement of randomly adsorbed H₂O is studied as a function of coverage and temperat ure. At low initial H_2O coverage the specular He waveform is dominated by the clustering of the isolated HO molecules. At higher HO coverage and temperature a second feature is manifest, which we interpret as the Oswald ripening of the 2-D islands. Adsorption and desorption kinetics are examined isothermally. Water, when fully clustered in two dimensions, gives rise to a He specular intensity that decreases linearly with coverage. Over essentially the entire sub-monolayer coverage regi m e the sample coverage changes linearly in time during both adsorption and desorption of H₂O. This requires that the desorption rate be independent of coverage and thus the desorption kinetics are zero-order. The zero-order kinetics are a consequence of the coexistence of a 2-D H₂O gas with a 2-D condensed H₂O phase on the Pt surface. At higher temperatures, depending on flux, non-zero order kinetics are observed which are indicitive of a transition to a single H₂O 2-D phase. Details of the experimental techniques and results will be presented. Pacific Northwest National Laboratory is a multiprogram National Laboratory operated for the Department of Energy by Battelle under Contract DE-AC067-76RLO 1830.

9:00am EC+SS-MoM3 Surface Chemistry of Solid Oxide Fuel Cells, R.J. Gorte, University of Pennsylvania INVITED

Fuel cells are an attractive method for electrical power generation because they offer the possibility of very high efficiencies compared to normal heat engines. One of the major hurdles preventing their implementation for a wide variety of applications is the fact that, until recently, only H₂ could be used as the fuel. We have recently demonstrated that stable power generation, without either internal or external reforming, can be achieved through the direct oxidation of hydrocarbons, including liquids, using a solid-oxide fuel cell (SOFC).¹ The anodes in these direct-oxidation SOFC were composites made of Cu, ceria, and yttria-stabilized zirconia (YSZ). In this talk, the methods for preparing these anodes will be described. It will be demonstrated that surface chemistry and structure are crucial for improved performance of these fuel cells. Attempts to control the surface chemistry and structure will then be discussed.

¹ S. Park, J. M. Vohs, and R. J. Gorte, Nature, 404 (2000) 265.

9:40am EC+SS-MoM5 Strategies for the Study of Methanol and CO Electrocatalysis on Solid Electrodes and Nanometer-Scale Supported Catalysts, C. Korzeniewski, G. Vijayaraghavan, L. Gao, Texas Tech University INVITED

The electrochemical oxidation of methanol and related small molecules has been of special interest in relation to fuel cell research. The development of fuel cells that operate below 100 °C on methanol, or H₂ has stimulated interest in the reaction steps involved in methanol and carbon monoxide oxidation at metal electrodes. In addition to being a by-product of methanol oxidation, carbon monoxide can also be present as an impurity in H. Adsorption of carbon monoxide on the anode catalyst generally degrades its performance. We have approached the study of methanol and carbon monoxide oxidation with the use of electrochemical techniques in combination with in situ infrared spectroscopy, atomic force microscopy (AFM) and wet-analytical methods. This presentation will focus on the surface electrochemistry of methanol and carbon monoxide at supported Pt and Pt-Ru catalysts. In situ infrared measurements are being performed with Vulcan carbon supported fuel cell catalysts. The carbon supported materials are adsorbed onto a smooth gold electrode to enable infrared sampling in a standard reflectance geometry. A thermostatted cell allows in situ infrared measurements between ambient and 80 °C. Similar to the bulk metals, thermal effects on methanol oxidation at nanometer-scale catalysts are stronger for Pt-Ru (atomic percent Ru = 50%) than Pt. The influence that metal particle size distribution and spatial arrangement on carbon supports has on methanol oxidation pathways is being investigated by depositing metal particles on highly ordered pyrolytic graphite. The surface electrocatalytic properties of the supported particles are investigated with cyclic voltammetry. AFM is used to determine the catalyst size distribution and spatial arrangement at different stages of preparation and electrochemical characterization. Properties of nanometer-scale metal particles in relation to methanol oxidation pathways will be discussed.

10:20am EC+SS-MoM7 Potential Application of Tungsten Carbides as Direct Methanol Fuel Cell (DMFC) Electrocatalysts, H.H. Hwu, J.G. Chen, University of Delaware

The Pt/Ru anode in direct methanol fuel cells (DMFC), though effective, is disadvantageous in terms of its prohibitively high costs and limited supplies. In this work, we are evaluating the effectiveness of tungsten and molybdenum carbides as alternatives to Pt/Ru electrocatalysts by studying their reactivities towards methanol, water, and carbon monoxide. Using Temperature Programmed Desorption (TPD) and High-Resolution Electron Energy Loss Spectroscopy (HREELS) the reaction pathways of these DMFC molecules on carbide-modified Mo(110), W(110), and W(111) can be understood. On both W(110) and W(111) carbide surfaces, methanol readily decomposes into gas-phase CO, methane, hydrogen, and surface carbon and oxygen. In addition, both tungsten carbide surfaces are active toward the dissociation of CO and water. Preliminary studies on the Mo(110) carbide surface also show strong decomposition activity toward methanol, but through a different pathway than either the W(110) or W(111) carbide surfaces. Results from parallel studies of DMFC molecules on thin film tungsten carbides will also be presented.

10:40am EC+SS-MoM8 Ru Nanoparticles Prepared by Decomposition of Ru₃(CO)₁₂ on Au (111): Structural Characterization and Chemical Properties, *T. Cai, Z. Song, Z. Chang, G. Liu, J.A. Rodriguez, J. Hrbek*, Brookhaven National Laboratory

Supported ruthenium metal particles prepared from ruthenium carbonyl have been shown as a most active catalyst for ammonia synthesis. In the emerging field of nanoscience, a goal is to make nanostructures with interesting functional properties. We have started a research program using metal carbonyls as precursors in the synthesis of nanoparticles on well-defined templates. In this study, we prepared and characterized a Au-supported Ru model catalyst under UHV by depositing metallic Ru on a Au (111) surface using triruthenium dodecacarbonyl, Ru₃(CO)₁₂, as a molecular precursor. We used the reconstructed Au (111) surface as an inert template for metallic cluster growth. Carbonyl adsorbs molecularly on the surface at 90 K and starts to dissociate at 280 K by CO elimination, as shown in TPD studies. The complete decomposition of the carbonyl occurs above 500 K, leaving metallic Ru on the surface with no significant C or O as detected by

XPS. Such an atomically clean Ru deposit is also obtained on Au (111) by MOCVD of $Ru_3(CO)_{12}$ at an elevated substrate temperature of 550 K. The morphology of the Ru nanoparticles investigated by STM and their chemical reactivity toward simple molecules (CO, N_2 , NH₃, O_2 , NO₂) studied by XPS and TPD will be discussed. The research was carried out at BNL under Contract No. DE-AC02-98CH10086 with the U.S. DOE (Division of Chemical Sciences).

11:00am EC+SS-MoM9 Development of a Microreactor System for Electrocatalytic Studies of Methanol Oxidation, *N. Arvindan*, *E.M. Stuve*, University of Washington

We report on the development of a microreactor for studies of methanol electro-oxidation on platinum catalysts. One of the primary benefits of the microreactor is the ease of temperature control and low consumption of reactants. Temperature can be adjusted and controlled nearly instantaneously over the range of 20 to 100 C. Higher temperatures are possible depending on the pressure limitations of the fluidic connec-tions to the microreactor. The microreactor enables studies of methanol electrooxidation at high temperatures to achieve accelerated kinetics and freedom from CO poisoning. Methanol oxidation is measured at constant potential following a step from a non-reacting potential. Accumulation of surface species like CO is subsequently measured by linear sweep voltammetry. These two measurements enable the overall oxidation rate of methanol to be compared with the CO oxidation rate. Initial results demonstrate clean voltammetry of polycrystalline platinum electrodes for all temperatures. Reaction studies over the range of 80 to 100 C show that methanol oxidation occurs at the same rate as CO oxidation, consistent with the series reaction path (methanol to CO to carbon dioxide) being the dominant mechanism. The results conclusively show that thermal desorption of CO is insignificant, even at temperatures as high as 95 C. At 95 C turnover rates vary from 0.1 to 1 per second for the respective potential range of 400 to 600 mV vs. RHE. These results show that unmodified polycrystalline platinum is an effect catalyst for methanol oxidation at 95 C and support the feasibility of high temperature direct methanol fuel cells. This work is supported by the National Science Foundation and the UW Center for Nanotechnology.

11:20am EC+SS-MoM10 Combined Atomic Force Microscope and Acoustic Wave Devices: Application to Electrodeposition, J.-M. Friedt, L. Francis, K.-H. Choi, A. Campitelli, IMEC, Belgium

We here present the development of an instrument based on a new combination of techniques including scanning probe microscopy (atomic force microscopy, AFM, in our case) and acoustic wave devices (quartz crystal microbalance - QCM - and acoustic wave resonators). We display the ways these two measurement techniques interact and show that their performances are not degraded through interaction. Using finite element analysis, we explain observations compatible with the generation of longitudinal acoustic waves in the liquid, creating standing wave patterns between the QCM sensing electrode and the AFM cantilever holder leading to resonance frequency instabilities of the QCM. QCM electrode vibration in liquid is also shown not to degrade AFM lateral resolution. We then show measurement results from electrodeposition of copper and silver on gold electrode obtained using this instrument, and demonstrate how the data from both techniques (QCM-D and AFM) are complementary. Since QCM-D allows simultaneous measurement of the resonance frequency at several overtones of the quartz crystal resonator as well as the dissipation (quality factor) of each of these overtones, we show how the relative frequency shifts of the overtones informs on the kind of interactions between the oscillating acoustic wave device and the surrounding media (electrodeposited layer and solution used for electrochemistry). This combined measurement was performed on AT-cut quartz resonators (QCM), SH-SAW lithium tantalate and quartz acoustic wave devices and Love mode quartz acoustic wave devices. Finally, we show that after identifying the types of interactions we can efficiently use electrodeposition as a mean of calibrating the sensitivity of acoustic wave devices. Sensitivities close to the theoretical values and compatible with previous values given in the literature are presented.

11:40am EC+SS-MoM11 Study of Bismuth Thin Film Electrodeposition and Oxide Formation on Au(111), C.A. Jeffrey, D.A. Harrington, University of Victoria, Canada, S. Morin, York University, Canada

Bismuth and bismuth oxide films have been well studied due to their magnetoresistive and semiconducting properties. In this work, the formation of electrodeposited bismuth thin films is studied using in-situ scanning tunneling microscopy (STM). Their growth mode and morphology provide useful information for the production of well-defined bismuth thin films. Electrodeposition of bismuth is performed on Au(111) in acidic solution and the bismuth film transformation to bismuth oxide in alkaline solution is

studied using in-situ atomic force microscopy (AFM). Our study of the underpotential deposition process indicate that the reconstruction of Au(111) is lifted by the adsorbed bismuth, resulting in the formation of gold islands at potentials negative of 0.170 V_{SCE} . Scans taken during the overpotential deposition process at potentials negative of -0.070 V_{SCE} reveal 'needle' growth starting at step edges. These needles propagate over the surface and eventually form relatively uniform films. Atomic resolution images of the needle structures show the nearly rectangular unit cell 3.9 Å x 4.3 Å that contains one bismuth atom. The shorter side of the unit cell lies in the direction of the growth axis of the needle. This reduced spacing results in preferential incorporation of surface diffusing atoms at the needle tip, as opposed to along the edge, and accounts for the anisotropic growth. Bismuth oxide was formed by first forming the bismuth layer in acidic solution followed by a gradual shifting of the solution pH to a value of 10. Under these conditions, the transformation to the oxide film is monitored as the potential is made more positive. Close to the potential where the formation of bismuth oxide is expected, the morphology changes abruptly; small isolated protrusions form on the needle structures and cover the entire surface. The surface oxide formed can be reduced back to bismuth and this results in a disordered Bi film.

Manufacturing Science and Technology Room: C-109 - Session MS+SE-MoM

In-Situ Monitoring and Metrology for Coating Growth and Manufacturing

Moderator: A. Diebold, International Sematech

8:20am MS+SE-MoM1 Product Development and Yield Enhancement through Failure Analysis of Integrated Circuits with Scanning Capacitance Microscopy, *P. Tangyunyong*, *C.Y. Nakakura*, Sandia National Laboratories

Scanning capacitance microscopy (SCM) has become a widely used metrology tool in the microelectronics industry due to its ability to measure two-dimensional free carrier profiles with nanometer-scale resolution. To date, SCM has been used primarily to characterize source/drain formation by imaging cross-sectioned, metal-oxide-semiconductor field effect transistors (MOSFETs). We have extended the role of SCM in our Fab from an off-line research instrument to a routinely-used failure analysis tool, active in providing feedback in new product development, process validation, and yield enhancement. The SCM measurement can be performed on any two-dimensions of the sample, thus providing unique information that cannot be obtained with other analysis techniques. This information has been instrumental in helping to identify several yieldlimiting defects in our CMOS device product line. In addition, SCM measurements are performed in-house with quick turnaround, yielding a considerable advantage over off-site analysis techniques, such as secondary ion mass spectroscopy. The methodology for performing both top-down (parallel to the wafer surface) and cross-sectional SCM measurements will be presented. We will show, in detail, several examples of how SCM information has been used to identify the root causes of device failures and discuss some of the corrective actions taken to reduce defects and improve yield.

This work was performed at and supported by Sandia National Laboratories under DOE contract DE-AC04-94AL85000. Sandia National Laboratories is a multi-program laboratory operated by Sandia Corporation for the United States Department of Energy.

8:40am **MS+SE-MoM2 Integrated CD Metrology for Poly Si Etching**, *G.P. Kota*, *C. Lee*, Lam Research Corporation, *T. Dziura*, *A. Levy*, KLA-Tencor Corporation

Advanced process control (APC) is gaining widespread use because of the costs associated with 300mm wafer processing and because of the stringent control required for CD and profile due to the shrinkage of critical feature dimension. APC can be used in Feed forward, Feed back and Fault detection control modes. The KT metrology module called iSpectra is integrated on to the Lam 2300 Versys etch platform. This modular design allows for real time APC. Integrated metrology also enhances the overall equipment efficiency. A comparison of iSpectra, CD-SEM, and xSEM results will be presented. iSpectra shows good correlation to the CDSEM measurements as well as x-SEM profiles. In addition, iSpectra repeatability is superior to conventional methods such as CD-SEM. It is common knowledge that 193nm PR shrinks during CDSEM measurements due to exposure of the PR to e-beam. This shrinkage has been measured to be up to 17nm after about 30 repeated measurements on the CDSEM. In comparison, the iSpectra measurement technique results in minimal CD shrinkage.

9:00am MS+SE-MoM3 Metrology for Manufacturing, U. Whitney, KLA-Tencor INVITED

9:40am MS+SE-MoM5 Measurements of Shallow Trench Isolation by Normal Incidence Optical Critical Dimension Technique, J. Hu, D. Shivaprasad, F. Yang, R. Korlahalli, Nanometrics, Inc.

Shallow Trench Isolation (STI) has emerged as one of the primary techniques for device isolation in complementary metal-oxide semiconductor (CMOS) technologies. This device isolation technology has become extremely important to satisfy the high density requirements of modern integrated circuits, It is of paramount importance to measure the critical dimensions of the STI structure. Currently used CD-SEMs cannot identify the rounding typically present at the bottom or top of the profile, and it is difficult to differentiate between the top and bottom line-width values. X-SEMs which can give the profile information require the destruction of the wafer. In this paper we present the work done on STI using the Optical Critical Dimension (OCD) technique. This technique measures line or trench profiles using Normal Incidence Polarized Reflectometry with a sensitivity to sub-50nm grating lines. In the OCD technique, a broadband polarized light beam is focused onto the grating surface, and the reflected 0th order is measured as a function of wavelength. The data obtained by measuring the grating structure gives a signature of the profile structure which is analyzed in real time using Rigorous Coupled Wave Analysis (RCWA). Since the data is fitted in real time, there is no requirement for library generation, which makes the analysis simpler and easier to extend to other structures without the need of lengthy re-generation of a new library of profile data. Data from STI wafers before and after ashing (removal of the developed resist) will be presented. Sensitivity to the oxide notching and repeatability data will also be presented.

10:00am **MS+SE-MoM6** The Evolution of Single Atomic Steps on vicinal Si(111) in NH₄F, *J. Fu*, National Institute of Standards and Technology, *H. Zhou*, University of Maryland, *J.A. Kramar, R. Silver*, National Institute of Standards and Technology

Determining the width of a feature or the scale in a pitch measurement with appropriate accuracy is fundamental for process control in state-of-the-art semiconductor manufacturing. To meet these needs as well as the future measurement and calibration needs of the emerging nanomanufacturing industry, the National Institute of Standards and Technology (NIST) has been pursuing research and development on techniques for the fabrication and measurement of atom-based dimensional standards. The key elements in the development of atom-based standards are the ability to prepare atomically ordered surfaces, and the ability to count the atoms making up the features of interest. One of the most difficult challenges in atom-based metrology has been the fabrication of an appropriate atomic template. Atomically ordered surfaces provide an intrinsic template which have both scale and orthogonality. Using Scanning Probe Microscopy(SPM), We have examined the surface produced by etching several different vicinal Si(111) sample in 40% NH_4F . In agreement with others, we find that deoxygenation of the etchant generally reduces the number of triangular etch pits. The formation of single atomic steps is evolved from these etch pits. These etch pits undergo nucleation, growth, merging, and corner rounding which can lead to single atomic steps. We also find that for maximum uniformity and minimum root mean square roughness, a certain minimum miscut angle is required. This angle is related to the maximum clear terrace width, which in turn is related to the relative aching rate of the step-edge sites and the terrace sites. The time evolution of the surface-smoothing etching process was also examined.

10:20am MS+SE-MoM7 Real Time in situ Spectroellipsometry, J.A. Woollam, B. Johs, J. Hale, J. A. Woollam Co., Inc. INVITED

This talk reviews applications of spectroscopic ellipsometry for in situ monitoring and control during deposition, thermal processing, and etching of surfaces and thin-films. In situ spectroscopic ellipsometry is valuable for calibrating film growth and etch rates, controlling the thickness of each layer in multi-layer structures, and investigating nucleation phenomenon. It is also useful for measuring surface and interfacial roughness, substrate and film optical constants (with and without surface oxides), alloy composition, and substrate temperature. There have been numerous challenges to implementing in situ spectroscopic ellipsometry, including how to deal with substrate wobble and the effects of windows, and how to accurately measure thickness and material properties during growth of large numbers of layers in multi-layer stacks. Solutions to these practical problems will be discussed, and example applications described. 11:00am MS+SE-MoM9 Real Time Process Control by Spectroellipsometry, D. Daineka, P. Bulkin, T. Novikova, B. Drévillon, CNRS, Ecole Polytechnique, France

In situ ellipsometry is well known to be the most sensitive, non-invasive tool for monitoring and control of thin film growth. In the fabrication of optical coatings and thin films in general the refractive index of the material is usually assumed to remain constant within a single layer. With such assumption only optical thickness of the layer can be controlled. For modern complex structures, however, even insignificant variation in the refractive index can be very detrimental to the final performance of the coating. Simultaneous real-time determination of refractive index and growth rate is required in order to comply with strict specifications. If the index departs from the pre-calculated target value, one has to adjust process parameters. In PECVD such control variables are gas flows of the precursors. We report on the closed-loop control of the silicon oxynitrides deposition by in situ phase modulated kinetic spectroellipsometry using a direct numerical inversion algorithm for the real-time reconstruction of refractive index and layer thickness. This technique is tested on constant index layers as well as on graded refractive index profiles and shown to be efficient and reliable.

11:20am MS+SE-MoM10 In-Situ Studies of the Amorphous to Microcrystalline Transition of Hot-Wire CVD Si:H Films Using Real-Time Spectroscopic Ellipsometry, *D.H. Levi*, *B.P. Nelson*, *J.D. Perkins*, National Renewable Energy Laboratory

In-situ real-time spectroscopic ellipsometry (RTSE) provides detailed information on the evolution of the structural and optical properties of Si:H films during growth.¹ We have used in-situ RTSE to characterize the morphology and crystallinity of hot-wire CVD (HWCVD) Si:H films as a function of substrate temperature T_s, hydrogen dilution R=[H]/[H+SiH₄], and film thickness d_b. Transitions from one mode of film growth to another are indicated by abrupt changes in the magnitude of the surface roughness during film growth. The degree of crystallinity of the film can be determined from the bulk dielectric function. We have studied the growth parameter space consisting of R from 0 to 14, Ts from 250°C to 550°C, and d_b from 0 to 1 µm. For each set of R and T_s values, the structural evolution of the film can be characterized by the shape of the surface roughness thickness d_s versus bulk thickness d_b curve. In contrast to studies done by Collins et al on PECVD growth of Si:H films, our studies of HWCVD growth find no conditions where d_s remains constant after coalescence of the initial nucleation centers. Most of the films grown within the range of parameters studied exhibit a secondary nucleation and coalescence signature. The transition between aSi:H and uc-Si:H growth is near the R=3 to R=4 dividing line. Initial coalescence of purely uc-Si:H material does not occur until R>8. We have verified the RTSE crystallinity classification using ex-situ Raman scattering.

¹ R.W. Collins, Joohyun Koh, H. Fujiwara, P.I. Rovira, A.S. Ferlauto, J.A. Zapien, C.R. Wronski, R. Messier, Appl. Surf. Sci., 154-155, 217-228 (2000).

11:40am MS+SE-MoM11 Post-Deposition Control of Resistivity and Anisotropy in ZnO Thin Films, J.S. Lewis, B. Stoner, C. Pace, MCNC

A method for post-deposition control of the resistivity of ZnO thin films has been developed, and a method for providing anisotropic sheet resistance in the plane of the film has been demonstrated. Military needs for real-time image processing can be met using thin film analog image processor (TAIP) devices. TAIP chips provide compact and power-efficient analog processing, including high- or low-pass spatial frequency filtering. The analog spatial filters are based on the RC time constant of the circuit, and therefore require thin films with controlled, repeatable sheet resistance in the range of $M\Omega/sq$. This range of sheet resistance can be difficult to achieve with good repeatability for inorganic films. ZnO thin films were sputtered from an undoped ZnO target by RF magnetron sputtering. The asdeposited sheet resistance of the films was in the range 5-50 k Ω /sq. Post deposition processing yielded films with sheet resistance in the range from the as deposited value to > 100 M Ω /sq. Target values of sheet resistance were obtained routinely. Using an in-situ monitor of sheet resistance during processing resulted in much better repeatability than that possible for asdeposited films. For TAIP chips, anisotropic sheet resistance in the plane of the film can allow more sophisticated algorithms for image processing. Post processing techniques were used to fabricate ZnO thin films with sheet resistance anisotropy ratios in the range of 2:1 to 25:1, and larger anisotropies should be possible. This work was sponsored by DARPA (contract no. DAAD19-00-1-0002).

Adsorption and Chirality

Moderator: B.E. Koel, University of Southern California

8:20am SS1-MoM1 STM Studies of the Role of Copper in Chlorosilane Desorption Mechanisms from Cl-exposed Cu/Si(111) Surfaces, D.V. Potapenko, S.E. Sysoev, A.V. Ermakov, D. Maithil, B.J. Hinch, Rutgers University

TPD experiments show that the presence of copper on a Si(111) surface significantly influences the desorption kinetics of chlorosilanes from chlorine-exposed Si(111) surfaces. The major desorption peak (of SiCl₂) occurs at ~600°C from Cl-covered Cu/Si(111) surfaces, and complex desorption kinetics are exhibited that indicate an active role of chlorine-free sites in the SiCl₂ desorption process. In contrast, SiCl₂ desorption from Si(111) surfaces, is observed at ~650°C and this follows comparatively simple second-order kinetics. Here we report on STM studies of the Cl-covered Cu/Si(111) surfaces, following low temperature (~450°C) restructuring and at the onset of chlorosilane desorption at 600°C. We will display evidence for the direct role of copper in the aggregation of Cl in compact Cl-containing regions during the high temperature chlorosilane desorption process. We will also discuss possible mechanisms of Cu-catalyzed desorption of chlorosilanes from the Si(111) surface.

8:40am SS1-MoM2 Dynamics of Oligomer Desorption from Surfaces, A.J. Gellman, K.R. Paserba, N. Vaidyanathan, Carnegie Mellon University A study of the desorption of long chain oligomers from surfaces has revealed that the measured desorption energies are non-linear in the oligomer chain length. This work has used alkanes, polyetheyleneglycols, and polyethyleneglycol dimethylethers with chain lengths in the range 5 to 60 atoms. These have been adsorbed on the surface of graphite at low temperature and the kinetics of desorption have been measured using temperature programmed desorption. Empirically we find that the desorption energies scale as the square root of the chain length. A model has been proposed for oligomer desorption that accurately accounts for the observed dependence of the desorption energy on chain length. The adsorbed oligomers can be considered to consist of segments that are attaching to and detaching from the surface independently. Within the context of transition state theory these partially detached oligomers are in equilibrium with a transition state to desorption which is fully detached from the surface. The energy of each of the detached states is simply proportional to the number of detached segments. The entropy is given by the number of ways of detaching segments and by the partition function for trans-gauche conformations about each detached bond. These energies and entropies determine the equilibrium constants for each of the partially detached species. These considerations can be formulated into an analytical expression for the measured desorption energy that accurately reproduces the experimental results. One of the interesting insights that our model provides is that the analytical expression for oligomer desorption energies exactly matches the predictions of Tolman's theorem. Because the oligomers on the surface can adopt a huge number of conformations this leads to a substantial non-linearity in the desorption energy as a function of chain length.

9:00am SS1-MoM3 D Abstraction by H on Si(111) Surfaces: Temperature and Coverage Dependence, F. Khanom, F. Rahman, A. Aoki, A. Namiki, Kyushu Institute of Technology, Japan

Influences of surface temperature T and D adatom coverage on direct abstraction (ABS) as well as collision-induced-desorption (CID) of surface D adatoms by H atoms have been studied on Si(111). We found that D₂ CID as a result of reaction H + D/Si --> D₂, obeys a third-order kinetics with respect to θ_D , ruling out the so-called hot atom mechanism. D_2 CID rate versus T_s curves were found to exhibit a close similarity in spectral line shape with a β_2 temperature-programmed-desorption (TPD) spectrum arising from a dideuteride phase. The spectral similarity between CID and TPD suggests that D_2 CID obey the same mechanism as for the β_2 TPD. In order to understand the underling mechanism we measured reaction order of the β_2 TPD. As a consequence, 1.5th-reaction order was obtained with respect to dideuteride coverage. The 1.5th reaction order suggests that three D atoms are involved in a single D₂ desorption, which rationalizes the thirdorder reaction observed in D2 CID. Regarding ABS to form HD molecules, HD rates were determined for various $\theta_{\text{D}}.$ As a result, we found that a firstorder kinetics prevails the HD ABS for low D coverage regime below 0.5ML, but strangely enough, a second-order kinetics becomes dominant for high coverage regime around 1.0 ML. The second-order kinetics suggests that a direct Eley-Rideal reaction mechanism as well as hot atom

mechanism are ruled out. We propose a new mechanism of hot complex mediated ABS and CID: the incident H atoms form a complex with D-Si system in the very early stages of sticking. ABS and dihydride formation occur competitively during the relaxation process of the hot complex.

9:20am **SS1-MoM4 Adsorption and Abstraction of H Atoms on the Graphite (0001) Surface**, *T. Zecho*, Max-Planck-Institut für Plasmaphysik (EURATOM Association), Germany, *A. Güttler, C. Drummer*, Universität Bayreuth, Germany, *X. Sha, B. Jackson*, University of Massachusetts, *J. Küppers*, Max-Planck-Institut für Plasmaphysik (EURATOM Association), Germany

The interactions of hydrogen atoms with graphite surfaces are of interest for many areas like astrophysics, plasma surface interactions in controlled fusion devices and diamond synthesises. Nevertheless most of the knowledge up to now is deduced from theoretical work and without experimental evidence. The present study has been performed in order to verify recent theoretical results on the interactions of hydrogen atoms with the graphite basal plane. Highly oriented pyrolytic graphite (HOPG-ZYH) was used and characterised by scanning electron microscopy (SEM) prior to the experiments. Hydrogen atoms were generated by thermal dissociation of hydrogen molecules in a tungsten capillary heated to 2000 K. Adsorption and abstraction were investigated by thermal desorption spectroscopy (TDS), electronic and vibrational energy loss spectroscopy (EELS, HREELS) and in situ measurment of the abstraction products. Admission of hydrogen atoms at low temperatures (100 K-300 K) leads to adsorption of hydrogen on graphite up to coverages of about 0.5 monolayer. In EEL spectra the intensity of the π -plasmon of graphite decreases upon hydrogen adsorption indicating a decreasing sp² character of surface carbon 2sp electrons. HREEL spectra allowed to determine the C-H normal and parallel vibrational frequencies which are close to theoretical predictions. Heating of H(D) covered graphite surfaces leads to desorption of hydrogen (deuterium) molecules with peaks between 300 K and 600 K. The thermal desorption peak maxima show a large isotope effect of about 50 K. The admission of deuterium atoms to H covered graphite surfaces leads to the release of HD and a very small amount of H2. The abstraction reaction shows a coverage dependent cross section which decreases from about 16 Å² at low coverages to about 4 Å² close to saturation.

9:40am SS1-MoM5 Experimental and Theoretical Characterization of the Vibrational Properties of Aminocarbyne Surface Intermediates, *B. Chatterjee, D.H. Kang,* University of Illinois at Chicago, *P. Mills,* North Central College, *M. Trenary,* University of Illinois at Chicago

Density functional theory (DFT) calculations and measurements using reflection absorption infrared spectroscopy have been used to characterize aminocarbynes on a Pt(111) surface. The three aminocarbynes considered are CNH₂, CNHCH₃ and CN(CH₃)₂. The CNH₂ species, known simply as aminocarbyne or as aminomethylidyne, is formed from HCN, methyl amine, or the hydrogenation of surface CN. Methylaminocarbyne, CNHCH $_{\!\!\!3}$, can be formed from the Nprotonation of methyl isocyanide (CNCH₃) or from the partial dehydrogenation of dimethyl amine, $HN(CH_3)_2$. Dimethylaminocarbyne, $CN(CH_3)_2$, is formed from the decomposition of trimethylamine, $N(CH_3)_3$. The DFT calculations were based on a model consisting of only two Pt atoms, as would be appropriate for bonding at a two-fold bridge site. Gaussian 98 with the B3LYP functional and a 6-311G** basis set along with effective core potentials for the Pt atoms was used. The calculations converged and optimized to reasonable geometries. For example, Pt_2CNH_2 converged to a C_{2v} symmetry structure with a CN bond length of 1.32 Å with calculated frequencies (using the appropriate scale factor of 0.9613) for the v(CN), δ (NH₂), and v_s(NH) fundamentals of 1393, 1564, and 3407 cm⁻¹, respectively, compared to experimental values for CNH₂ on Pt(111) of 1323, 1567, and 3363 cm⁻¹. The calculations successfully reproduce not only the measured vibrational frequencies, but also the relative intensities and the measured shifts that occur with various isotopic substitutions. Calculations using larger Pt clusters, which are much more time consuming, lead to only modest improvements. The results suggest that the internal vibrations of polyatomic adsorbates can be successfully calculated using models of the surface that are surprisingly simple.

10:00am SS1-MoM6 Adsorption and Adhesion Energies of Pb on (1x1)-MoC/Mo(001) by Single-crystal Adsorption Calorimetry, M.H. Smedh, S.F. Diaz, C.T. Campbell, University of Washington

The heat of adsorption, sticking probability and film growth mode of Pb adsorption was studied on a thin, ordered MoC film at 300 K. A several layers thick film of MoC displaying a (1x1) LEED pattern was grown by dissociating ethylene on hot Mo(100), following Frühberger.¹ The Pb atoms were deposited in a chopped molecular beam, with 0.1 s pulses containing 0.015 ML Pb every 2 s. The Pb beam flux was determined using a quartz crystal microbalance. The heat of Pb adsorption was measured by single-

crystal adsorption microcalorimetry, based on King's approach,² with a different heat detection scheme. The adsorption of a Pb pulse causes a transient heat input and temperature rise, detected by a pyroelectric polymer ribbon in contact with the backside of the sample.³ An initial heat of adsorption of 245 ± 5 kJ/mol was found. It stayed constant up to ~0.5 ML, then dropped smoothly up to 1 ML to ~195 kJ/mol, within a few percent of the heat of sublimation for Pb, where it remained constant up to ~ 8 ML. The implications of these results with respect to Pb-Pb repulsions and Pb mobility in the adlayer will be discussed. From the integral heat of adsorption at 8 ML, a Pb/MoC adhesion energy of ~180 µJ/cm² was obtained. This will be compared to results obtained from the contact angle of molten Pb drops. The sticking probability was found to be 0.96 initially, increasing linearly up to ~1 ML to 0.994 ± 0.003, where it remained for higher coverages. The growth mode of Pb on (1x1)-MoC/Mo(100) was further investigated by omparing the behavior of the Pb and Mo AES intensities as a function of the Pb coverage to different growth models.

¹B. Frühberger and J.G. Chen, Surf. Sci. 342 (1995) 38.

²C.E. Borroni-Bird and D.A. King, Rev. Sci. Instrum. 62 (1991) 2177

³J.T. Stuckless, N.A. Frei, and C.T. Campbell, Rev. Sci. Instrum. 69 (1998) 2427.

10:20am SS1-MoM7 Enantioselectivity on Naturally Chiral Surfaces, A.J. Gellman, J. Horvath, Carnegie Mellon University INVITED

Chirality is an omnipresent feature of the biochemical and biophysical world. The handedness of the molecules that form the basis of life creates the need for enantiomeric purity in the chemicals used for pharmaceutical and other bio-active purposes. Many of the processes used for synthesis and preparation of enantiomerically pure compounds rely on the use of chiral surfaces. The high Miller index surfaces of metals have chiral structures and can, in principle, be used for to control enantioselectivity in chemical processes. The kinked step structures of such surface are chiral and thus serve as chiral binding sites for a number of enantiospecific adsorption, desorption and surface reactions. As an example, the orientation of chiral molecules on chiral surfaces can be shown to depend on the relative handedness of adsorbate and substrate. This has been shown by study of the infrared reflection absorption spectra of 2-butanoxy groups on the Ag(643) surface. The intensities of the absorptions by R- and S-2-butanoxy groups are dependent on the handedness of the Ag(643) substrate. Similarly, the heats of adsorption of small chiral molecules such as R- and S-propylene oxide (CH3CH(O)CH2) and R-3-methylcyclohexanone are sensitive to the handedness of surfaces such as Cu(643). This has been observed using thermally programmed desorption measurements which reveal that the desorption kinetics of these chiral molecules are enantiospecific on chiral surfaces. They do not exhibit enantiospecificity on achiral surfaces such as Cu(111). In the course of this work we have been able to identify chiral adsorption sites on high Miller index metal surfaces. Most recently we have been able to demonstrate an enantioselective separation using such surfaces to purify a racemic mixture of 3-methylcyclohexanone. Understanding and controlling these enantiospecific properties poses some extremely interesting challenges for surface chemistry and surface physics.

11:00am SS1-MoM9 Self-assembly of Chiral Nanoclusters of Cysteine on Au(110)-(1x2), A. Kühnle, T.R. Linderoth, L. Molina, B. Hammer, F. Besenbacher, University of Aarhus, Denmark

We have performed a comprehensive STM-based study of the adsorption of the chiral amino acid cysteine, HS-CH2CH(NH2)-COOH, onto the missingrow reconstructed Au(110)-(1x2) surface under UHV conditions. In experiments where we deposit cysteine either as the pure enantiomeric forms or as the racemic mixture, we have identified a rich variety of chiral adsorption phenomena. The results are interpreted with the aid of density functional theory calculations. Previously, we have reported on the enantioselective dimerization of cysteine into homochiral molecular pairs and identified the atomic-scale interactions responsible for this intermolecular chiral recognition.¹ Here, we focus first on supramolecular chain-like assemblies of cysteine molecules that coexist with the molecular pairs. The chiral chains extend over several hundred Ångström and consist of two adjacent rows of cysteine molecules. Formation of these chains is accompanied by a pronounced surface reconstruction, involving the removal of two close-packed rows of gold atoms underneath each molecular double row, and is driven by the formation of hydrogen bonds between the carboxylic groups of the cysteine molecules in the rows. Secondly, we discuss the self-assembly of molecular nanoclusters of cysteine. When cysteine is deposited at a substrate temperature of 120 K, small, irregular agglomerates of molecules are formed. A remarkable transition is seen upon annealing to 270 K, where the molecules self-assemble into completely identical clusters with a size of 18 by 24 Å. The molecules appear to segregate into homochiral clusters when the racemic mixture is deposited.

¹ A. Kühnle, T.R. Linderoth, B. Hammer and F. Besenbacher, Nature 415, 891 (2002).

11:20am SS1-MoM10 Towards Epitaxial Growth of Chiral Metal Films on Metal Oxide Substrates, D.S. Sholl, A. Asthagiri, A.J. Francis, C. Niederbarger, L.M. Parter, P. Sakadar, Camagia Mellon, University

C. Niederberger, L.M. Porter, P. Salvador, Carnegie Mellon University Although intrinsically chiral metal surfaces have been demonstrated to have intriguing enantiospecific adsorption and electrochemical properties, current studies of these materials are performed using small single-crystal samples. To move towards practical applications of these surfaces, techniques for substantially increasing the surface area of these chiral films need to be developed. One avenue towards this goal is the controlled growth of thin metal films on suitable chiral metal oxide substrates. We will report theoretical and experimental results for the growth of Pt films on $\ensuremath{\mathrm{SrTiO}}_{\!\!3}$ substrates. This metal/metal-oxide pair was chosen because of the catalytic properties of Pt, the close lattice match between Pt and SrTiO₃, and the availability of SrTiO₃ as single crystal substrates. To control metal film growth on stepped metal oxide substrates it is necessary to understand the growth modes on the relevant atomically flat surfaces. We have studied Pt deposition on the non-polar SrTiO₃(100) surface and the polar SrTiO₃(111) surfaces using various experimental probes and ab initio Density Functional Theory. Our results identify the preferred binding geometries and film orientations of Pt films on these substrates. Xray diffraction and low energy electron diffraction confirmed epitaxial growth of the Pt films, with the number of in-plane orientations dependent on both the substrate temperature and the nature of the substrate surface. We are currently extending our studies to the deposition of Pt on intrinsically chiral SrTiO₃ substrates and will discuss the prospects for creating robust chiral metal films with this process.

11:40am SS1-MoM11 Novel Low-Temperature Reactivity of Model Bimetallic Surfaces with Monolayer Coverages, N.A. Khan, J.G. Chen, University of Delaware

Bimetallic surfaces have gained considerable interest in fundamental surface science research because of their unique catalytic activity and electronic properties. By studying these surfaces at an atomic level, we can gain more insight into the origin of these novel properties. In this study, we have used various surface science techniques (TPD, HREELS, NEXAFS, and XPS) to investigate the properties of model bimetallic surfaces. We have shown that the one monolayer Ni/Pt(111) surface exhibits novel chemical reactivity, unlike the pure Ni(111) or Pt(111) surfaces. Temperature-programmed desorption (TPD) results indicate that hydrogen has a lower binding energy to the 1 ML Ni/Pt(111) surface than on the other two surfaces.^{1,2} In principle, a weak metal - hydrogen interaction should lead to an increase in the hydrogenation activity of other species on the surface. We have used other catalytically important probe molecules, such as cyclohexene and thiophene to further investigate this hydrogenation activity. XPS and NEXAFS also showed that the oxidation state and density of unoccupied states of one monolayer Ni/Pt(111) are similar to that of bulk Ni(111). In addition to studying the Ni/Pt(111) surface, we have also investigated the Ni/W(110) surface for comparison. On the Ni/W(110) surface, the probe molecules also undergo hydrogenation at a low temperature. However, the maximum activity occurs at about 0.4 ML Ni. At this coverage of Ni, Schmidthals, et. al. have found a large amount of surface strain.³ We will attempt to correlate this lattice mismatch to a novel chemical reactivity seen on the 0.4 ML Ni/W(110) surface.

¹ H.H. Hwu, J. Eng Jr., J.G. Chen, J. Am. Chem. Soc. 124 (2002) 702.
² N.A. Khan, H.H. Hwu, J.G. Chen, J. Catal. 205 (2002) 259.

³ C. Schmidthals, et. al. Surf. Sci. 402-404 (1998) 636.

Surface Science Room: C-112 - Session SS2-MoM

Oxide Structure and Surface Chemistry

Moderator: T.E. Madey, Rutgers, The State University of New Jersev

8:20am SS2-MoM1 TPD Studies of the Chemistry of CCl₄ on Fe₃O₄ (2x2)-(111) Surfaces in the Presence of Adsorbed D₂O, K. Adib, G. Totir, J.P. Fitts, K.T. Rim, G.W. Flynn, R.M. Osgood, Jr., Columbia University Due to their abundance in the crust of the Earth and their high reactivity, the oxides of iron serve as ideal model mineralogical surfaces in environmental catalysis studies. The relevance of the environmental studies is enhanced by considering the effect of water on the reactivity of iron oxide surfaces. Natural single crystals of α -Fe₂O₃ were cut and polished in the (0001) orientation. They were processed in ultrahigh vacuum to produce a surface selvedge of Fe₃O₄ (111)- 2x2 and exposed at ~100 K to D₂O and CCl₄. The TPD studies of adsorbed D₂O indicate a rich surface chemistry with multiple desorption events extending to as high as ~ 800 K consistent with dissociative adsorption of D_2O on the Fe₃O₄ (111) surface. Previous TPD and XPS results indicate that in the absence of D_2O , CCl₄ dissociatively adsorbs on Fe₃O₄ (111) producing chemisorbed Cl and CCl₂ which upon subsequent heating of the surface, abstract lattice iron and oxygen atoms to desorb as FeCl₂ and OCCl₂, respectively. In the presence of adsorbed D_2O , it is observed that the production of FeCl₂ and OCCl₂ are substantially suppressed indicating that the D₂O fragments block the surface reactive sites. The evolution of the reaction products of CCl₄ with the Fe₃O₄ surface as a function of pre-adsorbed D₂O coverage will be presented.

8:40am SS2-MoM2 Variable Temperature Scanning Tunneling Microscopy Studies of a Natural Single Crystal a-Fe₂O₃(0001) Sample: Termination and Surface Chemistry with CCl₄ and Cl₂, K.T. Rim, T. Müller, J.P. Fitts, K. Adib, Columbia University, N. Camillone III, R.M. Osgood, Jr., Brookhaven National Laboratory, S.A. Joyce, Los Alamos National Laboratory, G.W. Flynn, Columbia University

Variable Temperature Scanning Tunneling Microscopy (VT STM) has been used to study the reactivity of the reduced surface of a natural single crystal α -Fe₂O₃(0001) sample. STM and LEED measurements reveal that the surface cleaned in ultrahigh vacuum is reduced and composed of a Feterminated Fe₃O₄ (111) region and an O-terminated Fe₃O₄(111) or biphase region. The Fe-terminated Fe₃O₄(111) region exhibits reaction with CCl₄ and Cl₂, but the O-terminated Fe₃O₄(111) (biphase) region does not undergo reaction. Reaction products (Cl) on the Fe- terminated Fe₃O₄(111) region were observed with STM at room temperature after the reduced surface was exposed to CCl₄ and Cl₂. Chlorines are found to occupy two distinct sites, Fe top sites and O vacancy sites when the surface is exposed to CCl₄ vapor. However Cl occupies only the top sites when Cl₂ is dosed on the surface. The O vacancy sites are created only after surface oxygen atoms are abstracted via reaction with CCl4 to produce phosgene. The reduced surface was exposed to CCl4 at 238K and the surface temperature changed from 238K to 600K in order to identify reaction products and intermediates (chlorine and dichloro-carbene) and to observe oxygen vacancies following oxygen abstraction from the surface. Related TPD, AES, and XPS results will also be presented to support the VT STM observations.

9:00am SS2-MoM3 Influence of Surface Composition on the Pyrite Mediated Dechlorination Kinetics of Alachlor, *H. Fairbrother*, *D.L. Carlson*, *M.M. McGuire*, *A.L. Roberts*, Johns Hopkins University

The effects of different pyrite surface compositions on the dechlorination kinetics of the herbicide alachlor were investigated. Chloroacetamides, including alachlor, are an important class of herbicides, which are encountered as ubiquitous contaminants in surface and groundwater. Currently, the understanding of the processes controlling the environmental fate and transformations of alachlor is somewhat fragmented. Alachlor can be dechlorinated by Fe(0). Because several iron sulfide minerals have been shown to dechlorinate low molecular weight alkyl and vinyl halides, we investigated the reactivity of alachlor with pyrite (FeS₂), a common minor constituent of sediments and aquifers. We found that the primary product is deschloroalachlor, the result of reductive dechlorination. This process may be important in natural systems, as previous work has identified deschloroalachlor in groundwater. In this study, we have employed a liquid cell directly coupled to a surface analysis chamber to examine the effect of surface defect sites on the pyrite mediated dechlorination kinetics of alachlor. The influence of surface chemical composition on the dechlorination of the organohalide alachlor (a herbicide) by pyrite was studied by XPS in conjunction with GC-MS. On natural pyrite surfaces, the dechlorination process exhibited first-order kinetics, indicative of a limited number of surface sites that were consumed during reaction. In contrast, pyrite surfaces modified by ion bombardment, which are dominated by sulfur vacancies, exhibited markedly different reaction kinetics characterized by an initial induction period of low reactivity during which time the surface is oxidized by water. These results indicate that monosulfide species are not responsible for alachlor reduction on pyrite. In a broader sense this study illustrates the intimate relationship that exists between surface chemical composition and reactivity at the liquid-solid interface.

9:20am SS2-MoM4 Adsorption and Desorption of Methanol on WO₃ (100) Surfaces, S. Ma, F.G. Amar, B.G. Frederick, University of Maine

We have investigated the role of intermolecular interactions, surface site heterogeneity, and surface diffusion during the desorption of methanol from the oxidized and reduced surfaces of (100) oriented, epitaxially grown WO₃ films on Al₂O₃(1-102) substrates. Ultra-violet photoelectron spectroscopy (UPS) showed that methanol adsorbed molecularly on the oxidized WO₃ surface but dissociatively on the reduced surface. On both surfaces, calibrated thermal desorption spectroscopy (CTDS) showed desorption of methanol in an asymmetric peak which shifts to lower temperature with increasing coverage, typical of water and alcohols on other oxide surfaces.

X-ray photoelectron spectroscopy (XPS) was used to characterize the surface by monitoring the W4f and valence band region, while separate STM studies indicate that the surface is heavily stepped. Monte Carlo simulations indicate that surface heterogeneity and rapid diffusion are consistent with the observed desorption spectra. By contrast, simulations on a homogeneous surface require repulsive intermolecular interactions, which is inconsistent with hydrogen bonding.

9:40am **SS2-MoM5 Interaction of Co₃O₄ Single-Crystal Surfaces with Water**, *M.A. Langell*, *D.A. Pugmire*, University of Nebraska-Lincoln, *W.H. McCarroll*, Rider University

Vacuum-annealed and vacuum-cleaved Co3 O4 single-crystal substrates have been characterized using the UHV surface analytical techniques of Auger electron spectroscopy, x-ray photoelectron spectroscopy, low energy electron diffraction and high resolution electron energy loss spectroscopy. Particular emphasis in this study has been placed on the characterization of surface oxygen, which often shows complex photoemission structure from core oxygen states, and of the tetrahedral/octahedral site occupancy of cobalt surface cations as it relates to the defect character of the spinel surface. These well-defined surfaces are subsequently probed by adsorption of H_2O , both at low ($\leq 10^{-6}$ Torr) and high (1-10 Torr) water vapor pressures. Dissociative adsorption to produce surface hydroxyls is an important process for air-exposed oxides and this mechanism was found to occur upon water exposure for the Co₃O₄ surface under UHV conditions. However, hydroxylation was most readily observed for stoichiometric surfaces upon electron or thermal activation of the water adsorbate. These surface species will be compared to hydroxyls generated under high vacuum and atmospheric conditions.

10:00am SS2-MoM6 Surface Chemistry of Calcined UO₂ Powders, A.J. Nelson, T.C. Meier, C.K. Saw, L.V. Griffith, Lawrence Livermore National Laboratory

High resolution X-ray photoemission spectroscopy (XPS) was used to examine the surface composition and chemical bonding of calcined UO₂ powders as a function of process parameters. It is believed that the surface composition of the powder grains ult imately affects packing density. XPS quantitative analysis revealed O/U ratios indicative of mixed uranium valences. In addition, high resolution U 4f_{7/2.5/2} core-level spectra revealed reoxidation of U^{4+} to U^{6+} for the lower temperatures, and a reduction of U^{6+} to $U^{4\ast}$ for the higher temperatures using $4 \overset{_{\sim}}{N}$ H_2/Ar. Reoxidation can also be affected by the presence of water or OH, and the powder samples calcined at the lower temperatures have the highest OH?/O2? peak area ratio. Also, electrons in the 6d, 5f, and 7s orbitals near the valence band maximum can participate in bond formation so long as adjacent atoms are capable of donating their electrons to these unfilled orbitals. The valence band electronic structure for the higher temperature calcinations clearly shows a stronger 5f emission peak near the Fermi edge, a feature that is indicative of a highly localized state. Results were correlated with bulk structural analysis using x-ray diffraction. This work was performed under the auspices of the U.S. Dept. of Energy by the University of California Lawrence Livermore National Laboratory under Contract No. W-7405-Eng-48

10:20am SS2-MoM7 Examination of the Redox Chemistry of Water with the Oxidized and Reduced Surfaces of CeO₂(111), M.A. Henderson, M.H. Engelhard, C.H.F. Peden, C.L. Perkins, S. Thevuthasan, Pacific Northwest National Laboratory

Ceria is important in automotive three-way catalysts because of its ability to store and release oxygen as reaction conditions oscillate between oxidizing and reducing conditions. The effect of such redox oscillations on adsorbate chemistry is not well understood, although the chemistry of water on oxide surfaces is known to depend on the surface's redox state.¹ Two groups have recently reported conflicting results for the interaction of water with reduced $CeO_2(111)$ films, with one group reporting Ce^{3+} oxidation² and the other reporting Ce^{4+} reduction.³ In both cases, the $CeO_2(111)$ films were thin (≤ 50 Å) and were grown on metal substrates (Ru(0001)² and Pt(111)³). We have studied the interaction of water with a 500 Å CeO₂(111) film grown on Y-stabilized ZrO₂(111). TPD measurements for varying coverages of water on either oxidized (800 K in O2) or vacuum reduced (at 850 K) CeO₂(111) are suggestive of predominately molecularly adsorbed water, and show no evidence for irreversible decomposition either in terms of water consumption or H₂/O₂ desorption. Complimentary core and valence band photoemission results show that adsorbed water does not increase or decrease the level of $\mathrm{Ce}^{3\scriptscriptstyle+}$ in the reduced $\mathrm{CeO}_2(111)$ surface, although water exposure at 600 K shows a slight increase in Ce³⁺ over that seen from annealing in UHV at the same temperature. Comparison of our results for the CeO₂/ZrO₂(111) system with those from thin CeO₂ films grown on metal substrates suggests that metal substrates may participate in water redox chemistry on ceria.

10:40am SS2-MoM8 Interface Mediated Defect Formation in Ultrathin Cerium Oxide Films, C. Castellarin-Cudia, S. Surnev, S. Eck, M.G. Ramsey, F.P. Netzer, Karl-Franzens-Universität Graz, Austria

The oxygen storage and release capabilities of cerium oxide are important factors for its use as an additive in the three-way catalyst for automotive emission control. The ceria can act as an oxygen pump, which under fuelrich conditions gives up oxygen, whereas under fuel-lean conditions it can take in oxygen. A key step in this process is the formation and destruction of oxygen vacancy defects at the ceria surface. Here we report the observation of defect formation, at the atomic level using STM, in ultrathin cerium oxide layers on a Rh(111) substrate surface. The ceria overlayers have been fabricated in situ by reactive evaporation of Ce metal onto the heated substrate (250°C) in an oxygen atmosphere, and reducing ambient conditions have been simulated by annealing in vacuum. Ceria overlayers on Rh(111) grow in a CeO2(111)-type structure and annealing of submonolayer coverages to ~500°C produces thin, well-ordered Ce-oxide island nanostructures. The island surfaces display atomic resolution in the STM and reveal a Moiré superstructure, as a result of the lattice mismatch between the oxide overlayer and the Rh substrate. Further annealing to ~600°C leads to partial reduction and an ordered array of oxygen vacancies, which form a defect superlattice of the same dimensions as the Moiré structure. Several defect signatures can be distinguished in the atomically resolved STM images. We propose that the defect superlattice is mediated by the metal-oxide interface, via a lattice-mismatch induced strain effect. This creates catalytically active sites for the preferential reduction of the ceria, i.e. the formation of oxygen vacancy defects, and constitutes a novel mechanism for the formation of interface-stimulated active centers. ^{*}Supported by the Austrian Science Foundation.

11:00am **SS2-MoM9 Identification of Defect Sites on Oxide Surfaces**, **Y.D. Kim**, J. Stultz, T. Wei, A.K. Santra, D.W. Goodman, Texas A&M University

Defect sites on oxide surfaces play an important role in various catalytic reactions, as well as in adhesion and in nucleation of metal clusters. Thus, identification and quantification of defect sites on oxide surfaces are important steps in the understanding of many catalytic reactions. Recently we have used several techniques to identify various defect sites on oxide surfaces including metastable impact electron spectroscopy (MIES), water and CO-temperature programmed desorption (TPD), MIES of adsorbed Xe (MAX), and electron energy loss spectroscopy EELS). MIES data for MgO(100) and SiO2 thin films are very sensitive to extended defect sites as well as point defect. Point defects result in the appearance of band gap states, whereas extended defects cause broadening of the O(2P) band. MAX data change significantly with increasing defect densities for various oxide surfaces. The adsorption of D2O and CO also has been used to identify various defect sites since their TPD spectra change significantly in the presence of defect sites. Recent EELS data acquired for low and highly defective oxide surfaces will also be discussed.

11:20am SS2-MoM10 Polar ZnO(0001)-Zn and ZnO(000-1)-O Surfaces: Geometric and Electronic Structure, Stabilization Mechanisms, O. Dulub *, U. Diebold, Tulane University

The geometric and electronic structure of the (0001)-Zn and (000-1)-O polar surfaces of ZnO were studied with Scanning Tunneling Microscopy (STM) and Spectroscopy (STS), as well as Low Energy Electron Diffraction (LEED). Sharp (1x1) LEED patterns were recorded for both surfaces. The STM images of the ZnO(0001)-Zn surface reveal flat triangular terraces of single step height (~2.6 Å), exhibiting two domains rotated by 180 degrees with respect to each other. STM shows a high density of triangular pits of various sizes and slightly rounded small holes. Triangular islands of different sizes were also observed on the terraces, and the smaller ones exhibit size-dependent special shapes. STM images from the O-terminated (000-1) surface reveal a quite different morphology. The surface is composed of flat, well ordered terraces without pits or added small islands. The terraces are separated mainly by double-layer high step edges (~5.2 Å) that include an angle of 120 degrees. STS indicates a slightly (but reproducibly) different electronic structure of the two polar surfaces. The filled states on the O-terminated face are shifted toward the Fermi level. Based upon the STM and STS results, two stabilization mechanisms are proposed for (0001)-Zn and (000-1)-O surfaces. A charge transfer from the O- to the Zn-terminated surface makes the latter more metallic. Since metallic Zn is known to have an extremely high vapor pressure even at low temperatures, it possibly evaporates off the surface.

Depleting the Zn-terminated surface of 1/4 of zinc atoms removes the infinite dipole moment and therefore stabilizes the crystal. The special shapes of the smallest ('magic') islands observed in STM images of the (0001)-Zn surface are consistent with the proposed model.

11:40am SS2-MoM11 The Polar O-ZnO(000-1) Surface: Stability and Interaction with Hydrogen, *M. Kunat*, *St. Gil Girol*, *U. Burghaus*, *Ch. Wöll*, Ruhr-University Bochum, Germany

The question about the stability of the polar surfaces of zinc oxide has been the topic of many experimental and theoretical investigations. Here we report on an investigation using the highly surface sensitive method of Heatom scattering (HAS). The clean, H-free surface shows (1x3) superlattice spots in He-atom diffraction scans. This finding is in contrast to previous work¹ where the presence of a (1x1) overlayer was found, but is in agreement with Taskers rule,² which predicts instabilities for polar oxide surfaces. After optimizing the preparation conditions for the O-ZnO(000-1) surface, in particular by employing annealing in an oxygen atmosphere, we were able to observe weak (1x3) spots not only with HAS but also in low energy electron diffraction (LEED). Exposure to hydrogen atoms leads to the disappearance of the (1x3) overlayer spots and the formation of a welldefined (1x1) diffraction pattern in both HAS and LEED, similar to the case of the Zn-ZnO(0001) surface previously studied in our laboratory.³ The formation of the H-atom overlayer is accompanied by a shoulder in the O1s XPS data, indicating the formation of OH-species. In addition first results of sticking coefficients of carbon monoxide as a function of hydrogen preexposure will be discussed.

¹ A. Wander, F. Schedin, P. Steadman, A. Norris, R. MCGrath, T.S. Turner, G. Thornton, and N.M. Harrison, Phys. Rev. Lett. 86 (2001) 3811.

² P.W. Tasker, J. Phys. C: Solid State Phys. 12 (1979) 4977.

³ Th. Becker, St. Hövel, M. Kunat, Ch. Boas, U. Burghaus, and Ch. Wöll, Surf. Sci. 486 (2001) L502.

¹ M.A. Henderson, Surf. Sci. Rep. 46 (2002) 1.

² Lj. Kundakovic et al., Surf. Sci. 457 (2000) 51.

³ U. Berner et al., Surf. Sci. 467 (2000) 201.

^{*} Morton S. Traum Award Finalist

Monday Afternoon, November 4, 2002

Electrochemistry and Fluid-Solid Interfaces Room: C-104 - Session EC+SS-MoA

Liquid-Solid Interfaces & Nanoscale Electrochemistry Moderator: S. Morin, York University

2:00pm **EC+SS-MoA1 Femtosecond Spectroscopy at the Metal/Liquid Interface**, *S. Roke, M. Bonn, A.W. Kleyn*, Leiden University, The Netherlands

Vibrational sum frequency generation spectroscopy is an ideal technique to study molecules at surfaces and at buried interfaces with a high degree of molecular specificity. The most powerful feature of this technique is its capability to monitor intramolecular vibrations of the first layer of molecules on the surface: it essentially allows one to look inside the molecules at the interface. The use of femtosecond laser pulses allows one to not only perform frequency domain measurements, but also time domain measurements. We have performed femtosecond time and frequency domain measurements on the acetonitrile/gold interface. Comparison of the time and frequency domain results showed that, although the two approaches are in principle equivalent they are sensitive to different physical aspects of the system. Time domain measurements are more clearly influenced by the inhomogeneity of adsorption sites, whereas frequency domain measurements are more subject to the homogeneous features of the spectral line broadening. To account for this we have extended existing models for calculating SFG spectra and free induction decay measurements. From the combination of the measurements and our model we have obtained information on the orientation and binding of acetonitrile to the gold surface and determined the nature and time scale of the decay of the vibrational polarization of the CH and CN stretch vibrations. The CN oscillators are distributed inhomogeniously across the surface and have a dephasing time of 1.65 ps. The CH stretch vibration however does not feel the inhomogeneity and dephases 2.5 times faster (T2 = 610 fs), because the methyl groups are further away from the interface.

2:20pm EC+SS-MoA2 Studies of the Interphase Region for Liquid Hexadecane Near a Au Surface, A.C. Oliver, J.E. Houston, Sandia National Laboratories

In this presentation, we explore the formation and properties of a solidlike"interphase" region near Au surfaces immersed in liquid hexadecane using interfacial force microscopy (IFM). We measure variations of the normal and lateral friction forces, as well as the conductance behavior, as a function of the relative interfacial separation. We show that this interphase layer passivates the normally strong bonding between two Au surfaces even at high applied stresses. In addition, no conduction is seen for this normally insulating layer until appreciable stresses are applied. By placing a voltage between tip and sample, we determine the thickness of the organized film from the behavior of the electrostatic force as a function of relative separation up to film contact. We show that at room temperature the interphase-layer thickness is ~7 molecular diameters, which increases with larger bias voltages. In addition, the lateral force shows appreciable friction before film contact for the larger voltages, indicating that the field is causing a local film organization. Data taken as a function of temperature indicates a decrease in the film organization. We discuss the implication of these results in the general context of the interaction of surface in liquid environments. Sandia is a multi-program laboratory operated by Sandia Corporation, a Lockheed Martin company, for the DOE under Contract DE-AC04-94AL85000.

2:40pm **EC+SS-MoA3 Surface Forces at Electrified Interfaces**, *J. Frechette*, **T.K. Vanderlick**, Princeton University

Electrodes specifically designed for the surface forces apparatus were developed to study adhesion between mica and polycrystalline gold at different applied potentials. Pull-off forces were a strong function of applied potential and dominated by electrostatic interactions. Adhesion measurements increased six-fold in a 150 mV window around the potential of zero charge. We compared these measurements using DLVO and JKR (Johnson-Kendall-Roberts) theory in the case of dissimilarly charged surfaces. We also investigated the effect of potential dependent adsorption, such as pyridine on gold, on electrostatic forces and adhesion. We observed a stronger influence of the adsorbate on adhesion measurements than on surface forces.

3:00pm EC+SS-MoA4 A New View of Ion Adsorption at Mineral-Fluid Interfaces with Synchrotron X-Ray Scattering, P. Fenter, Argonne National Laboratory, Z. Zhang, Northwestern University, M.L. Schlegel, Commissariat a l'Energie Atomique, France, C.Y. Park, L. Cheng, Argonne National Laboratory, K.L. Nagy, University of Colorado at Boulder, D.J. Wesolowski, Oak Ridge National Laboratory, M. Machesky, Illinois State Water Survey, M.J. Bedzyk, Northwestern University, N.C. Sturchio, University of Illinois at Chicago INVITED

Ion adsorption at mineral-water interfaces is a key component of the electrical double-layer, a classic problem in surface science, and is fundamental for understanding the mobility of elements in the environment. We describe direct in-situ measurements of the systematic trends in ion adsorption near rutile- and muscovite-water interfaces using synchrotron Xray scattering techniques (X-ray standing waves and X-ray reflectivity). These minerals represent two extremes in terms of location and origin of surface charge. The surface charge on rutile, an oxide, is determined by surface protonation reactions and is located above the mineral surface. In contrast, the surface charge of muscovite, a phyllosilicate, is determined by the permanent negative charge due to isomorphic lattice substitution below the mineral surface. The location of Zn^{2+} , Sr^{2+} and Y^{3+} ions were fully triangulated at the rutile(110)-water interface revealing unexpected differences in their adsorption geometries. Separate measurements were made of K^t, Cs⁺, Ca²⁺, Ba^{2+} and Zn^{2+} ion heights with respect to the muscovite(001)-water interface. Systematic trends in adsorption behavior will be discussed in the context of classical pictures of ion-mineral interactions (e.g., inner sphere vs. outer-sphere complexes) and by contrasting the different ion adsorption behavior at the rutile and muscovite surfaces. Research sponsored by the U.S. Department of Energy, Office of Basic Energy Science: Division of Chemical Sciences, Geosciences and Biosciences.

3:40pm **EC+SS-MoA6 Solution Composition Effects on Calcite Dissolution and Growth Processes**, *A.S. Lea*, *J.E. Amonette, D.R. Baer, N.G. Colton*, Pacific Northwest National Laboratory

We have examined the influence of a number of solution impurities on step motion and shape of pits during dissolution and growth on the cleavage surface of calcite. Mg^{2+} , in contrast to the other impurities (Ca^{2+} , Mn^{2+} , Sr^{2+} , Co^{2+} , Mg^{2+} , and CO_3^{-2}) we have studied, exhibits unique behavior by uniformly enhancing dissolution rather than retarding dissolution. Of the impurities that retard dissolution, Sr^{2+} and CO_3^{2-} demonstrate selective sorption to the most sterically accessible step site resulting in a substantial slowing of dissolution of this type of step. $\dot{M}n^{2\scriptscriptstyle +}$ and $Co^{2\scriptscriptstyle +},$ however, retard dissolution uniformly due to non-selective step sorption. For Mn²⁺, Sr²⁺, Co^{2+} , and Ca^{2+} , little impact on dissolution rate is seen until a threshold concentration is reached, whereupon near complete frustration of dissolution occurs upon further increase in impurity concentration. These results can be explained using a simple terrace-ledge-kink model that incorporates site-blocking and works equally well with metal ion or carbonate ion pair concentrations. This site-blocking model cannot explain the enhanced dissolution behavior of calcite in the presence of Mg^{2+} . In calcite growth processes, Ca2+ ions demonstrate preferred kink sorption sites, manifested by the unique pit shape observed during pit fill-in.

This work was supported by the Office of Basic Energy Science, Geosciences Research Program, U. S. Department of Energy. The work was conducted in the Environmental Molecular Sciences Laboratory, a U.S. Department of Energy user facility located at Pacific Northwest National Laboratory.

4:00pm EC+SS-MoA7 Investigation of Binary Oxide (V_2O_3) Thin Films as Electrodes for Rechargeable Micro Batteries using Li, A. Talledo, H. Valdivis, Universidad Nacional de Ingenieria, Peru, C. Benndorf, University of Hamburg, Germany

We report on the preparation of V_2O_5 thin films, their charcetrization and their application as electrodes in rechargeable micro batteries using lithium as counter electrode. The V_2O_5 thin films were deposited onto SnO coated glass by reactive rf sputtering of a V cathode using an Ar + O_2 atmosphere. The electrodes were characterized by their electrochemical behavior (IVcurves during charging and recharging using LiClO₄ +PC as electrolyte), Xray diffraction (XRD), X-ray and UV induced photoelectron spectroscopy (XPS and UPS) and infrared (IR) measurements. XRD measurements demonstrated that unannealed V_2O_5 films were amorphous with no sharp reflexes. Annealing to 350°C was sufficient to produce crystalline β - V_2O_5 . XPS spectra revealed the expected V/O ratio and the correct line positions. However, the O 1s peak was splitted into two components, one from the V_2O_5 component (530.8 eV). The other at 533.1 eV is attributed to the uptake of water from the atmosphere. The large uptake of water is consistent with a porous structure of the V_2O_5 thin film. The charged micro battery resulted in a maximum voltage of 3.4 V for the currentless circuit and a capacity of 34.5 mC/cm². With XPS we could demonstrate the migration of Sn into the V₂O₃ layer for the electrodes charged with Li. Further, UPS spectra from uncharged and charged V₂O₅ indicate a band gap narrowing due to the Li uptake, which is consistent with optical measurements. Our investigation contributes to the understanding and application of vanadium oxide thin films as cathodes for micro batteries.

4:20pm EC+SS-MoA8 Creating Beakers without Walls: Formation of Deeply-Supercooled Binary Liquid Solutions from Nanoscale Amorphous Solid Films, P. Ayotte, R.S. Smith, G. Teeter, Z. Dohnálek, G.A. Kimmel, B.D. Kay, Pacific Northwest National Laboratory

Supercooled liquids are metastable and their lifetimes are dictated by the kinetics for crystallization. Traditional experimental studies have used a variety of methods to suppress crystallization while cooling from the liquid phase. An alternate approach is to heat an amorphous solid above its glass transition temperature, Tg, whereupon it transforms into a deeplysupercooled liquid prior to crystallization. We employ molecular beams, programmed desorption (both TPD and isothermal) and FTIR vibrati onal spectroscopy to synthesize and characterize compositionally tailored nanoscale films of glassy methanol and ethanol. We demonstrate that these films exhibit complete diffusive intermixing and suppressed crystallization when heated above Tg. Fu rthermore, the resulting container-less liquids evaporate as continuously mixed ideal binary solutions while retaining their solid-like macroscopic shapes. This approach provides a new method for preparing deeply-supercooled liquid solutions in metastabl e regions of their phase diagram and for studying the kinetics of their phase separation and crystallization as they approach thermodynamic equilibrium. The applicability of this technique for studying aqueous liquid solutions will also be presented and discussed. P. A. is an NSERC Postdoctoral Fellow. Pacific Northwest National Laboratory is a multiprogram National Laboratory operated for the U. S. Department of Energy by Battelle Memorial Institute under contract DE-AC06-76RLO 1830.

4:40pm EC+SS-MoA9 Using NanomechanicaL Responses in Individual Systems from a Single C-C Bond to Single Cell, J. Gimzewski, University of California, Los Angeles INVITED

: The capability of the atomic force microscope has recently been extended as powerful tool to not only image molecules in real space in but also to explore the mechanical properties of single molecules in a wide range of environments ranging from ultra high vacuum to in vivo. In this talk I will present a series of experiments that span from individual cells in growth media to the forced rotation of a single carbon-carbon bond in a organic molecule, using AFM based techniques such as non-contact dynamic AFM. I will show that the ability to measure small forces and amplitudes in a range of environments enables unique insights into nanomechanical process such as the determination of the zepto Joule forces for molecular switches and the bility to monitor cell function. Additionally, I will also span these two extremes using liquid based nanomechanical probes of proteomic and genetic recognition processes.

Surface Science Room: C-108 - Session SS1-MoA

Surface Reactions: CO and NO Moderator: G. Fisher, Delphi Research Labs

2:00pm **SS1-MoA1 Bridging the Pressure Gap at the Atomic Level: CO/Pt(110) and CO/Pt(111)**, *E.K. Vestergaard*, *P. Thostrup*, *T. An*, *B. Hammer*, *F. Besenbacher*, University of Aarhus, Denmark

We have studied the adsorption of CO on Pt(111)¹ and Pt(110)² over 12 orders of magnitude, up to 1 bar, using high-resolution scanning tunneling microscopy.³ Here we demonstrate the possibility of bridging the pressure gap for these systems at the atomic level. For both surfaces, our new high-pressure STM results show that the adsorbate structures formed at high CO pressures are identical to high-coverage structures observed at low temperatures under vacuum conditions. Our findings are at variance with previous STM results where it was concluded that new structures develop at the platinum surfaces at high CO pressures. From these and other pertinent cases we attempt to extract general directions for making conjectures as to the high-pressure response of chemisorption systems.

¹ E. Kruse Vestergaard, P. Thostrup et al., submitted to Phys. Rev. Lett.

² P. Thostrup et al., Phys. Rev. Lett. 87, 126102 (2001)

³ E. Laegsgaard, P. Thostrup et al., Rev. Sci. Instr. 72, 3537 (2001).

2:20pm SS1-MoA2 Fluctuations and Bistability in CO Oxidation on Nanoscale Facets, D.-J. Liu, J.W. Evans, Iowa State University

Recent experiments of catalytic surface reactions, especially CO oxidation on nanoscale Pt field-emitter-tips,¹ provides tremendous new possibilities for modeling of surface reactions and for comparison with stochastic theories of chemical reactions. Particularly, in a chemical reaction with bistability, fluctuations can induce transitions between the two stable states for sufficiently small systems. We analyze a "hybrid" atomistic model mimicking CO oxidation on nanoscale facets of metal(100) catalyst surfaces. The model, which incorporate infinite CO diffusion and superlattice ordering of immobile O, display bistability for an infinite system. We focus on the probability distribution for the populations of adsorbed species, as well as dynamics of the fluctuations-induced transitions. An effective potential picture emerges from our analyses of kinetic Monte Carlo simulations. Qualitative behavior can be approximated by traditional master equation and Fokker-Planck equations, where the system size dependence and the approach to the critical point can be characterized by the mean-field behavior. Analysis of a generalized model with finite CO diffusion reveals the role of CO diffusion in the crossover from the mean-field to the equilibrium Ising-like behavior.

¹ Y. Suchorski et al., Phys. Rev. Lett. vol. 82, 1907 (1999).

3:00pm SS1-MoA4 In situ Monitoring of the Catalytic CO + NO Reaction on Pd(111) at 240 mbar: The Formation of Isocyanate, Ch. Hess, E. Ozenzoy, D.W. Goodman, Texas A&M University

The CO + NO reaction to form CO₂, N₂O and N₂ has been studied on a Pd(111) surface at pressures up to 240 mbar by using in situ polarization modulation infrared reflection absorption spectroscopy (PM-IRAS). At a pressure ratio of P_{CO}/P_{NO} = 1.5 and temperatures above 500 K, i.e., under reaction conditions, besides CO and NO, isocyanate is adsorbed on the surface as evidenced by isotope experiments. Below 0.1 mbar total pressure, however, no isocyanate formation was observed. The role of the isocyanate in the CO + NO on Pd(111) is discussed by comparison of the spectroscopic and kinetic results. In addition, kinetic measurements of the CO + NO reaction between 590 and 650 K showed an increase in the N₂O selectivity, a result of temperature-dependent changes of the ratio [NO]_a/[CO]_a. Within this temperature range, the apparent activation energy of the reaction was determined to be 54 \pm 21 kJ/mol.

3:20pm SS1-MoA5 Fundamental Studies of Function and Deactivation of NOx Storage Catalysts, E. Fridell, A. Amberntsson, P. Broqvist, J. Dawody, A.W. Grant, L. Olsson, M. Skoglundh, Chalmers University of Technology, Sweden INVITED

We have investigated the function of the different components in so called NOx storage catalysts regarding both the storage/reduction of NOx and deactivation by sulphur. These types of catalysts are used in lean burn applications for trapping NOx as nitrates, which in turn are reduced during lean conditions We have investigated model samples containing Ba compounds for storage of NOx and Pt and Rh as catalysts for oxidation and reduction reactions. We find that NO2 plays an important role in the storage mechanism as an oxidising agent. Two different mechanisms for this are discussed: The formation of surface peroxides and the oxidation of nitrites to nitrates. FTIR studies show that NOx is stored as surface nitrates. The stability of these species is also confirmed by first principle calculations. The sulphur deactivation is found to be more severe when SO2 is added during the rich phase than when SO2 is added during the lean period. This observation is found to be connected to the interaction between Pt and SO2. FTIR shows the formation of bulk sulphates both under lean and rich conditions. The influence of the choice of noble metals for the deactivation and regeneration was also investigated. It is found that Rh plays an important role for the regeneration after sulphur deactivation. Further, XPS studies show that the formation of platinum oxides is significant in the presence of NO2, especially for the Ba-containing samples. This has strong implications for the reactions.

4:00pm SS1-MoA7 Nitrite and Nitrate Formation from NO and NO2 Adsorption on Alkaline Earth Metal Oxide Surfaces, *M. Miletic*, University of Michigan, *P.J. Schmitz*, *W.F. Schneider*, Ford Research Laboratory, *J.L. Gland*, University of Michigan

Alkaline earth oxides surfaces are currently being explored as a means of trapping NOx species under excess oxygen conditions typical of lean burn (e.g. diesel) engine exhaust. These metal oxides have been proposed as active components in automotive NOx abatement strategies because of their role in effectively storing and releasing NOx under lean/rich exhaust cycling. However, molecular understanding of the adsorption and reactions of NO, and NO2 on alkaline earth oxide surfaces remains incomplete. A series of temperature programmed studies of NO and NO2 on alkaline earth oxide surfaces are reported here. These experiments, coupled with XPS and ab-initio studies, indicate that reactive chemisorption plays a unique,

adsorbate-specific role for both low and high temperature desorption. The effect of coverage on the molecular species is unexpected both in reactive adsorption and desorption on these oxide surfaces. Experimental and computational Density Functional Theory results are coupled, highlighting the importance of reactive configurations, charge transfer, surface-adsorbate Lewis acidity/basicity, and surface oxidation/reduction processes. Together, these approaches are used to form an integrated understanding of the driving forces behind nitrite and nitrate formation on alkaline earth oxide surfaces.

4:20pm SS1-MoA8 Adsorption and Reaction of NO on SrTiO₃ Surfaces, S. Azad, L.-Q. Wang, M.H. Engelhard, J. Szanyi, C.H.F. Peden, Pacific Northwest National Laboratory

The adsorption and reaction of NO on metal oxide surfaces has recently received considerable attention in relation to the efficient removal of toxic pollutants from automobile exhaust. In this study, the reactivity of NO on SrTiO₃ surfaces has been investigated using temperature programmed desorption (TPD) and x-ray photoelectron spectroscopy (XPS). On oxidized surfaces containing predominantly Ti4+ cations NO was found to be much less reactive and desorbed mainly as molecular NO around 250 K. Similar TPD spectra obtained for NO adsorption on SrTiO₃ prepared by sputtering or annealing the surface to 750 K, 850 K and 900 K in vacuum and in O2 suggested that thermal annealing of this surface did not affect the reactivity of NO with Ti⁴⁺ cation sites. However, a significant number of defects containing mainly Ti³⁺ (observed by XPS) that was created by Ar⁺ ion bombardment greatly increased the reactivity of the surface towards the adsorbed NO molecules. NO is reduced by the Ti³⁺ sites on these defected surfaces and the major decomposition products are N2 and N2O. Coadsorption of NO with CO on both reduced and oxidized surfaces has also been examined. The results of NO on $SrTiO_3\ surfaces\ will\ be\ compared$ with the results of ongoing studies of NO adsorption on Ce1- $_{x}Zr_{x}O_{2}/YSZ(111).$

4:40pm **SS1-MoA9 Structural and Chemical Properties of Ti/Pt(100)c(2x2) Second Layer Alloy - Evidence for Strong Ligand Effects**, *S. Hsieh, T. Matsumoto,* University of Southern California, *M. Batzill,* Tulane University, **B.E. Koel,** University of Southern California

We have investigated the structure and chemisorption properties of a Ti/Pt(100) surface alloy using AES, XPS, LEED, STM, XPD, ALISS, and TPD of CO and H₂. Samples were prepared by evaporating Ti onto a clean Pt(100)-hex reconstructed surface at 300 K. After annealing the sample to 800 K, a c(2x2) ordered LEED pattern was observed that sharpened as the temperature was increased to 920 K. Further annealing to 1000 K caused the LEED pattern to become diffuse, due to onset of disorder in the surface layers resulting from Ti diffusion into the bulk. Using XPD and ALISS, we have determined that Ti atoms in the Ti/Pt(100)-c(2x2) surface alloy are not present in the topmost layer, but instead, in the second layer. Thus, the surface layer is pure Pt. XPS results showed that the Ti 2p_{3/2} peak from the surface alloy is shifted about 1.4 eV from a thick Ti film, and the Pt 4f peak is shifted 0.1 eV, consistent with the formation of strong intermetallic bonds upon alloying. CO adsorbed reversibly on the alloy, desorbing in a broad peak with a maximum at 376 K, showing a strong downward shift of 132 K compared to CO desorption from clean Pt(100). Thermal desorption of H, was also studied and a similar peak shift toward lower temperatures was observed. In addition, much less H adsorbed on the Ti/Pt(100)-c(2x2) surface than on Pt(100). These results show that the second-layer Ti atoms exert a strong "ligand effect" on the Pt atoms at the surface, and this is a good model system for studying pure ligand effects at alloy surfaces.

5:00pm SS1-MoA10 Dissociation/Dehydrogenation of Hydrocarbons on NiAl(100), K.A. Layman, Y. Jiang, J.C. Hemminger, University of California, Irvine

HREELS has been used to study the reactivity of CO, CO_2 , acetone, and pyridine on NiAl(100) as a function of surface coverage and temperature following adsorption at 140 K. While CO adsorbs primarily associatively at low CO exposures, we observe that CO begins to dissociate on the NiAl(100) substrate after very high CO exposures (100-1000 L), as indicated by the formation of a predissociation CO stretch at ~1366 cm⁻¹. In addition, CO₂ interacts very strongly with the NiAl(100) surface, as indicated by the shifting of the asymmetric CO₂ stretch to ~2027 cm⁻¹. This shift is observed for CO_2 exposures as small as 0.1 L. In contrast, the adsorption of acetone and pyridine on the NiAl(100) substrate is nondissociative. Upon annealing the NiAl(100) surface after exposing the NiAl(100) single crystal to CO₂, acetone, or pyridine, the adsorbate begins to dissociate and/or dehydrogenate. After annealing the surface to approximately 260 K, the hydrocarbons begin to dehydrogenate. Further annealing to approximately 500 K results in the cleavage of the C-O or the C-N bond, forming Al_2O_3 or Al_xN_y thin films. The thin films of Al_2O_3 follow the phase temporal regimes exhibited for Al₂O₃ thin films grown by

exposing the NiAl(100) single crystal to oxygen. Further annealing of the Al_xN_y thin films results in a similar ordering/phase change as observed for the Al_2O_3 thin films.

Surface Science Room: C-110 - Session SS2-MoA

Nucleation & Growth of Metals on Oxides & Semiconductors

Moderator: D.Y. Petrovykh, Univ. of Maryland/Naval Research Lab

2:00pm SS2-MoA1 The Effects of Copper on the Hydrogen-Passivation of Si(001), A.R. Laracuente, L.A. Baker, L.J. Whitman, Naval Research Laboratory

Foreign adsorbates can alter the morphology of surfaces and often have a dramatic impact on film growth. Given that most semiconductor devices are fabricated in hydrogen-rich environments on silicon substrates, it is important to understand how adsorbates affect the surface morphology of H-terminated Si surfaces. Currently, we are studying how copper modifies the morphology of monohydride-terminated Si(001). In the experiments, clean Si(001) surfaces are first exposed to 0.3 monolayer of Cu and then passivated with atomic H under conditions that produce a monohydride surface. The samples are characterized at room temperature using scanning tunneling microscopy (STM) and Auger electron spectroscopy (AES). We find that the main effect of Cu pre-exposure is the formation of pits on the surface. The pits are about 3 nm x 3 nm in size and one atomic layer deep. It appears that Cu induces Si etching during the atomic H exposure. Furthermore, the "pitted" H-terminated surface is subsequently dosed with Cu to investigate the effects of the pits on the growth of Cu. We will present our STM and AES results, and an analysis of the pit size distribution.

2:20pm SS2-MoA2 Competing Classical and Quantum Effects in Shape Relaxation of a Metallic Island, *H. Okamoto*, *D. Chen*, Rowland Institute for Science, *T. Yamada*, NASA Ames Research Center

Pb islands grown on a silicon substrate transform at room temperature from the initially flattop facet geometry into an unusual ring shape with a volume-preserving mass transport process catalysed by the tip electrical field of a scanning tunnelling microscope. The formation of such ring shape morphology results from the competing classical and quantum effects in the shape relaxation. The latter also leads to a sequential re-growth on alternating strips of the same facet defined by the underlying substrate steps, showing for the first time the dynamical impact of the quantum size effect on the stability of a nanostructure.

2:40pm SS2-MoA3 Formation of Monodispersed Cobalt Nanoclusters on the Si₃N₄(0001)-4x4 Surface, C.-L. Wu, T.-B. Chou, S. Gwo, W.-C. Lin, National Tsing-Hua University, Taiwan, ROC, M.-T. Lin, National Taiwan University, Taiwan, ROC

A novel phenomenon of forming monodispersed Co nanoparticles at room temperature on a single-crystal Si₃N₄ dielectric thin film is presented. Results of very narrow size distributions with an average size of ~30 Co atoms have been obtained. We have found that cobalt clusters deposited on Si₃N₄ are stable with respect to cluster agglomeration/coalescence and thermal decomposition. Also, we have confirmed that the average size of Co clusters is independent of the deposition time and insensitive to the magnitude of the deposition flux. Therefore, their areal density can be controlled by the deposition time. The motivation for using a single-crystal Si₃N₄ support is two-fold. First, the dielectric support reduces chemical intermixing and electronic coupling $(\mathrm{Si}_3\mathrm{N}_4\xspace{is}$ is an excellent diffusion barrier with a bandgap energy of 4-5 eV) between metal clusters and the substrate compared with situations using semiconductor or metal surfaces. Second, the defect-free Si₃N₄ surface provides us a unique opportunity to study the formation of metal clusters without the influence of surface defects. Consequently, quantum effect can play an important role in the size control.

3:00pm **SS2-MoA4** The 'Three-Dimensional' Schwoebel-Ehrlich Barrier in Ag Crystallite Growth on Si(111), *W.X. Tang, K.L. Man*, Hong Kong University of Science and Technology, *H. Huang*, Hong Kong Polytechnic University, *M.S. Altman*, Hong Kong University of Science and Technology

Growth morphology will be affected, or even dictated, by kinetic limitations that may be present during growth. One such limitation, which has received a great deal of attention, occurs in growth at surfaces when there is a Schwoebel-Ehrlich (SE) diffusion energy barrier to atomic motion

descending a monolayer height step. We present evidence of an analogous 'three-dimensional' (3D) SE energy barrier to atomic diffusion across the ridge that separates two facets on a three-dimensional crystal. The 3D SE barrier stems from the reduced coordination at the ridge. Differences of the adatom formation energies on adjacent facets cause the 3D SE barrier to be asymmetric. Kinetically limited growth shapes of Ag crystallites on the Si(111) surface have been studied with low energy electron microscopy (LEEM) and diffraction (LEED). These growth shapes are in agreement with expectations from the asymmetry of the 3D SE barrier. LEEM observations of the modification of growth shapes caused by codeposition of surfactants are also consistent with modification of the 3D SE barrier caused by surface passivation. The 3D SE barrier is expected to be relevant to diffusion in the presence of multilayer height steps on surfaces, and is therefore also important for the development of film texture.

3:20pm **SS2-MoA5 Self-organization of Semimetal Bi on Si(111)**, *T. Nagao*, Tohoku University, Japan, *T. Kogure*, University of Tokyo, Japan, *J.T. Sadowski*, Tohoku University, Japan, *T. Sekiguchi*, *S. Hasegawa*, University of Tokyo, Japan, *T. Sakurai*, Tohoku University, Japan

We have studied the self-organization of epitaxially grown semimetal bismuth on Si(111) surfaces by in situ reflection high-energy electron diffraction (RHEED), scanning tunneling microscopy (STM), and 4-probe conductivity measurement. On the 7x7 surface, up to around 4ML, the system grows in a SK like manner: [102] oriented flat-top islands grow after completion of disordered wetting layer. Sharp height distribution of these flat-top islands peaked at 1.2nm was clarified in a wide growth temperature range (290-550 K) as well as wide deposition rate (0.1-2.0 ML/min), which indicates the significance of the dectronic effect in the film growth. After the connection of the flat-top islands, the growth mode switches to a nearly perfect FvM growth, and the connected layer selforganizes into a single-crystal ultrathin film with Bi(001)-1x1 surface as evidenced by in situ RHEED and ex situ XTEM. Four-probe measurements showed the largest resistance drop at around 4 ML followed by another gradual drop around 4-10 ML and finally approached to a conductivity only several times lower than the bulk value, unusual value for such thin films. The initial drop was associated with the percolation of the flat-top islands. The following gradual drop was assigned to the reduction in the (surface and bulk) roughness scattering, due to self alignment in the crystal orientation via drastic interfacial glide and mass transport of the flat-top nanocrystals which are initially loosely bound on the disordered wetting layer. The origin of this new type of electronic growth and its selforganization into perfectly ordered ultrathin film will be discussed in detail.

3:40pm SS2-MoA6 Controlling Island Size Distributions for Metals on Oxides: Cu and Ni Islands on TiO₂(110)-(1x2), J. Zhou, B.T. Long, D.A. Chen, University of South Carolina

Metal islands deposited on oxide surfaces are frequently used as model systems for understanding heterogeneous catalysts. In order to investigate how the surface chemistry of the metal islands may change as a function of island size, it is first necessary to produce islands with narrow size distributions. In these studies, Cu and Ni have been vapor-deposited onto a partially reconstructed TiO₂(110)-(1x2) surface and characterized by STM under UHV conditions. The key to achieving a uniform island size distribution for Cu on $TiO_2(110)$ -(1x2) is a low D/F ratio, where D is the diffusion rate for Cu on the surface and F is the Cu deposition or flux rate. When rate of deposition is high relative to diffusion, the incoming Cu atoms have a greater probability of encountering another Cu atom and forming a new island before they are able to diffuse across the surface and contribute to the growth of an existing island; in this case, small islands of uniform sizes are formed with high island densities. When the rate of diffusion is high relative to flux, the incoming Cu atoms are more likely to diffuse to an existing island before encountering other Cu atoms; in this case, Cu islands of varying sizes with lower island densities are formed. We have varied the D/F ratio by changing both the deposition rate and the temperature of the surface during deposition. In all cases, the lower D/F ratio yields a more uniform size distribution. Notably, the Cu islands grown on this partially reconstructed TiO₂(110)-(1x2) surface produce high island densities $(-5x10^{12}/cm^2 \text{ at } 2 \text{ ML})$ due to high defect densities on the titania surface itself. Larger islands Cu (~100 Å diameter) with uniform size distributions can be produced by deposition at room temperature followed by annealing at higher temperatures. Investigations of Ni island growth on the reconstructed titania surface are currently underway.

4:00pm SS2-MoA7 Surface Nanostructuring to Control Size and Composition of Individual Oxide Supported Nanoparticles, A. Kolmakov, University of California, Santa Barbara, D.W. Goodman, Texas A&M University

A key to the technological utilization of oxide supported metal nanoparticles as an active element in gas sensing devices and catalysts is an atomic level understanding of their role in the chemical reaction. The chemical and physical properties of nanoparticles dispersed on oxide surfaces exhibit a marked dependency on their size, shape, composition and electronic interaction with the support. To explore this avenue a umber of methods of producing and delivery of size selected clusters from the gas or liquid phase to the oxide surfaces have been developed during the last decade. Alternatively, recent achievements in single molecule and clusters spectroscopy with NSOM and SPM and TEM proved the feasibility of so called individual approach where instead of probing the ensemble of size selected particles, imaging and spectroscopy of the individual oxide supported nanoparticles with different sizes and composition is performed and compared during the single experiment. Using Ag, Au and alloy clusters supported on TiO₂ (110) as a model system, we demonstrate several experimental schemes for studying individual supported metal clusters using oxide surface nanostructuring in conjunction with SPM. Namely, on slightly reduced TiO₂ we create laterally confined and precisely located areas with controllably modulated defect densities by exploiting a "tip shadowing" technique to synthesize a nanostructured mask. Since the diffusion length of the adsorbate atoms and eventually the cluster nucleation density are strongly mediated by surface defect densities in these areas, a well-defined and controllable variety of cluster sizes is accessible for imaging and spectroscopy within the field of view of the SPM. A similar procedure is applied for tuning the doping level of individual, metal particles. The spectroscopic and morphological changes of the individual clusters were probed in situ while exposuring the sample to elevated pressure of reactive gases.

4:20pm SS2-MoA8 Nucleation and Sintering Kinetics of Pd on a-Al₂O₃(0001), S.L. Tait, Jr., L.T. Ngo, Q. Yu, S.C. Fain, Jr., C.T. Campbell, University of Washington

Low-temperature methane combustion for applications in electric generator turbines is catalyzed by Pd nanoparticles to minimize NO_x pollution. The reaction depends on the dissociation of methane molecules on the Pd surface. Nanoscale Pd particles contain coordinatively unsaturated Pd atoms, making them more active for the dissociation of CH4. We have studied the growth of Pd nanoparticles on the α -Al₂O₃(0001) surface. The alumina single crystal was cleaned by annealing in air and in vacuum. The cleanliness and structure of the surface were verified by XPS and LEED. Experiments were conducted on the unreconstructed 1x1 and the reconstructed $\sqrt{31x}\sqrt{31}$ R±8.9° surfaces. Wide terraces were observed on the surface with non-contact atomic force microscopy (NC-AFM). Submonolayer doses of Pd were deposited by vapor deposition. NC-AFM was used to observe the growth of Pd nanoparticles upon annealing. These measurements provide information about the Pd particle size, number density and morphology. The Pd showed a tendency to cluster at step edges. To measure Pd particle sintering kinetics and size effects thereon, temperature-programmed ion scattering spectroscopy was used to monitor the fraction of the surface covered by Pd particles continuously as the surface was heated at 1 K/s. The number density of the Pd particles was measured before and after heating using NC-AFM. Curiously, large regions of the surface were found to be void of clusters even at step edges. A mechanism involving the various elementary steps in atom and cluster migration is being developed to model the kinetics of sintering with physically reasonable parameters. Work supported by DOE-OBES Office of Chemical Sciences and the M. J. Murdock Charitable Trust. LTN supported by the IGERT Nanotechnology Fellowship.

4:40pm **SS2-MoA9** The Domain Boundary Barrier on Intermixed SbGe(001), *M. Li, E.I. Altman*, Yale University

The nucleation and growth of epitaxial Ge structures on the intermixed SbGe(001) surface below the Sb segregation temperature was studied using scanning tunneling microscopy (STM). The drastic changes in the density, shape and size of the epitaxial structures as a function of Sb concentration in the Ge(001) substrate reveal the favored nucleation of Ge ad-dimers on Ge instead of Sb. The lack of Ge epitaxial structures on Sb suggests the enhanced surface diffusion on Sb-passivated surface. The Ge epitaxial structures always situate in the proximity of domain boundary between mainly bean-shaped Sb dimer domains and Ge dimer domains in the substrate. A one-directional repulsive potential barrier at the Sb-Ge domain boundary is proposed that inhibits the diffusion of Ge dimers from Ge domains to Sb domains and thus the nucleation of epitaxial structure is confined to Ge domains.

Tuesday Morning, November 5, 2002

Biomaterials

Room: C-201 - Session BI+SS-TuM

Platforms for Non-fouling and Patterned Surfaces

Moderator: D.G. Castner, University of Washington

8:20am BI+SS-TuM1 Molecular Assembly and Micro-/Nanopatterning Techniques on Oxide-based Surfaces for Controlling Non-specific and Specific Interactions, M. Textor, ETH Zürich, Switzerland INVITED The assembly of multifunctional molecules at surfaces has become an important technique to design interfaces for biosensor applications and model surfaces for cell-biological studies. While alkanethiol self-assembled monolayers on gold surfaces are routinely used today, corresponding systems for oxide-based surfaces had first to be developed. The objective is to produce interfaces via cost-effective, robust techniques that allow the elimination of non-specific protein adsorption and the addition of ligands in controlled density to sense the biological environment. Poly(ethylene glycol)-grafted polyionic copolymers assemble spontaneously from aqueous solutions at charged interfaces resulting in well-defined, stable monolayers. The degree of interactiveness of the resulting surface with the bioenvironment can be controlled quantitatively through the design of the polymer architecture. If the polymer is functionalized with bioligands such as biotin, biosensor interfaces with quantitative control over ligand density can be efficiently produced. Chemical patterning of surfaces into adhesive and non-adhesive areas has become an important tool to organize in a controlled manner biological entities such as cells and biomolecules at interfaces. A novel surface modification technique is presented that uses a lithographically pre-patterned, inorganic substrate, which is subsequently converted into a pattern of biological contrast via area-selective molecular assembly processes. Biologically meaningful patterns of protein-adhesive and non-adhesive areas in a size range from micrometers to as small as 50 nm could be produced. Fluorescence microscopy, XPS, ToF-SIMS and AFM were used to control ex situ each surface modification step, while the kinetics of the surface reactions including the interaction with biological media were monitored in situ with an optical sensor (OWLS) and the quartz crystal microbalance (QCM-D) technique.

9:00am **BI+SS-TuM3** Orientation in Oligo(ethylene glycol) Functionalised Self Assembled Monolayers Adsorbed on Gold Depending on the Oligomer Length, *M. Zwahlen*, University of St Andrews, UK, *S. Herrwerth, W. Eck, M. Grunze*, University of Heidelberg, Germany, *G. Haehner*, University of St Andrews, UK

Oligo(ethylene glycol) (OEG) functionalised self-assembled monolayers (SAMs) have attracted considerable attention due to their protein repelling properties. The underlying mechanism is of high scientific relevance for future applications but has not yet been completely resolved. 'Steric repulsion', which describes the resistance to non-specific protein adsorption in the case of the polymer PEG does not explain the mechanism in densely packed SAM structures sufficiently. It has been suggested that one cru cial parameter for the interaction of OEG-modified surfaces with their environment is the orientation in the organic adlayer. This has motivated a number of structural investigations on OEG-SAMs. As a contribution to the ongoing discussion, we present a s tudy of the orientation in OEGfunctionalised SAMs adsorbed on gold. It was measured as a function of the number of EG units in the molecule using soft X-ray absorption spectroscopy (NEXAFS). The results and their implications on the vacuum structure of the OEG-films will be discussed. The data will be compared to those obtained with complementary experimental techniques under similar as well as under different environmental conditions.

9:20am BI+SS-TuM4 DOPA: A Novel Anchor for PEGylation of Biomaterials, J.L. Dalsin, P.B. Messersmith, Northwestern University

It is widely recognized that modification of biomaterial surfaces with biocompatible polymers is a useful strategy for controlling protein adsorption and cell interactions with materials. The physical or chemical immobilization of poly(ethylene glycol) (PEG) has routinely been used to limit biological fouling of surfaces. Many of the current PEGylation methods, however, are limited by high costs and complexity of synthesis. Most importantly, each of the present strategies vary widely depending on the characteristics of the substrate, and are typically different for metal, metal oxide, and polymer substrates. We are developing a new biomimetic strategy for anchoring PEG to biomaterial surfaces. Our approach is to utilize linear and branched PEGs end-functionalized with DOPA. DOPA is found in significant quantities in the adhesive proteins secreted by marine mussels for attachment to underwater surfaces, and recent evidence suggests

that the presence of DOPA promotes strong and durable adhesion of these proteins to metal, metal oxide, and polymer surfaces. Recently, it has been shown that DOPA-containing peptides adhere strongly to gold surfaces, mediated by metal-oxygen bonds formed between the catechol group of DOPA and Au atoms at the metal surface. In this study, we report our findings on the use of DOPA as an anchor for PEGylation of biomaterial surfaces. A variety surfaces were modified by adsorption of DOPAmodified-PEGs from solution, and the presence of PEG on the surface was confirmed with a number of surface characterization techniques, including XPS and TOF-SIMS. The behavior of cells on modified and unmodified gold surfaces was evaluated in an attempt to optimize the conditions for DOPA-mediated PEGylation of metals, metal oxides, and polymers.

9:40am BI+SS-TuM5 Characterization of Non-Fouling Surfaces by Matrix-Assisted Laser Desorption / Ionization Mass Spectrometry, G.R. Kinsel, J. Zhang, R.B. Timmons, M. Li, University of Texas at Arlington

Matrix-Assisted Laser Desorption / Ionization (MALDI) mass spectrometry has emerged in recent years as a powerful method for the mass spectrometric analysis of a wide range of biomolecules including proteins, oligonucleotides, polysaccharides, etc. An attractive feature of this analytical approach is the relative simplicity of the sample preparation. In principle, all that is required is that the analyte of interest be mixed with an appropriate "matrix" (typically a small, functionalized aromatic compound) and the two compounds allowed to co-crystallize on some type of support. In recent work, however, we have shown that the nature of the support can have a marked effect on the magnitude of the analyte MALDI ion signal. Specifically, we have shown that as the binding affinity of the support for the analyte increases, the analyte MALDI ion signal decreases. This relationship has been used to develop a quantitative method for the determination of the protein binding affinity of various materials based on a MALDI standard additions approach. In the present studies the MALDI method has been used to quantitate the protein binding affinity of a number of "non-fouling" surfaces. These surfaces include plasma polymerized PEO, plasma polymerized CH3OH, PEO-PU block copolymers, and PEO grafted surfaces. The "non-fouling" properties of these surfaces are compared with the protein binding affinity of other conventional polymers including PTFE, LDPE, etc. In addition, the binding properties of the various surfaces are examined with relation to a variety of peptides and modest sized proteins.

10:00am **BI+SS-TuM6 Polymerized Planar Biomembrane Assemblies**, *S. Saavedra*, University of Arizona

The utility of planar supported lipid bilayers (PSLBs) as protein-resistant coatings in molecular device technologies is hampered by the chemical and mechanical instability of these structures relative to (for example) alkylsiloxane self-assembled monolayers. We have been investigating cross-linking polymerization of diene-functionalized lipids as a strategy to enhance the inherent instability of PSLBs. The membranes are self-assembled by vesicle fusion, then polymerized in situ by a redox-initiated chemistry. In contrast to diacetylene-based materials, these new diene-based materials contain relatively few defects. They are stable to conditions that would destroy a fluid membrane (e.g. exposure to air, surfactants, solvents), yet retain the characteristic protein resistance of a fluid PSLB. Thus these structures appear to possess both the stability and inertness required for implementation of PSLBs in many technological applications. This talk will focus on preparation, characterization, and protein functionalization of diene-based PSLBs.

10:20am BI+SS-TuM7 Protein Binding at Biomembrane Interfaces, P.S. Cremer, Texas A&M University INVITED

We have used a combination of lithographic patterning techniques and microfluidics to spatially address fluid phospholipid bilayers at the liquid/solid interface. These systems are capable of multivalent ligandreceptor attachment chemistry. Moreover, on-chip designs allow for high throughput temperature, concentration, pH, and ionic strength measurements in an environment which closely mimics a cell membrane interface.

11:00am **BI+SS-TuM9** Surface Characterisation of Supported Lipid Layers, S.L. McArthur, M.W. Halter, V. Vogel, D.G. Castner, University of Washington

The boundaries of biological cells and organelles are defined by complex and dynamic membranes constructed from an array of lipids, proteins and carbohydrates. These interfaces have a range of specific functions and properties, one of which is their ability to prevent non-specific protein adsorption, making membrane mimics an attractive option for a variety of in vivo and in vitro biomedical implant and diagnostic applications. The development and characterization of complex biomimetic surfaces presents a challenge in terms of their initial formation, long-term stability and integrity in a variety of environments and the maintenance of bilayer fluidity. In this study we detail the development and chemical characterization of supported lipid monolayers. The structure was formed by coupling HEMA to a glass support and subsequently activating it with CDI to couple the headgroups of the lipid, dimyristoyl ethanolamine (DMPE). The success of the immobilization procedure was investigated by XPS and ToF-SIMS. A number of different lipid transfer regimes were explored. Results illustrated that the samples produced using Langmuir-Blodgett transfer at high pressure (20 mN/m) had the largest fraction of the transferred lipids remaining at the surface after 5 minutes sonication in ethanol. Fluorescence microscopy of the lipid layers showed that the presence of this limited number of anchored lipids acted to stabilize the monolayer and maintain its integrity without having a detrimental effect on layer fluidity.

11:20am BI+SS-TuM10 Purification of Mobile, Membrane-tethered Proteins in Micropatterned Supported Lipid Bilayers, L. Kam, T.D. Perez, W.J. Nelson, S.G. Boxer, Stanford University

Supported lipid bilayers are a unique system for studying fluidic membranes in a controllable in vitro format. A variety of methods for tethering proteins to supported bilayers provide a powerful reductionist model of cell-cell recognition and activation. However, contemporary methods for preparing membrane-tethered protein systems typically incur an immobile fraction; this population complicates and, at worst, subverts interpretation of experimental results. Here, we present a method for separating a population of mobile, GPI-tethered protein from an immobile fraction in a supported lipid bilayer. A GPI-modified protein based on the cell-cell adhesion protein E-cadherin was introduced into Egg PC vesicles by detergent dialysis. On a glass substrate, two adjacent and connected regions of supported lipid bilayer were created using a converging flow configuration. One region contained both mobile and immobile populations of GPI/cadherin while the other contained Egg PC alone. An electric field applied tangentially to the surface induced migration of the mobile, but not immobile, protein into the region of Egg PC, generating a purified population of these proteins which may then be isolated for analysis or further experimentation free from the immobile fraction. Importantly, this method is independent of the specific factors influencing protein mobility and thus generally applicable.

11:40am **BI+SS-TuM11** Spatial Control of Cell Attachment Using **Micropatterned Plasma Polymers**, *S.A. Mitchell*, *N. Emmison*, The Robert Gordon University, Scotland, UK, *A.G. Shard*, Sheffield University, England, UK

In recent years, there has been increased interest in the spatial control and regulation of cellular attachment and growth. Several techniques have been developed to produce surfaces with a well-defined chemical heterogeneity that are suitable for the rapid adhesion, spreading and proliferation of cells. Spatial control and sub-cellular pattern resolution has been successfully demonstrated by techniques such as micro-contact printing of selfassembled monolayers.¹ However, the labour intensive, time consuming preparation and ready oxidation of these surfaces limit the utility of these devices. Additionally, they are only applicable to substrates that are rarely used in biomedical devices. We have employed plasma polymerisation as an alternative method for the chemical patterning of surfaces, although the chemical composition of these surfaces is more difficult to control, this onestep procedure is rapid and cost effective.² The resulting surfaces have both a chemical functionality and a pattern resolution comparable to alternative techniques.³ They may be applied to virtually any substrate, including relatively rough surfaces such as tissue culture polystyrene, greatly increasing their applicability. We describe the patterned deposition of plasma polymers onto a variety of substrates and outline some of the advantages and limitations of the technique. Physicochemical characterisation of the plasma polymers is performed with XPS, AFM and contact angle analysis. The culture of mammalian cells on patterned substrates demonstrates their ability to spatially regulate cell attachment and spreading.

¹M Mrksich and G M Whitesides, Tibtech, 13, 228-235(1995)

²N A Bullett, R D Short, T OLeary, A J Beck, C W I Douglas, M Cambray-Deakin, I W Fletcher, A Roberts, C Blomfield, Surf. Interface Anal., 31, 1074-1076(2001)

³L Dai, H J Griesser, A W H Mau, J. Phys. Chem. B, 101, 9548-9554(1997).

Nanometer Structures

Room: C-207 - Session NS+SE+SS+MM-TuM

Nanotribology

Moderator: K.J. Wahl, Naval Research Laboratory

8:20am NS+SE+SS+MM-TuM1 Ultralow Friction Coatings and Surfaces, J.M. Martin, Ecole Centrale de Lyon, France INVITED From a technological point of view, very low friction in solid lubrication may be interesting in micromechanisms requiring neither friction noise nor instabilities, together with low power consumption. Theoretical approaches at the atomic scale coupled with experimental approaches using proximal probe techniques have been developed to study atomic scale friction behaviors and energy dissipation modes. The two limiting factors for friction reduction at the macro-scale are S0 (shear strength of the interface film) and a (pressure coefficient).¹ Approaching very low friction requires the reduction of both S0 and a below the MPa range. Thus lowering to zero friction would require the vanishing of both the adhesive and the external pressure. However these conditions are unlikely to be perfectly achieved in practice. Thus zero friction may not be possible. However, friction values in the 10-3 range or even less (near-frictionless sliding) have been experimentally reached in some practical situations. Here we examine ultralow friction by using a macro-scale sphere/plane contact configuration (maximum pressure of 1 GPa). Friction in the 0.001 range is associated with a shear strength of 1 MPa. We report experimental evidence of superlow friction with different coatings: pure molybdenum disulfide MoS2,² molybdenum dithiophosphate (Modtp) tribofilms and hydrogenated diamondlike carbon a-CH.

¹ I. Singer, J. Vac. Sci. Technol., A12(5), (1994) 2605.

²J.M. Martin, C. Donnet, Th Le Mogne and Th Epicier, Physical Review B 48, No 14, (1993) 10583.
³ C. Donnet et al, Surface and Coating Technology, 94, (1997) 456.

9:00am NS+SE+SS+MM-TuM3 Frictional Properties of Small Model Lubricant Molecules Adsorbed on VC(100), L.C. Fernandez-Torres, S.S. Perry, University of Houston, B.-I. Kim, Sandia National Laboratories

The frictional modification of the non polar (100) of vanadium carbide (VC) surface through small molecule adsorption at room temperature has been investigated from a fundamental perspective. These molecules represent the functionalities incorporated into lubricants and used to appropriately tailor the lubricant's properties and enhance its performance. Ultrahigh vacuum atomic force microscopy (AFM) has been employed to determine the changes in frictional response and interfacial adhesion. Scanning tunneling microscopy (STM) has been used to elucidate surface morphology. X-ray photoelectron spectroscopy (XPS) has been utilized to determine the composition of the species formed by the interaction of these adsorbates with the VC surface. This successful methodology has been developed during a recent investigation of ethanol, and in this study has been extended to other low molecular weight alcohols as well as an ester. The results will be rationalized in terms of chemical reactivity, adsorbate layer composition, extent of coverage, and changes in the interfacial shear strength and discussed in terms possible lubrication schemes.

9:20am NS+SE+SS+MM-TuM4 Adhesion and Deformation in Nanoscale Contacts between W(110) and Au(110) in Ultra High Vacuum, S.A. Smallwood, R.J. Lad, W.N. Unertl, University of Maine

Tribological phenomena change as the contact area decreases from macroscopic to atomic dimensions, but these changes are not well understood. We report studies of the force versus deformation behavior of contacts with diameters up to about 50 nm using well-characterized metal surfaces in ultra-high vacuum. These contact sizes are intermediate between those previously studied. The contacting bodies were a Au(110) single crystal and sharp tips of W wires. The W probes were cleaned by field evaporation and their atomic structure determined using field ion microscopy (FIM). All were terminated by (110) planes and radii varied between 12 nm and 24 nm. The probes were mounted in double cross-hair force sensors. After cleaning by sputtering and annealing cycles, the Au was transferred to a piezoelectric tube scanner and moved into tunneling contact with the probe. Deflection of the force sensor and electrical current were measured as the Au crystal was brought into mechanical contact to a predetermined maximum displacement and then withdrawn. Prior to the first yielding event, the data is well described by elastic contact mechanics theory. The reduced modulus of 61 $\hat{A}\pm$ 26 GPa agrees with the value calculated assuming bulk properties. The work of adhesion has an upper bound of about 0.3 J/m2. The first observable yielding events occur at a mean normal stress of 12 $\hat{A} \pm 2$ GPa, comparable to the values reported for larger probes, but half that reported for smaller contacts on Au(111). Hardness is about 6 GPa near the surface and decreases by about fifty percent at 8 nm indentation depth. Prior to first yield, contact conductance

remains far below one quantum. Deformation is confined to the Au. FIM demonstrates that the W probe is not deformed for penetrations as deep as its radius. Scanning tunneling microscopy shows that the indentation holes are asymmetric and that pile-up extends about one indentation diameter beyond the indent.

9:40am NS+SE+SS+MM-TuM5 Chemical Force Microscopy of Aluminium Oxide Surfaces, T.T. Foster, M.R. Alexander, UMIST, UK, E. McAlpine, Alcan International, UK, G.J. Leggett, University of Sheffield, UK

The combination of wettability, chemical force microscopy (CFM) and friction force microscopy (FFM) has been used to analyse changes at the oxide-covered surface of aluminium after magnetron sputter deposition. A model self-assembled monolayer (SAM) system was first developed to enable comparisons to be made with the more complex aluminium system. The monolayers were produced by self-assembly on Au (111) and Ag (111) substrates. The gold-coated AFM tips were modified with SAMs of alkanethiols terminated in a methyl or carboxylic acid group. Friction coefficients were measured for SAMs varying in chain length and terminal group chemistry. Using carboxylic acid modified tips; measurements were performed on the surface of aluminium. Adhesion forces were found to decrease with storage time in a desiccated environment, attributed to the adsorption of contaminant molecules from the atmosphere. In contrast the friction coefficient showed no significant change with storage time, presumably because the sliding tip, under loading, is able to displace contaminant molecules. Contact angle goniometry was used to study changes in surface wettability on the aluminium surface. The water contact angle increased linearly with the log of storage time, supporting the hypothesis that adsorption of hydrophobic contaminants modifies the aluminium surface. Contact mode characterisation of the aluminium oxide surface provided clear images of the oxide surface. A nitric acid-based cleaning procedure was developed that was capable of removing adventitious contamination and returning the aluminium oxide surface to condition that appears similar to the freshly deposited surface. This study clearly demonstrates the capability of CFM for characterising complex aluminium surfaces and studying changes in surface chemistry.

10:00am NS+SE+SS+MM-TuM6 Nanotribology and Related Structural Changes During Wear of Diamond-like Carbon Films, J. Goldsmith, E.A. Sutter, J. Moore, B Mishra, Colorado School of Mines, M. Crowder, Maxtor Corporation

Diamond-like carbon (DLC) thin films are used for wear and corrosion protection of magnetic disks, micro-electro-mechanical systems (MEMS), and tool bits. Magnetic information storage density increases when the readwrite head gets closer to the disk. The magnetic layers degrade very quickly without a good protective interface. The use of DLC thin films becomes increasingly popular as they can provide a protective surface due to their excellent tribological properties as low friction and high hardness. In both magnetic disks and MEMS applications, the DLC films are in the thickness range of 2 - 5 nm and in most cases are amorphous in structure. Characterizing the tribological and structural properties and identifying the wear mechanisms of DLC films on the nanoscale is a challenge. Here we present results on the nanotribology of the DLC films performed using both an atomic force microscope and a nanoindenter. We investigate the wear behavior of the DLC films and the role of transfer film. We find that the formation of transfer film plays an important role in providing low-friction. The nanotribological investigations are correlated with the structural changes that occur in the DLC film as well as in the transfer film detected using Raman spectroscopy and cross-sectional transmission electron microscopy.

10:20am NS+SE+SS+MM-TuM7 Tribology and Surface Forces in MEMS, J.S. Zabinski, Air Force Research Laboratory, S.T. Patton, K.C. Eapen, UDRI, S.A. Smallwood, Systran, Inc. INVITED

Microelectromechanical systems (MEMS) offer the potential to provide new capabilities and products for commercial and military applications. Simple devices are already common in the marketplace, but friction, stiction, and wear prevent reliable operation of more sophisticated types of MEMS devices that have contacting surfaces in relative motion. These tribological problems are fundamentally difficult to solve and are magnified because MEMS are expected to operate in very harsh environments, such as at elevated temperature and in space. The performance and reliability of MEMS are strongly dependent on the environment in which they operate. For example, moisture can cause device failure by stiction or it can provide excellent lubrication, depending on the device and the relative concentration of water vapor (i.e., relative humidity). Operation in vacuum is particularly severe and the wear mechanisms are different than in dry or moist environments. Methods to control system tribology include lubricant coatings, monolayers, and new materials. The tribological mechanisms operating in moist air through vacuum will be discussed along with strategies to control friction, stiction, and wear that have significantly improved MEMS reliability. In addition, the effects of storage on device performance will be presented.

11:00am NS+SE+SS+MM-TuM9 Tribological Measurement on MEMS Platforms¹, *M.T. Dugger*, *S.V. Prasad*, Sandia National Laboratories INVITED

Microelectromechanical systems (MEMS) fabricated using surface micromachining (SMM) and other lithographic techniques such as LIGA have resulted in actuators, counter-meshing gears and other moving mechanisms having complex tribological interfaces that are rough on the nanometer scale and have unusual surface morphologies. Meaningful friction and wear measurements of microsystems must be made at loads and speeds relevant to MEMS operation. Since friction and wear are properties of systems, measurements must also involve interactions of surfaces having the morphology and chemistry present in real devices. Experimental techniques for acquiring friction data during sub-micron displacement and under nanoNewton forces are critical for the fundamental understanding of energy dissipation and wear mechanisms in MEMS. However, experimental investigation of surface interactions in MEMS under relevant contact conditions requires techniques beyond those that are currently available. MEMS friction measurement platforms which bring real MEMS surfaces into contact are needed to define the design space, to investigate aging and failure mechanisms, and to validate models of friction and wear derived from fundamental studies. We have therefore developed both SMM and LIGA devices containing isolated tribological contacts from which quantitative friction forces can be extracted. These structures are used to investigate interface performance, degradation and failure mechanisms. Methods of quantifying static and dynamic friction in SMM and LIGA micromachined contacts will be presented. Examples will be shown of how these structures are being used to investigate degradation of monolayer lubricants and hard coatings for SMM devices, as well as the tribological behavior of metallic contacts in LIGA.

 1 Sandia is a multiprogram laboratory operated by Sandia Corporation, a Lockheed Martin Company, for the United States Department of Energy under contract DE-AC04-94AL85000.

Surface Science Room: C-108 - Session SS1-TuM

Hydrocarbon Catalysis

Moderator: J.L. Gland, University of Michigan

8:20am SS1-TuM1 The Role of Defects in Surface Resistivity: The Unusual Case of Sulfur on Cu(100), R.G. Tobin, Tufts University

Adsorbate-induced surface resistivity -- the change in electrical resistivity of a metal film when a gas adsorbs on its surface -- provides a simple but powerful probe of the dynamical interaction between conduction electrons and adsorbates.¹ The dominant mechanism is generally diffuse scattering of the electrons from the adsorbate, and the scattering cross section per adsorbate is usually nearly independent of adsorbate coverage. For sulfur on Cu(100), however, the resistivity increases rapidly with coverage up to a threshold, and then remains constant as the coverage increases further. This effect was first observed by Xu and Hirschmugl using infrared reflectance and a single crystal sample.² They attributed the rapid increase at low coverage to a large scattering cross section for S adsorbed on defect sites, with a near-zero cross section for S on terrace sites. In the present study the same behavior is seen in both the dc resistivity and the infrared reflectance of epitaxial Cu(100) thin films. The transition between the two scattering regimes, however, occurs at a higher coverage (~0.2 ML) than in the singlecrystal measurements (0.04 ML). The role of defects is investigated by quantitatively estimating the defect density from CO adsorption measurements, and by sputtering the surface before adsorption to increase the defect density.

1R.G. Tobin, Surf. Sci., in press.

²X.F. Xu and C.J. Hirschmugl, Surf. Sci. 490 (2001) 69.

8:40am SS1-TuM2 Chemistry of One-dimensional Metallic Edge States in MoS₂ Nanoclusters, *J.V. Lauritsen*, University of Aarhus, Denmark, *B.S. Clausen, H. Topsoe*, Haldor Topsoe A/S, Denmark, *F. Besenbacher*, University of Aarhus, Denmark

We report on interesting chemistry of MoS_2 nanoclusters, which we show to be able to hydrogenate and break up thiophene (C_4H_4S) molecules at unusual sites on the cluster edges. We associate this behavior with onedimensional metallic electron states located at the perimeter of the otherwise insulating nanoclusters. Since MoS_2 nanoclusters constitute the

basis of hydrotreating catalysts used to remove sulfur from oil products through the hydrodesulfurization (HDS) process, the kind of chemistry identified in this work has significant implications. Our approach exploits recent progress in the synthesis of a relevant catalyst model system, i.e. we can synthesize MoS₂ nanoclusters image them on the atomic-scale with STM.¹ With STM prominent electronic features are observed near the edges of triangular MoS_2 clusters, which are associated with 1D metallic edge states.² By adsorbing hydrogen and thiophene, we pin-point, in the STM studies, active sites on these metallic edge states and reveal signatures of thiophene reaction intermediates adsorbed onto the metallic edge state. At the cluster edges, we find that S-H groups form, which are involved in a hydrogenation reaction and subsequent C-S cleavage of thiophene. In an interplay with density functional theory we elucidate the reaction pathway and classify the adsorbed species as ring-opened thiolates. We have thus identified a new route for activating a relatively inert, sulfur containing molecule like thiophene. Unexpectedly, this process does not take place through direct interaction with the Mo atoms. Instead, metallic states on the fully sulfided edges have the ability to donate and accept electrons and thus act as catalytic sites just like ordinary metal surfaces.

¹ S. Helveg, J. V. Lauritsen et al. Phys. Rev. Lett. 84, 951 (2000).

² M. Bollinger, J. V. Lauritsen et al., Phys. Rev. Lett. 87, 196803 (2001).

9:00am **SS1-TuM3 Electron-Induced Dissociation and Reactions of Methyl Groups Adsorbed on Cu(110)**, *Y.L. Chan, P. Chuang*, National Taiwan University, Republic of China, *R. Klauser*, Synchrotron Radiation Research Center, Taiwan, Republic of China, *S.-H. Chien*, *T.J. Chuang*, National Taiwan University, Republic of China

Methylene was suggested in some prior studies to be the key species responsible for the propagation of long chain hydrocarbons from methyl groups on catalyst surfaces. So far, direct evidence to show the presence of such reaction intermediate remains elusive, particularly under UHV condition. With the combination of HREELS vibrational spectroscopy, TPD and LEED techniques, we have observed that CH₃(ads) groups adsorbed on Cu(110) can be dissociated by low energy electrons to form CH₂(ads). In subsequent thermal process, CH₂(ads) can react with coadsorbed CH₃(ads) to produce C₂H₄, C₃H₆ and C₄H₈ molecules desorbed from surface. The desorption peaks for the various alkenes center at the same temperature independent of the CH₂(ads) average surface concentration and exhibiting the first-order reaction kinetics. Furthermore, the product ratio of $C_{3}H_{6}/C_{2}H_{4}$ is found to be linearly proportional to the ratio of CH₂(ads)/CH₃(ads) concentrations. The results show that aggregation of the adsorbates and close proximity of the reactants in the form of twodimensional islands may be essential for the chain propagation reactions. In this study, the e-beam irradiation effects on molecular dissociation and desorption are investigated in the electron energy range of 5-70 eV. Preliminary report of these effects was given recently,¹ and a detailed account will be presented in this paper.

¹ P. Chuang, Y.L. Chan, S.-H. Chien, R. Klauser and T.J. Chuang, Chem. Phys. Lett. 354,179 (2002).

9:20am SS1-TuM4 Oxidative Coupling of Methane to Higher Hydrocarbons Using Li₂O/MgO Catalysts, J. Langohr, R. Heinisch, F. Behrendt, Technische Universität Berlin, Germany

Oxidative coupling of methane represents an important pathway to produce higher hydrocarbons especially those with two carbon atoms, i. e, ethane and ethane, representing a key component for chemical industry. The reaction scheme - which still is not completely understood -involves a number of steps with the heterogeneous formation of methyl radicals and the homogeneous recombination of methyl radicals to ethane as key parts. The second of these reactions is in competition with reactions leading to the total oxidation products carbon dioxide and water - a pathway occurring both homogeneously and heterogeneously. With respect to the concentration of methyl radicals the reaction order is one for the total oxidation but two for the formation of ethane. An increase of the concentration of methyl radicals should promote an increased production of the C2 hydrocarbons. For the example of a set of Li2O/MgO catalysts it is shown that an increase of the BET surface area - resulting in a higher number of active sites at the catalyst1s surface - results in an increased yield of C₂ hydrocarbons. By variation of the preparation technique (aqueous mixtures of various Li and Mg salts are dried and then calcinated at different temperatures and periods of time) catalysts are produced which indeed show an increase in methane turn-over - without losing selectivity for C_2 hydrocarbons - with increasing surface area. The BET surface area is varied between 0.3 and 4.2 ml/g. Ongoing experiments aim at further increasing this surface area. Modifications of the preparation technique will include calcination under low-pressure conditions and on carrier materials having high surface areas themselves, e.g., polyurethane foams or activated carbon.

9:40am SS1-TuM5 The Dynamics of Alkane Adsorption on Pt(111), Pd(111) and Ni(111): Prediction from One Metal to Another?, C.-L. Kao, Stanford University, J.F. Weaver, University of Florida, R.J. Madix, Stanford University INVITED

The adsorption and reaction of alkanes on metal surfaces is fundamental to hydrocarbon catalysis. In order to adsorb the kinetic energy of the incident molecule must be dissipated in the gas-surface collision. To develop a predictive capability for the adsorption probabilities of alkanes on surfaces we have combined molecular beam methods with molecular dynamics simulations. The objective is to determine simple empirical potential parameters that govern the alkane-metal interaction from experimental measurements for a single alkane-surface combination and to use these parameters to predict trapping probabilities for other alkanes on other surfaces. A single set of potential parameters, determined from measurements of the trapping probabilities of ethane on Pt(111) can be used to predict the trapping probabilities of C3-C5 alkanes on Pt(111) and ethane and propane on Pt(110). More recently, these predictions have been extended to C1 - C5 alkane trapping on Pd(111). Palladium and platinum have similar lattice constants and Debye temperatures, differing primarily in their atomic mass, and thereby offer a good first order test of the predictive capability of the molecular dynamics simulations. Indeed, the trapping probabilities for Pd(111) are accurately predicted. Generally, the trapping probabilities for a given alkane are higher on Pd(111) due to the lower mass of the palladium atoms. The simulations show the importance of both the excitation of lattice vibrations and cartwheel rotational motion in affecting trapping. Predictions for Ni(111) are potentially more challenging, since the Ni-Ni force constants are much higher and both the mass and lattice parameter differ significantly from those of platinum. The theory correctly predicts that the adsorption probabilities on Ni(111) are lower than those for both Pt(111) and Pd(111). In general trapping probabilities are predicted to within about 50%.

10:20am SS1-TuM7 Molecular Mechanisms of Propylene Adsorption and Oxidation on the Stepped Pt(411) Surface, H.D. Lewis, D.J. Burnett, A.M. Gabelnick, University of Michigan, D.A. Fischer, National Institute of Standards and Technology, J.L. Gland, University of Michigan

The influence of surface defects on the chemistry of propylene adsorption and oxidation was investigated using temperature-programmed reaction spectroscopy (TPRS) and in-situ fluorescence yield soft x-ray techniques on the stepped Pt(411) surface. Mass spectrometer based TPRS studies show that propylene adsorbed on Pt(411) at 100 K undergoes disproportionation and decomposition to propylene, propane, hydrogen and surface carbon. Reacting coadsorbed propylene with excess oxygen, complete oxidation occurs with oxydehyrdogenation to water preceding skeletal oxidation to carbon dioxide. Based on the qualitative mechanistic understanding from TPRS, in-situ oxidation experiments were performed in oxygen pressures up to 0.02 Torr. The mechanism is the same in flowing oxygen, and preadsorbed propylene is completely oxidized by 475 K. The 280 K initiation temperature for oxydehydrogenation is independent of oxygen pressure, while the initiation temperature for skeletal oxidation is oxygen pressure dependent beginning at 370 K in 1 x 10⁻⁵ Torr oxygen and decreasing to 300 K in 0.02 Torr oxygen. A stable intermediate is observed after oxydehydrogenation is complete. The molecular mechanism for propylene oxidation on Pt(411) with both propylene and oxygen in the gas phase was also studied. With increasing oxygen pressure less propylene is adsorbed and the onset temperature for deep oxidation decreases. Taken together, results indicate that the inhibition of oxygen adsorption is important in limiting this complex oxidation reaction. Results for propylene oxidation on this stepped surface are compared to studies on Pt(111) to delineate the role of surface defects in this interesting surface reaction network.

10:40am **SS1-TuM8 Catalytic Arene Oxidation on Supported Platinum Nanoparticles**, *A.L. Marsh*, University of Michigan, *G.E. Mitchell*, The Dow Chemical Company, *D.A. Fischer*, National Institute of Standards and Technology, *J.L. Gland*, University of Michigan

The cleanup of volatile organic compounds from industrial emissions is a current environmental issue that requires knowledge of molecular-level mechanisms for catalytic processes. Aromatics such as benzene, toluene, and chlorobenzene are often present in emissions because of their stability. However, these molecules can be removed by oxidation over nanoparticulate-supported catalysts. In order to better understand the mechanisms of catalytic oxidation, the reactions of benzene, toluene, and chlorobenzene on a commercial alumina-supported platinum catalyst have been characterized both in vacuum and in the presence of oxygen. Molecular-level mechanisms for both decomposition and oxidation have been determined using Temperature-Programmed Reaction Spectroscopy. The structures of intermediates present during oxidation or decomposition have been identified using Fluorescence Yield Near-Edge Spectroscopy.

Comparisons will be made to the chemistry on the Pt(111) surface in an effort to show the effects of particle size and of the support. Substantial substituent effects on the chemistry of the aromatic ring are also observed. This molecular-level understanding of these reactions will aid in tailoring catalysts for the efficient cleanup of industrial emissions.

11:00am **SS1-TuM9 In situ XPS Investigation of the Methanol Oxidation Over Copper**, *H. Bluhm*, *M. Hävecker*, *A. Knop-Gericke*, Fritz Haber Institute of the Max Planck Society, Germany, *V.I. Bukhtiyarov*, Boreskov Institute of Catalysis, Russia, *D.F. Ogletree*, *M. Salmeron*, Lawrence Berkeley National Laboratory, *R. Schlögl*, Fritz Haber Institute of the Max Planck Society, Germany

We have used in situ X-ray photoelectron spectroscopy (XPS)¹ in combination with mass spectrometry to investigate the partial oxidation of methanol to formaldehyde over a polycrystalline copper sample. The experiments were performed at a methanol to oxygen flow ratio of 3:1 (total pressure 0.4 torr) in the temperature range from 300 K to 750 K. The correlation of in-situ XPS spectra of the copper surface and the simultaneously obtained mass spectrometer data (which show the catalytic activity) allow us to draw conclusions about the electronic state of the catalyst under reaction conditions. Valence band and Oxygen 1s spectra show that after the onset of the catalytic reaction at T>550 K the copper surface has a metallic character. The Oxygen 1s spectra reveal that at least two different oxygen species with binding energies (BE) of 529.7 eV and 531.4 eV, respectively, are present at the catalytically active Cu surface. The O 1s peak at 529.7 eV is assigned to chemisorbed oxygen at the Cu surface. The integrated intensity of the chemisorbed oxygen peak is proportional to the amount of formaldehyde that is produced in the catalytic reaction. The peak at 531.4 eV is assigned to subsurface oxygen. The formaldehyde yield increases linearly with the integrated intensity of the subsurface oxygen peak, up to a concentration of the equivalent of about one monolayer of subsurface oxygen. A further increase of the amount of subsurface oxygen does not lead to an increase of the formaldehyde yield.

¹ D.F. Ogletree, H. Bluhm, G. Lebedev, C.S. Fadley, Z. Hussain, M. Salmeron, submitted to Rev. Sci. Instrum.

11:20am SS1-TuM10 Determination of the Adsorption Site of a Polyatomic Adsorbate Using Vibrational Spectroscopy and ab initio Calculations: Methoxy and Ethoxy on Cu(100), P. Uvdal, M.P. Andersson, Lund University, Sweden

Using infrared vibrational spectroscopy and ab initio electronic structure calculations of small metal cluster models we have determined the adsorption site of methoxy and ethoxy on Cu(100). The experimental intramolecular vibrational frequencies are very well reproduced by the model cluster representing the four-fold hollow adsorption site. In contrast calculated frequencies for intermolecular modes modeled by clusters representing bridge and on-top adsorption is not not reproduce as well.

11:40am SS1-TuM11 A Model Catalyst with Selectivity Controllable Functions: The Effects of Frequency in Thickness Extension Mode Resonance Oscillation on Ethanol Decomposition Over a Thin Ag Film Deposited on a Ferroelectric z-cut LiNbO₃ Single Crystal, N. Saito, Y. Yukawa, H. Nishiyama, Y. Inoue, Nagaoka University of Technology, Japan The resonance oscillation of acoustic waves is generated on a poled ferroelectric crystal by a piezoelectric effect. We have shown that the thickness extension mode resonance oscillation (TERO) has the ability to remarkably change the reaction selectivity over thin metal catalysts deposited on a zcut $LiNbO_3$ (z-LN) crystal.¹ The TERO has a series of resonance frequencies (the first, the second, the third and so on) determined by the crystal constants. A z-LN crystal shows 3.5(first), 10.8 (second) and 17.9 (third) MHz. It is interesting to see the frequency effects on TEROinduced selectivity changes. In the present work, the TERO of 10.8 and 17.9MHz were employed for ethanol decomposition on a thin Ag film catalyst deposited, and the results were compared with those reported previously for 3.5MHz. The TERO of 10.8 and 17.9 MHz at 1.5W caused the enhancement of ethylene production without significant changes in acetaldehyde production. The selectivity for ethylene production, Se, increased from 62% without the TERO to 96% for 3.5MHz, 85% for 10.8MHz and 75% for 17.9MHz. The selectivity increases became small with increasing resonance frequency. Laser Doppler measurements showed that the TERO generated randomly distributed standing waves vertical to the surface. With increasing frequency, the magnitude of the waves, corresponding to lattice displacement, decreased (98 nm for 3.5 MHz, 28 nm for 10.8 MHz and 15 nm for 17.9MHz at 1W), whereas the number of the standing waves per unit area increased remarkably. In photoelectron emission spectroscopy, the TERO shifted the threshold energy of photoelectron emission from Ag surface by 0.08-0.25eV. The present results indicate that the magnitude and the density of standing waves

strongly related to activity enhancement and selectivity changes. A mechanism of the frequency-dependent TERO effects is discussed. ¹ N.Saito and Y.Inoue, J.Chem. Phys. 133,469(2000).

Surface Science

Room: C-110 - Session SS2-TuM

Diffusion & Growth on Metal Surfaces

Moderator: M. Salmeron, Lawrence Berkeley National Laboratory

8:20am **SS2-TuM1 Long Jumps in the Surface Diffusion of Large Molecules**, M. Schunack, **T.R. Linderoth**, F. Rosei, E. Laegsgaard, I. Stensgaard, F. Besenbacher, University of Aarhus, Denmark

While the surface mobility of atomic adsorbates has been studied extensively, similar investigations of large organic molecules are very scarce. Here, we report a detailed variable-temperature Scanning Tunneling Microscopy investigation of the one-dimensional diffusion of two largish molecules, decacyclene (DC) and hexa-tert-butyl-decacyclene (HtBDC), on a Cu(110) surface. The molecular diffusion was studied by acquiring series of STM-images at substrate temperatures of 172-200 K and 218-251 K for HtBDC/DC, respectively. Surprisingly, we find that long jumps, i.e. adsorbate transitions spanning multiple lattice sites, play a dominating role for the diffusion of DC and HtBDC. The root mean-squared (RMS) jump lengths are as large as 3.9 and 6.8 Cu lattice spacings, respectively. The presence of long jumps is revealed by a new and simple method of analysis, which we have tested quantitatively by kinetic Monte Carlo simulations. The dominating role played by long jumps is in strong contrast to previously investigated adsorbate systems where diffusion typically occurs by jumps between nearest neighbor sites. Our results furthermore demonstrate the possibility of tailoring molecular diffusion properties: DC and HtBDC both have the same aromatic plane, which interacts strongly with the surface. In the case of HtBDC, however, the plane is raised away from the surface by spacer groups, resulting in an approximately four orders of magnitude higher diffusion constant compared to DC. The higher diffusivity results both from the larger RMS jump length and from a reduction of the activation barrier for diffusion from 0.73 to 0.59 eV.

8:40am SS2-TuM2 Observation of the Motion of Individual Leadoxide Molecules on Reconstructed Au(111) Using Scanning Tunneling Microscopy, M.C. Robinson, A.J. Slavin, Trent University, Canada

Ultra-thin metal oxides are of great technological importance, so it is necessary to understand how these films grow, beginning at the molecular level. In this study we have used scanning tunneling microscopy (STM) to observe the room-temperature diffusion of lead-oxide molecules, most probably PbO, on the reconstructed Au(111) surface at coverages below 0.06 monolayers (ML). To our knowledge, this is the first direct observation of the diffusion of metal-oxide molecules. The existence of mobile molecules suggests that, at least in some cases, oxide layer formation may be driven by the same processes governing metal-on-metal growth. If the motion is not tip-induced, then an upper limit for the molecule diffusion energy is 0.7 eV, based on the motion of the molecules between successive STM images. Atomic resolution is lost above 0.06 ML, probably because the Au reconstruction is lifted allowing a large increase in the rate of adatom diffusion.

9:00am SS2-TuM3 Initial Stages of Transition-Metal-Assisted Carbon Nanotube Growth: A First-principles Study*, Z. Zhang, Oak Ridge National Laboratory, Q. Zhang, The University of Texas at Arlington, J.C. Wells, Oak Ridge National Laboratory, X. Gong, Fudan University, China INVITED

The initial stages of catalytic growth of single-wall carbon nanotubes (SWNT) on transition metal clusters and surfaces are investigated using the first-principles molecular dynamics method. Selected nickel surfaces and magic-sized nickel clusters have been used as a paradigm for this type of catalyst. The method is based on density-functional theory using the local-density approximation with gradient corrections (GGA). The computation scheme is based on the expansion of valance electrons in a plane wave basis. The ultra soft pseudopotentials for nickel (Ni) and carbon (C) are employed to describe their interaction with ionic cores. The energetics involved in the elemental processes of SWNT growth, such as adsorption, diffusion, and nucleation of carbon atoms on the elemental facets of Ni magic clusters as well as on the different Ni surfaces, is investigated and compared, with the objective of identifying the precise role of catalytic clusters. We also investigate the energeticc involved in the possibility of a

concerted motion in the atom supply and growth of a baby nanotube on a given surface.

* Research sponsored by the Material Sciences and Engineering Division Program of the Department of Energy (DOE) Office of Science and by the Laboratory Directed Research and Development Program of Oak Ridge National Laboratory (ORNL), managed by UT-Battelle, LLC for the US DOE under Contract No. DE-AC05-000R22725 with UT-Battelle, LLC, and the National Science Foundation (NSF).

9:40am SS2-TuM5 Water Diffusion and Clustering on Pd(111), T. Mitsui, Lawrence Berkeley National Laboratory, M.K. Rose, E. Fomin, University of California, F. Ogletree, M. Salmeron, Lawrence Berkeley National Laboratory

The adsorption, diffusion and the formation of clusters of water molecules on Pd(111) has been studied by scanning tunneling microscopy. Water adsorbs in the form of isolated molecules at 40 K. With the help of STM movies of the molecular random walk and of atom-tracking techniques we studied the process of diffusion and cluster formation. When two water molecules meet they form a dimer, then a trimer and so on. The mobility of dimers and trimers was found to be nearly three orders of magnitude larger than that of single molecules. Pentamers and larger clusters are immobile at 40 K, although changes in their conformation were observed. Hexamers with a cyclic configuration are particularly stable. They grow with further coverage forming a commensurate hexagonal honeycomb with ($\sqrt{3x}\sqrt{3}$)R30° structure relative to the Pd(111) substrate.

10:00am SS2-TuM6 A New Mechanism of Mo Growth on Au (111) by Chemical Vapor Deposition from a Mo(CO)₆ Precursor, Z. Song, T. Cai, Z. Chang, G. Liu, J.A. Rodriguez, J. Hrbek, Brookhaven National Laboratory

Chemical vapor deposition (CVD) of metal carbonyls has been attractive for decades in both making supported metal catalysts and fabricating electronic devices. In most of the previous morphology studies of metal deposition on Au (111), the physical vapor deposition (PVD) method was used to prepare the samples. So far, it is not clear what to expect for the growth of metals from CVD of metal carbonyls. In this study, a Mo submonolayer has been grown by CVD of Mo(CO)₆ on a reconstructed Au (111) at a substrate temperature of 500 K and studied by STM. The Mo(CO)6 molecules decompose on the Au(111) surface at elevated temperatures and form Mo nano-scale clusters. The Mo clusters grow on both upper and lower steps and at elbows of the Au (111) herringbone structure at low coverages. New clusters are formed with increasing Mo coverage and found preferentially within the fcc troughs and randomly at elbows. In contrast to the Mo-PVD, where Mo clusters form well-ordered arrays by decorating all elbows of Au template, the Mo-CVD clusters aggregate without coalescing and develop ramified islands of clusters. An auto-catalyzed carbonyl decomposition is proposed to explain a facile formation of Mo clusters before they anchor on the surface. The Mo growth at upper steps can be attributed to the presence of CO, that modifies locally the surface potential of Mo. This research was carried out at BNL under Contract No. DE-AC02-98CH10086 with the U.S. DOE (Division of Chemical Sciences).

10:20am SS2-TuM7 Vacancy-Mediated and Exchange Diffusion in the Pb/Cu(111) Surface Alloy, B.S. Swartzentruber, M.L. Anderson, M.J. D'Amato, P.J. Feibelman, Sandia National Laboratories

To understand the formation and stability of surface alloy systems, it is important to know the fundamental atomic-intermixing and mass-transport processes. Using STM measurements and first-principles DFT calculations we have explored them for the formation and evolution of the Pb/Cu(111) surface alloy. When Pb atoms are deposited on Cu(111), they place exchange with surface Cu atoms forming a 2-d surface alloy phase. At low coverage, thermodynamics favors a random distribution of Pb atoms in the surface layer. However, upon deposition, the Pb atoms take the easy path, forming metastable stripes of high Pb concentration embedded near steps. Over time, equilibrium is reached through the much slower decay of this initially non-uniform concentration profile. We measure the kinetics of mass transport, using STM, by following the motion of individual embedded Pb atoms and also the time evolution of the concentration profile. By analyzing the statistics of the local motion we find the most likely process to be one in which diffusion of the embedded Pb atoms occurs via exchange with thermal surface vacancies. There is also a minority process occurring much less often - wherein an embedded Pb atom exchanges with a thermal Cu adatom and travels over long distance before re-embedding into the surface layer. Although this minority process rarely occurs, the long length scale over which it transports Pb atoms makes it a crucial ingredient of the overall mass transport process as measured in the decay of the concentration profile. Sandia is a multiprogram laboratory operated by Sandia Corporation, a Lockheed Martin Company, for the United States Department of Energy under contract DE-AC04-94AL85000.

10:40am SS2-TuM8 Ultrathin Transition Metal Films on W Surfaces -Conditions for Surface Alloy Formation, J. Block, E. Schroder, Chalmers University of Technology and Gothenburg University, Sweden, J.J. Kolodziej, Rutgers, The State University of New Jersey, J.W. Keister, J.E. Rowe, North Carolina State University, **T.E. Madey**, Rutgers, The State University of New Jersey

We report theory and experiment for the formation of alloy layers in the growth of transition metal films on W surfaces. When W(111) is covered by monolayer films of certain metals (Pt, Pd, Ir, Rh, Au), followed by annealing to T>750 K, the surface becomes covered with three-sided pyramids of nanometer-scale dimensions, having {211} planes as facet sides. High resolution soft x-ray photoelectron spectroscopy using synchrotron radiation is employed to study metal films (Pt, Pd, Ir, Rh) on W(111) and W(211). Surface core level shifts of $4f_{7/2}$ photoemission peaks indicate that single physical monolayers of these metals are stable against thermal rearrangement. In contrast, when multilayer films of Pd, Pt, Ir, Rh are annealed above 700-1000 K, tungsten atoms diffuse into the overlayer to form alloy films. We also characterize ultrathin Pd and Pt films on W(211) by first-principles density-functional theory (DFT) methods. Both to confirm the formation of alloy from theory and to help characterize the alloy, we present studies of Pd and Pt films with included W atoms. The DFT methods allow us to suggest the energetically preferred structures. We studied both pseudomorphically-grown alloy films and alloy films with the atomic positions locally optimized by minimizing the Hellmann-Feynman forces. The DFT calculations are consistent with the experimental observations.

11:00am SS2-TuM9 Metastable Pb Microcrystals on Ru(0001) Formed by Oxygen Segregation*, D.B. Dougherty, K. Thuermer, J. Reutt-Robey, E.D. Williams, University of Maryland

Microcrystals formed after dewetting a continuous Pb film grown on Ru(0001) have provided a convenient model system for understanding a variety of surface mass transport issues.^{1,2} In particular, the relaxation of crystallites toward thermodynamic equilibrium has been studied in detail. Here we report the formation of an unusual metastable crystallite shape and its STM tip induced rapid decay. Combined AES and STM investigations show that this new behavior is the result of minute amounts of oxygen that segregates from the substrate into the Pb. AES is used to observe the segregation of oxygen from the Pb/Ru interface to the surface of the continuous Pb film upon post-deposition annealing. This effect, when combined with the absence of any other detectable contamination explains the presence of nearly spherical crystallites on a surface for which the overwhelming majority have long since decayed to a steady, facetted shape. The decay of the unusual crystallites is induced by repeated scanning of an STM tip, suggesting the removal of a low-mobility oxygen species. This interpretation is consistent with previous observations of the effect of oxygen on single crystal Pb(111) surfaces³ and our Auger analysis. The highly nonequilibrium tip-induced decay is compared with the previously studied decay of Pb microcrystals. * Work supported by UMD-NSF-MRSEC.

 1 K. Thuermer et al., Step Dynamics in 3D Crystal Shape Relaxation. Phys. Rev. Lett 87 186102 (2001)

² A. Emundts et al., Experimental Absolute Step and Kink Formation Energies on Pb(111) Vicinal Surfaces. Surf. Sci. 496 L35-42 (2002)

 3 L. Kuipers et al., Jump to Contact and Neck Formation Between Pb Surfaces and a STM tip. Surf. Sci. 340 231-244 (1995).

11:20am SS2-TuM10 Selforganized Nanostructures at Vicinal Surfaces, N. Nöel, T. Maroutian, L. Douillard, H.-J. Ernst, CEA Saclay, France

The use of intrinsic instabilities in epitaxial growth is currently actively explored as a promising pathway for lateral nanostructuring of surfaces as a cost-effective alternative to lithography based schemes. The origin of these instabilities is traced back to the presence of an excess energy barrier for adatom diffusion over descending steps, the Ehrlich-Schwoebel barrier. Upon growth of Cu on vicinal Cu templates a step-meandering instability develops, resulting in an in-plane patterning of the surfaces at the nanometer scale with a temperature- and flux-dependent characteristic wavelength.¹ The step width increases with time (coverage) according to a power law with exponent 1/3. This experimental finding is at variance with currently existing theories.²

¹T. Maroutian et al., Phys. Rev. Lett. 83, 4353, (1999); idem, Phys. Rev. B 64, 165401 (2001)
²M. Rusanen et al., Phys. Rev. B 65, 41404 (2002).

11:40am **SS2-TuM11** Azimuth Dependent Nanogroove Greation by Grazing Ar^+ Bombardment on Cu(001), *H. Wormeester*, *M.M. Ovsyanko*, *A.A. Mewe*, *G. Stoian*, *B. Poelsema*, University of Twente, The Netherlands Grazing incidence 800 eV Ar^+ sputtering on a Cu(001) surface leads to the formation of nanogrooves in which only 3 layers are involved.¹ We found with high resolution LEED (SPA LEED) that the distance between the

nanogrooves L depends on the azimuthal orientation of the incident ions, with a larger distance L for incidence along <100> than <110>. Extrapolation to zero time shows that initially no azimuthal dependence of L is noticable. The time dependent behaviour, however, shows a much larger separation speed for [100] oriented nanogrooves. The creation and azimuth dependent development of these nanogrooves will be discussed. ¹Phys. Rev. Lett. 86, 4608 (2001).

Surface Science Room: C-112 - Session SS3-TuM

Metals, Adsorbates, and Defects on TiO₂

Moderator: R.L. Kurtz, Louisiana State University

8:20am SS3-TuM1 Effects of Cluster Size and Deposition Energy on Adsorption and Sintering Behavior of Metal Nanoclusters on Öxide Supports, M. Aizawa, S. Lee, University of Utah, J. Lee, Seoul National University, Korea, S.L. Anderson, University of Utah INVITED Size-selected metal nanoclusters on oxide supports are prepared by deposition of pre-formed, mass-selected cluster ions, allowing impact energy to be varied over a wide range. The samples thus prepared, are probed by a combination of XPS, AES, ISS, and TPD, providing insight into changes in oxidation state, morphology, and chemical behavior, induced by varying deposition conditions, thermal processing, and exposure to adsorbates. Results will be presented for Ni_n and Ir_n on TiO_2 . In both cases, the clusters appear to be stable with respect to breakup or sintering for a range of deposition energies on room temperature substrates. Significant morphology changes are observed following exposure to adsorbates. Both the adsorbate interation strengths and morphology changes are strongly size dependent.

9:00am SS3-TuM3 Bonding of Gold Nano-Clusters to Vacancies on Rutile TiO₂(110), E. Wahlström, R. Schaub, University of Aarhus, Denmark, N. Lopez, Technical University of Denmark, A. Ronnau, University of Aarhus, Denmark, J.K. Norskov, Technical University of Denmark, F. Besenbacher, University of Aarhus, Denmark

We have studied the early stages of Au cluster nucleation on defective rutile TiO₂(110) using scanning tunneling microscopy (STM). STM images and STM movies show a diffusion controlled growth mechanism. Room temperature STM movies show that the smallest stable clusters have a radius > 0.6 nm, while at 140 K not even single gold atoms seem to diffuse on the surface. It is also shown that a correlation exists between a decrease in density of bridging oxygen vacancies and growth of Au clusters at all investigated temperatures. This is direct evidence of a strong interaction between Au atoms and single atomic oxygen vacancies. Density functional theory calculations support these findings.

9:20am SS3-TuM4 The Chemical and Catalytic Activity of Au/TiO2(110) towards Sulfur Dioxide, Z. Chang, J.A. Rodriguez, G. Liu, T. Jirsak, J. Hrbek, J. Dvorak, Brookhaven National Laboratory, A. Maiti, Accelrys Inc.

Bulk metallic gold typically exhibits a very low chemical and catalytic activity. Recently gold has become the subject of a lot of attention due to its unusual catalytic properties when dispersed on some oxide supports. Gold particles supported on titania are active catalyst for the low temperature oxidation of CO, the selective oxidation of propene, and photocatalytic oxidations used for environmental cleanup. We used synchrotron-based high-resolution photoemission and first-principles density-functional slab calculations to study the interaction of gold with titania and the chemistry of SO₂ on Au/TiO₂(110) surfaces. Au/TiO₂ is much more chemically active than metallic gold or stoichiometric titania. On Au(111) and rough polycrystalline surfaces of gold, SO2 bonds weakly and desorbs intact at temperatures below 200 K. For the adsorption of SO₂ on TiO₂(110) at 300 K, SO₄ is the only product. In contract, Au/TiO₂(110) surfaces fully dissociate the SO₂ molecule under identical reaction conditions. Interactions with titania electronically perturb gold, making it more chemically active. Furthermore, our experimental and theoretical results show quite clearly that not only gold is perturbed when gold and titania interact. The adsorbed gold, on its part, enhances the reactivity of titania by facilitating the migration of O vacancies from the bulk to the surface of the oxide. In general, the complex coupling of these phenomena must be taken into consideration when trying to explain the unusual chemical and catalytic activity of Au/TiO2. The research was carried out at BNL under Contract No. DE-AC02-98CH10086 with the U.S. DOE (Division of Chemical Sciences).

9:40am SS3-TuM5 STM Studies of Titanium Oxide Adlayers on a Pt(100) Surface, T. Matsumoto, University of Southern California, M. Batzill, Tulane University, S. Hsieh, B.E. Koel, University of Southern California

Pt supported on titanium oxide catalysts exhibit effects termed SMSI (strong metal support interaction). In order to probe aspects of this chemistry, thin films of titanium oxide on Pt single crystal surfaces have been observed by using surface science techniques, but most studies focused on titanium oxide films that fully covered the surface. In this study, submonolayer coverages and ultrathin films of titanium oxide on Pt(100) were observed by STM, LEED and XPS, and we report several new, ordered structures. These titanium oxide structures were produced by annealing to 800-1300 K after the deposition of Ti in an oxygen atmosphere or additional oxidation with NO_2 and O_3 after Ti deposition. A (3×5) structure of Ti₂O₃ was found after annealing above 800 K. This structure could also be produced by O3 oxidation of the Pt3Ti surface alloy produced on Pt(100). Our proposed structural model suggests that the thin film of titanium oxide with the (3×5) structure covers the Pt(100) surface fully. Several other locally ordered structures were found by annealing below 1000 K after additional oxidation of the (3×5) structure with NO₂ and O₃. These were more oxidized than Ti_2O_3 , and were changed to the (3×5) structure after annealing to 1000 K.

10:00am SS3-TuM6 Oxygen Vacancies on TiO₂(110) : An STM Study of Adsorbate Mediated Diffusion, R. Schaub, E. Wahlström, A. Ronnau, E. Laegsgaard, I. Stensgaard, F. Besenbacher, University of Aarhus, Denmark

Time resolved fast Scanning Tunneling Microscopy (STM) experiments reveal a spatially correlated diffusion of oxygen vacancies present on the rutile TiO₂(110) surface. The diffusion is observed to occur exclusively perpendicular to the oxygen bridging rows of the (1x1) reconstructed surface. This unexpected behavior is unambiguously assigned to trace amounts of adsorbates present on the surface which mediate the oxygen vacancy diffusion. Based on high resolution STM movies, a novel atomistic diffusion mechanism is proposed.

10:20am SS3-TuM7 Oxygen Vacancies as Active Sites for Water Dissociation on Rutile TiO₂(110), P. Thostrup, R. Schaub, University of Aarhus, Denmark, N. Lopez, Technical University of Denmark, E. Laegsgaard, I. Stensgaard, University of Aarhus, Denmark, J.K. Norskov, Technical University of Denmark, F. Besenbacher, University of Aarhus, Denmark

Water dissociation on $\mathrm{TiO}_{\!2}$ is of fundamental interest as an example of a simple surface chemical process with significant applications. In addition, TiO_2 is the material of choice for photochemical hydrogen production from water and for biocompatible implants. Earlier experimental studies report a minor degree of water dissociation on TiO₂(110) while theoretical studies predict the dissociated state, or mixed dissociated-molecular states, to be most energetically favorable. Thus, even for this simple process we do not have a clear picture of the dissociation energetics and the active site for dissociation. Through an interplay between scanning tunneling microscopy experiments and density functional theory calculations, we determine unambiguously the active surface site responsible for the dissociation of water molecules adsorbed on rutile TiO₂(110). Oxygen vacancies in the surface layer are shown to dissociate H₂O through the transfer of one proton to a nearby oxygen atom, forming two hydroxyl groups for every vacancy. The amount of water dissociation is limited by the density of oxygen vacancies present on the clean surface exclusively. The dissociation process sets in as soon as molecular water is able to diffuse to the active site.

¹ R. Schaub, P. Thostrup et al., Phys. Rev. Lett. 87, 266104 (2001).

10:40am SS3-TuM8 The Influence of Subsurface, Charged Impurities on the Adsorption of Chlorine at TiO₂(110), M. Batzill, B. Katsiev, Tulane University, E.L.D. Hebenstreit, Lawrence Berkeley National Laboratory, W. Hebenstreit, Optical Coating Laboratory, Inc., U. Diebold, Tulane University

A fundamental surface science study on the influence of single, subsurface dopants on the chemical surface properties is presented. In particular the adsorption of chlorine atoms on TiO₂(110) samples modified by low concentrations of impurities were investigated. Subsurface impurity atoms were identified by scanning tunneling microscopy and spectroscopy. This analysis established that positively charged impurity atoms, most likely substitutional vanadium atoms, are present in some samples. Areas of about 2 nm in diameter around these impurities are imaged as protrusions in empty state STM images. This is consistent with a downward band bending induced by positively charge impurity atoms. Adsorption studies of Cl at room temperature on these samples showed that Cl atoms avoid chemisorption in the vicinity of these impurity atoms. Cl is an acceptor-like adsorbate that is negatively charged at the surface. The suppressed adsorption is explained by an increased local electron affinity due to the only partially screened positively charged impurities. This lowers the energy gain for adsorption of Cl at the surface and thus renders adsorption sites close to impurities as energetically disfavored compared to unaltered surface areas.

11:00am **SS3-TuM9 Lower 3-fold Hollow Site of K on TiO₂(110)1x1,** *G. Thornton, C.L. Pang, C.A. Muryn,* Manchester University, UK, *V.R. Dhanak*, Daresbury Laboratory, UK

Recent calculations by San Miguel et al (J. Phys. Chem. B 105 (2001) 1794) and Bredow et al (Surf. Sci. 418 (1998) 150) both predict that the low coverage bond site of K on TiO2(110) is the so called lower three fold hollow site. This involves two bridging O atoms and an in-plane O. In our work we have tested this prediction at a K coverage of 0.15 ML using a combination of surface extended X-ray absorption fine structure (SEXAFS), scanning tunneling microscopy (STM), and non-contact atomic force microscopy (NC-AFM). The polarisation dependence of the SEXAFS data rules out the atop, bridge and upper three fold hollow sites, and are consistent with the lower three fold hollow predicted by theory, with a K-O distance of 2.63 ű0.03 Å. In addition to elements of the clean surface STM image, images of the K dosed surface contain wide dark rows running along the [001] direction. These are about 3 nm in length and centered along the dark bridging oxygen rows such that the two adjacent 5-fold coordinated Ti rows are not imaged. These presumably arise from Kinduced blocking of the tunneling current, either by charge transfer to Ti 3d states, or because there are no empty states of K near EF. The clustering of alkali metal sites is consistent with molecular dynamics simulations. In the absence of useful topographic information in STM, we turn to NC-AFM images of TiO2(110)1x1, where the [001] direction bright rows arise from bridging O atoms. In addition to straight rows characteristic of the clean surface, zigzag rows are observed on the Kdosed surface, presumably arising from K atoms alternately occupying sites on either side of a bridging O row, as predicted by theory.

11:20am SS3-TuM10 Electronic and Geometric Structure of Anatase TiO₂(101) and (001) Single Crystals, A.R. Kumarasinghe, W.R. Flavell, A.G. Thomas, A.K. Mallick, D. Tsoutsou, G.C. Smith, UMIST, UK, **R.L.** Stockbauer, Louisiana State University, M. Grätzel, R. Hengerer, Swiss Federal Institute of Technology

Scanning tunnelling microscopy (STM), low energy electron diffraction (LEED) and resonant photoemission studies on single crystal anatase TiO₂ (101) 1x1 and (001) 1x4 surfaces are reported. The (101) surface exhibits triangular shaped large terraces/steps leading to a saw tooth like structure. The steps are monatomic and are ~ 4Å high. Atomically resolved STM images show that the (101) surface has a bulk (1x1) termination and is unreconstructed. Defect states which are clearly observed in atomica lly resolved images can be created on clean (101) surfaces following sputter anneal cycles. Bright features are seen on atomic rows are most likely due to adsorbed molecules.¹ A defect peak is observed near 1 eV BE in UPS and is thought to arise from the loss of surface oxygen. This state is investigated using I/V measurements from scanning tunnelling spectroscopy (STS). Ti 3p-3d resonant photoemission of the surfaces are compared with earlier work from rutile TiO₂ (110) and features in the valence band at around 6 and 8 eV BE are assigned regions of weak and strong Ti-O hybridisation respectively. The defect peak is observed at around 1 eV BE for both surfaces following surface defect creation and is thought to arise from Ti³⁺. This peak can be removed by gentle heating in oxygen.² Constant initial state spectroscopy reveals differences in cation-anion hybridisation between the two surfaces, while repeated sputtering shows the (001) surface to be more resistant to the creation of O vacancies than the (101) face.

¹ W. Hebenstreit, N. Ruzycki, G. S. Herman, Y. Gao, and U. Diebold, Phys Rev B, 62, 24, (2000).
² A.G. Thomas, W.R. Flavell, A.R. Kumarasinghe. A.K. Mallick. D. Tsoutsou, G.C. Smith, R. L. Stockbauer, M. Grätzel and R. Hengerer (in preparation).

11:40am SS3-TuM11 Interactions of Oxygenated Hydrocarbons with Stoichiometric and Defective SrTiO₃(100) Surfaces: Role of Surface Structures and Defects, *L.-Q. Wang*, *S. Azad*, *K.F. Ferris*, *M.H. Engelhard*, Pacific Northwest National Laboratory

Molecular interactions on metal oxide surfaces are influenced by the surface structures and by the presence of surface defets. Adsorption and reactivity of oxygenated hydrocarbons on metal oxide surfaces have recently received considerable attention due t o the environmental concerns. In this study, we examined the interactions of a series of oxygenated hydrocarbons with stoichiometric and defective SrTiO₃(100) surfaces using x-ray photoelectron spectroscopy (XPS), temperature programmed desorption (TPD), and electronic structure calculations. The goal of this study is to have a fundamental understanding of the role of surface structures and defects on the adsorption and reactivity of these oxygenated hydrocarbons on metal oxide surfaces. SrTiO₃(100) was chosen as our model surface not

only because of its heterogeneous and photo-catalytic activities but also because investigation of oxygenated hydrocarbons on single crystal oxide surfaces is very rare. This presentation compares the interaction o f acetaldehyde with that of methanol, ethanol and formic acid on the same surface. Since aldehydes are weaker than carboxylic acids and stronger than alcohols, the comparison of their reactivity on the surface is very interesting. It was found that methan ol, ethanol and acetaldehyde adsorb molecularly whereas formic acid goes through dissociative adsorption on stoichiometric SrTiO₃(100) surface. As comparable with studies on other oxides such as TiO₂, adsorption and protonation of weaker acids such as methanol, ethanol and acetaldehyde are found to depend more on the surface structures than stronger acids such as formic acid and these results are in good agreement with our theoretical calculations. However, decomposition and redox reactions of methanol, ethanol, and acetaldehyde take place when surface defects are created by Ar⁺ sputtering. In addition, such surface defects change the reaction pathway for formic acid.

Tuesday Afternoon, November 5, 2002

Biomaterials

Room: C-201 - Session BI+SS-TuA

Molecular Recognition Surfaces

Moderator: M.J. Tarlov, National Institute of Standards and Technology

2:00pm BI+SS-TuA1 Medard W. Welch Award Address: The Biointerface Examined in Five Dimensions, *B.D. Ratner**, University of Washington INVITED

Twenty years ago, we had no such word as "biointerface." Now we use that word almost routinely to suggest surface-localized events between biological systems and solid surfaces (solids that vary in solidity from almost fluid to hard). To examine with a new perspective this burgeoning field, five facets of the biointerface will be explored. The five faces of the biointerface will be: temporally (and historically), spatially, molecularly, entrepreneurially and virtually (in computer space). Studies from our groups at the University of Washington and from others in the field will be presented. The talk will aim at defining the new field of the biointerface, relating it to "classical" surface science and highlighting opportunities.

2:40pm BI+SS-TuA3 "Smart" Biomolecular Conjugates, P.S. Stayton, A.S. Hoffman, N. Malmstadt, C. Hu, S. Kulkarni, University of Washington One of the hallmarks of biological systems is their ability to change important properties in response to environmental cues. We have been developing stimuli-responsive biomolecular materials for biosensors. diagnostics, affinity separations, microfluidic devices, and chip/array devices that exhibit responsiveness to specific environmental cues. For many of the diagnostic and sensor technologies that utilize biomolecular recognition properties, there is a continuing need for better control routes. Current environmental methods are relatively harsh and can lead to damage of biomolecules and cells. In addition, the environmental signals are typically large general solution changes and thus not targeted to selective recognition components. The stimuli-respon sive biomolecular materials allow reversible control over protein recognition properties by utilizing small changes in environmental conditions or signals. The "smart" polymers reversibly cycle between an extended and hydrophilic random coil, and a collap sed, hydrophobic state that is reduced in average volume by ca. 3fold. When the smart polymers are attached at defined protein side-chains, typically by genetically engineering cysteine or lysine residues, the polymers serve as sensors and actuators to c ontrol access of ligands or su bstrates to binding or catalytic sites. This general approach targets mild environmental signals to specific polymer-protein conjugates, and thus for example allows differential control of different antibodies in a device by using conjugated polymers that are sensitive to different signals (e.g. antibody 1 with pH, antibody 2 with temperature, antibody 3 with light). They can thus allow multiplexing control in complex mixtures, and are thus relevant to a number of different diagnostic and sensor formats.

3:00pm **BI+SS-TuA4 Molecular Recognition Mediated Fabrication of Protein Nanostructures by Dip-Pen Lithography**, J. Hyun, S.J. Ahn, W. Lee, S. Zauscher, A. Chilkoti, Duke University

The spatially controlled immobilization of biomolecules on solid surfaces at the nanometer length-scale is driven by the possibility of fabricating new sensors and actuators that will enable detection and actuation at the single molecule level. This communication describes how dip-pen nanolithography (DPN) in combination with the high-affinity streptavidinbiotin, protein-ligand system provides a simple and versatile "bottom-up" approach to create nanoscale biomolecular architectures in a step-wise fashion. This method involves the fabrication of nanoscale features by patterning a self-assembled monolayer (SAM) of a COOH-terminated alkanethiol on a gold substrate by DPN, followed by covalent immobilization of a high-affinity small-molecule ligand (biotin) onto the nanopatterned SAM and subsequent molecular recognition of its protein binding partner (streptavidin) from solution. We fabricated streptavidin nanostructures with lateral feature sizes in the range of 10-400 nm by this method, and have shown that the streptavidin nanopatterns can be used as a template to pattern biotinylated molecules of interest from solution. Because the binding of the final, target molecule is mediated by a highly specific molecular recognition interaction that occurs solely in the patterned region against a non-fouling background, this approach should allow

patterning a biomolecule of interest directly from complex mixtures such as cell lysate without purification, which is not possible with alternative DPN methods that involve physisorption or covalent conjugation.

3:20pm **BI+SS-TuA5** Threading DNA Through a Nanopore: Applications for Analyte Detection, J.J. Kasianowicz, S.E. Henrickson, B. Robertson, National Institute of Standards and Technology, H.H. Weetall, EPA, M. Misakian, National Institute of Standards and Technology INVITED

We recently demonstrated that single-stranded DNA (ssDNA) can be driven electrophoretically through a solitary Staphylococcus aureus alphahemolysin (alpha-HL) ion channel. In an effort to use this model system to understand DNA transport in biological systems, we show that the partitioning of ssDNA into the pore depends on the side to which the polymer is added and on the magnitude of the applied potential. Kramer's reaction rate theory was used to estimate both the height of the energy barrier for polymer translocation and the integral number of charges on ssDNA that interact with the barrier. In a related research effort, we illustrate three experimental results that suggest the interaction between polymers and a single nanopore can be used to quantitate analyte concentration and type. First, the probability that ssDNA enters the alpha-HL channel is proportional to the polymer concentration. Second, analyte binding to sites on ssDNA predictably alters the ability of the polymer to thread through the pore. Third, different ssDNA homopolymers induce current blockade patterns that are characteristic of the nucleotide type. We compare this method to other channel-based detection schemes. Finally, we show that modified polynucleotides might prove useful as "molecular rulers" for probing the structure of nanopores.

4:00pm **BI+SS-TuA7 Novel Immunosensor Interfaces based on Mixed Self-Assembled Monolayers of Thiols on Gold, F. Frederix**, M. Boesmans, K. Bonroy, W. Laureyn, A. Campitelli, IMEC, Belgium, M.A. Abramov, W. Dehaen, G. Maes, KULeuven, Belgium

The two components that make up a biosensor are the biological recognition layer, which selectively binds the analyte, and the transducer which translates this recognition event into an electrical signal. The increasing miniaturization of biosensor transducers (and thus of their active areas) and the demand for sensitivity, require a fully evaluated and optimized covalent immobilization of antibodies. Our research is therefore not only focusing on the transducer but also on the biological interface. This biological recognition layer mainly determines the specificity, stability, reproducibility, and durability of the biosensor as a whole. Our strategy is to achieve the above-mentioned properties based on mixed Self-Assembled Monolayers on gold. The realization of a biological recognition interface encompasses various aspects. Cleanliness and structural properties of the gold surface are very important for perfect SAM formation and were therefore optimized. Novel thiols able to couple antibodies or to mitigate non-specific adsorption were synthesized and evaluated, along with new molecules for blocking. The mixed monolayer formation of these novel thiols was characterized using contact angle measurements, XPS, cyclic voltammetry, and GA-FTIR. The immobilization of proteins on mixed SAMs is the most important step in the realization of immunosensors because it determines the activity of the antibodies and therefore the sensitivity. Random and orientated immobilizations of (chemically modified) antibodies on mixed monolayers of thiols were compared using Surface Plasmon Resonance. The enhanced sensitivity (< 0,1 ng/mL) and selectivity (no non-specific adsorption) were compared to commercially available biological recognition layers. In summary, we will show the importance of the biological recognition layer for the global performance of a biosensor and how the sensitivity can be drastically enhanced by modifications on the biological interface of an immunosensor.

4:20pm **BI+SS-TuA8 Electrostatic and Fluorescence Sensing of DNA Hybridization at Electrode Surfaces**, *R.M. Georgiadis*, *J. Wang, L.K. Wolf, A.W. Peterson*, Boston University

Current microarray technologies, based on specific probe-target hybridizations, often suffer from nonspecific surface interactions. In addition, for surface immobilized probes, thermodynamic equilibrium conditions may not be reached without excessively long incubation times and hybridization may be kinetically or sterically inaccessible for some probe sequences or for some surface probe densities. In previous work on perfectly matched duplexes, we have shown that probe density is a controlling factor for DNA hybridization at surfaces. Here, we expand our studies to investigate probe density effects for mismatched sequence or targets that access different binding locations on the immobilized probe. To improve mismatched hybrid discrimination we detect different dissociation

* Medard W. Welch Award Winner

profiles for matched and mismatched 25-mer targets from surfaceimmobilized probes in the presence of an applied repulsive electrostatic field and present denaturation profiles for surface-bound hybrids obtained by continuously varying the applied electrostatic surface field. Finally, we examine the immobilization and hybridization of covalently-bound molecular beacons on gold surfaces using surface plasmon resonance (SPR) spectroscopy and fluorescence spectroscopy.

4:40pm **BI+SS-TuA9** Characterization of DNA on Gold: A **Quantitative Surface Science Approach**, *D.Y. Petrovykh*, University of Maryland - College Park / NRL, *H. Kimura-Suda, M.J. Tarlov*, National Institute of Standards and Technology, *L.J. Whitman*, Naval Research Laboratory

Covalent attachment of thiolated DNA onto gold surfaces is one of the most common methods for immobilizing aqueous DNA onto solid substrates. The formation of the DNA film in this case is thought to closely resemble that of alkanethiol self-assembled monolayers (SAMs). DNA films in modern applications, e.g. DNA microarrays, are < 10 nm thick with submonolayer surface coverage, which means that the traditional surface characterization techniques can be employed to complement biochemical analysis. We are applying XPS, FTIR, and ellipsometry to systematically quantify the chemical structure and coverage of self-assembled singlestranded DNA (ssDNA) films. Thymine (T) has the simplest structure of the four nucleotide bases: a single ring with two N atoms. Moreover, the environment of the two N atoms is so similar that the resulting XPS peak is consistent with a single N1s state in a polymer-like material. Backbone P atoms produce a base-independent single P2p peak. N and P are not subject to significant contamination, so the peak intensities can be used to estimate the coverage of immobilized DNA. N1s chemical shifts together with the base-dependent N/P ratio can confirm the presence of specific polynucleotides on the surface. The coverage determined by XPS is linearly correlated with base-specific IR features and agrees with absolute values obtained from radiolabeling measurements. We will also discuss how the XPS and IR spectra of dT-polynucleotide films can provide information about other basic properties of ssDNA films, such as uniformity and orientation, as well as issues of damage, degradation and contamination.

5:00pm **BI+SS-TuA10** Antibacterial Coatings of Immobilised Furanones, *H.J. Griesser*, *S. Al-Bataineh*, University of South Australia, *B.W. Muir, H. Thissen, M. Willcox*, CRC for Eye Research and Technology, Australia

The formation of bacterial biofilms and subsequent infections can cause serious complications in the use of biomedical devices such as catheters, and broadly effective technology is lacking. Nature has, however, addressed very effectively the problem of microbial colonisation of surfaces. For instance, the red alga Delisea pulchra secretes brominated furanones that prevent its microbial colonisation. These compounds are thought to interfere with bacterial quorum sensing by their chemical similarity with homoserine lactone, an important bacterial regulator. We have immobilised various furanones onto synthetic surfaces and tested the efficiency of such coatings in bacterial colonisation assays. A broadly applicable covalent immobilisation strategy involves nitrene chemistry, with light-activated reaction between furanones and azido aniline coupled onto a surface hydrogel interlayer. This allows coupling of furanones without reactive substituents but is non-selective with regard to molecular orientation and location of attachment. Other strategies require functionalised furanones, for example reaction between a hydroxylated furanones and surface isocyanate groups; such furanones can be more difficult to synthesize. Work to date has produced substantial reductions in bacterial colonisation, but not to the high degree required in clinical applications. Investigations now focus on the interactive effects of furanone molecular composition, immobilisation chemistry and surface density. An interesting finding is that these compounds are effective when surface immobilised although the classical microbiological model of homoserine lactone action requires entry into the microbial interior. This dichotomy calls for detailed surface characterisation of furanone coatings, including study of whether the entire population of surface-bound molecules is indeed covalently linked and thus non-diffusible and acting via a different mechanism to stifle bacterial colonisation.

Organic Films and Devices Room: C-102 - Session OF+SS+EL+SC-TuA

Organic Molecular Films

Moderator: H. Fairbrother, Johns Hopkins University

2:00pm OF+SS+EL+SC-TuA1 Reactivity of Polymers Containing Nitrogen and Oxygen Functional Groups with Vapor Phase Metal Atoms, A.J. Wagner, G. Wolfe, D.H. Fairbrother, The Johns Hopkins University

The surface reactions during the initial stages of polymer metallization are crucial in determining bonding and adhesive characteristics with native and plasma treated polymers. In this study, we have compared the reactivity of different nitrogen and oxygen containing functional groups with a variety of vapor phase metal atoms during the initial stages of metallization. The reactivity of different nitrogen containing functional groups during the vapor deposition of Ti, Fe, Ni, Cu and Au on Nylon 6, containing an amide group (-NH-(C=O)-and nitrogen implanted Poly(ethylene) (N-PE) containing a mixture of C-N, C=N and CN groups was studied. In addition, the reactivity of vapor phase metal atoms with specific functional groups was also investigated using a nitrile (CN) terminated self-assembled monolayer (CN-SAM). For each of the metals studied except Au reaction with Nylon 6 and N-PE resulted in the formation of the metal-nitride (MN), although the extent of reaction increased in the order Ti > Fe > Ni ~ Cu, scaling with the MN bond strength. Experimental evidence, however, indicated that the different nitrogen containing functional groups present in the nitrogen-modified PE were not equally reactive. Ti and Fe also reacted with the C=O functional group in Nylon 6 to form their respective oxides while Cu, Ni and Au were unreactive with the C=O functional group. Metal nitride formation was also observed during evaporation of Ti and Fe on the CN-SAM although Cu and Au were unreactive towards the CN functional group. In contrast, metal carbide production was only evidenced during reactions with Ti. Results from this investigation will be interpreted in terms of the relative bond strengths associated with specific functional groups within the polymer and potential product species (e.g. metal oxide, nitrides).

2:20pm OF+SS+EL+SC-TuA2 A New Crystalline Form of Pentacene: pi-stacked Thin Films Grown on Au(111), J. Kang, X.-Y. Zhu, University of Minnesota

The recent demonstration of pentacene and related molecules in highmobility field effect transistors (FETs), including superconducting FETs, has attracted great interest in this class of organic semiconductors. Carrier mobility is known to depend intimately on crystalline quality. In order to establish a molecular level understanding of structure-property relationship, we have carried out a scanning tunneling microscopy (STM) and spectroscopy (STS) study of the growth of crystalline pentacene thin films on Au (111). The use of high bias voltage (~ 5 V) and low tunneling current ($\sim 1pA$) has enabled us to image, with molecular resolution, the growth of a new crystalline phase of pentacene well beyond the first a few layers. High resolution imaging shows that pentacene molecules form a pi-stacked crystalline phase with their long-axis parallel to the surface. This is attributed to the strong molecule-surface interaction, which seeds the growth of this new crystalline phase.

2:40pm OF+SS+EL+SC-TuA3 Vapor Deposition and Polymerization of Low-k Polycyanurate Films, J.N. Russell, Jr., V.J. Bellitto, B. Bartlett, MJ Brooks, P.G. Santangelo, A.W. Snow, Naval Research Laboratory INVITED

Future microelectronics will require advanced materials and processes for smaller, faster and more robust devices. Polymers address these needs and range from ultra-low permittivity materials to molecular semiconductors. Developing and understanding solventless deposition processes such as vapor deposition polymerization is important for producing conformal, voidless polymer films. One class of low-k polymers, polycyanurates, shows promise as a vapor depositable material. Yet little is known about the surface chemistry of the cyanate functionality and the conditions required for surface polymerization. Initially the surface chemistry of key functionalities in the monomer and polymer are examined using model compounds such as phenyl cyanate and triazine on Al(111). Aluminum was chosen because it is used for interconnects in microelectronics. Then, the in situ vacuum deposition and polymerization chemistry of NCO-CH2(CF2)6 CH2-OCN (F6Cy) is studied on Al, Cu, and Si surfaces. The vapor deposited F6Cy monomer film undergoes a photo-induced cyclotrimerization process to form cross-linked cyanurate networks with a permittivity of 2.1 at 1 GHz.

Optical lithography is a common technique for the formation of electronic devices on semiconductor substrates. Here we show an analogous technique that allows the introduction of a reactive functional group (-COCl) onto an alkylated Si substrate, or onto any substrate that contains C-H groups. The importance of the -COCl group stems from its high reactivity with amino and hydroxyl groups. Our new method consists of exposing a C-H containing surface to a gaseous mixture of N2 and oxalyl chloride ((COCl)2) and then illuminating with 35 nm light. The UV photons form free radicals from the oxalyl chloride that then react with the C-H containing surface. We have shown using wetting, XPS, elipsometry and FT-IR spectroscopies that we have been able to form acid chloride functional groups on surfaces. By using simple optical masks we have shown that this functionalization occurs only where the sample is exposed to light. The key step to understanding the reaction mechanism for the surface reaction is understanding the formation and subsequent reaction of the radicals formed from the oxalyl chloride. Previous liquid phase reaction studies of oxalyl chloride with adamantane led to the suggestion that at 266 Cl is the primary radical formed, while at 355 nm the primary radical is the COCl radical. We have looked at the formation of radicals as a function of wavelength to analyze dissociation mechanism, and product energy distributions as well as the effect of pressure on radical formation. The minimum feature size which can be made using this method is given by the diffusion length of the radical. Thus the quenching must be understood and optimized to have controlled patterning of surfaces.

3:40pm OF+SS+EL+SC-TuA6 Characterization of Ultrathin Organic Films via Near-edge X-ray Absorption Fine Structure Spectroscopy, T.M. Willey, University of California Davis and Lawrence Livermore National Laboratory, A.L. Vance, T. van Buuren, C. Bostedt, A.J. Nelson, L.J. Terminello, Lawrence Livermore National Laboratory, C.S. Fadley, University of California Davis and Lawrence Berkeley National Laboratory Self-assembled monolayers (SAMs) and other thiol compounds adsorbed on Au(111) surfaces have become increasingly important for achieving surface attachment and orientation of complex molecules. Surface-attached molecular species containing catenanes and rotaxanes promise to play a vital role in achieving molecular-scale electronics and other devices.¹ Only through a rigorous understanding of the structure and properties of such molecular monolayer species can a rational synthesis of these hybrid materials be realized. Orientation of chemical bonds and thus the orientation of molecules can be precisely determined with near-edge x-ray absorption fine structure (NEXAFS) spectroscopy. Here, we present NEXAFS results on the configuration of surface-attached fundamental building-blocks of such systems, including a simple surface-attached rotaxane and its constituents. This rotaxane consists of a crown ether ring, threaded by a molecule bound to the gold at one end and providing an athracene stopper at the other.² Investigating films of the stopper molecule only vs. the complete rotaxane we confirm the presence of the crown ether in the complete molecule. We present the orientation of the anthracene stopper and crown ether ring with respect to the surface by deconvoluting their respective features in the NEXAFS.

Acknowledgements: This work is supported by the U.S. Department of Energy, BES Materials Sciences under contract W7405-ENG-48, LLNL; at the ALS under contract number DE-AC03-76SF00098 at LBNL; and at the SSRL under contract number DE-AC03-76SF00515 at SLAC. ¹ Collier et al., Science 289, 1172-5

² Kolchinski et al., Chem. Commun., 1998, 1437-8

4:00pm **OF+SS+EL+SC-TuA7** Interfaces with Evaporated Short Chain Polyaniline, B. Xu*, A.N. Caruso, M. Bai, Y. Ovchenkov, S. Ducharme, B. Doudin, P.A. Dowben, University of Nebraska-Lincoln

The interface properties of evaporated short chain polyaniline (PANI) were investigated by X-ray photoemission spectroscopy (XPS), inverse photoemission spectroscopy (IPES), as well as angle integrated photoemission spectroscopy (UPS). With sodium doping, the valence bands, conduction bands as well as the characteristic core levels show consistent shifts to the higher binding energy. Sodium, as an electron donor, when added to the polyaniline system, results in increased electron populations in the polyaniline bands --- effectively filling the almost completely filled band. In the case of iodine doping, all the states shifted to lower binding energy. Iodine, as an electron acceptor, effectively depletes the electron population in the occupied bands polyaniline. There is no abrupt interface formed between sodium or iodine and polyaniline, as demonstrated by the angle-resolved XPS. By comparison, the interface between polyaniline and another poly(vinylidene fluoride with trifluoroethylene) copolymer (PVDF-TrFE) is quite abrupt. A PN diode

was made by evaporating PANI (p type) on the top of PVDF-TrFE (n type). The results presented here should apply to the problems associated with improving heterojunction polymer devices.

4:20pm **OF+SS+EL+SC-TuA8** Controlled p-Doping of Organic Molecular Films, W. Gao, A. Kahn, Princeton University

We investigate the controlled electrical p-doping of the hole-transport organic molecular material α -NPD with the strong electron acceptor tetrafluoro-tetracyano-quinodimethane (F4-TCNQ) using ultraviolet and inverse photoelectron spectroscopies (UPS/IPES), and in-situ I-V measurements. We previously examined p-doping of ZnPc co-evaporated with F4-TCNQ,1 and found an excellent energy match between the ionization energy (IE) of ZnPc (5.28eV) and the electron affinity (EA) of F₄-TCNQ (5.24eV), demonstrating host HOMO-to-guest LUMO charge transfer. The ZnPc thickness dependence of I-V data further demonstrated a 7 orders of magnitude increase in hole current injected from Au due to tunneling through the doping-induced narrow depletion region at the metal/organic interface.² In the present study, we show that $\alpha\text{-NPD}$ (IE=5.52eV) is also efficiently doped with E4-TCNQ. The hole injection current increases by almost 5 orders of magnitude when only the first 80Å of α -NPD away from the metal/organic interface is doped, and increases by another factor of 10 when the entire organic film is uniformly doped. However, the doping-induced movement of EF toward the HOMO appears to be more restricted than in ZnPc. Having excluded extrinsic effects like surface photovoltage, we propose that the substantial (~0.2 eV) ionizationinduced relaxation of molecular energy levels moves the "doped" α -NPD HOMO upwards, and thus pins E_F deeper into the gap than for ZnPc, which is a planar molecule with a negligible relaxation energy (< 0.05 eV). This interpretation is further confirmed with UPS study of the host material growth on a film of the dopant molecules. We also show that molecular level alignment at organic/organic interfaces is controllable by dopinginduced dipole. Work supported by the NSF (DMR-0097133).

¹ W. Gao and A. Kahn, Appl. Phys. Lett., 79, 4040 (2001)

² W. Gao and A. Kahn, Organic Electronics (in press).

4:40pm **OF+SS+EL+SC-TuA9** Processable Optically Transparent Thin Films of Conducting Polymers, B.D. Martin, N. Nikolov, R. Shashidhar, Naval Research Laboratory

A major problem in the area of electronically conducting polymers is that attempts to enhance their electrical conductivity by adding ionic dopants are always accompanied by a decrease of optical transparency. In this study we show how molecular self-assembly of small carbohydrate molecules can decouple the optical transparency and electrical conductance of conducting polymer films. When a carbohydrate such as glycerol, which is essentially a non-ionic hydrogen bonding dopant, is added to a commercially available conducting polymer suspension (Baytron P), the carbohydrate forms an intercalated, hydrogen bonded sandwich between the ionic pairs of the conducting oligomer unit and its supporting polymer suprastructure. This results in a pronounced increase of the distance between the ion pairs, and hence, to decreased electrostatic interaction. As a consequence there is an enhanced mobility of the ions and hence an increased conductivity without an accompanying increase in optical absorption. This behavior, which is in striking contrast to the normally observed trends in conducting polymers doped with traditional ionic dopants, is very important to the development of plastic liquid crystal displays (LCDs) and organic light emitting diode (OLED) displays.

5:00pm **OF+SS+EL+SC-TuA10 Optical Properties of Ordered Ultrathin Films of PTCDA**, *R. Nitsche*, *H. Proehl, S. Mannsfeld, T. Dienel, T. Fritz*, TU Dresden, Germany

Research activity on molecular solids has gathered pace in recent years as these materials have a wide range of interesting properties, emerging industrial interest with real applications at the horizon, and possible future applications that will enable electronics to move into the nanoscale. High quality samples, precise structural data, and a detailed understanding of the physical properties is essential, with special emphasis on thin films and interfaces. In this respect, the use of highly controlled growth techniques like Organic Molecular Beam Epitaxy (OMBE) is becoming more and more important, aiming at high quality thin films with controlled crystal structure and morphology, therefore displaying well defined physical properties. In our contribution we will discuss the special optical properties of ultrathin films of an archetypal organic material, namely PTCDA (perylene-3,4,9,10tetracarboxylic-3,4,9,10-dianhydride). Highly ordered organic thin films on a gold single crystal have been prepared by means of OMBE with submonolayer to multilayer coverage. All films were structurally characterized by combining Scanning Tunneling Microscopy (STM) with Low Energy Electron Diffraction (LEED), clearly indicating epitaxial growth in the point-on-line mode. Differential Reflection Spectroscopy (DRS, a variant of reflection absorption spectroscopy) both ex situ and in

situ has been applied to measure the optical characteristics of those films. The results clearly show that ultrathin layers have different optical properties as compared to thicker films, which in turn match the results known for long from polycrystalline samples. The results are further compared to thin films grown on mica to discuss the influence of different substrates.

Surface Science Room: C-108 - Session SS1-TuA

Ultrafast Phenomena & Dynamics at Surfaces

Moderator: B.D. Kay, Pacific Northwest National Laboratory

2:00pm SS1-TuA1 Electron Dynamics at Surfaces, T. Fauster, University of Erlangen, Germany INVITED

Two-photon photoelectron spectroscopy permits the study of the time evolution of electronic states at surfaces with femtosecond resolution. Image-potential states at metal surfaces provide examples for various fundamental processes in electron dynamics: exponential decay, dephasing, quantum beats and interband scattering. At semiconductor surfaces the relevant time scales can be of the order of picoseconds. For dangling bond states on Si(100) intraband and interband scattering lead to a delayed buildup and slow decay of the electron population.

2:40pm SS1-TuA3 Observation of Isotope Effect in Femtosecond Laser-Induced Desorption of O₂/Pd(111), D.P. Quinn, T.F. Heinz, Columbia University

A significantly higher yield for femtosecond laser-induced desorption is observed for $^{16}O_2$ than for $^{18}O_2$ in the saturated co-adsorbed $^{16}O_2$ + $^{18}O_2/Pd(111)$ system. Similar isotope effects 1 have been reported for conventional photochemistry and electron-stimulated desorption. Such isotope effects have also been used to examine reaction mechanisms for femtosecond laser-induced surface processes. $^{2.3}$ In the present case, investigations of the $O_2/Pd(111)$ system have demonstrated that the desorption process is mediated by the substrate electronic excitations induced by the femtosecond laser pulses. The observation of a significant isotope effect is compatible with such an electronic mechanism, but implies that the adsorbed molecules are out of equilibrium with the electronic degree of freedom of the substrate during the desorption process. We consider this phenomenon in the context of both DIMET⁴ and electronic friction models of the adsorbate-substrate coupling.

¹ T.E. Madey et al., J. Chem. Phys. 52, 5215 (1970).

² R.J. Finley et al., Chem. Phys. Lett. 274, 499 (1997).
³ M. Bonn et al., Science 285, 1042 (1999).

⁴ J.A. Misewich et al., Phys. Rev. Lett. 68, 3737 (1992).

3:00pm SS1-TuA4 Time Resolved Femtosecond Laser Desorption from Ionic Crystals, W.P. Hess, A.G. Joly, K.M. Beck, Pacific Northwest National Laboratory, J.T. Dickinson, Washington State University

We have used femtosecond laser pulse pairs to measure the positive ion yield, from wide band-gap single crystals, as a function of time-delay between pulses. The two-pulse technique allows direct observation of solid state and surface dynamics on a femtosecond timescale. We find the ion yield, from 265 nm irradiated MgO, KBr, and LiF, depends critically on the time delay between pulses. For example, the Mg+ desorption yield displays three distinct features; a coherence peak, followed by rise, and decay features. In contrast, the yield of K+ and Li+ from KBr and LiF display only the coherence peak and picosecond decay features. The observed thresholds suggest, that although the ion desorption mechanism is dominated by defect photoabsorption, significant electron-hole pair production may contribute to the desorption mechanism following femtosecond excitation. The picosecond lifetimes correspond well with known electron-hole lifetimes in each material. We hypothesize that fs laser desorption may be related to the creation of electron hole pairs. By determining the ultrafast time-dependence we hope to reveal details of the ion desorption mechanism.

3:20pm SS1-TuA5 On the Detection of Chemically-Induced Hot Electrons in Surface Processes: from X-ray Edges to Schottky Barriers, *J.W. Gadzuk*, National Institute of Standards and Technology

The potential involvement of electron-hole pair excitations in atomic/molecular processes such as sticking/adsorption/dissociation at metal surfaces has long been debated, particularly by those previously involved with similar issues in electron spectroscopies of localized core levels in solids. Of special relevance here are the fundamental studies of Müller-Hartmann et al.¹ on the dynamic response of Fermi systems to transient localized perturbations as subsequently applied to problems in non-adiabatic surface dynamics.² Recent experiments have detected hot electrons produced when various gases were adsorbed on a thin metal film that formed a Schottky barrier with an n-type Si substrate upon which the film was deposited.³ Drawing on analogies with electron-hole pair shakeup in spectroscopic processes which lead to the xray edge singularity, a theoretical model for the electronically non-adiabatic effects is presented here that accounts for the observed initial hot electron production, roughly 10^{-3} - 10^{-2} electrons per incident strongly-interacting adsorbate such as O, H, and NO₂ on Ag. Since the fundamental physical content of the x-ray edge model is the Fermi-level phase shift associated with the localized perturbation and the rate at which it is switched on, straightforward connections with friction-based models⁴ are easily established in an intuitively satisfying way.

¹E. Müller-Hartmann, T. V. Ramakrishnan, and G. Toulouse, Phys.Rev.B 3,1102(1971).
²J. W. Gadzuk and H. Metiu, Phys.Rev.B 22,2603(1980); ibid. 24,1866(1981).

3B. Gergen, H. Nienhaus, W. H. Weinherg, and E. W. McFarland, Science 294,2521(2001); H. Nienhaus, Surface Sci. Repts. 45,1(2002).

⁴K. Schönhammer and O. Gunnarsson, Phys. Rev.B 27,5113(1983).

3:40pm SS1-TuA6 Kinetics and Dynamics of CO Oxidation on Oxygen Precovered Gold Nanoclusters Supported on Titania, C.B. Mullins, T.S. Kim, J. Stiehl, C.T. Reeves, R.J. Meyer, University of Texas at Austin INVITED

Studies of the kinetics and dynamics of carbon monoxide oxidation have been carried out on a titania single crystal surface with a (110) orientation and decorated with gold nanoclusters. The investigations employed molecular beam surface scattering techniques as well as thermal desorption mass spectrometry and Auger electron spectroscopy. An rf-powered plasma jet source was used to create a beam of atomic oxygen which was used to populate the surface with oxygen adatoms. After the surface was prepared a molecular beam of carbon monoxide was directed at the surface in order to study oxidation of CO as a function of oxygen coverage and surface temperature. There is a maximum in the reactivity as a function of oxygen coverage and surface temperature. Competing processes, such as adsorption and desorption, will be discussed as well as the effect of adsorbed oxygen upon the surface reactivity of the gold nanoclusters.

4:20pm SS1-TuA8 O₂ and NO Island Formation on Al(111), J.Z. Sexton, A.C. Kummel, University of California, San Diego

The oxidation of aluminium is a fundamentally important process that is not well understood. Scanning tunneling microscopy was employed to study the mechanisms for the oxidation of Al(111) with thermal Q and NO at medium to high oxygen coverage regime (20-50% ML). The STM-UHV studies provided the following observations: 1) Oxygen islands on the Al(111) surface, prepared with thermal oxygen, are elongated and noncompact. 2) Al(111) step edges change shape upon Q chemisorption to relieve strain from oxide islands. 3) Islands produced with thermal nitric oxide (NO) produce round, compact islands in contrast to the non-compact, elongated islands formed with thermal oxygen. 4) Above a critical oxygen coverage (30-40% ML), Al-atom protrusions appear within oxygen islands. These protrusions increase with increasing coverage and indicate the onset of the phase transition from isolated chemisorbed oxygen islands to an ionic Al₂ O₃ amorphous layer. 5) Pre-existing oxygen features can locally enhance the sticking coefficient. This local enhancement of oxygen adsorption on the Al(111) surface is likely due to a perturbation in the local electronic structure surrounding an oxygen feature. The enhanced O₂ chemisorption results from lattice strain coupled to a work-function change in the proximity of pre-existing oxygen islands. The lattice strain at high oxygen coverages eventually yields the phase transition to amorphous Al₂ O₃.

5:00pm SS1-TuA10 Adsorption Dynamics and Desorption Kinetics of Argon and Methane on MgO(100), Z. Dohnálek, R.S. Smith, B.D. Kay, Pacific Northwest National Laboratory

The adsorption dynamics and desorption kinetics of Ar and CH_4 on MgO(100) are studied using a combination of molecular beam scattering and temperature programmed desorption (TPD). Both Ar and CH_4 exhibit an initial trapping probability that de creases dramatically with increasing kinetic energy and is independent of incident angle indicating adsorption is a barrier-less process obeying total energy scaling. The trapping probability for both adsorbates increases roughly linearly with the increa s ing coverage in the first layer. Such behavior can be described by a simple model involving constant but different trapping probabilities on clean and adsorbate covered MgO(100) with fast intra-layer diffusion leading to preferential filling of the bar e M gO(100). Analogous behavior is observed for trapping on the second and third layers and indicates layer-by-layer growth of the adsorbate overlayer with layer dependent trapping probabilities. Analysis of the TPD spectra yields desorption energies of 8.5

a nd 13 kJ/mole for Ar and CH₄, respectively in agreement with previous measurements and theoretical calculations. The total energy scaling observed for the initial trapping of Ar and CH₄ on MgO(100) is in sharp contrast with the normal en er g y s caling previously observed for these species on Pt(111). These differences indicate that the adsorbate-substrate interaction is laterally smooth on Pt(111) and highly-corrugated on MgO(100). Pacific Northwest National Laboratory is a multiprogram National Laboratory operated for the Department of Energy by Battelle under Contract DE-AC06-76RLO 1830.

Surface Science Room: C-110 - Session SS2-TuA

Atmospheric Surface Chemistry

Moderator: C.H.F. Peden, Pacific Northwest National Laboratory

2:00pm SS2-TuA1 Surface Chemistry of Size-Selected Soot Nano-Aerosol Particles, J.T. Roberts, K.K. Higgins, A. Wensmann, M.R. Zachariah, University of Minnesota

A method has been developed to conduct surface chemistry and extract surface kinetic rates from size-selected aerosol nanoparticles. The measurements encompass broad ranges of particle size, phase, and composition. Results will be presented on the growth and oxidation of soot nanoparticles (particle radius between 10 and 40 nm). The particles are investigated for changes in surface area using on-line nanoparticle characterization instrumentation. Experiments emphasize two classes of reactive conditions: h igh temperature oxidation by O_z and NO_x , and room temperature addition of hydrocarbons. We believe these to be the first measurements of soot oxidation and condensation kinetics that have been conducted on size-selected particles. Th e result s are important because soot emission from combustion sources is dictated by the competing surfaces processes of growth and oxidation. More generally, the results represent one of the first kinetic and mechanistic studies of gas-phase nanoparticle reactivity.

2:20pm SS2-TuA2 Uptake and Reaction of Ozone on NaCl and Bromide-doped NaCl, J.N. Newberg, J.C. Hemminger, University of California, Irvine

Sea-salt significantly affects the chemistry and composition of the marine boundary layer. For example, gas-phase bromine compounds resulting from sea-salt aerosol particles and sea ice have been implicated in tropospheric ozone depletion events in the arctic spring time, as well as in the deposition of mercury from the atmosphere in the marine troposphere. While there have been significant advances in our knowledge of gas-phase and bulk aqueous-phase reactions of sea-salt, little is known about the fundamental surface interactions of sea-salt with important gas-phase constituents (e.g., O₃ and OH) at the air-particle interface. This is due in part to the paucity of conventional atmospheric chemistry methods with the ability to monitor surface reactions on a fundamental molecular-level. Using X-ray photoelectron spectroscopy (XPS), we monitored the surface chemistry of solid sea-salt substrates upon exposure to ozone. Past studies under steadystate conditions indicate that O3 is essentially unreactive towards dry and aqueous NaCl in the dark. Our results show unequivocally that under UHV conditions and continuous exposure to O₃, oxygen uptake occurs on NaCl. For NaCl doped with bromide, an increase in oxygen uptake was observed. Moreover, as the amount of doped bromide increased, the total uptake of oxygen increased. Based on our experimental results and ab initio calculations, it is suggested that the products of the surface reaction of O3 on dry bromide-doped NaCl yield ClO and BrO. Neither of these species has been reported in the XPS literature. Exposing the bromide-doped NaCl samples to water vapor leads to the segregation of Br to the salt surface. Exposure of this surface enriched Br to ozone leads to enhanced uptake of oxygen, likely in the form of BrO.

2:40pm SS2-TuA3 XPS Study on Surface Segregation of Bromide in Bromide-doped NaCl Crystals by Water Vapor Exposure, K. Inazu, J.T. Newberg, J.C. Hemminger, University of California, Irvine

Drastic decrease of trophospheric ozone in the Arctic at polar spring has been observed accompanying an increase of particulate bromide.¹ The chain reactions involving sea salt bromide were proposed to be responsible for the ozone depletion.² While current model calculations for the tropospheric ozone depletion have applied the available abundance of bromide for the atmospheric reactions estimated from the bromide concentration in bulk sea water, the availability of bromide in sea salt particles must be reevaluated if the selective surface enrichment of bromide takes place on sea salt particles. In order to verify the feasibility of the surface bromide enrichment in sea salt particles, water-vapor exposure experiments were conducted for bromide-doped NaCl (100) single crystals with different bromide concentration using X-ray photoelectron spectroscopy and scanning electron microscopy. Segregation of bromide to the surface of the NaCl crystals uniformly doped with bromide at Br/Cl ratio below the level in sea water was observed even when the crystals were exposed to water vapor at lower pressure than the deliquescence points of NaCl and NaBr. The initial segregation rate of bromide was dependent on water vapor pressure and steeply increased when the employed water vapor pressure approached the deliquescence point of NaBr. At the initial stage of the segregation, segregated NaBr crystallites were highly dispersed on the crystal with ca. 0.2 µm on a side. As segregation proceeded by further water vapor exposure, the NaBr crystallites fused each other to achieve threedimensional growth similarly to the case of water-induced reorganization of the ultra thin nitrate film formed by the reaction of NaCl single crystal with nitric acid.3

¹L. A. Barrie et al., Nature, 334, 138(1988).

²K. W. Oum et al., Geophys. Res. Lett., 25, 3923-3926(1998).

³J. C. Hemminger, Int. Rev. Phys. Chem., 18, 387(1999).

3:00pm SS2-TuA4 Chemical Reactions Induced by Ionizing and Electron-beam Irradiation in Organohalide/Water (Ice) Films, C.C. Perry, Johns Hopkins University, N.S. Faradzhev, Rutgers, The State University of New Jersey, A.J. Wagner, C. Vecitis, G. Wolfe, D.H. Fairborther, Johns Hopkins University, T.E. Madey, Rutgers, The State University of New Jersey

We report on the reactions of organohalides (CCl₄, CHCl₃, CH₂Cl₂, PhCl, CF₂Cl₂) in water (ice) films (~50 nm) at ~100K under the influence of ionizing and electron beam irradiation using reflection-absorption infrared spectroscopy, Xray photoelectron spectroscopy and mass spectrometry. The final neutral gas phase products of electron-stimulated degradation of chlorocarbons CCl₄, CHCl₃, CH₂Cl₂, and PhCl, were identified as CO₂, CO, and HCl. Product species identified in the film include a thermally stable partially chlorinated $(C_x Cl_y)$ overlayer, CO_2 , H_3O^+ and Cl^- . Phosgene $(COCl_2)$ was also observed except in the case of PhCl. For CCl_4/H_2O mixtures, the product branching distributions are sensitive to the films initial H_0/CCl_4 composition. In CCl_4 rich films, the dominant reaction products in the film were C_2Cl_4 and the C_xCl_y overlayer; CO was the dominant gas phase species. In H₂O rich films, CO₂ becomes dominant at the expense of C₂Cl₄ and C_xCl_y species. For films concentrated with CCl₄ chlorine is lost principally into the gas phase while in water rich films chlorine is partitioned principally as HCl, producing $\mathrm{H}\mathrm{O}^{\scriptscriptstyle +}$ and Cl . In contrast, Freon-12 (CF₂Cl₂) / water mixtures subject to ebeam or X-ray irradiation produced carbonyl fluoride (COF₂), a major source of fluorine in the stratosphere. $H_3O^{\scriptscriptstyle +}$ and CO_2 were also detected as stable reaction products as well as Cl and F, consistent with a recent study of negative ion yields in ESD from CF2Cl2/water films. The decomposition rate of different organohalides in ice film under electron beam irradiation varied dramatically (~100): Freon being much more sensitive to electron exposure than the chlorocarbons.

3:20pm SS2-TuA5 Heterogeneous Uptake of HNO₃ in the Troposphere: From Sand to Cirrus, *M.A. Tolbert*, University of Colorado, Boulder INVITED

One longstanding issue in tropospheric chemistry is the observation that the ratio of HNO₃/NO_x often shows atmospheric values two to ten times lower than those modeled. This implies either a missing sink of HNO₃, a missing source of NO_x species, or a missing conversion from HNO₃ to NO_x in the models. There are several dominant particle types in the free troposphere that may provide surfaces for loss of HNO₃. In this paper, we present laboratory studies of HNO₃ uptake on two systems modeling global tropospheric particulate: ice surfaces representative of cirrus clouds and mineral particles representative of atmospheric dust. The results from current laboratory experiments will be discussed and, where possible, comparisons with recent atmospheric data will be presented.

4:00pm SS2-TuA7 Surface Chemistry of Oxide and Carbonate Particles in the Atmosphere, V.H. Grassian, B.J. Krueger, S. Carlos-Cuellar, University of Iowa

While there is a growing body of evidence which suggests that reactions on mineral aerosol may play an important role in the troposphere, there is very little understanding of what chemistry occurs on the surface of these particles. The focus of this talk is on recent laboratory studies of surface reactions of inorganic and organic acids found in the atmosphere on oxide and carbonate particles. These particles are used as laboratory surrogates for mineral aerosol. Kinetic measurements are made of these potentially important atmospheric reactions so as to quantify the rates of these reactions. Spectroscopic measurements along with atomic force and scanning electron microscopy provide additional information about surface reaction mechanisms. The laboratory data are then used as input into atmospheric chemistry models in order to assess the importance of these surface reactions in the troposphere.

4:20pm SS2-TuA8 Variable-Temperature Studies of Sulfur Dioxide Reactions with Carbon Clusters, W.T. Wallace, Georgia Institute of Technology, A.J. Leavitt, State University of West Georgia, M.G. Arredondo, Georgia Institute of Technology, D. Doby, State University of West Georgia, R.L. Whetten, Georgia Institute of Technology

The variable-temperature reactions of SO₂ with thermalized carbon cluster anions, C_N , are reported. Carbon clusters were produced via laser vaporization of a graphite rod and exposed to a dilute SO₂:He mixture in a pulsed variable-temperature flow tube reactor (FTR). The products of these reactions were detected using time-of-flight mass spectrometry. A series of reactions were monitored at FTR temperatures of 96 °C, 73 °C, 55 °C, 47 °C, 38 °C, and 24 °C. At all temperatures, the products C_NO and $C_NO_2^$ were detected corresponding to the depletion of the parent C_N^- concentration in the mass balance for selected values of N = 8 to 40. At each increasing temperature, the reaction was driven closer to completion when compared to C_N^- :SO₂ reactivity at room temperature. These studies probe the reactive nature of atmospheric soot with SO_x that are linked to respiratory problems.

4:40pm SS2-TuA9 Heterogeneous Reactivity of Ozone on Mineral Oxides, A.E. Michel, C.R. Usher, V.H. Grassian, University of Iowa

Mineral aerosols, or wind-blown soil particles, are emitted into the atmosphere where they can provide numerous sites for the heterogeneous reaction, physisorption and chemisorption of tropospheric gases. Understanding the role of mineral aerosol in the troposphere is important for its potential impact on chemical processes in the atmosphere. Laboratory measurements of the various processes are desired for the development of accurate atmospheric computer models. The uptake of ozone on various mineral oxide particles was observed using a Knudsen cell apparatus equipped with a quadrupole mass spectrometer. Mineral oxide samples included both commercially available powders (α -Al₂O₃, α -Fe₂O₃ and SiO₂) and authentic dusts (Saharan sand and China loess). Initial reactive uptake coefficients, γ_{BET} , were measured for the various particles and ranged from 10⁻⁵ to 10⁻⁴. In this investigation, it was observed that both the mineral oxide powders and authentic dusts exhibited catalytic behavior towards the destruction of ozone. Additionally, variations in the reactivity of the authentic dusts were observed as a function of sample treatment.

5:00pm SS2-TuA10 Alkali Halide Nanocrystal Growth and Etching Studied by AFM and Modeled MD Simulation, *S. Garcia-Manyes*, *A. Verdaguer*, University of Barcelona, Spain, *P. Gorostiza*, University of California at Berkeley, *F. Sanz*, University of Barcelona, Spain

Adsorption of water on alkali halides single crystals plays a key role in many fields ranging from interstellar dust grains, biochemistry, industrial applications and environmental processes, such as nucleation of clouds or sea salt spray. To understand the atomistic details of the wetting and dissolution processes that take place in, we combined Atomic Force Microscopy and Molecular Dynamics to study the adsorption of water vapor on a stepped (100)-oriented crystals surface prepared by cleavage. The AFMicroscope, placed in a humidity-controlled chamber is used to induce local step nanostructures forming hillocks. A few seconds of contact between the cantilever tip and the crystal surface are enough to create a hillock of a few monatomic steps due to the water neck formed on account of capillary forces. The shape and distribution of the monatomic steps in the formed hillock follows the minimization of the interface free energy established between the aqueous ionic solution and the air phase in order to reduce surface tension. After hillock creation the AFM tip is retracted and the hillock starts to dissolve and ions migrates until the hillock disappears. Terraces in the hillock disappear one by one, from the upper one to the lowest in order to minimize again the free energy of the whole system. We have studied creation and free evolution of hillocks for alkali halides single crystals by AFM under chosen humidity conditions. Imaging during experiments is performed in tapping mode so as to reduce the surface perturbation. We performed molecular dynamics simulations of the interface between the single crystal and water using a hillock-like surface model and results are compared with experimental data in order to understand the dynamics of the system. Ionic migration, steps mobility and dissolution directly calculated by the simulations have been used to modeling the hillock evolution according to experimental data.

Surface Science Room: C-112 - Session SS3-TuA

Metal/Oxide Surfaces

Moderator: C.A. Ventrice, Jr., University of New Orleans

2:00pm SS3-TuA1 High Quality Nanoscale Interfaces between Metals and Metal/Oxides: Co on Fully Hydroxylated Sapphire, S.A. Chambers, T. Droubay, Pacific Northwest National Laboratory, **D.R. Jennison**, T.R. Mattsson, Sandia National Laboratories

We present experimental and theoretical results that show Co metal deposited on fully hydroxylated alpha-Al2O3(0001) at room temperature produces a chemical reaction that leads to laminar growth of the metal film. A fraction of the initial metal dose is oxidized, and a concomitant amount of hydroxyl is reduced, resulting in hydrogen being released. The resulting Co cations are within the top layer of the oxide. These bind ionically to the substrate, but are also bound to neighboring metal atoms. Stronger interfacial binding results and near layer-by-layer metal growth is achieved, with good metal morphology just beyond the third layer. We propose direct hot reactions are responsible and many other metals and oxides should display this phenomenon. All work was supported by the US Dept. of Energy.

2:20pm SS3-TuA2 The Interaction and Reactivity of Hydrocarbons on Hydroxylated g:Al₂O₃/NiAl(100), K.A. Layman, J.C. Hemminger, University of California, Irvine

 γ -Al₂O₃ is an important industrial catalyst and catalyst support. The surface OH groups on bulk γ -Al₂O₃ influence the Brönsted acidity and metal dispersion on these catalysts. However, the detailed understanding of A l₂O₃ surfaces has been limited because of the complexity of the surface hydroxyl groups. We are able to grow highly-ordered and well-defined thin films of hydroxylated γ -Al₂O₃ which model bulk γ -Al₂O₃ by exposing the NiAl(100) substrate to 100 L H₂O at 1000 K. Unlike bulk γ-Al₂O₃, these films exhibit a single OH stretch at 3711 cm⁻¹ (FWHM approximately 100 cm⁻¹). This frequency is indicative of non-interacting OH groups bonded to 2 or 3 Al atoms. We have used HREELS to study the interaction and reactivity of hydrocarbons, such as acetonitrile, pyrazine, 2,6-dimethylpyridine, and ammonia, on our thin films of hydroxylated γ -Al₂O₃ following adsorption at 140 K. These molecules interact with surface OH groups, forming acid-base complexes. Complex formation causes the OH bond strength to decrease and the OH stretch to shift to lower frequency. We have observed that the magnitude of the OH shift depends on both the basicity and adsorption orientation of these hydrocarbons. Correlation of the OH frequency shift with the gas basicity of the adsorbate allows us to assign a pK_a to the surface OH groups. The hydrocarbons can also interact with the surface Al³⁺ cations. In the case of ammonia, this interaction leads to disruption of an N-H bond and the formation of surface NH₂ and OH species.

2:40pm SS3-TuA3 Calculations of the Free Energy and Structure of Alpha-Alumina (0001), M. Finnis, A. Marmier, Queens University, UK INVITED

We report a study of the excess free energy of this surface using two different shell models (S1 and S2) and an ab initio (AI) model in which the total energy was obtained from self-consistent pseudopotential calculations using the local density approximation. We apply the quasi-harmonic approximation to estimate the phonon contribution to the free energy. The surface energies with S1 and S2 bracket the AI result. They also show that only two k-points are needed to sample the phonons in the Brillouin zone with good accuracy. A six layer slab is thick enough for obtaining all contributions to the surface free energy, which converges faster with slab thickness than the mean square amplitudes of atomic vibration, and in fact the latter diverges for a finite slab. Anharmonicity is insufficient to account for the discrepancy beween calculated and experimental surface relaxations. A stoichiometric AI-terminated surface is predicted to be stable over all but very low (close to decomposition of the oxide) and very high (> 1 atmosphere) oxygen partial pressures, in agreement with experiment.

3:20pm **SS3-TuA5 Effect of Annealing on the Crystallization of Ultrathin Al₂O₃ Film on NiAl(110),** *T.T. Lay***,** *M. Yoshitake***, National Institute for Materials Science, Japan**

 Al_2O_3 is a wide band gap insulator and it is reported that clear band gap exits in 0.5nm-thick well-ordered Al_2O_3 grown on NiAl(110).¹ It has high potential of application in metal-insulator-metal(M-I-M) electron emitter which needs wide gap insulator. Oxygen dose rate, oxidation temperature and annealing are important parameters for well-ordered film. In our previous work, good crystalinity of Al_2O_3 layer was obtained by optimizing the dose rate and oxidation temperature.^{2.3} In the present work, change in

crystalinity and surface composition due to annealing time is analyzed. NiAl(110) single crystal was put inside the UHV system and 1200L oxygen was introduced under pressure 5 x 10⁻⁷ torr at 670K. After oxidation the specimen was annealed at 1070K. The oxide layer was amorphous before annealing and crystalline Al₂O₃ appeared after annealing. Crystal structure and surface composition were measured by LEED and XPS every hour during annealing. Intensity ratio of Al₂O₃ and NiAl spots was measured from LEED patterns. The intensity ratio is directly related to crystalinity and it increases linearly with annealing time. After 6 hours annealing, the ratio became saturated and there was less change by further annealing. The surface composition of O. Al and Ni changed only at the early stage of annealing and were almost constant one hour later. It is likely that the amount of oxygen contributed to well-ordered crystalline oxide is almost decided at oxidation. Annealing at 1070K for certain period of time is important for epitaxial growth of well-ordered oxide layer.

¹ R.M. Jaeger, H.Kuhlenbech, H.J.Freund, M.Wuttig, W. Hoffmann, R. Franchy and H. Ibach, Surf. Sci., 259,235(1991),

² M. Yoshitake, B. Mebarki and Thi Thi Lay, Surf.Sci. Lett., in press.,

³ Thi Thi Lay, M. Yoshitake and B. Mebarki, J.Vac. Sci. Technol., submitted.

3:40pm **SS3-TuA6 Ab-Initio Calculations of Pristine and Doped ZrO₂ Tilt Grain Boundaries**, *Z. Mao*, Northwestern University, *E.C. Dickey*, The Pennsylvania State University, *S.B. Sinnott*, University of Florida

The structure of the cubic-ZrO₂ symmetrical tilt sigma 5 (310)/[001] grain boundary is examined using density functional theory within the local density and pseudopotential approximations. Several pristine stoichiometric grain boundary structures are investigated and compared to Z-contrast scanning transmission electron microscopy and electron energy loss spectroscopy results. The lowest-energy grain boundary structure is found to agree well with the experimental data. When Y³⁺ is substituted for Zr⁴⁺ at various sites in the lowest-energy grain boundary structure, the calculations indicate that Y³⁺ segregation to the grain boundary is energetically preferred to bulk doping, in agreement with experimental results.

4:00pm **SS3-TuA7 Role of the Stress in the Epitaxy of Silver on the Basal Planes of Zinc Oxide**, *J. Jupille*, Groupe de Physique des Solides, France, *S. Djanarthany*, Laboratoire des Geosciences, France, *D. Abriou*, Laboratoire CNRS/Saint-Gobain, France, *N. Jedrecy*, Laboratoire Mineralogie-Cristallographie, France, *R. Lazzari*, *G. Renaud*, CEA-Grenoble, France

In general late transition metals and noble metals poorly wet oxide surface oxides. However, rather high values of the critical coverage (onset of the formation of the second atomic layer [Campbell, Surf. Sci. Rep. (1997)]) have been observed for platinum, copper and silver. The present paper reports on two different $(0001)_{ZnO}//(111)_{Ag}$ epitaxies for silver on the oxygen- and zinc-rich basal planes of zinc oxide. The [20-20]_{Zn0} //[220]_{Ag} orientation relation (OR I), corresponding to a misfit of + 2.75 %, is obtained on surfaces which are only prepared by annealing under oxygen. The $[11-20]_{ZnO}//[220]_{Ag}$ orientation relation (OR II, rotated by 30° with respect to OR I) is observed after an ion bombardment of the surfaces. It corresponds to a misfit of 11 %. The two epitaxies show both a perfect reproducibility and a good thermal stability. Low energy electron diffraction, transmission electron microscopy and X-ray diffraction (XRD) measurements demonstrate that (i) the ion bombardment strongly increases the size of the surface domains (narrowing of diffraction spots and rods) and that (ii) OR II, which corresponds to within 0.11 % to a 9Ag/8ZnO lattice coincidence, does not show any stress even at the onset of the film growth. It is concluded that the OR II is favoured by large ZnO domains while the OR I, which shows a better fit on short range, appears on surfaces of poor crystalline quality.

4:20pm **SS3-TuA8 Vanadium Oxide Nanostructures on Rh(111): Novel Oxide Phases at the Interface**¹, J. Schoiswohl, S. Surnev, S. Eck, M.G. Ramsey, **F.P. Netzer**, Karl-Franzens University Graz, Austria

Ultrathin layers of materials develop novel physical and chemical properties due to confinement and interfacial proximity effects, which are not shared by their respective bulk phases. Here we report a study of thin vanadium oxide layers on Rh(111) surfaces using STM, STS, LEED, and XPS with synchrotron radiation. We have fabricated vanadium oxide nanostructures on Rh(111) by reactive evaporation of vanadium metal in an oxygen atmosphere onto the heated substrate surface and have characterised the atomic structures of the V-oxide with STM (STS) and LEED; the oxidation state of the oxide layers have been followed by XPS. We find a complex phase diagram of oxide structures as a function of oxide coverage and temperature, and observe a range of well-ordered two-dimensional oxide phases with novel structural properties. At submonolayer coverages higher oxidation states ($\geq 4^+$) prevail [($\sqrt{7x}\sqrt{7}$) and/or ($\sqrt{13x}\sqrt{13}$) structures], whereas the oxidation state converges to 3^+ and a bulk-type V₂O₃ phase forms for thicker layers (> 2-3 ML). The monolayer phase is distinguished by a Moiré-type STM structure, resulting from the lattice mismatch between the ordered oxide overlayer and the substrate. Reduced oxide phases are obtained after vacuum annealing treatments, displaying a fascinating structural complexity, with e.g. (5x5), (5x3 $\sqrt{3}$), (9x9) and other structures. ¹Supported by the Austrian Science Foundation.

4:40pm **SS3-TuA9 Room Temperature Growth and Thermal Sintering** of Ag and Pd on Flat Ultra-thin SiO₂ and MoO₂ Films, *A.K. Santra*, *B.K. Min, D.W. Goodman*, Texas A&M University

The initial growth morphology of Ag and Pd particles has been investigated on epitaxial ultra-thin MoO2(100) and SiO2 films using STM. The room temperature growth of Ag and Pd particles is invariant with respect to the thickness of the SiO2 film, however, with increasing surface temperature the Pd particles undergo a 3DA" 2D transition on a 0.5nm thick SiO2 film and increase in particle size on films with a thickness >0.8nm. In contrast, Ag particles on a MoO2(100) substrate show striking differences with respect to the particle size distribution as a function of the oxide film thickness at room temperature. These results indicate that the initial growth and thermal sintering of metal particles depend critically on the strength of the metal-support interaction. The preparation procedure for these flat ultrathin films on Mo(112) will be discussed relative to the LEED and highly resolved STM data. Furthermore, STS data indicate that a minimum thickness (3 - 4 Si-atomic equivalent layers) is necessary to obtain a bulklike band-gap for SiO2 ultra-thin films, in excellent agreement with results recently reported by Muller and co-workers [Nature 399 (1999) 758] for Si/SiO2/Si gate-oxide samples.

5:00pm SS3-TuA10 Structure and Properties of SnOx Wetting Layers and Crystallites on Pt(111), *J. Kim*, University of Southern California, *M. Batzill*, Tulane University, *D. Beck*, University of California-Los Angeles, *B.E. Koel*, University of Southern California

Tin-oxide films were grown on Pt(111) substrates by oxidation of Sn/Pt surface alloys using NO₂ exposures or by deposition of Sn in an NO₂ ambient gas. Based on the wide variety of structures of tin-oxide films that we have reported previously [Phys. Rev. B 64, 245402/1 (2001)], we now report detailed characterization of the vibrational and electronic properties of each structure using XPS, UPS, ELS, and HREELS. XPS confirmed the existence of three Sn states that have been labeled previously as metallic, "quasimetallic", and oxidic Sn. We conclude that the "quasimetallic" state results from oxidized Sn that is still alloyed within the Pt surface layer. UPS identified a SnO₂ stoichiometry for multilayer tin-oxide films. HREELS was used to identify characteristic vibrational modes for the different monolayer films. SnO₂ crystallites, although only a few monolayers high and tens of nanometers in width, remarkably exhibit bulk-like vibrational and electronic properties.

Tuesday Afternoon Poster Sessions

Surface Science Room: Exhibit Hall B2 - Session SS-TuP

Surface Science Poster Session

SS-TuP1 In-situ Observation of Chemical State of a Si Electrode Surface during a Galvanostatic Oscillation in Fluoride Electrolytes Using Infrared Absorption Spectroscopy, Y. Kimura, J. Nemoto, M. Niwano, Tohoku University, Japan

Electrochemical etching of silicon (Si) is an important technique for the fabrication of micro- and nano-structures on Si, and therefore, it has been extensively investigated theoretically and experimentally. It is well known that when an anodic potential below about 1 V is applied to a Si electrode, porous silicon (PS) forms in the vicinity of the surface. Interestingly, when a higher anodic potential, several volts or more, is applied to a Si electrode, an oscillation in the anodic potential or the anodic current density takes place. Previously, the oscillation has been interpreted as being due to alternative formation and removal of silicon oxide on the Si electrode surface. However, the chemistry of a Si electrode surface during galvanostatic oscillation has not been fully understood. In this study, we have investigated a galvanostatic oscillation phenomenon during anodization of a silicon (Si) crystal electrode in fluoride electrolytes using infrared absorption spectroscopy in multiple internal reflection geometry (MIR-IRAS). We confirm that the electrode surface is covered with a thin oxide layer during the course of galvanostatic oscillation. We observe a weak oscillation of the oxide thickness that synchronizes with the oscillation of an anodic potential. We also find that when the anodic potential falls to its minimum, hydrogen-substituted oxide (suboxide, Si(O₃)-H) forms on the electrode surface. We propose a model of galvanostatic oscillation in which it is assumed that an decrease in the anodic potential is due to the formation of pits in the oxide over layer and low-quality oxides containing Si(O₃)-H species are preferentially formed at the pit sites. We suggest that formation of an inhomogeneous oxide layer plays a crucial role for the galvanostatic oscillation phenomenon.

SS-TuP2 What Governs the Si(100) Low Temperature Phase? - Study by STM and LEED, S. Yoshida, O. Takeuchi, K. Hata, H. Shigekawa, University of Tsukuba, CREST, Japan

Through the recent intensive study on the low temperature phase of Si(100) by Scanning Tunneling Microscopy (STM) and Non-Contact Atomic Force Microscopy, symmetric dimmer, c(4x2)/p(2x2), and c(4x2) phases have been confirmed to exist below 30K, giving rise to the controversy on the ground state of Si(100). In addition to these structures, we recently succeeded in observing a single p(2x2) phase by STM at 10K for the first time, and have studied the conditions for the appearance of all these phases. For example, although c(4x2) phase easily appears in the case of p-type Si(100), particular sample conditions are necessary for the observation of the p(2x2) single phase; (1) n-type, (2) high dope, and (3) very low defect density. Furthermore, for the n-type Si(100) surface, we have succeeded in the direct observation of the phase transition between p(2x2) phase (lower temperature side) and c(4x2) phase (higher temperature side) by STM and LEED measurements. These obtained results suggest the great importance of the dopant and defect influences on the Si(100) surface phase transitions. Tip induced effect will also be discussed.

SS-TuP3 Stability Studies of Monolayers on Scribed Silicon to Water, Air, and Xray, G. Jiang, T.L. Niederhauser, S.D. Davis, M.R. Linford, Brigham Young University

The stability of alkyl monolayers on scribed silicon to air, water, and/or Xrays was investigated. Monolayers were prepared by scribing silicon surfaces in the presence of reactive liquids (1-pentene, 1-decene, 1hexadecene, methyl iodide, 1-iodopetane, 1-iododecane, 1-butanol, 1bromopentane, and 1,4-dibromobutane) with a computer-controlled diamond-tipped instrument. In all cases some initial oxidation of the underlying silicon surface was observed by X-ray photoelectron spectroscopy (XPS), which increased with time until the O1s/Si2p XPS ratio reached a stable level (after 100 - 200 hours). In the case of silicon scribed under the iodoalkanes, the iodine to silicon ratio by XPS decreased with time until it also reached a stable value. The C1s/Si2p XPS ratios for all surfaces remain essentially constant after all exposures to air and water, which indicates that monolayers of 1-alkenes and 1-haloalkanes on scribed silicon are quite stable. Kinetics measurements using water contact angles on scribed patches and water capacity measurements of hydrophobic corrals on silicon show trends similar to the XPS results. In general, hydrophobic corrals retained much of their capacity to hold water. Surface oxidation is

shown to take place at the silicon surface. It is suggested that iodine is lost by hydrolysis of surface Si-I bonds. Finally, no change in the amount of C, O, or Br at the surfaces was observed by XPS after 3 - 4 hr of illumination with monochromatic Al Ka Xrays, indicating that XPS analyses can be performed on monolayers on scribed silicon without substantially damaging them.

SS-TuP4 Bevel Crater SIMS for Auger Analysis of Laterally Oxidized AlGaAs/GaAs Multilayers, S.A. Wight, G. Gillen, P. Chi, A. Fahey, A. Roshko, K. Bertness, National Institute of Standards and Technology

Recently, in support of a project to engineer strain in compound photonic semiconductors, we employed a combination of Secondary Ion Mass Spectrometry (SIMS), Auger Electron Spectroscopy (AES), and Scanning Electron Microscopy (SEM) to characterize MBE grown, laterally wetthermal oxidized, Al.98Ga.02As layers in an attempt to determine compositional uniformity through the oxide layers. Typical samples for this study consist of alternating layers of $Al_xGa_{1-x}As$ (where x is between 0.90 and 1.0) and GaAs. Each AlGaAs layer is 80.0 nm thick and is separated from adjacent layers by 150 nm of GaAs. The surface is capped with 200 nm of GaAs. Each sample has a series of trenches (spaced 100 µm apart) etched through the multilayer to expose the buried AlGaAs layers. The lateral extent of oxidation was designed to be 25 µm from the trench edge. An external raster waveform was used in place of the standard digital raster to produce bevel craters on a commercial SIMS instrument. Beveled samples were analyzed using O2+ and Cs+ microbeam imaging in the SIMS and by AES/SEM in a commercial scanning Auger instrument. Bevels were cut in AlGaAs samples using Cs, O and Ga + primary ion beams at several different energies. Both Cs+ and Ga+ beveling produced very distorted bevels resulting from the large sputter rate differences between oxidized and unoxidized regions and a high degree of surface topography as determined by SEM imaging. Best results were obtained by using O2+ bombardment for bevel production. Currently, we are using Ar+ sputtering at a few keV impact in the Auger instrument to remove the primary beam oxygen before analysis.

SS-TuP5 Oxygen Reactivity of Clean and Au-induced High-Index Si Surfaces, J.C. Moore, J.L. Skrobiszewski, A.A. Baski, Virginia Commonwealth University

We have studied the oxygen reactivity of the clean high-index Si(5 5 12) surface, as well as nearby Au-induced facet planes. The (5 5 12) surface is oriented approximately midway between the (001) and (111) planes and forms a single-domain, row-like reconstruction. When submonolayer coverages of Au are deposited and annealed on Si(5 5 12), the surface undergoes significant restructuring to form a variety of nearby facet planes. In this work, we use scanning tunneling microscopy to investigate the O₂ reactivity of these various surfaces for a range of temperatures (600 to 800 °C), pressures (10^{-7} to 10^{-6} Torr), and exposures (50 to 200 Langmuirs). At lower temperatures (<700 °C), Q exposure of the clean (5 5 12) surface results in disordered oxide growth, similar to that previously observed for the low-index Si surfaces. At higher temperatures (>700 °C), etching is observed via step retraction and subsequent pinning by small islands, presumably due to oxide growth. The density of these islands decreases at higher temperatures (800 °C), indicating that oxide etching dominates in this temperature regime. With regard to the Au:Si(5 5 12) system, for oxygen exposures of ~100 L and moderate temperatures (700 to 750 °C), oxide island formation is seen on the lower Au coverage (337) facets, but no etching or oxidation is observed on higher coverage facets such as (5 5 11). This behavior indicates enhanced stability of the higher coverage Auinduced surfaces, which is consistent with he passivating nature of this adsorbate.

SS-TuP6 The Origin of the Metallic States on Ge(100) Surface, *C. Jeon*, Sungkyunkwan University, Korea, *C.C. Hwang, K.-J. Kim, T.-H. Kang, B. Kim*, PAL, POSTECH, Korea, *C.-Y. Park*, Sungkyunkwan University, Korea

Semiconductor surfaces exhibit a temperature-induced metallization upon raising temperature. Photoemission spectroscopy (PES) and low-energy electron diffraction (LEED) studies on Ge (100) surface, Kevan and Stoffel, observed a metallic state above 130K whose intensity increases as temperature rises.¹ At the same time, a c(4x2) LEED pattern was observed to convert to a 2x1. A similar increase in metallicity with temperature (up to about 900K) on the Si(100) was reported in a recent study.² In this work, angle resolved ultra-violet PES was utilized to investigate the metallization on the Ge(100) surface from room temperature up to 900K. The metallic state was observed at about 580 K around two symmetric points without any change in LEED pattern. Based on these results, we'll discuss the difference and similarity between the origin of the metallic surface states of the Ge and Si(100) surfaces.

¹ S. D. Kevan, N. G. Stoffel, Phys. Rev. Lett. 53, 702, 1984

² C. C. Hwang et al., Phys. Rev. B 64, R201304, 2001

SS-TuP7 Two-dimensional Electronic Excitations in a Metallic Monolayer on a Semiconductor Surface, *T. Inaoka*, Iwate University, Japan, *T. Nagao*, Tohoku University, Japan, *S. Hasegawa*, University of Tokyo, Japan, *T. Hildebrandt*, *M. Henzler*, University of Hannover, Germany

There exists a surface-state band at the Si(111)-($\sqrt{3x}\sqrt{3}$)-Ag surface created by depositing a monolayer of Ag on the Si(111) surface. An electron system in this band forms a realistic two-dimensional (2D) conduction-electron system. Recently, 2D plasmons (PLs) in this electron system have been clearly observed by high-resolution electron energy-loss spectroscopy in a broad wave-number range including PL decay due to electron-hole pair (EHP) excitations. In the present work, by means of the local-fieldcorrection (LFC) theory, we evaluate the exchange-correlation (X-C) effects on the above electronic excitations. We compare three cases, namely, (i) random-phase approximation, (ii) Hartree-Fock approximation, and (iii) STLS approximation formulated by Singwi, Tosi, Land, and Sjölander. The X-C effects are neglected in (i), only the X effect is considered in (ii), and both the X and C effects are taken into account in (iii). We determine the electron density and the electron effective mass so that the calculated results in (iii) accord with the experimental ones. Our calculations give a good description of the experimental results of the energy dispersion and the energy-loss intensity of the 2DPL. When the X or both the X and C are switched on, with increase in wave number q, the dispersion curve begins to shift downward, and decays away due to EHP excitations at a smaller q value. Simultaneously, the integrated resonance intensity of the 2DPL in the energy dependence of the energy-loss function declines more quickly at smaller q values. This effect is more conspicuous in (iii) than in (ii). Our electron system has a large effective Bohr radius, and consequently a high effective density, because our electron system lies on a semi-infinite dielectric medium. However, owing to low dimensionality, the X-C effects appear remarkably in the 2DPL with increase in q.

SS-TuP8 Formation pf Platinum Silicides on Si as followed by AES and XRD, *J. Liday*, Slovak University of Technology Bratislava, Slovakia, *M. Jergel*, CINVESTAV-IPN, Mexico, *P. Vogrincic*, *I. Hotovy*, *R. Kosiba*, Slovak University of Technology Bratislava, Slovakia, *G. Ecke*, Technical University of Ilmenau, Germany

Auger electron spectroscopy was used for depth profiling of platinum silicide thin layer formed as a result of annealing of 43 nm platinum layers deposited on Si (111). The factor analysis was utilized for interpretation of Auger spectra. The stoichiometry of silicide layers was determined by X-ray diffraction in both Bragg-Brentano and grazing incidence (at angles 0,5°, 1°, 1.5° and 2°) geometries in order to distinguish the depth distribution of intermediate platinum silicide phases (Pt₃Si, Pt₂Si, PtSi).

SS-TuP9 Experimental and Computational Studies of the Adsorption of Allyl Alcohol on the Si(100) Surface, L. Zhang, A.J. Carman, S.M. Casey, University of Nevada

In order to determine which mechanism, oxygen-addition or cycloaddition, plays a dominant role in governing the adsorption of organic molecules on silicon surfaces, the adsorption of a bi-functional molecule, allyl alcohol, on the Si(100)-(2x1) surface was investigated experimentally using Auger electron spectroscopy (AES), thermal desorption spectroscopy (TDS), and low-energy electron diffraction. The AES studies show that the surface adsorption of allyl alcohol is similar to the adsorption of the monofunctional molecule n-propanol, and is different from the adsorption of propene, based on final coverage comparisons. TDS results show that both allyl alcohol and n-propanol have no desorbing parent molecular species, while propene desorbs molecularly from this surface. Both allyl alcohol and propanol display desorption products consistent with the loss of water during decomposition. Computational studies were also performed using density functional theory and cluster models of the surface, in order to compare with the results from the experimental studies. Both the computational and experimental studies indicate that the oxygen-addition mechanism is most likely the favored path over [2+2] cycloaddition-type reactions with the Si(100) surface.

SS-TuP10 Stochastic Motion of 7x7 Kinks at Monoatomic Step Edges, T. Fukuda, S. Maeda, H. Nakayama, Osaka City University, Japan

Control of steps on the surface have been regarded as one of the promising technique for future electronic devices.¹ Synthesis of artificial step arrangement can be achieved by photolithographically patterned substrates followed by thermal treatment. Because an individual step movement is governed by the detail balance between attachment and detachment of

surface adatoms at step edges, the study of adatom kinetics is a crucial issue for understanding and controlling of step configuration. Here we propose a method for measuring migrating adatoms and step movements below the 7x7-"1x1" transition temperature.. Microscopically, meandering steps consist of long straight segments with well defined orientations and short segments called kinks. On the Si(111) surface, these kinks are expected to be quantized by the 7x7 reconstruction and their widths and strides are limited within the 7x7 period. Even in thermal equilibrium, these kinks will stochastically fluctuate by attaching or detaching adatoms. So, the individual kink can be regarded as one dimensional "Brownian particle". In this study, we made an in situ measurement of the kink motion by the hightemp. STM and found the kink is really Brownian particle. Because the chemical potential around the kink is uniform in thermal equilibrium, there is no net mass transport between the surface adatoms and the kink site. The Brownian kink, therefore, will not diffuse but restore its position. The kink velocity follows gaussian distribution and its standard deviation is a measure of the diffusion constant of the kink, which is closely connected to the adatom diffusion constant. The temperature dependence of the standard deviation showed an activation type behavior with an energy of ~0.87 eV, compared with the adatom diffusion energy of 0.75±0.2 eV on the Si(111) 7x7 surface.²

¹T.Ogino et al., Appl. Surf. Sci. 107 (1996) 1.
²Voigtlander et al., Phys. Rev. B51 (1995) 7583.

SS-TuP11 Atomic Structure of Bare Si Dimer on H/Si(100) Surface, C.C. Hwang, POSTECH, Korea, C. Jeon, Sung Kyun Kwan University, Korea, K.-J. Kim, T.-H. Kang, K.W. Ihm, B. Kim, POSTECH, Korea, C.-Y. Park, Sung Kyun Kwan University, Korea

When H adsorbs on the Si(100) surface, H bonds preferentially to Si dangling bonds and can form monohydride, Si-H. The structural, electronic, and chemical properties of the Si(100) surface are considerably modified by H adsorption. Recently, partially Hdesorbed Si(100)2x1-H surfaces by thermal annealing or photon irradiation have received much attention, for example, due to its increasing chemical reactivity to H_{k} .¹ The modified chemical property could be strongly related to the atomic structure of bare Si dimer. It has been reported from scanning tunneling microscopy experiments that untilted dimers, which are different from those on the clean 2x1, are responsible for the exotic phenomenon. Contrary to this assertion, our synchrotron radiation photoemission spectroscopy results obtained at PAL in Korea² show that bare Si dimers are tilted and similar to those on the clean Si(100)2x1 surface. In this presentation, we will provide Si 2p core level and valence band spectra from partially H-desorbed surfaces and discuss possible origins of the chemical reactivity.

¹ E. J. Buehler and J. J. Boland, Science 290, 506 (2000).

 2 C. C. Hwang et al., Phys. Rev. B 64, R201304 (2001).

SS-TuP12 Shape Transformation of Silicon Trenches during Hydrogen Annealing, *H. Kuribayashi*, *R. Hiruta, R. Shimizu*, Fuji Electric Corporate Research and Development, Ltd., Japan, *K. Sudoh, H. Iwasaki*, Osaka University, Japan

In trench gate MOSFETs, trench corner rounding, which is caused by surface self-diffusion during heat treatments, is significant for the gate oxide reliability. Though the evolution of a crystal shape through surface self-diffusion during heating in vacuum has been extensively investigated, it has not been sufficiently studied in specific ambient, which is applicable to semiconductor process. In this work, we have studied the shape transformations of silicon trenches through surface self-diffusion during annealing in hydrogen ambient. The trench stripes on Si(001) with a depth of 3µm were fabricated by RIE technique with HBr contained gas plasma, where the trench sidewall surface orientation was chosen to be (110) and (-110). Then the samples were annealed at 1000°C in hydrogen ambient at various hydrogen pressures. The cross-sectional profiles of the trenches were observed by SEM after cleaving the substrates along the trench stripes. The observed time evolution of trench shapes was well reproduced by numerical simulation based on Mullins' continuum theory.1 Thus we confirmed that the evolution of the trench-shape was due to Si surface selfdiffusion. From comparison between the time scales in the experiment and the simulation, the diffusion coefficient was estimated to be about 2x106nm²/sec at 5.3kPa, which is smaller than that at vacuum ambient.² It was found that the rate of shape transformation decreased with increasing hydrogen pressure, showing strong pressure dependence of the diffusion coefficient. In the symposium, we are going to discuss the dependence of silicon surface on hydrogen pressure in detail. In addition, the behavior of atomic steps on the trench sidewall surfaces, which was observed by AFM, will be also discussed.

¹W.W.Mullins, J.Appl.Phys.28,333(1957) ²Yang et al., Surf.Sci.356,101(1996).

SS-TuP13 Adsorption and Photodissociation of 4-Haloanilines on GaN(0001)-(1x1), V.M. Bermudez, Naval Research Laboratory

Photochemical reactions of organic molecules on semiconductor surfaces are of interest as a means of synthesizing patterned structures with specific chemical functionalities. The adsorption of 4-chloro- and 4-iodoaniline on the GaN(0001)-(1x1) surface, and the effects of subsequent exposure to near-UV or vacuum-UV radiation, have been studied using primarily UV photoemission and electron energy loss spectroscopies, supported by ab initio quantum-chemical modeling. Both 4-haloanilines adsorb via the molecular NH₂ group, with the phenyl ring intact, as does aniline itself.¹ Like aniline, both are very reactive with the clean GaN(0001)-(1x1) surface, requiring only a small dose to achieve saturation coverage (ca. 0.29 molecules/surface site). 4-Iodoaniline is photochemically active as an adsorbate on GaN, as expected from its apparent behavior in non-polar solvents. UV radiation promotes dissociation of the molecular C-I bond, leading to the transfer of I to available sites on the GaN surface. The molecular C-I bond is intact prior to irradiation, as suggested by the changes in ELS and UPS data seen to result from UV exposure. The photochemical activity of 4-chloroaniline adsorbed on GaN is at present uncertain, but it appears to be relatively inert, again consistent with its behavior in non-polar solvents. Similar results were obtained for both n- and p-type GaN, suggesting that the photochemistry is not mediated by excited carriers from the GaN substrate.

¹ V.M. Bermudez, Surf. Sci. 499 (2002) 109, 124.

SS-TuP14 RHEED and STM Study of Initial-stage Structural Change of Si(100) Surface Induced by Exposure to Ethylene Gas and Annealing, *T. Takami*, Visionarts Inc., Japan, *I. Kusunoki*, Tohoku University, Japan

The initial stage of the structural change in clean Si(100) - 2 X 1 surface induced by annealing at 913 K and exposure to ethylene gas has been studied by reflection high-energy electron diffraction (RHEED) and scanning tunneling microscopy (STM). Transmitted bulk Si and particle SiC spots appeared on the RHEED patterns of the ethylene-exposed Si(100) surface. The obtained STM images were in accordance with the respective RHEED patterns. At the flat area of the exposed surface where the RHEED pattern showed twice the periodicity of surface spots and transmitted bulk Si spots, the STM image showed 2 X n (n=6,7,8,9,10,11,12) reconstruction. The obtained 2 X n STM image depended on the bias voltage.

SS-TuP15 Structure of Stable Si(6 9 17) Facet on Si(5 5 12), Y.Z. Zhu, S.H. Cho, W.X. Quan, J.M. Seo, Chonbuk National University, Korea

Up to now, it has been known that the stable facet parallel to the atomic row of Si(5 5 12) is Si(113). In the recent structural studies on Si(5 5 12) using STM, it has been found that there exists another stable facet, Si(6 9 17), whose azimuthal angle is 97 degree-off from the atomic row and polar angle is 6.2 degree-off from Si(5 5 12). As this (6 9 17) facet appears at differently inclined surfaces, it is not simply due to miscutting. Although Si(6 9 17) facet is nearly vertical to the atomic row, it consist of 1.92 nm wide (337) terraces and single (011) steps, of 0.195 nm height, connecting such narrow (337) terraces. The unit cell of (6 9 17) contains a pair of tetramers and π -7 chain which is quite similar to those of (337) subsections composing of Si(5 5 12). As the (6 9 17) facet is always accompanied by defects like grain boundaries, it can adapt smoothly-bending facets as well as straight facets. It can be concluded that it is essential to form such flexible (6 9 17) facets in order to relieve the local strain with various directions.

SS-TuP16 Interfactant-mediated Growth of Ultrathin Bismuth Films on Si(111), J.T. Sadowski, T. Nagao, Y. Fujikawa, S. Kuwano, T. Sakurai, Tohoku University, Japan

Semimetal bismuth (Bi) has quite distinctive electronic properties due to its covalent-like bonds, highly anisotropic Fermi surface and low carrier concentrations. The small carrier effective masses and the very long mean free path result in large MR effects observed in bulk single crystals of Bi. However, fabrication of high quality bismuth films with nanometer thickness, required for the technological applications, still appears to be difficult. Recently, we have found that ultrathin Bi layers deposited at room temperature on the Si(111)-7x7 surface exhibit 2D growth after forming initial rough transition layer, and self-organizes into a single crystal ultrathin film nearly perfectly aligned to the Si substrate. In this paper we report the scanning tunneling microscopy studies of the role of the interfactants of Au-induced surface superstructures in the growth of flat, very well ordered, ultrathin Bi films on Si(111) surface. The morphology of the Bi ultrathin film was found to be modified by the presence of interfactant surface superstructures since the growth kinetics is modified by the change in the diffusion length, nucleation density, and the interface free energy due to the modification in the atomic as well as domain-wall configuration. In the systematic study, the morphology and detailed atomic

structure of the Bi layer grown on the various Au-induced surface superstructures such as 5x2, α -root3xroot3, and β -root3xroot3-Au will be discussed and compared with the results of the direct Bi growth on the Si(111)-7x7 surface, as well as with growth on otherwise modified interfaces such as α -root3xroot3 and β -root3xroot3-Bi superstructure.

SS-TuP17 Measurement of the Dependence of Bulk Defects on the Reactivity of the $TiO_2(110)$ Surface, S.N. Thornburg, J.M. Burst, C.A. Vantrice, Ir. University of New Orleans II, Dichold Tulana University

Ventrice, Jr., University of New Orleans, U. Diebold, Tulane University Missing-atom point defects at metal oxide surfaces often enhance the reactivity of these surfaces towards the adsorption of simple molecules. A previous study of the adsorption of S on the TiO₂(110) surface found that the reactivity of this surface at temperatures >120°C was enhanced by the presence of bulk missing-oxygen defects.¹ This was determined by measuring the S 2p uptake with x-ray photoelectron spectroscopy as a function of reduction time. However, this was performed on a new Ti O2 crysta l, so the influence of bulk impurities on the uptake of S was difficult to determine. A technique for reoxidizing dark blue, bulk-reduced, TiO_{2} crystals has been developed that allows us to return these crystals to a defect f ree clea r state. The degree of bulk reduction is monitored using optical spectroscopy and temperature dependent resistivity measurements with a four point probe. Optical spectroscopy measurements for both the dark blue and clear crystals show the same ab sorption edge at 3.0 eV, which corresponds to the bulk band gap of TiO₂. However, the dark blue crystals also show a strong absorption below 2.6 eV. Photoemission measurements of the S uptake, O reduction, and S peak shift at 250°C and room t emperature have been performed on both dark blue and clear crystals. At room temperature, the S saturates at approximately one monolayer coverage for both clear and bulk reduced crystals. At 250°C, the adsorbed S replaces the first few layers of oxygen atoms. The rate of S adsorption is found to depend on bulk reduction, but at a reduced rate as compared to the measurements on a new crystal. This indicates that bulk contaminants in new crystals are also influencing the S adsorption rate.

¹E. L. D. Hebenstreit et al., Surf. Sci. 486, L467 (2001).

SS-TuP18 FT-IR Investigation of Water Adsorbed on a-Al₂O₃ and MgO at 296 K, *H.A. Al-Abadleh*, *V.H. Grassian*, University of Iowa

Fundamental studies of water adsorption on oxide surfaces are of great interest as the water/oxide interface plays an important role in many if not all environmental chemical processes. In these studies, transmission FT-IR spectroscopy is used to investigate the adsorption of water on α -Al₂O₃ (0001) and MgO (001) surfaces. The FT-IR spectra of the (0001) surface of α -Al₂O₃ and (001) surface of MgO single crystals are measured in the presence of 0.2 to 20 Torr H₂O vapor pressure corresponding to 1 to 95% relative humidity (RH) at 296 K. The adsorption of D₂O on the single crystal surfaces of on α -Al₂O₃ and MgO is also carried out in order to obtain additional insight into the behavior of adsorbed water. Water adsorption on nitrate-coated oxide single crystal surfaces are also carried out to investigate the effect of adsorbed ions on the hydrogen bonding network of water on oxide surfaces. The FT-IR spectra are analyzed so as to quantify the amount of water adsorbed on these oxide surfaces under ambient conditions and to determine more about the nature of the adsorbed water layer.

SS-TuP19 Ozone Reactivity on Processed Mineral Oxide Particles, C.R. Usher, A.E. Michel, V.H. Grassian, University of Iowa

Wind-blown mineral dust from arid and semi-arid regions can be transported over large distances in the troposphere. The reaction of dust with trace atmospheric gases can result in the presence of organic and inorganic surface coatings. These coatings will alter the surface chemistry of mineral dust with other tropospheric species. In this study the reactivity of ozone on mineral oxides (e.g. α -Al₂O₃ and SiO₂) that had been previously reacted with nitric acid, sulfur dioxide and organics has been measured. Comparison of the kinetics of ozone decomposition on previously reacted particles to particles that have not been reacted shows that the reactivity can either increase or decrease depending on the nature of the coating. Insight into these reactions is obtained by FT-IR spectroscopy of the coated oxide particle surface before and after exposure to ozone.

SS-TuP20 Adsorption of Vesicles to Titanium Dioxide: Effect of Vesicle Size and Lipid Composition, *I. Reviakine*, University of Houston, *F. Rossetti*, ETH Zurich, Switzerland, *A.N. Morozov*, University of Leiden, The Netherlands

Adsorption of intact vesicles has been shown to be the first step in the formation of supported phospholipid bilayers.^{1,2} While the process of supported bilayer formation has been investigated in significant detail, that of vesicle adsorption has received much less attention. Experimental² and theoretical³ studies indicate that the extent of deformation of the adsorbed vesicles determines whether they will form a Supported Vesicular Layer

(SVL) or a Supported Phospholipid Bilayer (SPB). Bending rigidity of the bilayer and vesicle size control the extent of vesicle deformation on a given surface. This study has therefore focused on investigating the effect of these two parameters on the properties of an SVL formed on the surface of TiO₂, where vesicles used in this study adsorbed but did not form SPBs. A combination of spectroscopic (Quartz Crystal Microbalance with Dissipation measurement, QCM-D) and microscopic (Atomic Force Microscopy) techniques was used to follow the adsorption process. Voight model was used to interpret QCM-D response ⁴ and the results were compared with the Random Sequential Adsorption model.

¹ Keller and Kasemo, Biophys J. 1998, 75, 1397.

² Reviakine and Brisson, Langmuir 2000, 16, 1806.

³ Seifert U., Adv. Phys. 1997, 46, 13.

⁴ Voinova et al., Physica Scripta 1999, 59, 391.

SS-TuP21 Perchlorate Reduction on Irradiated Titania Studied by LITD-FTMS, XPS, and IC, K.D. Lormand, D.P. Land, E.L. Pyatt-Rudolph, University of California-Davis

Inorganic contaminants in water supplies have been a concern for decades, due to possible deadly health effects. Perchlorates, in particular, have posed a major concern as of late due to their irreversible and damaging effects on the human thyroid, long residence time in water sheds, and resistance to existing catalysts used in water treatment. However, preliminary studies have shown that oxidized surfaces of titanium exposed to ultraviolet radiation reduce perchlorates in aqueous solutions effectively. The reaction mechanism of this reduction has been studied using laser induced thermal desorption- Fourier transform mass spectroscopy, x-ray photoelectron spectroscopy, and ion chromatography. A new chamber that allows for the rapid introduction of samples reacted in aqueous solution into UHV for analysis was used for the LITD-FTMS studies. Reacting the perchlorate solutions with the titania catalyst at atmospheric pressures allows for a more inclusive reaction mechanism due to the incorporation of atmospheric water, carbon dioxide, nitrogen, and oxygen. Surface species are seen both in the LITD-FTMS experiments as well as in the XPS studies, while species that do not adhere to the catalyst surface can be seen in the IC solution studies. Studies show that LITD-FTMS of perchlorate and its oxy-chloride derivatives do not have distinct enough fragmentation patterns to be studied by LITD-FTMS. XPS and IC studies have indicated that titania, in a thin film form, is a slow, but effective catalyst for the reduction of perchlorate. Higher surface area titania, like nano-particulate titania, may prove faster in the reduction of perchlorate to chloride.

SS-TuP22 Electron- and Photon-stimulated Desorption of Alkali Atoms from a Lunar Sample and a Model Mineral Surface¹, *B.V. Yakshinskiy*, *T.E. Madey*, Rutgers, The State University of New Jersey

To investigate mechanisms for the origin of alkali atoms in the atmosphere of the Moon, we are studying the electron- and photon-stimulated desorption (ESD and PSD) of K atoms from a model mineral surface (SiO₂ film), and ESD and PSD of Na atoms from a piece of lunar basalt. X-ray photoelectron spectroscopy demonstrates the existence of traces of Na in the lunar sample. To permit increased signal for detailed measurements of desorption parameters (appearance thresholds, yields, energy distributions), a fractional monolayer of Na is predeposited onto the lunar sample surface. An alkali atom detector based on surface ionization and a time-of-flight technique are used for ESD/PSD measurements, together with a pulsed electron gun, and a mechanically-chopped and filtered mercury arc light source. We find that bombardment of the alkali covered surfaces by UV photons or by electrons with energy E>4 eV causes desorption of hot alkali atoms. The results are consistent with the model developed to explain our previous measurements of sodium desorption from a silica surface² and desorption of K atoms from water ice:³ charge transfer from the substrate to the ionic adsorbate causes formation of a neutral alkali atom in a repulsive configuration, from which desorption occurs. The data support the suggestion that PSD by UV solar photons is a dominant source process for alkalis in the tenuous lunar atmosphere.

¹supported in part by NASA

²B. V. Yakshinskiy and T. E. Madey, Surf. Sci. 451(2000) 160

³B. V. Yakshinskiy and T. E. Madey, J. Geophys. Res. 106, E12(2001) 33303.

SS-TuP23 The Periodically-Stepped NiO(100) Surface and the Adsorption of Bromobenzene, S. Chapman, M.A. Langell, University of Nebraska-Lincoln

Periodically-stepped NiO(100) was prepared and characterized the surface with Low Energy Electron Diffraction, (LEED), Auger Electron Spectroscopy, (AES), and XRay Photoelectron Spectroscopy, (XPS) to model surface defects relevant to heterogeneous chemical processes. All solid materials, including single crystal surfaces, possess irregular steps and other defects. These step defects, model undercoordinated sites that initialize catalytic and other chemical behavior. The NiO(100) single crystal was cut, polished, and oriented with regular repeating steps of seven-atom terrace width. LEED diffraction patterns are characteristic of an ordered step array with appropriate terrace and step height dimensions. Preliminary results show bromobenzene adsorbs onto stepped NiO(100) surface at 133K. The XP spectra of 515L of the adsorbate give two distinct carbon peaks separated by 4.5eV and the Ni 2p region peaks exhibit minimal structure loss. Thermal Desorption Spectrometry, (TDS), shows the majority of physisorbed bromobenzene desorbing molecularly by 190K and smaller adsorbed ring fragments around 280K. Studying a surface of characterizable defects of known density helps further the understanding of the first initial steps occurring in a chemical reaction and in the fabrication of nanostructure materials.

SS-TuP24 MCS and KMCS of Adsorption Probabilities: The Autocatalytic Adsorption Phenomenon, J. Stephan, University of Potsdam, Germany, U. Burghaus, Ruhr-University of Bochum, Germany

An increase in the coverage, Θ , dependent adsorption probability, $S(\Theta)$, with increasing coverage, i.e. an auto-catalytic adsorption phenomenon which is called for now adsorbate-assisted adsorption, has frequently been observed for the adsorption of prototype molecules on quite different surfaces. However, the effect has rarely been addressed theoretically. We present a steady-state Monte Carlo (MČS) version of the modified Kisliuk model which is consistent with the energy, E_i, dependence of the phenomenon and includes the effect of surface defects on $S(\Theta)$. Although steady-state MCS lead already to a better understanding of the microscopic scenario than analytical models, the influence of the adsorption temperature, T_s , on $S(\Theta)$ can in principle not be studied. We therefore present additionally first results of a time-dependent (kinetic) Monte Carlo simulation scheme (KMCS) which can account in principle also for the T_s dependence of $S(\Theta)$. The MCS schemes are tested for different adsorption scenarios (such as the Kisliuk and Langmuirian dynamics) and especially for the auto-catalytic adsorption. Furthermore, a comparison of the simulations with experimental data for CO adsorption on both polar (O- or Zn-terminated) ZnO surfaces [Th. Becker, et al., JCP 113 (2000) 6334] will be shown. Although the scheme can be applied to other adsorption systems, the polar surfaces of ZnO are a perfect test system for the algorithm which is mainly based on the differences in the mass-mismatch of the adsorbate (CO) and the surface atoms (O or Zn).

SS-TuP25 Synchrotron Radiation Xray Photoelectron Spectroscopy Study of Thermal Effects on Nb Surface Oxides¹, *Q. Ma*, *P. Ryan, J. Freeland, R.A. Rosenberg*, Argonne National Laboratory

We report a recent xray photoelectron spectroscopy study of thermal effects on the oxides grown in air on crystalline Nb surfaces. Both angleresolved and glancing-incidence x-ray photoelectron spectroscopy techniques were used in this study. The samples were annealed at 430 °K and 540 $^{\circ}$ K for various lengths of time. We will demonstrate that the reduction of the insulating Nb₂O₅ layer to lower oxidation states is primarily an interface-mediated reaction. Annealing at 430 °K produces a semiconducting, layered oxide with a composition of NbO_x that changes from x = 2.5, 2.0, 1.5, 1.0, to 0.5 across the oxide. Annealing at 540 °K produces a metallic oxide layer with a composition that is mainly NbO_{0.5}, but changes continuously and rapidly near the oxide surface. A photoelectron diffraction effect is observed on the 540-K annealed surface, which possibly indicates the formation of an ordered, but faceted, oxide layer. Oxygen readily diffuses into the Nb substrate by annealing at 540 °K. However, oxygen diffusion proceeds predominantly within the oxide in the case of annealing at 430 °K.

¹This work is supported by the U.S. Department of Energy, Office of Basic Energy Sciences, under Contract No. W-31-109-ENG-38.

SS-TuP26 Active Sites of Photocatalyst for Water Decomposition of RuO₂-dispersed pblock Metal Oxides Involving In³⁺, Ga³⁺, Sn⁴⁺ and Ge⁴⁺ with d¹⁰ Configuration, J. Sato, H. Nishiyama, N. Saito, K. Ikarashi, Y. Inoue, Nagaoka University of Technology, Japan

The development of solid photocatalysts to produce hydrogen from water has been among important issues. The photocatalysts discovered so far have been the transition metal oxides with d⁰ configuration. In aiming at finding a new photocatalyst group, we have focused on the p-block metal oxides with d¹⁰ configuration.¹ In the present study, MIn₂O₄, MGa₂O₄, M₂SnO₄ (M = Mg, Ca, Sr, Ba), and Zn₂GeO₄ were employed, and the effects of M on the photocatalytic activities were examined. For photocatalytic decomposition of water, RuO₂ were loaded on p-block metal oxides by an impregnation method. MIn₂O₄ (M= Ca,Sr) have pentagonal-prism-like tunnel structures with two distorted InO₆ octahedra each. For M = Ca and Sr, hydrogen and oxygen were stably evolved in repeated run under Xe lamp light illumination, whereas little activity was observed for M= Ba. The activity of M₂SnO₄ (M= Ca, Sr, Ba) was remarkably large for M= Ca and M= Sr, but negligible for M= Ba. The SnO₆ octahedra of M= Ca and M=Sr were distorted, whereas those of M= Ba were normal, indicating the contribution of the deformed octahedra to photocatalysis. In MGa₂O₄ (M=Mg, Sr, Ba), the activity was observed for M=Sr and M=Ba, but not for M=Mg, for which there existed correlation between photocatalytic activity and distorted metal-oxygen units. The present study clearly demonstrates that the distorted metal-oxygen units play an important role in the photocatalysis, which is possibly related to the efficiency of photoexcited charge formation. The p-block metal oxides with d¹⁰ configuration is concluded to form a new photocatalyst group for water decomposition.

¹ J. Sato, N. Saito, H. Nishiyama, and Y. Inoue, J. Phys. Chem., 105, 6061 (2001).

SS-TuP27 How Thick is my Oxide?, D.D. Allred, S. Lunt, Brigham Young University

"How thick is the oxide on this sample?" is a question is frequently heard in the lab. After a thin film is removed from the deposition system, exposing it to air on its top surface, it can begin to tarnish. I will review our work in determining the kinetic constants required to answer the question posed, to estimate the thickness of the tarnish layer as a function of time and temperature for several thin film metal exposed to laboratory air at temperatures near ambient for times up to several thousand hours. The thickness and composition of the tarnish layer is important, particularly when it is to be used in an application, such as for gate oxides for ULSI devices, for which understanding and controlling the thickness of ultrathin oxide layers is important. Our EUV optics deposition group also labors in an area where the thickness of ultrathin post deposition films is extremely important. We have looked for a single, or set of, papers which would help us answer this question for materials of interest for the extreme ultraviolet optics (EUV) community. Since the data could not be found in the literature, we resolved to measure and report them. We have studied the tarnishing of a variety of very thin metal films (typically 3-30 nm) including: Al, several of the 3-d metals (e.g. Sc, V, Cr, Fe), one each of the 4d (Ru) and 5d (W) metals and U, and UO2 in laboratory air at temperatures near ambient for several months. We have used spectroscopic ellipsometry, AFM, XPS, and low-angle x-ray diffraction in this work. The tarnish formed is not the familiar bulk oxide for Al and some other cases. We will focus particularly our progress in understanding the stages of oxidation in the 2-6 nm range, thicker than is usual for surface studies but thinner than most corrosion work. We will also show that EUV reflectance is itself a sensitive tool for measuring the thickness of ultrathin oxide films such as SiO2 and UO2.

SS-TuP28 New Insights into Self-Assembled Monolayer Structure and Dynamics, *S.B. Darling**, *S.J. Sibener*, The James Franck Institute at The University of Chicago

We have studied the effect of adsorption of a low-density alkanethiol monolayer on the state of the Au(111) reconstruction. It is commonly believed that the substrate deconstructs following formation of a thiolate self-assembled monolayer, but our results suggest this is not always the case. Helium diffraction from 1-decanethiol (C10) and 1-octanethiol striped phase monolayers is exploited to establish the surface nearest-neighbor spacing and to illustrate a unit cell corresponding to the long dimension of the $(23x\sqrt{3})$ reconstruction. Complementary scanning tunneling microscopy data are also presented that show persistence of the reconstruction during growth of a decanethiol striped phase monolayer and no evidence for vacancy islands typically associated with deconstruction. Our model involving a still-reconstructed substrate is consistent with all of the available data. Furthermore, the low-energy surface vibrational structure of the $(11.5x\sqrt{3})$ striped phase of C10 has also been studied. Energy-transfer spectra for this system exhibit a dispersionless inelastic feature at 8 meV. We assign this to the frustrated translation of the entire molecule vibrating with polarization perpendicular to the surface. These results further the understanding of the forces that govern nanoscale self organization.

SS-TuP29 Oxygen Induced Reconstructions and Epitaxial Growth of MoO2(100) on Mo(112) : A Combined STM and LEED Study, B.K. Min*, A.K. Santra, D.W. Goodman, Texas A&M University

Oxygen chemisorption followed by oxidation of Mo(112) has been investigated in detail by the use of low energy electron diffraction (LEED) and scanning tunneling microscopy (STM). Oxygen-induced p(2x3)-O, p(1x2)-O and p(1x3)-O missing row reconstructed surface structures are observed using STM and are shown to be dependent on the substrate temperature during oxygen adsorption. Atomically resolved STM data explain the undulated LEED pattern observed for the p(1x3)-O surface. This is the first direct demonstration of the epitaxial growth of MoO2(100) on a Mo(112) surface where the p(1x3)-O reconstructed surface is shown to be the precursor. A new oxide surface has been observed that corresponds to the c(2x2) reconstruction of MoO2(100) and correlates with the onset of oxide formation. Oxidation at 1250K produces a mixture of MoO2 and MoO3 (3:1) as determined by XPS and AES.

^{*} Morton S. Traum Award Finalist

Wednesday Morning, November 6, 2002

Organic Films and Devices Room: C-102 - Session OF+EL+SS+SC-WeM

Metal-Organic Interfaces

Moderator: L.J. Guo, University of Michigan

8:20am OF+EL+SS+SC-WeM1 Interfaces between Metals and Conjugated Organic Materials: From Physisorption to Covalent Bonding, N. Koch, Princeton University, J. Ghijsen, Facultes Universitaires Notre-Dame de la Paix, Belgium, A. Rajagopal, Rutgers University, C. Chan, Princeton University, J.J. Pireaux, Facultes Universitaires Notre-Dame de la Paix, Belgium, J. Schwartz, A. Kahn, Princeton University INVITED

The electronic properties of interfaces formed between conjugated organic materials (polymers and small molecules) and other organic and inorganic materials are of paramount importance in terms of the performance of organic-based devices (e.g., light emitting diodes, thin film transistors). The alignment of energy levels at such interfaces is a direct consequence of the physical and chemical interactions between the materials. Using mainly photoemission spectroscopy (PES), we show that the nature of interaction between low work function metals and phenylene-based electroluminescent oligomers and polymers covers the whole range from physisorption (aluminum and samarium) to chemical reduction (calcium), and to charge transfer reactions (alkali metals). Although PES is a very powerful experimental tool to determine electronic properties of interfaces, great care must be taken in the interpretation of the data when wide band-gap materials, such as conjugated organic materials, are being investigated. We demonstrate that the observation by PES of a finite density of occupied states at the Fermi-level on an organic film in which alkali metal atoms have been intercalated does not necessarily imply metallicity nor the presence of negative polarons (radical anions), as previously proposed. From a combination of ultraviolet PES and Kelvin probe measurements, evidence is obtained that the substrate and the surface of the organic film are not necessarily in thermodynamic equilibrium, leading to potential misinterpretations of the Fermi level position at the surface of organic films.

9:00am OF+EL+SS+SC-WeM3 Structural and Electronic Properties of the Interfaces between Au(111) and the Organic Semiconductors Pentacene and p-sexiphenyl, C.B. France, P.G. Schroeder, B.A. Parkinson, Colorado State University

Thorough understanding of the interface between organic semiconductors and metal contacts is important because of charge transfer events that take place in new devices based on organic semiconductors. Transistors¹ and photovoltaic devices² have been fabricated using pentacene as the organic semiconductor. In the interest of understanding the structural and electronic environments of these interfaces we have investigated thin films of pentacene and p-sexiphenyl on the Au(111) surface in ultrahigh vacuum using multiple characterization techniques. The entergetics of these heterojunctions have been measured using photoemission spectroscopy. Large interfacial dipole barriers exist at the interface of both systems. Temperature programmed desorption has been used to investigate the binding environment of the organic semiconductors on the metal substrate. Two different binding environments have been uncovered for both molecular semiconductors on the Au(111) substrate. Scanning tunneling mic roscopy has been used to investigate the coverage dependant structures that are formed by thin films of semiconductor molecules on the Au(111) surface. Pentacene was found to generate many overlayer structures at differing film thickness. Structures found on low coverage, monolayer and multilayer films will be discussed.

¹ Schön, J. H.;Berg, S.;Kloc, C.;Batlogg, B. Science 2000, 287, 1022.

² Schön, J. H.;Kloc, C.;Bucher, E.;Batlogg, B. Nature 2000, 403, 408. .

9:20am OF+EL+SS+SC-WeM4 Growth of Organic Molecules on Ferromagnetic Substrates for Hybrid Organo-metallic Spintronic Devices, M.V. Tiba, O. Kurnosikov, B. Koopmans, J.T. Kohlhepp, C.F.J. Flipse, W.I.M. de Jonge, U.S. Schubert, Eindhoven U. of Technology, CNM, The Netherlands

Motivated by the success of polymer based- and molecular electronics, a challenging new field is emerging. Recent work has demonstrated the feasibility of hybrid organo-metallic spintronics, in which the spin degree of freedom is explicitly being used. Application in future magnetic sensor and memory technology has been proposed. Improved characteristics of such devices require very clean interfaces, therefore deposition of organic molecules in UHV environment is desirable. A severe complication of growing ordered structures of organic molecules on transition metal

ferromagnetic substrates is their high reactivity. In this work we investigate the influence of substrate passivation on the bonding to the substrate (and hence the molecular ordering) for different organic molecules. Selection of the molecules is based on their electronic properties as well as their tendency to form well ordered layers. In the particular case of PTCDA molecules deposited on a Ni(111) substrate we show that quarter monolayer of oxygen reduces enough the reactivity of Ni to enable the molecules to form an ordered structure.¹ Current activities aiming at the fabrication of organo-metallic hybrid magnetic tunnel junctions having polycrystalline Co electrodes and organic barriers will be addressed as well.

¹ M.V.Tiba et al. Surf. Sci. 498 (2002) 161.

9:40am **OF+EL+SS+SC-WeM5 Controlling Metallic Contacts to Molecular Electronic Devices**, *A.V. Walker*, *T.B. Tighe*, *O. Cabarcos*, *B.C. Haynie*, *D.L. Allara*, *N. Winograd*, Pennsylvania State University

In the development and design of molecular electronic devices, it is vital to understand the nature of the metal-organic monolayer interaction. To fully characterize these interactions, we employ a multi-technique approach using time-of-flight secondary ion mass spectrometry (ToF SIMS), infrared spectroscopy (IRS), x-ray photoelectron spectroscopy (XPS) and density functional theory (DFT) calculations. Using an unfunctionalized molecular wire (4-[4?-(phenylethynyl)-phenylethynyl]-benzenethiol) monolayer on Au, we demonstrate that the metal-monolayer contact can be varied from complete destruction of the monolayer to contact formation at the monolayer terminus to complete penetration through the layer. For example, we show that upon deposition of Cu or Ag, the Cu and Ag atoms simultaneously interact with the terminal phenyl ring and penetrate to the Au/S interface. In contrast, Au penetrates through the monolayer at all coverages studied. By using metals specifically tailored for the chemistry of the device molecule as well as for electronic states, the characteristics of the metal-molecule contact can also be controlled. These types of data provide a foundation for rational design of contacts in molecular electronic devices.

10:00am **OF+EL+SS+SC-WeM6 DLC Thin Film as Electron Injection Layer in Organic LEDs**, *M. Cremona*, Pontificia Universidade Catolica do Rio de Janeiro, Brazil, *R. Reyes*, Universidad Nacional de Ingeniería, Perú, *C.A. Achete, P.I. Guimarães, S.S. Camargo, Jr.*, Universidade Federal do Rio de Janeiro, Brazil

Recently, there has been an increased interest in organic light emitting diodes (OLEDs) due of their potential applications to color flat panel displays and in new optoelectronic components. These devices are assembled using three organic molecular materials: an electron injection layer, the emitting one and finally the hole injection layer. However, in most cases the electron injection is more difficult to achieve than hole injection. In this work two different diamond like carbon (DLC) thin films cathode were used to decrease the electron injection barrier. The first kind were nitrogen-doped amorphous hydrogenated hard carbon films deposited by rf glow discharge from methane-nitrogen mixtures onto the TPD/Alq₃ layer structure thermally deposited. DLC films were obtained for different N₂ partial pressures (bias voltage V_b=â€"370 V and total pressure P=8 Pa). Next, amorphous carbon nitride thin films (a-CN_x) have been deposited using a rf diode sputtering system onto the same organic structure. In this case the DLC films were deposited in reactive nitrogen-argon atmospheres. The partial pressure of nitrogen ranged from 0% to 100% at two different deposition pressures (P = 2 Pa and P = 8 Pa). In both cases a thick (150 nm) aluminum electrode were deposited onto the whole structure. The deposition process for the organic compounds is performed in high vacuum environment (6x10⁶ Torr) on glass substrates coated with an hole injecting ITO transparent layer. A preliminary investigation was conducted on the properties of the OLED device with the two DLC intermediate layers. The relationship between the properties of the DLC deposited films on the electroluminescent characteristics of the different devices are investigated. The refractive index of the DLC film deposited, their conductivity and optical absorption, the OLED I-V curves, a preliminary photoluminescent and electroluminescent OLED results are presented and discussed.

10:20am **OF+EL+SS+SC-WeM7** Self-assembly of Molecular 1D wires on Cu(110), Y. Naitoh, F. Rosei, P. Thostrup, M. Schunack, F. Besenbacher, University of Aarhus, Denmark

The adsorption of a large organic $C_{90}H_{98}$ molecule, known as the Lander molecule, is studied by Scanning Tunneling Microscopy (STM) on a Cu(110) surface.¹ By exposing the surface to low doses of oxygen at elevated temperatures, we form a nanopattern of alternating bare Cu(110) regions and (2x1)-O reconstructed regions aligned parallel to the [001] direction. The oxygen-induced reconstruction reveals a long-range ordering of Cu-O rows 20-50 Å wide. When deposited on this template, Lander

molecules adsorb preferentially on bare Cu regions. By tuning the oxygen dosing, thereby adjusting the lateral periodicity of the template, and by varying molecular coverage in a controlled manner we can form long 1D rows of molecular wires. This type of assembly opens new possibilities for ordering organic molecules on surfaces.

¹ F. Rosei et al., Science 296, 328 (2002).

10:40am **OF+EL+SS+SC-WeM8 Dip Pen Nanolithography on Insulating Substrates**, *S.E. Kooi*, *P.E. Sheehan*, *L.J. Whitman*, Naval Research Laboratory

Methods of assembling nanoscale components at chosen locations on a surface are needed to produce nanoscale electronic and sensor devices. Dip pen nanolithography (DPN) has been successful in producing such features as small as ~10 nm wide and one monolayer thick in several different molecule - surface combinations. The most studied systems have been alkyl and aryl thiol depositon on gold surfaces; however, DPN has also been demonstrated for inorganic salts on silicon, biomolecules on gold, and silazanes on semiconductor surfaces. We explore the application of DPN to write functional molecules on a technologically important insulating surface, namely silicon oxide. We have written several different trichlorosilane molecules directly onto thermally-grown silicon oxide substrates. By choosing an appropriate trichlorosilane and post-deposition chemical modification of the written molecules, we can direct the deposition of other nanostructures (such as carbon nanotubes, semiconducting nanowires, or nanoparticles). For example, by writing 10undecenyltrichlorosilane onto silicon oxide, we can create a terminal carboxylic acid group with a post-deposition chemical oxidation. Subsequent deprotonation of the patterned carboxylic acid groups produces a negative charge that directs the deposition of positively-charged nanostructures. The ability to place nanoscale components at chosen locations on a surface, in combination with traditional (e-beam) lithographic techniques, opens up the possibility of interfacing nanoscale components with traditional devices.

Surface Science Room: C-110 - Session SS+EL-WeM

Nucleation & Growth of Semiconductors

Moderator: B.S. Swartzentruber, Sandia National Laboratories

8:20am SS+EL-WeM1 Nucleation and Epitaxial Growth of Gallium Nitride on Sapphire (0001) using Ion-beam-assisted Molecular Beam Epitaxy, *B. Cui*, *I.P. Steinke*, *P.I. Cohen*, University of Minnesota

Molecular beam epitaxy (MBE) is a far from equilibrium growth technique that relies purely on thermal energy to provide high quality thin films. At the relatively low temperatures used a key limitation is often the widely disparate adsorptive and diffusive properties of the film constituents. To provide additional control over the growth kinetics, we have used a low energy ion beam from a Kaufman source to impinge on the surface at low glancing angle of about 4 degrees. First experiments examined the nucleation and growth of GaN on the basal plane of sapphire. The sapphire substrates were pretreated in an ion flux and then annealed for cleaning. The sapphire was then nitrided at 1100K for about 10 min. Then GaN was nucleated by a sequence of adsorption and annealing steps. Finally, a very thin film of GaN was grown under conditions of excess Ga. Ammonia was the nitrogen source throughout. For comparison a GaN film was grown under identical procedures but using an ion beam. An Ar ion beam at 300 eV with a current of 20 micro A/cm2 was incident on the sample after a few of the initial nucleation steps were carried out. Atomic force micrographs of the resulting films showed films with a granular structure. The grains were nearly doubled in size. Small islands apparent in the normal growth were not present when the films were grown using the ion beam. The evolution of the island sizes is compared to a rate equation model of the ion-assisted growth. Partially supported by the National Science Foundation and the Office of Naval Research.

8:40am SS+EL-WeM2 STM Characterization of Ge Nucleation on Ge(001), M. Li, E.I. Altman, Yale University

The initial stage of Ge homoepitaxial growth has been studied using scanning tunneling microscopy (STM). When 0.12 ML of Ge was deposited on the Ge(001) surface at 310 K, <130>-oriented metastable clusters dominated the surface with very few epitaxial dimer rows oriented across the substrate dimer row. Increasing the Ge coverage to 0.18 ML led to an increase in the density of epitaxial dimer rows. Metastable dimers disappeared at the same Ge coverage but at a higher growth temperature of

420 K, which can be explained by the competing process of the transition from metastable dimers to stable epitaxial dimers against that of the coalescence of metastable dimers to form <130>-oriented metastable clusters. At the same temperature, a myriad of epitaxial structures including single buckled B dimers, single nonbuckled dimer rows with ends terminated by either B and D dimers or D dimers only; single buckled dimer rows; pairs of buckled dimer rows with local c(4x2) structures; pairs composed of one buckled and one nonbuckled dimer rows; as well as larger epitaxial islands were first observed. The observed islands as well as second-layer nucleation elongate preferably along 2x direction of the islands and substrate respectively, which can be explained by 1) the fast diffusion of ad-dimers along 1x direction (dimer row direction) of the islands and substrate; and 2) the strong capture probability of diffusing addimers along 2x direction of the islands and substrate. Nonbuckled SA steps and nonbonded SB steps, which were claimed not to exist on stepped and singular Ge(001) surfaces, were populated on single dimer rows. The interactions between various steps of epitaxial structures and neighboring dimers are also discussed.

9:00am SS+EL-WeM3 High Resolution Large Area STM Analysis of Nucleationless Island Formation in SiGe/Si(100), P. Zahl, P.W. Sutter, J.S. Palmer, E.A. Sutter, Colorado School of Mines

We present an STM analysis of quantum dot (QD) island self-assembly in lattice-mismatched heteroepitaxy. A primary objective of recent research on QD growth is the creation of long-range ordered arrays of QDs of uniform size, a major technological milestone that would pave the way for application of these nanostructures in electronic and optoelectronic devices. The formation of epitaxial QD islands is generally assumed to involve nucleation, a statistical process that would severely impede QD organization. Our recent observations by atomically resolved large area STM document the complete transition from initial surface roughening to the formation of faceted QDs in the heteroepitaxial SiGe/Si(100) system. QD self-assembly occurs in a coninuous process that avoids nucleation.¹² Combining growth with in-situ STM, we analyze the surface morphology evolution with increasing coverage. The key aspect of this analysis is the capability of our system to acquire very large STM scans (up to 400nm x 1000nm with 0.1nm resolution), with an unprecedented combination of image detail and statistics. The 2xn reconstruction and step meandering are analyzed at lower coverages, with the goal of identifying mechanisms that induce long-range order in the nucleationless islanding process. Statistical information is extracted using a SPA-LEED^{3,4} like analysis of STM images in reciprocal space. At higher coverages the surface gets micro-rough and a transition to 3D growth of faceted, pyramid shaped QDs occurs. The arrangement and influence of the surrounding micro-rough area is analyzed in detail, depending on germanium concentration and growth conditions.

¹ P. Sutter and M.G. Lagally, Phys. Rev. Lett. 84, 4637 (2000)

² R.M. Tromp, F.M. Ross, and M.C. Reuter, Phys. Rev. Lett. 84, 4641 (2000)

³ Spot Profile Analysing-LEED

⁴ M. Horn-von Hoegen, Z. f. Kristallographie 214, 591, 727 (1999), I+II.

9:20am SS+EL-WeM4 Scanning Probes and Transition States: Uncovering the Low-barrier Si ad-dimer Diffusion Mechanism on Si(001) by its Electric Field Dependence, *T.R. Mattsson*, *B.S. Swartzentruber*, Sandia National Laboratories, *R. Stumpf*, Motorola Labs, *P.J. Feibelman*, Sandia National Laboratories

Surface diffusion and reactions occur on a picosecond time scale, making direct observation of their atomic mechanisms difficult. Yet, understanding these processes is necessary to control the evolution of surfaces at the nanoscale. We show that the electric field dependence of barriers for surface diffusion and other surface processes can be used to discriminate between different proposed atomic mechanisms. Using density functional theory calculations, we show that "piecewise diffusion", the previously accepted atomic mechanism for ad-dimer diffusion on Si(001), where the ad-dimer partly splits during the transition, has the opposite field-dependence to what is observed. It therefore cannot be the dominant mass-transport mechanism. We describe an alternate process wherein the ad-dimer "walks" along the dimer row, combining rotational and translational motions. This process has a low barrier at zero electric field and a field dependence in agreement with measurements. This approach, comparing the measured and calculated effects of an electric field, is not limited to diffusion on semiconductors, but can also be used to study, e.g., dissociative adsorption barriers. Thus, the electric field in a scanning probe should not be considered a nuisance which is to be corrected for by extrapolating results to zero field, but instead a tool that helps us study states otherwise inaccessible. T.R.M. acknowledges support from the Motorola/SNL computational materials CRADA. Sandia is a multiprogram laboratory operated by Sandia Corporation, a Lockheed Martin Company, for the United States Department of Energy under Contract DE-AC04-94AL85000.

9:40am SS+EL-WeM5 Simulations of Surface Diffusion on Amorphous Silicon, A.S. Dalton, E.G. Seebauer, University of Illinois Surface diffusion over amorphous materials plays a governing role in an increasing variety of applications, including reflow of amorphous metals and oxides, and nanostructure formation for electronic memory devices. However, there exists little literature describing diffusion on amorphous surfaces. The structural and energetic heterogeneity of amorphous surfaces should lead to diffusivities that differ significantly from crystalline ones. Our recent experimental work has confirmed that that activation energy for surface-self diffusion on amorphous Si (a-Si) differs significantly from that for crystalline Si (c-Si), and that the activation energy is temperature dependent. Here we describe the results of molecular dynamics simulations to gain atomistic insights into these phenomena. Calculations using a modified Stillinger-Weber potential confirm marked differences between diffusion parameters on a Si vs. c-Si, with lower activation energies for a Si. Collective motions involving two or three atoms play a significant role, as do long hops over several atomic diameters. Both hopping motion and formation of mobile atoms can be described with distribution functions, which ultimately give rise to temperature-dependent Arrhenius parameters for diffusion.

10:00am SS+EL-WeM6 Relaxation of a Single Silicon Mound during Silicon Deposition on the Si(111)(7x7), A. Ichimiya, Y. Tsutsui, Nagoya University, Japan

Isolated single three dimensional (3D) silicon mounds on the Si(111)(7x7)surface between 700K and 800K have been produced using a tip of a scanning tunneling microscope (STM). Produced 3D mounds are like pyramids with certain facets for the both surfaces. Indices of main facets of the mounds on the Si(111) surface are {311} and small facets are {221}. Without silicon deposition, the pyramid begins to decompose just after the deposition. During the decomposition of the mound, the facets of the pyramid transform into multi-bilayer steps. Finally the mound becomes a bilayer (2D) island with a truncated triangle shape. When silicon atoms are deposited on the surface with retracting the STM tip, the decay rate is reduced due to increasing chemical potential on the surface. For deposition of 5×10^{12} atoms at 700K, the mound is grown slowly just after the production. The height of the mound decreases and the top of the pyramid is truncated. The facets of {311} increase the area and the {221} facets are reduced. Then the pyramid becomes truncated pyramid with stable height of about 10 bilayers. Shapes of the bottom and the top layers are just triangles while these shapes become truncated triangles during decay of the mound without deposition. The difference between the shapes with and without deposition is due to the difference of the chemical potentials on the silicon surface. Therefore the {311} facets of the pyramid become dominant and the $\{221\}$ facets disappear at growth mode of silicon on the Si(111). The behavior of the pyramid during deposition has been expected that the shape changes into two dimensional island, and the {221} facets remain, because silicon mounds tend to two dimensional island during growth on silicon surfaces. It is noted that the present result is different from expectation from the results of the decay process of the pyramid on the Si(111).

10:20am SS+EL-WeM7 Morphology of Crystal Growth on Vicinal Surfaces: MBE and H-assisted MBE Growth on Laser-textured Ge(001), A. Raviswaran, D.G. Cahill, University of Illinois

We delineate the growth conditions of temperature, substrate vicinality, and concentration of surface adsorbates that produce rough and smooth crystal growth of Ge by molecular beam epitaxy. Ge(001) substrates are modified by laser texturing to produce a large range of vicinalities $0<\theta<10^\circ$ within a 5 µm diameter laser-dimple. We then deposit Ge on these modified substrates over a wide range of growth temperatures $150<T<450^\circ$ C, with and without an atomic hydrogen flux of 10^{13} cm² s¹, and characterize the morphologies by atomic-force microscopy. Hydrogen flux suppresses the growth-mound instability at low vicinality and reduces the epitaxial critical thickness at large vicinality. Highly-elongated mounds continue to dominate the morphology to surprisingly high growth temperatures; at even higher temperatures, the morphology of vicinal surfaces is dominated by stepbunching instabilities and the formation of low angle facets. Hydrogen adsorbates continue to play a role in the growth morphology at T=450°C when the steady-state hydrogen coverage is only a few percent.

10:40am SS+EL-WeM8 Characterization of Si(100) Homoepitaxy Grown in the STM at Low Temperatures, *H. Grube*, *G.W. Brown*, *M.E. Hawley*, Los Alamos National Laboratory

We explore the growth of low-temperature bulk-like Si(100) homoepitaxy with regard to microscopic surface roughness and defects. We characterize films grown at different temperatures up to 500K in-situ by means of an effusion cell added to our UHV-STM. The development of novel architectures for future generation computers calls for high-quality homoepitaxial Si(100) grown at low temperature.¹ Even though Si(100) can

be grown crystalline up to a limited thickness,² the microstructure reveals significant small-scale surface roughness³ and defects specific to low-temperature growth.⁴ Both can be detrimental to fabrication and operation of small-scale electronic devices.

- ¹ B. Kane, Nature 393, 133 (1998)
- ² DJ Eaglesham, J. Appl. Phys., 77, 3597 (1995)
- ³ RJ Hamers et al., J. Vac. Sci. Technol. A 8, 195 (1990)

 4 MJ Bronikowski et al., Phys. Rev. B, 48, 12 361 (1993) .

Surface Science

Room: C-112 - Session SS-WeM

New Opportunities and Technique Innovations

Moderator: A.R. Laracuente, Naval Research Laboratory

8:20am SS-WeM1 Surface Vibrational Spectroscopy Beyond the Harmonic Approximation: Experiments and ab initio Calculations of Ethoxy Adsorbed on Cu(100), *M.P. Andersson*, *P. Uvdal*, Lund University, Sweden

We compare high sensitivity experimental reflection-absorption IR spectra of ethoxy adsorbed on Cu(100) with ab initio calculations. The high sensitivity allows for detection of binary combinations of CH bend modes, i.e. overtones and combination bands. As their presence cannot be explained using a strictly harmonic approximation, we include anharmonic effects in the ab initio treatment as well. Calculations at the harmonic level are performed for an ethoxy-Cu17 cluster with a hybrid DFT method. Anharmonic effects are computationally more demanding and are therefore calculated for the free ethanol molecule using the same method and basis set as for the cluster. The anharmonic effects are then added through a standard expression involving third and fourth derivatives of the energy. The method allows for inclusion of both intramode anharmonicity and anharmonic resonance effects such as Fermi resonances due to accidental degeneracy. The experimental spectrum is reproduced in detail, including CH bend overtones and combination bands in resonance with CH stretch fundamentals. The mean absolute deviation is only 10 cm-1 and all intensities are also very well reproduced.

8:40am SS-WeM2 Development of a Time-of-Flight HREELS Using Pseudorandom Modulation, *R.H. Jackson, Z. Yang, L.J. LeGore, P. Kleban, B.G. Frederick,* University of Maine

We have constructed a prototype high resolution Time-of-Flight HREELS utilizing pseudorandom modulation. The instrument is comprised of an LK-3000 HREELS, a custom designed TOF analyzer with a double mu-metal shielded 1.5m flight tube, a Bradbury-Neilsen Gate modulator, a microchannel plate detector, and a Fast Com Tek time to digital converter with 250 ps time bins. The electron optics have been shown to pass a beam of electrons to the detector with energies as low as 0.5eV over a 1m flight length. The TOF spectra are recovered using the Lucy maximum likelihood deconvolution algorithm. Initial measurements show that the method can recover well resolved <4meV peaks at 6eV flight energies to within the capability of the current data acquisition electronics. We will present the methodology for using and calibrating the instrument and show loss spectra of PTFE films comparing the TOF and conventional spectra.

9:00am SS-WeM3 The STM as Operative Tool: Physics and Chemistry with Single Atoms and Molecules, K.H. Rieder, Free University Berlin, Germany INVITED

Recent progress in using the scanning tunneling microscope (STM) for manipulation of individual atoms and molecules is reviewed. Topics include - build-up of artificial nanostructures by lateral manipulation (pulling, pushing, sliding) - determination of physical properties like electron phase relaxation lengths in artificial structures - manipulation and contacting of complex molecules as well as manipulation into parts of molecules with consequences to molecular electronics - induction of all steps of chemical reactions with tips funcionalized by vertical manipulation - investigation of electronic and vibrational influences upon electron induced formation of ice clusters - experiences with attempts to transfer manipulation techniques from metal surfaces to thin insulating films. * In collaboration with: Gerhard Meyer (IBM ZRL), Francesca Moresco, Karina Morgenstern, Ludwig Bartels (UC Riverside), Kai-Felix Braun, Stefan Falsch (PDI-Berlin), Saw-Wai Hla (Ohio State Univ.), Reinhold Koch (PDI-Berlin), Jascha Repp (IBM ZRL), Jens Schulz (PDI-Berlin), Sven Zaphel (Createc) 9:40am SS-WeM5 Microscopic Nature of the Interaction of Water with Noble Metal Surface, *H. Fukidome*, *Y. Kim*, RIKEN, Japan, *Y. Sainoo*, University of Tsukuba, Japan, *T. Komeda*, RIKEN, Japan, *H. Shigekawa*, University of Tsukuba, Japan, *M. Kawai*, RIKEN, Japan

Interaction of water on solid surfaces has been one of the central issues in science.It has been, however, hard to microscopically investigate the interaction of water with solid surfaces by traditional macroscopic spectrscopies, such as infrared spectroscopy and electron energy-loss spectroscopy. One of the reasons for this is that water can form various types of cluster owing to its hydrogen-bonding. A STM-IETS, which can do a spectroscopy at a sinlge-molecular level,¹ was used in our work in order to microscopically study the interaction of water with Pd(110) surface. In our STM-IETS spectra of water monomer, a huge and asymmetrical feature appeared a 57 meV. This can be assigned to the frustrated translational mode of water perpendicular to the surface (Tz).² On the contrary, no feature was absent at 57 meV in a spectra of water tetramer. The abovementioned asymmetrical lineshape of the Tz mode of water monomer arises from the interference between elastic and inelastic tunneling processes. More interestingly, the lineshape of the Tz mode drastically changed within the molecule. This drastic change is caused by the mixing of two molecular orbitals that are responsible for the tunneling processes associated with Tz mode. A comparison between our STM-IETS results and a detailed theory now under construction would tell the microscopic picture of the interaction of water molecules with metal surfaces that has ever remained to be seen.

¹ B.C. Stipe, M.A. Rezaei, and W. Ho, Science 280 (1998) 1732.

² R. Brosseau, T.H. Ellis, and M. Morin, J.Vac.Sci.Technol. A8 (1990) 2454.

10:00am SS-WeM6 First Principles Simulation for NC-AFM Images of Si(111) Ö3xÖ3-Ag Surface, N. Sasaki, University of Tokyo and Japan Science and Technology Corp. (JST), Japan, S. Watanabe, M. Tsukada, University of Tokyo, Japan

Quantitative, or sometimes even qualitative interpretation of non-contact atomic force microscopy NC-AFM images is extremely difficult, which contracts with the case of STM (scanning tunneling microscopy). Therefore theoretical simulations of NC-AFM images based on the first-principles density functional theory play very important role for the analyses of the experimental date. Effects of the tip structure and atom kind dependence can be also clarified, by the theoretical simulation. There have been some extrordinary features have been experimentally reported for the Si(111) $\sqrt{3x\sqrt{3}}$ surface(refferd to $\sqrt{3}$ -Ag hereafter), which await theoretical explanation. Recently Scanning Tunneling Microscopy (STM) experiment of $\sqrt{3}$ -Ag surface have been reproduced well based on the assumption of fluctuated Ag atoms among different energetically stable phases of Inequivalent-Triangle (IET) structures¹ without the tip effects using Monte Carlo simulation.² However NC-AFM experiments of the $\sqrt{3}$ -Ag surface at room temperature³ have not been fully understood yet. Important point here is that, in the case of NC-AFM, the tip effects are much stronger than in the case of STM, which give remarkable influences on the surface dynamics. Therefore in this work, NC -AFM images of $\sqrt{3}$ -Ag surface at both room and lower temperatures have been reproduced by DFT calculations.45 First we report that calculated images successfully reproduce experimental ones for both room temperature⁵ and lower one. For the room temperature image, thermal fluctuation is described by the weighted average of the two IET phases with the Boltzmann factor counting the difference of the interaction energies. Energetically stable IET structure appears in the lower temperature image. Thus it is clarified that, as far as only the room temperature NC-AFM experiment is observed, we cannot obtain information of truly stable IET structure of $\sqrt{3}$ -Ag surface.Next we show a remarkable tip-height dependence of the lower temperature NC-AFM images. In this case the Hydrogen-terminated Si tip is used. As the tip approaches the surface the NC-AFM image pattern changes from that of IET phase to HCT phase, and another IET phase. We explain this transition from the standpoint of the atom relaxation of tip-surface system. Thus our calculated results mean that Scanning Probe Microscopy (SPM) has an ability of not only directly observing dynamic feature of the surface but also mechanically controling the surface structures.

- ¹ H. Aizawa, M. Tsukada, N. Sato, and S. Hasegawa, Surf. Sci. 429, L5c09 (1999).
- ² Y. Nakamura, Y. Kondo, J. Nakamura, and S. Watanabe, Surf. Sci. 493 206 (2001).
- ³ Y. Sugawara et al., Surf. Interface Anal, 27, 456 (1999).
- ⁴ N. Sasaki, S. Watanabe, H. Aizawa, M. Tsukada, Surf. Sci. 493, 188 (2001).
- ⁵ N. Sasaki, S. Watanabe, M. Tsukada, Phys. Rev. Lett. 88, 046106 (2002).

10:20am SS-WeM7 Single Molecular Motion and Reaction Induced by STM Inelastic Tunneling, Y. Sainoo, RIKEN and Tsukuba University, Japan, Y. Kim, T. Komeda, M. Kawai, RIKEN, Japan

Inelastically tunneled electrons using STM device enable vibration excitation of individual molecules applicable to vibration spectroscopy, mode selective reaction and so on. Here we present that the selective excitation is ruled reflecting the symmetry of adsorbed molecules and that the vibrationally excited molecules may react along the reaction coordinate through their multiple excitation state. Examples for selective excitation are given for trans-2-butene on Pd(110) surface where methyl groups are lifted towards vacuum and butadiene with flat-laying geometry. The C-H stretching vibration is clearly observed for trans-2-butene and not for butadiene. Symmetry of the adsorbed states for both adsorbates is determined by XAS and HREELS. Motions of isolated cis-2-butene molecule on the Pd(110) surface at 4.7 K between four equivalent positions were induced and monitored with tunneling electrons of scanning tunneling microscope (STM). These motions were consisted with two different flip-flop motions, and clear threshold energy indicated the existence of different potential barriers for the corresponding motions. The strong dependences of these motions rate on the tunneling current support multiple vibrational excitation mechanism via inelastic tunneling process.

10:40am SS-WeM8 Dry De-intercalation in Layered Compounds upon Controlled Surface Charging in XPS, Y. Feldman, A. Zak, R. Tenne, H. Cohen, Weizmann Institute of Science, Israel

2H platelets and inorganic fullerene-like (IF) MS_2 (M=W,Mo) powders, intercalated with alkaline (A=K,Na) atoms,¹ are studied using controlled surface charging (CSC) in XPS.² The degree of intercalation, expressed in terms of A/M concentration ratios, is found to tightly correlate with the presence of 'open' (hk0) edges, typically absent from the closed IF nanoparticles. Under strong electric fields, applied by an electron flood gun, diffusion process is negligible with low flood gun voltages, indicating that a critical field is needed for this type of dry de-intercalation. Diffusion rates out of 2H matrixes are generally higher than in corresponding IF samples, while those of K are far better than Na. These observations, closely related with the initial intercalation efficiency, provide helpful information about the actual intercalation states and their diffusion mechanisms.

¹ A. Zak, Y. Feldman, H. Cohen, V. Lyakhovitskaya, G. Leitus, R. Popovitz-Biro, E. Wachtel, S. Reich and R. Tenne, JACS 124, 4747 (2002).

² I. Doron-Mor, A. Hatzor, A. Vaskevich, T. van der Boom-Moav, A. Shanzer, I. Rubinstein and H. Cohen, Nature 406, 382 (2000).

Wednesday Morning Poster Sessions

Surface Science

Room: Exhibit Hall B2 - Session SS-WeP

Surface Science Poster Session

SS-WeP1 Study of Polymethylmethacrylate Removers for Electron Beam Lithography through Quantitative Surface Roughness Characterization by AFM, *Q. Hang*, *D. Hill, G.H. Bernstein*, University of Notre Dame

As nanotechnology approaches molecular scales, issues of surface contamination by unremoved resists will play an important role in device fabrication. Electron beam lithography (EBL) of polymethylmethacrylate (PMMA) resist is still among the most widely used nanofabrication techniques, so it is relevant to study its residual contamination on both exposed and unexposed surfaces using a variety of resist removers. Besides preventing good metal adhesion, the resulting contaminant-induced surface roughness reduces the ability to characterize deposited molecular patterns by atomic force microscopy (AFM). We are aware of no systematic, quantitative study of surface roughness after removal of PMMA by different solvents toward determining the least amount of residual resist. The ideal stripper exhibits high affinity for both the polymer (as quantified by the lowest Flory-Huggins interaction parameter) and the substrate, the latter aimed at reducing the solid-liquid surface energy. We characterized the effectiveness of several different strippers: acetone, dichloromethane (DCM), a mixture of acetone and DCM (volume ratio 1:1), 1,2dichloroethane (DCE), a mixture of acetone and DCE (volume ratio 1:1), and the commercial PMMA remover NanoTM Acryl Strip (MicroChem), on two different molecular weights of PMMA. Environmental AFM was used to investigate SiO₂ surfaces before and after PMMA was applied and removed by those strippers. The effects of electron beam exposure of the PMMA will also be presented. Power spectral density and root mean square surface roughness analyses showed that DCM and DEC are the best PMMA removers, and can produce the same surface roughness as the original SiO₂ surface (i.e. no contamination). Estimates of the polymer-solvent, Flory-Huggins, interaction parameters and surface-solvent interfacial energy (from contact angle measurements) satisfactorily predict the effectiveness of the solvents

SS-WeP2 Functionalization and Patterning of C-H Containing Surfaces Using Oxalyl Chloride, G. Husseini, E.T. Sevy, M.C. Asplund, M.R. Linford, Brigham Young University

Functionalized and patterned surfaces are of great utility in a variety of areas of science and technology. One particularly useful functional group is the acid chloride, which readily reacts with amines and alcohols. Here we describe a facile gas-phase method of patterning acid chloride groups onto C-H containing surfaces. Basically, a surface that contains C-H groups, e.g., alkylated silicon or polyethylene, is introduced into a flow-through cell that has a quartz window. A mixture of N2 carrier gas with a low concentration of oxalyl chloride then flows through the cell at room temperature. The surface is next illuminated with 365 nm light, which is known to cause dissociation of oxalyl chloride. Surface reactions then occur that introduce the -COCl group onto the surface where the surface was illuminated and nowhere else. In particular, clean silicon surfaces are first alkylated with dimethyloctadecylchlorosilane. Acid chloride groups are then introduced onto the surface as mentioned above, followed by characterization using XPS, FTIR, ellipsometry and contact angle goniometry. XPS confirms the presence of chemically shifted carbon. FTIR confirms the presence of carbonyl groups. Optical ellipsometry shows an increase in film thickness. Contact angle goniometry shows a decrease in water contact angles. The main advantage of this work is that silicon surfaces can be easily derivatized with an acid chloride in a one-step-photochemical-gas-phase reaction. We are in the process of extending this work to perform photolithographic patterning of surfaces. The resulting functional groups can be used to attach molecules, including biomolecules such as DNA and peptides.

SS-WeP3 Functional Group Effects on the Adsorption of Organics on Silicon Surfaces, S.M. Casey, L. Zhang, A.J. Carman, University of Nevada

Computational studies have been undertaken using density functional theory and cluster models of the Si(100) surface in order to compare the adsorption pathways for small organic molecules that contain different functional groups. The efficiency of nitrogen-addition via the amine group can thus be compared to the efficiency of [2+2] cycloaddition via the alkene group or oxygen-addition via the alcohol group in this manner. By variation

of the functional group, the relative reactivity of these groups with the silicon surface dimers can be surmised. Both nitrogen-addition and oxygen-addition appear to be favored adsorption pathways compared to the [2+2] cycloaddition pathway. A clear preference between the two addition channels is more difficult to determine, however. The results from these computations compare favorably with results from experimental studies of the adsorption of allyl amine, propananine, allyl alcohol, propanol, propene, and 3-amino-1-propanol on this surface.

SS-WeP4 The Formation and Segregation of Carbon at a Ni(111) Surface, H. Nakano, J. Ogawa, H. Hirashima, J. Nakamura, University of Tsukuba, Japan

The formation and segregation of carbon at Ni surfaces are important as initial processes for synthesis of carbon nanotube by Ni catalysts. We have studied the carbon formation by the Boudouard reaction $(2CO -> C + CO_2)$ and the decomposition of ethylene ($C_2H_4 \rightarrow 2C + 2H_2$) using scanning tunneling microscopy (STM), Auger electron spectroscopy (AES) and low energy electron diffraction (LEED). It was found that the behavior of the carbon deposition was very different between the Boudouard reaction and the ethylene decomposition. As for the Boudouard reaction, the carbon was formed at step edges on Ni(111), which immediately diffused into the bulk at 400 - 500 K. The carbon dissolved in the bulk then segregated to the subsurface at low temperatures of 300 - 400 K. The segregation rate was greater at lower temperatures. A single domain of carbide islands located along the step edges was clearly observed by STM, which was explained by the growth of the island initiated at the step edge. On the other hand, no such segregation was found for the carbon formation by the decomposition of ethylene. The decomposition took place on the terrace leading to an isolated unit or carbide short strings without forming islands. The difference in the decomposition behavior was ascribed to that in the site of carbon formation. That is, CO should dissociate at the step edge on Ni(111), while ethylene should decompose to carbon at the terrace site. We have also examined the effect of sulfur upon the carbon formation on Ni(111). Interestingly, no significant poisoning effect was observed upon the formation rate of carbon for both Boudouard reaction and ethylene decomposition.

SS-WeP5 Surface Characterization of Dendrimer-Encapsulated Pt Nanoparticles, *B.T. Long*, *F. Parsons*, *J. Gao*, *C. Murphy*, *D.A. Chen*, University of South Carolina

The ability to prepare metal nanoparticles with narrow size distributions has many potential applications in the field of heterogeneous catalysis. Platinum nanoparticles with uniform size distributions can be prepared from solution in the presence of poly(amidoamine) generation 4 starburst dendrimers. The resulting Pt nanoparticles have diameters of ~1.5 nm and are encapsulated by the dendrimers. These dendrimer-encapsulated metal nanoparticles have been spin-coated on mica and Au surfaces and imaged by tapping mode AFM and STM. At higher concentrations, the surface is covered by a single-layer dendrimer film while at lower concentrations, dendrimer aggregates are observed. Our goal is to remove the dendrimers from the Pt particles, which can then be used for catalytic studies. Thermal gravimetric analysis experiments have shown that the dendrimer begins to decompose at approximately 200°C, but decomposition is not complete at temperatures below 400°C. Ultrahigh vacuum studies will be used to further address the decomposition of the dendrimers. Specifically, the species that remain on the surface at various stages of dendrimer decomposition will be characterized by X-ray photoelectron spectroscopy. Gaseous products that desorb from the surface during decomposition will be monitored by temperature programmed desorption.

SS-WeP6 Dimethyl Methylphosphonate Reaction on Metal Nanoparticles Deposited on a TiO₂(110)-(1x2) Surface, J. Zhou, K. Varazo, D.A. Chen, University of South Carolina

The thermal decomposition of dimethyl methylphosphonate (DMMP) on supported copper and nickel nanoparticles has been investigated under UHV conditions by scanning tunneling microscopy (STM), X-ray photoelectron spectroscopy (XPS) and temperature programmed desorption (TPD). Our STM studies have shown that Cu particles grown on a TiO₂(110)-(1x2) surface at room temperature have a uniform particle size distribution. By annealing the surface to higher temperatures, the particle size can be increased while maintaining narrow size distributions. XPS studies of DMMP adsorbed on small Cu nanoparticles (35 Å diameter) indicate that molecularly adsorbed DMMP is the main species at room temperature. Heating to 350 K results in P-C and P-OCH3 bond scission and the formation of two distinct phosphorous-containing species on the surface. Between 350 K and 700 K, the molecular DMMP continues to

decompose, producing methane and hydrogen as the major gaseous products as observed by TPD. Upon heating to 800 K, all of the carbon is removed from the surface, but 30% of the original phosphorous signal is still observed up to 1000 K. DMMP reaction on the titania surface has also been studied. The surface chemistry of DMMP on larger Cu particles (70-100 Å diameter) will be investigated in order to understand if the size of the Cu particles affects DMMP chemistry. Furthermore, DMMP decomposition on Ni particles of various sizes will also be investigated.

SS-WeP7 S K-edge NEXAFS and S 1s XPS Studies of L-cysteine on Transition Metals, Y. Matsumura, S. Yagi, Y. Nakano, Nagoya University, Japan, E. Ikenaga, S.A. Sardar, J.A. Syed, Hiroshima University, Japan, K. Soda, Nagoya University, Japan, E. Hashimoto, K. Tanaka, M. Taniguchi, Hiroshima University, Japan

We have paid attention to L-cysteine [HSCH₂CH(NH₂)COOH] and investigated the adsorption behavior on polycrystalline Cu, Mo and Ni substrates by S K-edge Near Edge X-ray Absorption Fine Structure (NEXAFS) and S 1s X-ray Photoelectron Spectroscopy (XPS) techniques. The sample was prepared by adsorbing L-cysteine molecules on clean metal surfaces in an aqueous solution at room temperature. Curve fitting of the S K-edge NEXAFS spectra reveals that there is a peak at around 2470eV. The NEXAFS spectra clarifies L-cysteine molecule dissociates for Ni. In the S 1s XPS spectra a sharp peak and a shoulder structure appear at around 2473eV and 2470eV, respectively. The peak deconvolution of the XPS spectra reveals the presence of three S chemical states, which are L-cysteine molecule, thiolate and atomic sulfur. The result of NEXAFS is consistent with that of XPS qualitatively. Keywords: NEXAFS, XPS, L-cysteine, adsorption behavior, Cu, Mo, Ni.

SS-WeP8 Structural, Electronic and Catalytic Properties of Clean and Overlayer-Covered Ir(210), *I. Ermanoski*, *W. Chen, M.J. Gladys, J.S. Quinton, T.E. Madey*, Rutgers, The State University of New Jersey, *M.D. Ulrich, J.E. Rowe*, North Carolina State University

We report results on the structure, morphology, electronic and catalytic properties of the Ir(210) surface - clean as well as covered with gaseous and metallic overlayers. The atomically rough Ir(210) surface is morphologically unstable: When Ir(210) is covered with more than 0.6 ML of oxygen and annealed, pyramidal facets exposing {110} and {311} surfaces develop on the initially planar surface. We have used a variety of methods to characterize this surface, including LEED, STM and high resolution soft X-ray photoelectron spectroscopy (HRSXPS) using synchrotron radiation. To prepare an oxygen-free faceted surface, we use catalytic CO oxidation at ~500 K to react the oxygen off and "freeze" the surface in its pre-prepared faceted state. HRSXPS has been employed to investigate core-level features of all the surfaces mentioned. The Ir 4f7/2 core levels are fitted with Doniach-Sunjic lineshapes. Surface and bulk peak identifications are supported by measurements at different photon energies (different electron escape depths) and variable photoemission angles. All of the surface components (first, second and third layer peaks) are identified with core-level shifts positioned at higher binding energies with respect to the bulk. This result is in contrast to previous reports of binding energy inversion on the Ir(100) surface. Using TPD we find evidence for structural sensitivity in a surface reaction, i.e. differences in the chemical reactivity of on the planar and faceted surfaces. Overlayers of Pd and Pt exhibit structural changes upon annealing, and HRXPS measurements show changes in the core-level properties of the overlayers. Supported by US DOE and ARO.

SS-WeP9 Surface Stress Induced during the Formation of Alkanethiol Self-Assembled Monolayers on Gold-Coated Cantilevers, *M. Godin*, *O. Laroche, V. Tabard-Cossa, B. Seivewright*, McGill University, Canada, *P. Williams*, Acadia University, Canada, *B. Lennox, P. Grütter*, McGill University, Canada

Functionalized alkanethiol self-assembled monolavers (SAM) have proven to be quite versatile in producing sensing layers that are both selective and reactive to specific target molecules during chemical or biochemical sensing. By self-assembling these sensing layers onto the surface of standard atomic force microscope (AFM) cantilevers, we can design micromechanical sensors that are tailor-made to respond to very specific chemical signals. The surface stress induced at the sensing layer during chemical sensing is directly measured as a deflection of the cantilever.¹ We have developed a new method² of obtaining quantitative surface stress measurements from cantilever deflection signals that does not require the knowledge of the cantilever's Young's modulus, which is often difficult to estimate when different sensing layers are used or for commonly used SiNx. We systematically investigated the self-assembly process of alkanethiol monolayers on gold in order to model the surface stress buildup during chemical sensing, ultimately aiming to optimize the sensor's response. In particular, we studied the kinetics of alkanethiol SAM formation by

combining real-time, in-situ, surface stress and thickness measurements. A differential micromechanical sensor was used to measure the surface stress evolution during SAM formation on gold-coated cantilevers from the vapor phase, while thickness measurements were performed by ellipsometry with sub-monolayer sensitivity. Results clearly demonstrate that analyte introduction and cell geometry play a determinant role in the structural development of the SAM, which not only affects the final stress values achieved, but also the kinetics during SAM buildup. Such considerations are crucial when optimizing sensor response through modeling or when comparing results achieved with different sensor systems.

¹R. Berger et al. Science 276, 2021 (2000) ²M. Godin et al. APL 79, 551 (2001).

SS-WeP10 Characterization of Functionalized Thiol-SA-Layers on Au using TP-SIMS and Polyatomic ToF-SIMS, *M. Schröder, J.C. Feldner, S. Sohn, H.F. Arlinghaus,* Westfälische Wilhelms-Universität, Germany

Functionalized monolayer substrates provide the basis for biosensor chips and other biorecognition systems. Several factors, such as type of SA layer building molecules, their functional headgroups and the different parameters concerning the immobilization process, influence the physical, chemical and biochemical properties of these substrate surfaces. We investigated different thiol classes, such as alkanethiols, $C_n H_{2n+2}S$, alkanethiol derivatives and aromatic thiols, with different functional headgroups, e.g. NH₂, COOH or OH, immobilized onto Au-substrates. Thiols with functional headgroups could be linked to larger biomolecules such as DNA and proteins in order to design biosensor-chips for diagnostics. To link NH2-terminated molecules to carboxyllated surfaces, we used 1-ethyl-3-(3-dimethylaminopropyl)-carbodiimide (EDC) to catalyze the formation of an amide bond. Another possibility for linking such molecules to a surface is to bind an NH2-terminated thiol to the gold and use di-(n-succinimidyl)-carbonate (DSC) as a crosslinking mediator. The different reaction steps were monitored using time-of-flight secondary ion mass spectrometry (ToF-SIMS). We carried out ToF-SIMS measurements on SA-layers of different alkanethiols to investigate the time, concentration, and chain length dependence of the layer formation. Also, the influence of primary ion mass and of primary ion constituents on the secondary ion yield was investigated. With temperature-programmed SIMS (TP-SIMS), we were able to compare the desorption temperatures of different thiols, e.g. alkanethiols and their derivatives, and to investigate the influence of functional headgroups on the surface binding energy. From the obtained data it can be concluded that ToF-SIMS and TP-SIMS are useful techniques for investigating physical properties of SA-layers and for controlling crosslinking reactions to optimize e.g. binding conditions of DNA or PNA.

SS-WeP11 Low Temperature STM Investigation of Halosubstituted Biphenyls on Copper Surfaces, L. Bartels, B.V. Rao, Q. Zhang, University of California at Riverside

4,4'-Di-bromo-biphenyl was adsorbed on a Cu(111) single crystal surface in ultra-high vacuum at 25K. The preferred adsorption site and the mobility of the species were investigated. 4,4'-Di-bromo-biphenyl was found to adsorb primarily at step edges on the surface with the long axis of the molecule aligned parallel to the step edge. High-resolution images reveal the individual, substituted benzene rings. Their separation is in good agreement with the value expected from the literature. In contrast, adsorption at nitrogen temperatures does not permit STM investigation of the unreacted species on the surface. STM images are poor and high fluctuations in the tunneling current point to a mobility of the adsorbate beyond the time-scale of the feedback loop. Retracting the tip several nanometers from the sample, the tunneling current does not vanish completely in a reliable fashions. This points to the spontaneous polymerization of 4,4'-di-bromo-biphenyl to long tethers on the surface.

SS-WeP12 Adsorption Behavior of L-cysteine on Transition Metals (Ni, Cu) in Aqueous or Methanol Solution Studied by S K-edge NEXAFS and XPS, S. Yagi, Y. Matsumura, Y. Nakano, Nagoya University, Japan, E. Ikenaga, S.A. Sardar, J.A. Syed, Hiroshima University, Japan, K. Soda, Nagoya University, Japan, E. Hashimoto, K. Tanaka, M. Taniguchi, Hiroshima University, Japan

Adsorption behavior of a sulfur-containing amino acid molecule on transition metal surface has been interested in a bio-catalytic and surface reaction fields. In this study, we have studied the adsorption behavior of the L-cysteine amino acid [HSCH₂CH(NH₂)COOH] on polycrystalline Ni and Cu surfaces by sulfur K-edge Near Edge X-ray Absorption Fine Structure (NEXAFS) and sulfur 1s X-ray Photoelectron Spectroscopy (XPS) techniques. The sample was prepared by scratching the substrate in the aqueous or methanol solution of the L-cysteine at room temperature. In the NEXAFS spectra, a significant difference of the first peak (1s-to- σ^* (S-C)) shape was obtained between two kinds of Ni samples, which were prepared

in the aqueous and methanol solutions. Curve-fitting results of the NEXAFS spectra indicates that the L-cysteine on Ni in the aqueous solution dissociates. On the other hand, the L-cysteine in the methanol solution on Ni does not dissociate. Keywords: NEXAFS, XPS, L-cysteine, adsorption behavior, Ni, Cu, aqueous solution, methanol solution.

SS-WeP13 LEED and HREELS Study of Methane Physisorbed on Ag(111), *M. Sakurai*, *T. Nanba*, Kobe University, Japan

The structure of methane monolayer physisorbed on a Ag(111) surface was observed by LEED. The picture was recorded with suppressed electron current using cooled CCD camera in order to minimize the electron stimulated desorption of adsorbed methane. We have observed that the anomalous feature in the IV curve of very low energy electron scattered from this system at 40K depends on the ambient pressure of methane, with which the physisorbed layer is in equilibrium. By the present measurement, the LEED pattern indicated that the lattice of methane molecules forms hexagonal structure with rotationally commensurate direction with the substrate lattice. The LEED spots were somewhat obscure and had broadened nature in azimuthal direction at the equilibrium conditions; however, they became sharp ones when the substrate was cooled to 25K. We have also performed vibrational spectroscopy of adsorbed methane molecules by HREELS and anomaly in the vibrational excitation cross section (i.e. inelastic IV curve) has been observed. The relation between the IV curve and structure will be discussed.

SS-WeP14 Adsorption and Reaction of NO, CO and O₂ on Cu(100) at Low Temperatures Studied by Infrared Reflection Absorption Spectroscopy, C.-W. Yi, Texas A&M University, C.M. Kim, Kyungpook National University, Korea, D.W. Goodman, Texas A&M University

The adsorption and reaction of NO, CO, and O2 on Cu (100) have been investigated in the temperature range 21 - 200 K using infrared reflection absorption spectroscopy (IRAS). NO forms dimers within the monolayer and multilayer regime at 21 K. The dimer, in turn, converts to N2O above 60 K. A strong lateral interaction between coadsorbed NO and CO at 21 K results in the NO and CO molecules tilting from the surface normal by approximately 45 degree. CO interacts strongly with chemisorbed dioxygen on Cu(100) within the temperature range 50 - 100 K resulting in the vibrational frequency of CO being blue-shifted by 25 cm-1. These studies provide new insights into the molecular interactions that are precursors to reactions between CO and NO/O2.

SS-WeP15 Artificial Control of Reaction Selectivity in Methanol Oxidation and Ethanol Decomposition on Pt, Pd and Ag Catalysts by Dynamic Lattice Displacement of Thickness Extension Mode Resonance Oscillation, Y. Yukawa, N. Saito, H. Nishiyama, Y. Inoue, Nagaoka University of Technology, Japan

Selectivity is a very important factor in heterogeneous catalysis, and it is highly desirable to precisely control it in an artificial manner. We have employed the thickness extension mode resonance oscillation (TERO) of acoustic waves. In the present work, the TERO effects on the selectivity of methanol oxidation and ethanol decomposition on Pt, Ag and Pd catalysts were studied. To change the resonance frequencies of the TERO, four z-cut LiNbO₃ single crystals with different thickness of 0.3, 0.5, 1.0 and 2.0 mm were used: the first resonance frequencies were 11.2 MHz for 0.3 mm thick crystal, 7.3 MHz for 0.5 mm, 3.6 MHz for 1.0 mm and 1.8 MHz for 2.0 mm. A Pt, Ag or Pd film was deposited at 100 nm on the crystals. For methanol oxidation on Pt, the major products were CO2, HCHO and HCOOCH₃. The TERO of 3.6 MHz accelerated the production of CO₂ and HCHO, but little HCOOCH₃. With increasing rf power, the selectivity for HCHO production increased from 9% without TERO, reached a maximum level of 18% at 0.5 W, and decreased. For the same reaction on Pd, the selectivity increased monotonously with increasing rf power. For ethanol decomposition on a Ag catalyst, the TERO accelerated the ethylene production without affecting acetaldehyde production. With increasing resonance frequencies, the selectivity for ethylene production increased, passed through a maximum at 7.3 MHz and decreased. Laser Doppler measurements showed that the magnitudes of standing waves (lattice displacement) caused by the TERO attenuated monotonously with frequency, whereas the number of the standing waves per area increased remarkably. The dependence of selectivity on the resonance frequency is discussed based on the contribution of the magnitudes and density of lattice displacement.

SS-WeP16 Oxygen Adsorption on Cu-9%Al(111) Studied by LEED and AES, M. Yoshitake, S. Bera, Y. Yamauchi, W. Song, National Institute for Materials Science, Japan

Cu-based alloys have been used for electric cables for long time. In the field of microelectronics, Al had been used for electrical wiring. However, it became clear that electro-migration occurs in Al that causes breaking of

wires in minute wirings. Due to this problem, Cu wiring is used in mostadvanced microprocessors. Cu metal is more corrosive than Al and Cubased alloys with a small amount of Al is expected to solve problems both on electro-migration and corrosion. The initial stage of corrosion is oxygen adsorption. We studied surface segregation of Al on Cu-9%Al(111) and oxygen adsorption on the surface with/without Al segregation in UHV by LEED and AES. It was found that Al segregates on the surface to form $(\sqrt{3}x\sqrt{3})$ structure and the structure vanishes above 320C to give (1x1) structure while Al still segregates. The specimen was exposed to oxygen at different temperatures. The amount of oxygen uptake was not structure dependent but temperature dependent. Below 320C, only a small amount of oxygen adsorbed. Between 325 and 600C, oxygen adsorbed surface showed amorphous LEED pattern. The specimen was annealed at 800C after oxygen exposure. When the specimen was exposed oxygen below 600C, the oxygen Auger intensity decreased significantly by annealing and the annealed surface showed ($\sqrt{3x}\sqrt{3}$) structure at room temperature. When the specimen was exposed to oxygen at 600C, diffused spots developed newly in LEED pattern but the pattern disappeared after 800C annealing while oxygen Auger intensity stayed almost constant. Exposing the specimen to oxygen at 725C resulted in clear spots in LEED pattern, which were attributed to $(7/\sqrt{3}x7/\sqrt{3})$ structure.

SS-WeP17 The Diffusion of Single CO Molecules and Dimers on Pd(111), T. Mitsui, Lawrence Berkeley National Laboratory, *M.K. Rose, E. Fomin,* Lawrence Berkeley National Laboratory and University of California, Berkeley, *D.F. Ogletree, M. Salmeron,* Lawrence Berkeley National Laboratory

The diffusion of individual CO molecules on Pd(111) has been studied by scanning tunneling microscopy in the temperature range 40-50 K. By following the random walk motion as a function of temperature an activation energy barrier of 0.116 \pm 0.005 eV and a pre-exponential factor of $10^{-3.5}~{\rm cm}^2{\rm -sec}^{-1}$ were determined. Attractive interactions between CO molecules give rise to the formation of dimers that diffuse as a unit. Diffusion rates for dimers and energy parameters for the pair potential between CO molecules were also obtained. Coadsorbed hydrogen more than doubles the diffusion barrier of CO monomers.

SS-WeP18 Pd adatom-Adatom Interactions on the W (211) Surfaces, T.-Y. Fu, Y.-J. Hwang, National Taiwan Normal University, ROC, T.T. Tsong, Academia Sinica, Taiwan

Adatom-adatom interactions play an important role in controlling the formation of surface layers, thin film growth and catalysis. Direct observations in the field ion microscope make it possible to determine the probability P(R) of finding two atoms at a separation R at equilibrium on a surface at temperature T. The free energy of interaction F(R) can be obtained from the relation: P(R) is proportional to exp[-F(R)/kT]. On W (211) planes, the interactions of two Pd atoms are studied in following cases: two Pd atoms in the same channel, in two nearest neighboring channels, in two next nearest neighboring channels, and so on. When two Pd atoms are in the same channel, they combine easily to form a dimer of bond length 2.74 Å and the dimer can diffuse along the channel. In the other cases, the oscillatory behaviors of interactions along the channel direction are observed. The more is the number of the separate channels, the smaller is the interaction energy maximum. The energy maximum in the same channel, two nearest neighboring channels, and two next nearest neighboring channels are 37.5 meV, 23.0 meV, and 9.0 meV, respectively.

SS-WeP19 Temperature Dependence of Self-Assembled Pb Domains on Cu(111), *R. van Gastel*, *N.C. Bartelt, G.L. Kellogg*, Sandia National Laboratories

Pb deposited on Cu(111) organizes into self-assembled domain patterns.¹ It has been hypothesized that stress differences between the Pb/Cu surface alloy-phase and the Pb overlayer phase stabilizes the domains.¹ The domain patterns can be ordered arrays of dots (``droplet" or ``inverted droplet" phase) or alternating rows (``striped" phase). Their structure evolves as a function of Pb coverage. The feature size, area fraction and degree of long range order of the domain patterns also show a strong dependence on temperature. To understand this behavior, we have investigated the temperature dependence of the domain boundary energy by studying the thermal fluctuations of striped patterns. We observed an increase in thermal fluctuations with increasing T. Our measurements show that the boundary energy decreases by a factor three in the temperature range 570 K to 640 K. Since theory predicts that the stripe width decreases with decreasing boundary energy, this observation can explain the observed T dependence of the stripe pattern. The absolute value of the boundary energy provides an estimate of the surface stress - we discuss this number in the context of first principles calculations. We have also measured the change in area fraction with temperature of the surface alloy and overlayer phases. We observe a decrease in area fraction of the surface alloy phase with increasing T. We

attribute this change in area fraction mainly to a change in the Pb-density of the alloy phase. This work was performed at Sandia National Laboratories, a multiprogram laboratory operated by Sandia Corporation, a Lockheed Martin Company, for the U.S. Department of Energy under Contract DE-AC04-94AL85000.

¹R. Plass, J. Last, N. C. Bartelt and G. L. Kellogg, Nature 412, 875 (2001).

SS-WeP20 Using Ti Interlayers as an Interface Stabilizer to Promote Epitaxial Growth of Fe on Al(100) Surfaces¹, C.V. Ramana, R.J. Smith, Montana State University, B.S. Choi, Jeonju University, Korea

An approach is described to promote epitaxial growth of thin metal films on single-crystal metal substrates by stabilizing the interface with an extremely thin metallic interlayer. A single atomic layer of a metal is deposited at the interface prior to the growth of the metal film of interest to produce an abrupt, epitaxial interface in a system that is otherwise duracterized by interdiffusion or chemical roughness. The stabilized interface prevents interdiffusion and serves as a template for ordered film growth. Using high-energy He+ backscattering and channeling techniques along with low-energy electron diffraction and low-energy He+ scattering, it is demonstrated that an atomically thin layer of Ti metal deposited at the Fe-Al interface, a system well known for considerable intermixing at room temperature, prevents interdiffusion and promotes the epitaxial growth of Fe films on the Al(100) surface. The resulting structure is observed to be stable for temperatures up to about 200 C.

¹Work Supported by NSF Grant DMR-0077534.

SS-WeP21 Surface Structural Studies of Epitaxial Ag/Ni/Pt(111) and Ni/Ag/Pt(111) Ultrathin Films, *C.W. Su*, *Y.W. Chu*, *H.Y. Ho*, *C.S. Shern*, National Taiwan Normal University

The introduction of Ag films on the epitaxial x ML Ni/Pt(111) metal surface, x=1-5, as the capping layer Ag/Ni/Pt(111) or the buffer sandwich Ni/Ag/Pt(111) was investigated by means of Auger electron spectroscopy (AES) and ultraviolet photoelectron spectroscopy (UPS) in UHV. The evidences from monitoring the initial annealing temperature of the Ag/Ni/Pt(111) corresponded to the signals began to decrease in AES show that 1 ML overlayer of Ag retards the bulk diffusion of the Ni atoms toward the Pt substrate. Compared with our previous study,¹ the initial temperatures of the system capped with Ag are higher than those capped without it. As for the behavior of atomic exchange, from Ni/Ag to Ag/Ni, has been observed on the annealed Ni/Ag/Pt(111) surface. Ag atoms migrate to the top at about 400 K and then reach an exchanging equilibrium at a high temperature. The thicker the Ni films, the higher the equilibrium temperature. The variations of electronic valence band by UPS though the annealing processes also attracted ours attention. In additional to the variations of the Fermi edge intensities and of the Ag-Ni hybrid d-band peaks during annealing, an extra peak in UPS appears gradually with the binding energy at about 11 eV on either the spectra of the Ag/Ni/Pt(111) or the Ni/Ag/Pt(111) even the temperature up to 825 K. The heating brought about the changes was contributed to additional chemical adsorption emerged from the surface. The most interesting case was the density of state (DOS) unexpectedly affected by an extra positive or negative bias on the sample. The shift of the UP spectra and the variation of the DOS were also remarkable. Finally, the possible explanations of the phenomena are to be discussed.

¹C. W. Su, H. Y. Ho, C. S. Shern, and R. H. Chen, Surface Science 499, 103 (2002).

SS-WeP22 The Importance of Pb-Vacancy Attraction on Diffusion in the Pb/Cu(001) Surface Alloy, *M.L. Anderson*, *B.S. Swartzentruber*, Sandia National Laboratories

Vacancy-mediated diffusion has recently been shown to be a dominant mass transport mechanism on the Cu(001) surface.¹ Not only are vacancies responsible for self-diffusion of surface-layer Cu atoms, but also for diffusion of impurity atoms such as Pd, In, and Pb, embedded in the surface layer. We use atom-tracking STM to measure the diffusion of embedded Pb atoms directly as a function of temperature to extract the diffusion energies. We find a Pb-vacancy attraction that dramatically affects the diffusion statistics. A diffusion event consists of a "burst" of a series of rapid exchanges between an embedded Pb atom and a surface vacancy. The population density of surface vacancies and their migration energy in the Cu surface layer govern the burst-to-burst time interval statistics. Because a single diffusion event entails a number of Pb-vacancy exchanges, the net displacement of Pb is often much more than a single lattice constant. The details of this displacement distribution are measurably affected by the Pbvacancy interaction. The long length scale of the displacement distribution due to Pb-vacancy attraction is in stark contrast to Pd, which has a repulsive interaction. The energetics extracted from the measurements in comparison with first-principles calculations lead to a better understanding of the driving forces responsible for surface alloy formation and kinetics. Sandia is a multiprogram laboratory operated by Sandia Corporation, a Lockheed

Martin Company, for the United States Department of Energy under contract DE-AC04-94AL85000.

¹ J. B. Hannon, et al., Phys. Rev. Lett. 79, 2506 (1997); R. van Gastel, et al., Phys. Rev. Lett. 86, 1562 (2001); M. L. Grant, et al., Phys. Rev. Lett. 86, 4588 (2001).

SS-WeP23 Bias Voltage Dependence of Apparent Local Barrier Height at Constant Tip-Sample Separation, *S. Yagyu*, *M. Yoshitake*, National Institute for Materials Science, Japan

The bias voltage dependence of apparent local barrier height (LBH) corresponding to "work function" at nanometer-scale has been measured by STM on Au (111) surface with Au tip at constant tip-sample separation (CS). The obtained main result is that in the bias voltage range of I-V curve showing nearly straight (ohmic), the LBH does not depend on the bias voltage and beyond this range the LBH decrease with increasing the bias voltage. The bias voltage dependence has been reported at relatively high bias voltage above 1.5 V. However, these reports had been measured at constant current (CC) conditions generally used in STM / LBH measurements. To measure its dependence under CC, the bias voltage is varied, which causes change in separations. In this situation, the measured results contain both effects (bias voltage and separation). Therefore, to measure the effect of bias voltage on LBH truly, the separation effects have to be eliminated. We have measured bias voltage dependence of LBH at CS using the current on I-V curve, and have compared results at CS with CC. At CS measurements, in the ohmic range (below 0.1V), LBH does not depend on bias voltage within the experimental error. Beyond this range, that is off ohmic, LBH decrease with increasing the bias voltage. On the other hand, at CC measurements, the range of I-V curve showing the ohmic and a slightly off the ohmic, the LBH increase with increasing the bias voltage, because of the increasing in separation. Beyond this range, LBH decreases with increasing the bias voltage as CS case, indicating that separation does not affect any more.

SS-WeP24 Electronic Friction at the High T_c Superconductor-Adsorbate Interface, *X.F. Hu*, *P. Guptasarma*, University of Wisconsin-Milwaukee, *R.W.C. Hansen*, Synchrotron Radiation Center, *C.J. Hirschmugl*, University of Wisconsin-Milwaukee

Electronic friction at a substrate-adsorbate interface can be examined using grazing incidence Infrared Reflection Absorption Spectroscopy (IRAS). Adsorbed molecules provide extra scattering sites for substrate electrons in metallic substrates with electron mean free paths longer than the skin depth. This electron energy loss is observed as a broad absorption feature in the change in reflectivity with and without adsorbates. In superconductors, substrate electrons have varying mean free paths above and below the superconducting transition temperature. We will present IRAS results for CO adsorbed on surfaces parallel to and perpendicular to the ab-plane in near-optimal doped (Tc \sim 95K) large single crystals of Bi₂Sr₂CaCu₂O_{8+y} (BSCCO). The single crystal was grown by the float-zone technique in an infrared image furnace. Measurements were taken both above and below the superconducting transition temperature at the Synchrotron Radiation Center.

SS-WeP25 An UHV Analytical Tribometer to Evidence Tribochemistry, *T. Le-Mogne*, *J.M. Martin*, Ecole Centrale de Lyon, France

Increasing demands in the mechanisms of lubricant additives and thin films have resulted in the development of new tribometers coupled with surface analysis techniques. In this paper the so-called AES/XPS analytical tri botester is presented. In-situ surface analyses inside and outside wear scars without air exposure are possible thanks to a tribometer directly installed in the UHV analytical chamber. Two experimental approaches are developed to study the tribochemical reactions of lubricant additives. The first one consists in UHV friction experiments on tribological films previously formed. Thanks to AES and XPS mapping, the good friction reducing properties of molybdenum dithiophosphate (MoDDP) are explained by the formation of MoS2 in the sliding contact. The second one studies the reactivity of fresh surfaces with gaseous compounds which are chemically representative of lubricant additives. Interesting results have been obtained by comparison between 1-hexene and n-hexane on steel at different partial pressures.

SS-WeP26 Coupling of XPS and XANES to Characterize Sulfides in Films Formed from Lubricant Additives, *M.I. De Barros, J. Bouchet, T. Le-Mogne, J.M. Martin,* Ecole Centrale de Lyon, France

The nature and properties of each species formed in both the antiwear action of zinc dithiophosphate (Zndtp) and in the friction reduction of molybdenum dithiocarbamate (Modtc) are investigated. Special attention was carried out to the advantage of coupling two surface analytical techniques on the Zndtp, Modtc and Zndtp/Modtc combination tribofilms: XPS and XANES spectroscopies. XANES is a bulk analysis of the film compared to XPS which is much more surface sensitive. A Cameron-Plint friction machine was used to generate large tribofilm areas in mild/severe tribological conditions. First XANES spectroscopy at the P K-edge, Mo K-edge and S K-edge was carried out in order to investigate any differentiation between phosphate and sulfides. Afterwards, an XPS analysis was performed in the same location of the tribofilm. Special attention has been paid to the deconvolution of Fe2p, Zn2p, S2p, Mo3d and O1s photopeaks and Auger ZnLMM lines. Analytical results are discussed and compared with theoretical predictions from the Chemical Hardness model for Zndtp, Modtc and Zndtp/Modtc tribofilm formation.

SS-WeP27 Scanning Tunneling Microscopy Studies of a Cu₃Pt(111) Surface and Its Dependence on Preparation Conditions, K.T. Rim, T. Müller, G.W. Flynn, Columbia University, A.V. Teplyakov, University of Delaware

A single crystal Cu₃Pt (111) sample was studied using Scanning Tunneling Microscopy (STM) and Low Energy Electron Diffraction (LEED). The preparation conditions in ultrahigh vacuum have been analyzed by varying annealing temperatures following Ar⁺sputtering on the alloy surface. The STM study reveals that, despite a sharp 1x1 LEED pattern at three different annealing temperatures (825, 845, and 855K), the alloy surface changes from very corrugated to atomically flat over a relatively narrow temperature range. When the sample is annealed at 845K following Ar⁺ sputtering, 10-20nm wide terraces are formed and an ordered 2x2 phase is observed. The atomically resolved STM image of the ordered 2x2 surface shows that bright protrusions correspond to Pt atoms surrounded by Cu atoms that appear dark. This ordered 2x2 phase covers approximately 10 - 15% of the surface, and a chemically mixed, disordered 1x1 phase covers approximately 85 - 90% of the surface. The 2x2 ordered phase also exhibits some defects and antiphase boundaries. Along the step edges of terraces, Pt atoms alternate with Cu atoms, and very few Pt-Pt pairs are observed on the terraces. The chemical reactivity of these two distinct surface phases with respect to HCl and 1-hexene will also be described.

SS-WeP29 Studies of Ballistic Electron Emission Microscopy on p-n Junction Structures, E.R. Heller, J.P. Pelz, C. Tivarus, The Ohio State University

One class of experiments using Ballistic Electron Emission Microscopy (BEEM) makes nm-scale studies of hot-electron transport through a deposited film¹ or 'stack' of metal films (e. g. magnetic multilayers)² and/or insulating layers (e. g. magnetic tunnel junctions).³ For this class of experiments, a high quality (non-leaky) metal/semiconductor Schottky has been required to block thermal electrons. However, desired film deposition techniques (e.g. sputtering) and non-ideal surface preparation often produce very leaky and non-uniform Schottky barriers, making BEEM studies complicated or impossible. We will discuss an alternate approach for such studies which uses a buried pn junction in the semiconductor as the thermal electron blocking layer. We find this permits much higher signal-to-noise for sample structures which are incompatible with good Schottky barriers. By putting the blocking layer inside the bulk of the semiconductor, a leaky or non-ideal metal/semiconductor interface becomes largely irrelevant. A well-designed pn junction still can have low hot-electron attenuation⁴ and extremely good rejection of thermal electrons. We will also discuss related on-going approaches which can permit BEEM studies at reduced temperatures with sensitivity down to the aA (10⁻¹⁸ amp) level. This work was supported by NSF Grant No. DMR-0076362.

¹Lu R. P. et al., J Appl. Phys. 87, 5164 (2000).

²W. H. Rippard and R. A. Buhrman, Appl. Phys. Lett. 75, 1001 (1999).

³W. H. Rippard, A. C. Pirella, and R. A. Buhrman, Appl. Phys. Lett. 78, 1601 (2001).

⁴L. D. Bell et al., Phys. Rev. B 48, 5712 (1993).

SS-WeP30 Monolayer Functionalization of Atomic Force Microscopy Tips for Chemical Sensitive Imaging, *L.W. Zilch*, *A.T. Woolley*, *M.R. Linford*, Brigham Young University

While atomic force microscopy (AFM) provides nanoscale information of surface topology, it is often incapable of detecting chemical differences between regions on surfaces. Thus, the usefulness of this technique increases when the AFM tip is chemically modified so as to perform chemical force microscopy. It is then possible to relate tip forces to both surface topology and chemical interactions between the tip and the surface. We are currently working on modifying silicon AFM tips with a variety of organic monolayers using gas and liquid phase silanes (on silicon oxide) or using 1-alkenes (on hydrogen-terminated silicon). Monolayers are advantageous because they do not substantially degrade the resolution of the technique by increasing the radius of curvature of the tip. After coating the tip with a monolayer we then intend to perform a variety of gas phase reactions in the presence of these coated tips to introduce useful functional groups onto them. Ultimately we intend to create an all gas-phase process for functionalizing AFM tips. We will use the resulting AFM tips to study

surfaces that have regions of different hydrophobicities and chemical functionalities. Two suggested substrates for testing these tips are silicon and gold surfaces microcontact printed with silanes and thiols, respectively.

SS-WeP31 Contrast Mechanisms of Secondary Electron Images from Electron, Ion and X-Ray Excitation, Y. Sakai, T. Tazawa, Y. Iijima, JEOL Ltd., Japan, C. Nielsen, JEOL Inc., T. Ichinokawa, Waseda University, Japan

The atomic number (Z2) effect of the secondary electron yields for metals was compared by using secondary electron microscope (SEM), secondary ion microscope (SIM) imaging and X-ray photoelectron spectroscope (XPS) imaging. The atomic number (Z2) effect of the secondary electron yields for metals has recently experimented in secondary electron microscope (SEM) and secondary ion microscope (SIM) imaging (1). The Z2 dependence of the secondary electron yields is opposite to each other and the brightness of the secondary electron image by electron bombardment increases with increasing Z2, while the brightness of the secondary ion image by Ga+ or Ar+ ion bombardments decreases with increasing Z2. In this experiment, the Z2 dependence of the secondary electron yields in electron and X-Ray excitation are the same and opposite to that in ion excitation. The brightness of the secondary electron images by X-Ray bombardment increase with increasing Z2. These phenomena have been found by this experiment and compared with a difference of emission mechanisms for electron, ion and X-Ray bombardment for metal. The experiment was carried out by using an X-ray photoelectron spectroscope (JPS-9010MC). A photoelectron analysis for XPS has become a well- recognized in surface chemical analysis. The secondary electron peak at about 1 to 20eV was not used for the chemical analysis. But this peak will use for imaging observation, because the intensity of its is higher than the photoelectron peaks. A scanning secondary electron images by X-Ray excitation were measured by a stage scanning imaging method. The analyzing area was selected with the 200um aperture and scanned with a motor controlled stage. A specimen is the plate of Al, Cu, Ag and Au. The secondary electron energy from each metal as excited Mg-Ka(1253.6eV) and monochrometored Al-Ka(1486.6eV) was measured with a hemi-spherical electron analyzer at a constant retarding method (0.6%). For metal, the Z2 dependence of the secondary electron yields in X-Ray excitation increases with increasing Z2.

SS-WeP32 How Old is Surface Science?, *E. Paparazzo*, Consiglio Nazionale delle Ricerche, Italy

Some philosophical and literary testimonies from the Classical World on solid surfaces are reviewed, and their implications discussed in the light of Surface Science. While Plato (V-IV century BC) thought the surface to be a real, material entity, Aristotle (IV century BC) considered it but a merely conceptual abstraction having no existence of its own. Subsequently, the Stoic philosopher Posidonius (I century BC) regarded plane surface as existing both in thought and in reality, although the implications involved in his view were remarkably different from those of Plato's. While Aristotle's view enjoyed a virtually unanimous consensus in antiquity, some passages in book 34 of the Elder Pliny's Naturalis Historia (I century AD) make a notable exception, as they refer to the surface of metal objects as to a region whose nature and behavior are quite different from those of the bulk: in other words, this bears witness to what appears to be an "ante litteram" example of Surface Science. Indeed, Pliny records the peculiar and dramatic ways in which these surfaces are affected by physico-chemical agents from the environment, and he also describes the remedies which best mitigate the effects of such phenomena. Further analogies between "old" and "modern" Surface Science are considered: purely-geometrical Plato's surface is found to compare favorably to a single-crystal surface, whereas the "corporeal" surface involved in Posidonius' view is best likened to an air-oxidized, or otherwise ambient-modified surface. I shall finally argue that the longstanding dominance of Aristotle's view from antiquity onwards has greatly delayed theoretical speculation into solid surfaces.

Wednesday Afternoon, November 6, 2002

Electronic Materials and Devices Room: C-107 - Session EL+SS+SC-WeA

Semiconductor Film Growth and Oxidation

Moderator: R.K. Ahrenkiel, National Renewable Energy Laboratory

2:00pm EL+SS+SC-WeA1 Scanning Tunneling Microscopy and Spectroscopy of Gallium Oxide and Indium Oxide Deposition on GaAs(001)-(2x4), *M.J. Hale, J.Z. Sexton, University of California, San Diego, S.I. Yi, Applied Materials, D.L. Winn, A.C. Kummel, University of California, San Diego*

The surface structures formed upon deposition of Ga2O and In2O onto the technologically important As-rich GaAs(001)-(2x4) surface have been studied using scanning tunneling microscopy (STM) and spectroscopy (STS), low energy electron diffraction (LEED), and density functional theory (DFT) calculations. At submonolayer coverage, the initial bonding sites are different for Ga2O and In2O adsorptions due to the different activation barriers for the two oxides to chemisorb at various sites onto the surface. In₂O initially bonds in the trough between the arsenic dimer rows, whereas Ga₂O first inserts into the top layer arsenic dimer rows. Conversely, at elevated surface temperatures, both Ga2O and In2O form a crystalline monolayer. Both oxides form crystalline (2x1) surface reconstructions that are electronically unpinned: there are no states within the band gap. Although both oxides form a (2x1) surface reconstruction, the surface structures differ. At monolayer coverage the Ga2O/GaAs surface has a much larger step density while the In₂O/GaAs surface shows a broad distribution of row oxide spacing. The DFT calculations confirm the observed surface structures and show that both oxides form unpinned surfaces because the bonding to these oxides restore the charge on the first and second layer As and Ga atoms to near bulk values.

2:20pm EL+SS+SC-WeA2 Structure-Sensitive Oxidation of the Indium Phosphide (001) Surface, G. Chen, University of California, Los Angeles, S.B. Visbeck, Siemens & Shell Solar Gmbh, Germany, D.C. Law, University of California, Los Angeles, R.F. Hicks, University of California, Los Angeles; AVS fellow

Abstract The properties of oxide/semiconductor interfaces significantly affect the performance of indium phosphide-based electronic and photonic devices. In this study, indium phosphide films were grown on InP (001) substrates by metalorganic chemical vapor deposition (MOCVD). Then the samples were transferred to an ultrahigh vacuum system, and annealed at 623 and 723 K to produce the (2x1) and delta(2x4) reconstructions with phosphorus coverages of 1.0 and 0.125 ML, respectively. These structures were exposed to unexcited molecular oxygen, and the reaction characterized by X-ray photoelectron spectroscopy (XPS), reflectance difference spectroscopy (RDS) and low energy electron diffraction (LEED). At 298 K and above, the In-rich InP (001) surface rapidly oxidizes upon exposure to O2. The oxygen dissociatively chemisorbs onto the delta (2x4), inserting into the In-P back bonds and the In-In dimer bonds. By contrast, the P-rich (2x1) reconstruction does not absorb O2 up to 500,000 L at 298 K. Above 453 K, the (2x1) becomes reactive with oxygen inserting into both the In-P back bonds and the phosphorus dimer bonds. Based on these results, we conclude that the oxidation of indium phosphide (001) is highly structure sensitive. This means that the oxide/semiconductor interface formed on InP devices can vary widely depending on the process history.

2:40pm EL+SS+SC-WeA3 The Addition of Sb and Bi 'Surfactants' during GaN Growth by Metal Organic Vapor Phase Epitaxy, T.F. Kuech, L. Zhang, H.F. Tang, J. Schieke, M. Mavrikakis, University of Wisconsin - Madison INVITED

The addition of certain impurities has been shown to modify the growth behavior of several lattice-mismatched epitaxial semiconductor systems, most notably SiGe-Si. Of the many impurities studied, antimony and bismuth have been shown to act as 'surfactants' during SiGe epitaxy altering the critical thickness and surface morphology. Such impurities have not been studied in detail in other systems, such as GaN and related materials. We present data on the role and effect of isoelectronic centers, Sb and Bi, on the structure and properties of GaN epilayers during metal organic vapor phase epitaxy. The Sb addition slightly improved the optical and structural properties of GaN epilayer at a low level of Sb incorporation. The addition of Sb resulted in changes in the GaN surface morphology, which was further explored by the lateral overgrowth epitaxy technique through the changes in the growth rates and the facet formation. The presence of Sb in the gas phase greatly enhanced the lateral overgrowth rate and altered the formation of the dominant facets. While Sb altered the growth facet present during LEO, only a small amount of Sb was incorporated into the GaN, suggesting that Sb may be acting as a 'surfactant' during the GaN MOVPE growth. Sb addition produces surface conditions characteristic of a Ga-rich surface stoichiometry indicating both a possible change in the reactivity of NH₃ and/or enhanced surface diffusion of Ga adatom species. Other changes in the surface chemistry and transport were studied by the use of state-of-the-art periodic self-consistent DFT calculations. Bismuth has also been studied as a surfactant to alter the surface chemistry and defect structure during the GaN growth. Bi addition resulted in a decrease in surface roughness as measured by atomic force microscopy while no significant Bi was incorporated over a broad range of gas phase concentrations.

3:20pm **EL+SS+SC-WeA5** Surface Reaction Study of Tungsten Nitride Precursors Decomposition on Si(100)-(2 x 1), Y.-W. Yang, Synchrotron Radiation Research Center, Taiwan, J.-B. Wu, Y.-F. Lin, H.-T. Chiu, National Chiao-Tung University, Taiwan

Reaching an atomic-scale understanding of the surface reaction pathways followed by precursors during MOCVD thin-film growth is a daunting task. We have been studying the transition metal nitride growth on both Cu and Si surfaces. Here, we report a thermal decomposition study of WN precursor on Si(100)-(2 x 1) using TDS and synchrotron-based XPS techniques. The studied precursors are (t-BuN)₂W(NHBu-t)₂ and (t-BuN)₂W(NEt₂)₂ and their structural characteristics consist of the presence of both W-N and W=N bonds and either the presence or the absence of β -H that influences the thermolysis of the precursors. XPS data show that the metallic tungsten already forms for a submonolayer dose of the precursors at room temperature, suggesting the complete abstraction of the amine ligands by the dangling bonds on Si(100) surface. The evolution of hydrocarbon and amine species during the pyrolysis are followed by the TDS and the results suggests the similarity to the amine adsorption on Si(100). High temperature annealing produces silicon carbides and silicon nitrides. In stark contrast, no metallic tungsten is ever formed during the pyrolysis of the same precursors on Cu(111) and the formation of tungsten nitride is secured through the gradual loss of excessive amine ligands. Based on these results, possible surface reaction mechanism and the structural effect of the precursor are to be discussed.

3:40pm EL+SS+SC-WeA6 Thermal Decomposition and Desorption Study of Tetrakis(diethylamido)zirconium(TDEAZr) on Si(100) for MOCVD and ALD of ZrO₂, K. Yong, J. Jeong, S. Lim, Pohang University of Science and Technology, Korea

Tetrakis(diethylamido)zirconium (TDEAZr) is used as a zirconiumprecursor to deposit zirconium oxide by metal-organic chemical vapor deposition (MOCVD) and atomic layer deposition (ALD). Surface reaction study of precursors can aid in describing the kinetics of MOCVD and ALD. Surface reaction and desorption of TDEAZr $(Zr(N(C_2H_5)_2)_4)$ on Si(100) were studied using temperature programmed desorption (TPD), X-ray photoelectron spectroscopy (XPS) and Auger electron spectroscopy (AES). During TPD, ethylethyleneimine, diethylamine, acetonitrile, ethylene and hydrogen desorbed as main decomposition products of diethylamido, which was chemisorbed on Si(100) through the scission of zirconiumdiethylamido bond in TDEAZr. The formation of silicon-carbide and silicon-nitride was observed on the surface after TPD runs. These results indicated that a complete decomposition of diethylamido also proceeded. A reaction pathway model of TDEAZr/Si(100) was proposed. Also, the coadsorption of TDEAZr with water on Si(100) was studied.

4:00pm EL+SS+SC-WeA7 Reactions of Organosulfur Compounds with Si(100) for Chemically Controlled Epitaxy of II-VI Semiconductors on Si(100), Z. Zhu, A. Srivastava, R.M. Osgood Jr., Columbia University

The growth of silicon-based quantum devices requires precise control of ultrathin Si/wide-bandgap-semiconductor/Si heterostructures. We have investigated the initial stages of chemistry-based low-temperature epitaxy using organosulfur precursors. The approach uses the chemical insight gained from organic functionalization of Si.¹ Thus we have studied the reaction of $(CH_3S)_2$, CH_3SH , $(CH_3)_2S$ with Si(100) at room temperature, under UHV conditions for atomic layer growth of functional-group-terminated sulfur on Si(100). This reaction is the first step in the layer by layer self-limiting epitaxy of ZnS, for example, on Si(100). AES studies indicate that each of these organosulfur compounds have different reaction kinetics with the Si(100) surface and reach different levels of sulfur saturation coverage. The differences observed for $(CH_3S)_2$ and $(CH_3)_2S$

reactions have been shown to be explained by the relative bond strengths and the number of sulfur atoms present in the adsorbate molecule. Our TPD studies from 25-825°C show no sulfur-related desorption. Instead AES studies confirm that sulfur atoms remain on surface until ~ 525°C and then diffuse into the Si(100) substrate upon further annealing. TPD studies also indicate evolution of H₂ at temperatures similar to those obtained for H₂ desorption from saturated atomic H on Si(100). In our studies methyl desorption also occur at T > 650°C, temperatures higher than that of H₂ desorption. The amount of m/e = 15,16 fragments is dependent on the organosulfur compound examined. Chemical strategies are now being explored to grow layers of Zn on methyl-terminated sulfur layer as shown in the epitaxy using sequential H₂S/dimethyl cadmium dosing on ZnSe.²

¹Bent SF, J Phys Chem B, 106(11): 2830-2842, 2002.

²Luo Y, Han M, Slater DA, Osgood RM, J Vac Sci Tecnol A 18(2): 438-449, 2000.

4:20pm EL+SS+SC-WeA8 Kinetics and Mechanism of Adsorption and Ultrathin Oxide Growth by Ozone on Si(100)2x1 and Si(111)7x7, K. Nakamura, A. Kurokawa, H. Nonaka, S. Ichimura, National Institute of Advanced Industrial Science and Technology (AIST), Japan

Ozone is one of the promising oxidants to synthesize an ultrathin oxide film on silicon surfaces for the near-future MOSFET because of rapid oxidation rate at low substrate temperature, negligible thickness of structural transition layers in the oxide film, etc.¹ However, to control the thickness of an oxide film precisely and accurately,² kinetics and mechanism of initial oxide growth must be clarified. Thus, in this paper, we discuss chemistry of adsorption and ultrathin oxide growth by ozone on silicon surfaces. Si(100)2x1 and Si(111)7x7 were exposed to highly concentrated (>80%) ozone gas and monitored by x-ray photoelectron spectroscopy (XPS) and second harmonic generation (SHG). Kinetic analysis has suggested that initial dissociative adsorption of ozone on Si(100)2x1 and Si(111)7x7 proceed with the mechanism of leaving only one oxygen atom on the surface and of desorbing the other two, possibly, as a molecular oxygen. This adsorption, in contrast to that of oxygen, was featured with structureinsensitive kinetics, no activation barrier for the dissociation, and high sticking probability close to unity. After the adsorption was completed, first three oxide layers were synthesized by random adsorption of oxidant species on each layer in the consecutive manner. The formation of three layers led to the further growth of an oxide film with ozone with linear growth kinetics, but not with molecular oxygen. Each of these initial ozoneoxide layers has distinctively different activation energy for its growth: they were estimated 0 eV, 0.34 eV, 0.68 eV, and 0 eV for first, second, third, and above fourth layers on Si(100), respectively, enabling accurate control of the thickness of an oxide film.

¹K. Nakamura, S. Ichimura, A. Kurokawa, K. Koike, G. Inoue, and T. Fukuda, J. Vac. Sci. Technol. A 17 (1999) 1275.

²K. Nakamura, A. Kurokawa, and S. Ichimura, Jpn. J. Appl. Phys. 39 (2000) L357.

4:40pm EL+SS+SC-WeA9 Stress-induced Dissociative Chemisorption of Oxygen on Si(001), *M. Yata, Y. Uesugi-Saitow*, National Institute for Materials Science, Japan

We have investigated the role of surface stress in dissociative adsorption process of O₂ on Si(001)-2x1by supersonic molecular beam technique. The tensile stress was externally applied on the surface along[110] direction. The Si(001)-2x1surface reconstructs by dimerization of atoms in adjacent rows. In areas of the surface separated by an odd number of monoatomic steps the orientation of the dimer bonds is rotated by 90° giving 2x1 and 1x2 orientational domains. Their domain populations are changed to relax the stress at the surface and the kinetics of the change depend on the surface temperature.¹ Below room temperature, the domain populations were almost equal during the molecular beam experiments. Two co-existing dissociation channels are seen, a trapping-dissociation channel at low translational energy of incident Q and a direct activated channel at high translational energy.² In case of the trapping-dissociation, $O_{\!2}$ molecule is trapped to a precursor state and undergoes a kinetic competition between desorption and dissociation. We have estimated a difference in activation barrier heights between desorption and dissociation at 30 meV. The initial dissociative sticking probability for low translational energy of incidence increases as the tensile stress increases. This indicates that trapping-mediated dissociation is enhanced by the stress. We have found that the difference in the activation barrier heights between desorption and dissociation decreases as the stress increases. We will discuss the change of dissociation dynamics with the tensile stress in detail.

¹ F. K. Men, W.E. Packard and M. B. Webb, Phys. Rev. Lett. 61(1988) 2469.

² B. A. Ferguson, C. T. Reeves and C. B. Mullins, J. Chem. Phys.110(1999)11574.

5:00pm EL+SS+SC-WeA10 Direct Detection of D₂O and D₂ on D/Si(111) Surfaces under O Atom Exposures, F. Rahman, F. Khanom, A Acki S. Inanaga A. Namiki Kuuchu Institute of Technology, Ianan

A. Aoki, S. Inanaga, A. Namiki, Kyushu Institute of Technology, Japan Initial oxidation stage of D/Si(111) surfaces by atomic oxygen (O) have been studied from the absorption point of view. O/D/Si(111) co-adsorbed surfaces were prepared by various O exposure on 1.25ML D/Si(111). TPD measurement shows nearly 50% reduction of D adatoms from the surface for 2 min O exposure indicating the D adatoms abstraction by incident O atoms. Measurement of desorbing species have been done with a QMS during O exposures on the 1ML D/Si(111) surface for various surface temperatures (T_S). D_2O as well as D_2 molecules were observed. Rate curves of both species show an initial rate jump and then a gradual increase having a peak, which is followed by a nearly exponential decay with exposure time. Both D₂O and D₂ rates vs. T_S curves show similar line shape to the similar plot of D₂ rates vs. T_S curve obtained for the reaction system of H + $D/Si(111) \rightarrow D_2$. In a previous work, the later reaction was understood as due to the so-called β_2 TPD desorption arising from a dideuteride phase. Therefore, we consider that the O induced D₂ formation proceeds along the same mechanism as for the β_2 -channel TPD. Regarding D_2O formation, it is significant and interesting since the reaction takes place as a result of picking up two D adatoms by single O atom upon collision. We will propose a possible mechanism to explain the O-induced D₂O formation on the D/Si(111) surfaces.

Homeland Security Room: C-209 - Session HS+SS+BI-WeA

Chemical and Biological Detection

Moderator: J.N. Russell, Jr., Naval Research Laboratory

2:00pm HS+SS+BI-WeA1 Photonic Crystals Derived from Nanocrystalline Porous Si: Applications in Detection of Chemical Warfare Agents, Explosives, Pollutants, and Biochemicals, M.J. Sailor, University of California, San Diego INVITED The optical properties of nanostructured porous silicon films are exploited for a variety of sensor applications. With appropriate modification of the electrochemical preparation conditions, multilayered structures can be generated that behave as photonic crystals. These structures can be encoded and used as remote sensors for chemicals. For example, small particles of nanoencoded microporous Si are used to detect chemicals by measurement of the intensity of reflected light from a remote laser probe. The particles contain a periodic porous nanostructure that defines the code. The periodic structure forms a Rugate reflector which displays sharp maxima in the optical reflectivity spectrum at wavelengths that are controlled by the etch parameters. The intensity and wavelength of reflected light is determined in part by the refractive index of the porous nanostructure, which can be modified by adsorption of vapors within the porous matrix. Using a 10 mW laser as an optical probe and telescope collection optics, detection of ethanol, acetone and toluene vapors has been achieved at a distance of 20 m. Control experiments using water vapor at comparable partial pressures show very little response, demonstrating selectivity towards the hydrocarbon analytes. Examples of irreversible detection and reversible sensing modes for explosives, nerve warfare agents, and various biochemicals will also be discussed. A catalyst can be incorporated into the nanomaterials to provide specificity for nerve warfare agents. For example, rapid detection of a fluorophosphonate is achieved by catalytic decomposition of the agent to HF and subsequent detection of the HF in the porous silicon interferometer. The catalyst system can be integrated on the silicon chip and consists of a TMEDA[Cu(II)] catalyst (TMEDA = tetramethylethylenediamine) encapsulated in cetyltrimethylammonium bromide (CTABr) micelles. An operational battery-powered unit has been constructed and tested on the live nerve warfare agent Sarin. These devices are all compatible with conventional Si microfabrication technologies.

2:40pm HS+SS+BI-WeA3 Magnetic Labeling and Microarray Detection of Biomolecules, L.J. Whitman, Naval Research Laboratory INVITED

NRL is developing two novel biosensor systems using magnetic microbeads to probe for target biomolecules specifically bound to receptor-patterned surfaces, with an initial focus on detecting biological warfare agents.^{1.2} The microbeads ærve both as reporter labels and as force transducers to allow "force discrimination" - a technique developed at NRL that greatly reduces the background signal-enabling the identification of single biomolecular ligand-receptor interactions with high sensitivity and specificity. Assays using magnetic labeling and force discrimination have been developed for a variety of bacteria, viruses, and protein toxins (immuno-sandwich assays), and for oligonucleotide microarrays (hybridization assays). How the assays are incorporated into a practical sensor system depends on how the specifically bound beads are detected. We are currently perfecting two detection approaches, an optical system that images beads captured on a patterned nanoporous membrane, and a chip-based sensor system that directly detects beads using an array of giant magnetoresistive (GMR) magnetic field microsensors. The optical system has achieved sensitivities of 10 pg/ml for proteins, $10^{2.5}$ cfu/ml for bacteria, and 10^3 pfu/ml for viruses. Using a single GMR sensor, we have successfully detected 1 fM of DNA in a 30 µL sample with only 15 min of hybridization. I will discuss how the interplay between surface chemistry, sensor design, and microfluidics determines the overall performance of our biosensor systems. Supported by ONR, the DoD JSTPCBD, and DARPA.

¹Lee et al., Anal. Biochem. 287, 261 (2000).

²M. M. Miller et al., J. Mag. and Mag. Mat. 225, 138 (2001).

3:20pm HS+SS+BI-WeA5 Optical Microarrays for Chemical and Biological Detection, D.R. Walt, Tufts University INVITED

We have used coherent imaging fibers to make fiber-optic chemical sensors. Sensors can be made with spatially-discrete sensing sites for multianalyte determinations. We are investigating the limits of our ability to create high-density sensing arrays containing thousands of microsensors and nanosensors. Micrometer- and nanometer-sized sensors have been fabricated by etching the cores of the optical imaging fiber to create wells and loading them with micro and nanospheres. Such arrays can be employed for making genosensors for bio-agent detection. We have also created optical sensors based on principles derived from the olfactory system. A cross-reactive array of sensors is created such that specificity is distributed across the array's entire reactivity pattern rather than contained in a single recognition element. The ability to use such information-rich assemblies for broad-based chemical sensing will be discussed.

4:20pm HS+SS+BI-WeA8 Real-time Detection of TNT Using Microcantilevers with Microcyclic Cavitand Coatings¹, N.V. Lavrik, T. Thundat, G. Muralidharan, P.G. Datskos, Oak Ridge National Laboratory

Real-time detection of nitroaromatic aromatic explosive compounds in various environments is a highly significant task in forensics, anti-terrorist activities and global de-mining projects. In particular, ability to detect trace levels of trinitrotoluene (TNT) in air and soil could greatly reduce continued fatalities from land mines among civilians and be a measure in tracking and locating explosive materials. In our work, we address this challenge of detecting TNT vapors in gaseous environment by using an innovative, highly sensitive microcantilever transducer combined with a chemically sensitive molecular coating based on the macrocyclic cavitand of a calixarene family. We measured responses to vapors of TNT and its analogs, 0-mononitrotoluene and 2,4-dinitrotoluene vapors in the range of temperatures of 298 K to 318 K. Our results were used in order to estimate the limits of detection (LODs) for these compounds and optimize the temperature regime of the designed detection system. In the case of TNT, the steady state responses were large, however, the response kinetics was significantly elongated, which is consistent with an analyte depletion model. As compared to more traditional surface acoustic wave sensors with a proven potential for detection of TNT, our approaches offer a simpler, lowcost alternative without sacrificing the performance. The reported results together with these advantages of microcantilever based gas detectors clearly indicate a viable technological approach to mass produced detectors of explosive materials.

¹ This work was supported by the U.S. Department of Energy and Micro Sensor Technologies, Inc. Oak Ridge National Laboratory is operated for the U.S. Department of Energy by UT-Battelle under contract DE-AC05-96OR22464.

4:40pm **HS+SS+BI-WeA9 A New Nanoscale Platform for Gas Sensor Applications**, *A. Kolmakov*, *Y. Zhang, G. Cheng, M. Moskovits*, University of California Santa Barbara

The application of metal and semiconductor nanowires as solid state gas sensors has been an area of tremendous promise currently limited by challenges related to nanowire growth and device fabrication. We present an approach for fabricating individual and arrays of nanowires of a variety of metals and metal oxides with tunable, uniform diameters and length in the range of 10-100 nm and 5-200 micrometers, respectively, configured for gas sensing application. The materials successfully employed include Pd, Ag, Cu, Pb, PbO, CuO and SnO₂. Arrays of nanowires were fabricated in hexagonal close-packed nanochannel alumina templates. Electrodes deposited on the surfaces of these nanostructures provides electrical contacts which with the incorporated heaters determines the device architecture. Based on this method we explored the electronic and structural properties of Pd and SnO₂ nanowires using HRTEM, XPS and Auger spectroscopy. Chemical reactivity and gas sensitivity toward hydrogen and carbon monoxide of individual and assemblies of ca 10⁹ Pd and SnO₂ nanowires were assessed using conductivity measurements and TPD

analysis. This approach constitutes a novel platform for micro- and nanosensor application.

5:00pm **HS+SS+BI-WeA10 Metal Phthalocyanine Thin Films as Gas Sensors**, *L. Lozzi*, *S. Santucci*, INFM and University of L'Aquila, Italy, *C. Cantalini*, University of L'Aquila, Italy

Metal Phthalocyanine (MPc) thin films have shown interesting properties as gas sensor, in particular for NO2. The wide variety of different available molecules, changing both the central atom and/or the chemical structure of the outer benzene rings, allows a fine modulation of the film sensing properties. In this work we will present our result on the interaction between oxidating gases (O2 and NO2) and different MPc films. We have deposited thin films (about 50 nm thick) of Copper Phthalocyanine (CuPc) and Exadecafluoro-copper-phthalocyanine (F16CuPc) onto Si3N4 substrates, for the spectroscopic characterizations, and onto Pt interdigital circuits, for the gas sensing tests. These films have been analysed both as deposited and after different thermal annealing. The electrical sensing analyses have shown a sizeable decrease of the film resistivity during the film exposure to NO2, even at very low concentration (up to 100 ppb). We have studied the electronic structure by means of the X-ray and ultraviolet photoemission spectroscopies (XPS-UPS) after the exposure to NO2 and O2 both at room and at higher temperature, in order to investigate the surface reactivity of these samples and in particular the preferential adsorption sites.

Surface Science Room: C-108 - Session SS1-WeA

Gas-Surface Dynamics

Moderator: J.J. Boland, University of North Carolina at Chapel Hill

2:00pm SS1-WeA1 Interaction of Gas-phase H Atom with Metal Surfaces : Cu(111) vs Pt(111), S.J. Lee, J. Kim, J. Lee, Seoul National University, Korea

The gas-phase H atoms of thermal energy impinging upon metal surface undergo reflection, adsorption, or abstraction of a surface H atom. The probability of each process strongly depends on the inelastic nature of the H-metal surface collision. Inelastic energy loss via phonon excitation is expected to be quite inefficient because of the light mass of H atom. Recently, Nienhaus et al. (1) have experimentally shown that H atom collision with metal surfaces induces e-h pair excitation. Then, one can raise the following interesting questions; 1) Is eh pair excitation a dominant inelastic loss mechanism in H-metal surface collision? 2) If it were the case, what would be the effect of electronic band structure of metal in its interaction with H atom? In order to gain further insight into these questions, we have measured and compared the initial sticking probability(S₀), saturation coverage(θ_s), and abstraction cross section(s_{abs}) for hydrogen atom at Cu(111) and Pt(111) at 90K. We measure S=0.72, $\theta_s{=}0.95ML,$ and $s_{abs}{=}1.30\text{\AA}$ for Pt(111) and S_0{=}0.45, $\theta_s{=}0.32ML,$ and sabs=5.5Å for Cu(111). We interpret the results in terms of e-h pair excitation whose efficiency is determined by the electron density of state at the Fermi level.

2:20pm SS1-WeA2 Anomalous Reactive Scattering: Hyperthermal Energy Collisions of State-selected Bromine Ions on Pt(111), P.L. Maazouz, M. Maazouz, D.C. Jacobs, University of Notre Dame

The dynamics of scattering state-selected atomic and molecular bromine ions on Pt(111) are investigated across the hyperthermal energy regime (5 -100 eV). Scattered ionic products are measured with mass-, angular-, and velocity-resolution. Scattered Br_2^{-1}/Br^{+} product distributions are measured as a function of the incident Br_2^{-1}/Br^{+} collision energy, vibrational energy, and surface temperature. The yield for both atomic and molecular projectiles reveals an unusual behavior where negative ion conversion is most efficient for incident velocities near 7.6 km/sec. This sharp peak in the yield shifts to lower velocities with increasing surface temperature. A detailed analysis of the products' velocity distributions suggests an important interplay between charge transfer and energy transfer in this system.

2:40pm SS1-WeA3 Hyperthermal Ejection of Atomic Cl from the Reaction of Cl₂ on the Al(111) Surface: Evidence of a Nonadiabatic Electron Harpooning Mechanism, G.C. Poon, T.J. Grassman, A.C. Kummel, University of California, San Diego

Resonantly Enhanced Multiphoton Ionization (REMPI) and Time-of-Flight Mass Spectroscopy (TOF-MS) have been used to demonstrate that the reaction of Cl_2 on the low work function Al(111) surface proceeds via a

prompt nonadiabatic electron harpooning process. As Cl₂ approaches the Al(111) surface, an electron harpoons from the surface, suddenly converting Cl₂ to Cl₂. This places the molecule high on the repulsive portion of the Cl₂ potential curve leading to rapid dissociation into Cl and Cl fragments. The Cl proceeds toward the surface and sticks while Cl is ejected into the gas phase. An experimentally observable signature of this harpooning process would be a hyperthermal translational energy of the ejected fragment, whose energy is determined by the vertical transition between Cl₂ and Cl₂ and should be nearly independent of incident translational energy. Three beams of Cl₂ were prepared by seeding with translation energies ranging from 0.989 eV to 0.105 eV. Each of the three Cl₂ beams was directed at the surface at three incident angles: 0°, 20°, and 40°. The translational energy of the ejected Cl was shown to be a weak function of the incident translational energy. For 0.989 eV normal incidence Cl₂ the ejected Cl had a translational energy of 0.147 eV, while 0.105 eV normal incidence Cl_2 produced ejected Cl of 0.100 eV. Therefore, for incident Cl₂ with a velocity of 535 m/sec, the ejected Cl atoms were accelerated to a velocity of 740 m/sec. This acceleration of ejected Cl compared to incident Cl2 is consistent with a nonadiabatic process that converts electronic to kinetic energy.

3:00pm SS1-WeA4 Degradation of Alkanethiol Self Assembled Monolayers under Hyperthermal O Bombardment, T. Tzvetkov, X. Qin, D.C. Jacobs, University of Notre Dame

We present experimental results on the reaction of 5-20eV O⁺ with alkanethiol self-assembled monolayers (SAMs). Decanethiol or 1H, 1H, 2H, 2H-perfluorodecanethiol are used to form well-ordered SAMs on a clean gold surface. Scattered ionic products, formed as a result of hyperthermal O⁺ ion bombardment, are collected with angle-, energy-, and mass-resolution. Chemical modifications in the SAM layer are monitored by X-ray photoelectron spectroscopy (XPS). Efficient removal of H from alkanethiol SAMs is observed at all incident energies. With increasing collision energy, C-C bond cleavage becomes important, as various scattered species of $C_n H_m$ or $C_n F_m$ radicals are observed, and the stoichiometry of the irradiated SAM is altered. The experimental results help us to understand the mechanisms of polymer degradation under O bombardment at hyperthermal incident energies.

3:20pm SS1-WeA5 Charge Transfer in Low Energy Li Ion Scattering from Halogen-covered Metal Surfaces, Y. Yang, J.A. Yarmoff, University of California, Riverside

Resonant charge transfer (RCT) for 400-3000 eV Li ions scattered from iodine- and bromine-covered Fe(110) and Ni(100) surfaces is probed with time-of-flight spectroscopy. RCT with alkali ions has traditionally been considered to reflect the overlap between the local surface potential and the ionization level of the exiting ion. In this work, it is shown that the local charge density can also influence the RCT process. For example, iodine would be expected to adsorb with some net negative charge, thereby producing a dipole directed into the surface that would raise the work function. In contrast, iodine decreases the work function, and the neutralization probabilities for Li singly scattered from the I sites are always higher than for scattering from metal sites. Thus, there is a local effect involved in RCT for this system. Bromine adsorption does not change the work function significantly, but still the neutralization probabilities for scattering from Br sites are larger than from the substrate. These results suggest that the local charge density does plays a significant role in determining the RCT probability.

3:40pm SS1-WeA6 Adsorption and Radiation Induced Decomposition of SF₆ on Ru(0001), N.S. Faradzhev, D.O. Kusmierek, B.V. Yakshinskiy, T.E. Madey, Rutgers, The State University of New Jersey

Electron stimulated desorption ion angular distribution (ESDIAD) and temperature programmed desorption (TPD) techniques have been employed to study the adsorption and radiation-induced decomposition of fractional monolayers of octahedrally-coordinated SF₆ physisorbed on Ru(0001) at 25K. TPD reveals predominantly molecular adsorption of SF₆, which desorbs from 3 weakly-bound states below 100K. ESDIAD of both F⁺ and F ions at 25K demonstrate "halo-like" patterns, and heating the substrate to ~90K results in formation of hexagonal angular distributions for both ions. ESD of F and F occurs via different mechanisms but from the same chemical states of molecular SF₆, which appears to be adsorbed via three F atoms, with the other three pointed away from the surface. At low temperatures, the F atoms have a random azimuthal orientation, while upon annealing, lateral ordering occurs in two complementary domains. Prolonged electron beam exposure leads to dissociation of SF_6 , and formation of SF_x (x=0 to 5) fragments. F ions escape only from undissociated molecular SF₆, while F⁺ ions also originate from dissociation fragments; both normal beams and off-normal beams are seen in hexagonal F⁺ ESDIAD patterns, and intensities vary with electron exposure. Electron

exposures ${>}10^{16}$ e/cm² result in complete decomposition of SF_{6} , as verified by TPD and ESDIAD.

4:00pm **SS1-WeA7 Dynamical Behaviors of GaCl on GaAs Surfaces by Pulsed Molecular Beam Scattering**, *M. Ohashi*, National Institute of Advanced Industrial Science and Technology (AIST), Japan, *M. Ozeki*, Miyazaki University, Japan

Gallium chloride (GaCl) is an important precursor in the growth of compounds containing Ga and plays an important role in halide vapor-phase epitaxy (VPE) and hydride VPE. The GaAs layer grown on a GaAs(001) substrate is completely mirror-like without surface defects, but the layer grown on a GaAs(110) substrate is slightly hazy. The cause of these results is unclear. As the initial process in GaAs epitaxial growth is defined that GaCl molecule trapped into a precursor state in GaCl/GaAs surface system, this precursor plays an important role in growth. The reason that a high quality layer can be grown on a GaAs(001) substrate but not a GaAs(110) substrate has not clarified because the dynamical behaviors in the precursor states of GaCl on these surfces, such as activation energy and desorption rate have not been clarified. We investigated the adsorption mechanism of GaCl on the GaAs(001) and GaAs(110) surfaces based on angular distribution and the temperature dependence of GaCl time of flight spectra reflected from these surfaces. These well-defined surfaces are prepared by molecular beam epitaxy system connected with molecular beam scattering apparatus. The angular distribution of reflected GaCl consists of two parts; inelastic direct scattering contribution and thermal desorption of trapped molecules on the GaAs(001) and GaAs(110) surfaces. We divided the time of flight spectra of thermally desorbed GaCl into the component with activation energies of 92 kJ/mol corresponding to GaCl trapping well on GaAs(001) 2x4 surface and the components with 54 kJ/mol on GaAs(110) 1x1 surface Trapped GaCl desorbed rabidly from the GaAs(110) 1x1 surface compared to GaAs(001) 2x4 surface. These results suggest that the interaction between GaCl molecules and GaAs surface deeply influences the quality to large grown on GaAs substrates. Most of above this work was supported by New Energy and Industrial Technology Development Organization (NEDO).

4:20pm SS1-WeA8 A New Mechanism for Ion-Stimulated Surface Processes at Low Energies, Z. Wang, E.G. Seebauer, University of Illinois Ion surface interactions at low energies (<100 eV) characterize an increasingly diverse array of material processing steps in ion beam assisted deposition (IBAD), plasma enhanced deposition, reactive ion etching (RIE), and other applications. Overall process behavior in these applications often reflects a delicate balance among several competing kinetic effects. The governing kinetic phenomena are often tacitly considered to lie at one of two poles: physical effects where momentum matching dominates, and chemical effects involving thermal activation of atomic bonds according to Arrhenius expressions. Here we report molecular dynamics simulations of low-energy noble gas atoms impacting Si and Ge surfaces, and describe a new phenomenon that lies at neither pole. The simulations, backed by experiments on surface diffusion, exhibit a surprising new form of tradeoff between the ion energy threshold for point defect formation and substrate temperature. Because of the vast difference in scales between ion energies and thermal energies, the tradeoff resembles an elephant being balanced by a mouse on a seesaw. The effect originates from instantaneous nonuniformities in net surface potential induced by thermal vibrations, which dramatically affect the locality of momentum transfer to the surface and greatly amplify the effect of temperature. This amplification may offer a new means for selecting specific elementary rate processes during plasma processing or ion beam assisted deposition by judicious tuning of temperature and ion energy.

4:40pm SS1-WeA9 Photochemistry of Caged Molecules: CD₃Cl in Ice, *M. Asscher*, *Y. Lilach*, Hebrew University of Jerusalem, Israel

The interaction of two similar coadsorbed dipolar molecules, HO and CD_3Cl , has been studied over Ru(001) under UHV conditions. The complementary techniques of δP -TPD and work function change in a $\delta \phi$ -TPD mode were employed. Post-adsorption of water leads initially to compression, reorientation and then to the formation of CD_3Cl layers that are encapsulated between amorphous solid water layers. These caged molecules are explosively desorb at 165K. Unique photochemical reactivity is displayed by the trapped methyl chloride molecules upon irradiation by 6.4 eV photons from an ArF excimer laser. Radical chemistry based on hot, photochemically generated methyl fragments, lead to the formation of longer chain hydrocarbons as well as oxygenated products. The relevance of these observations to the origin of interstellar hydrocarbons is discussed.

Structure and Chemistry at Metal Surfaces

Moderator: B.J. Hinch, Rutgers University

2:00pm SS2-WeA1 Real Time Monitoring of the Structure and Morphology of Growing Nanoparticles by Grazing Incidence Small and Wide Angle X-ray Scattering, in situ, in UHV, *G. Renaud*, CEA-Grenoble, France INVITED

Islands of nanometer size grown on substrates display a set of fascinating properties, which are of interest for both basic and applied research. They include model catalysts made of supported metallic particles whose reactivity and selectivity can be adapted to given needs, single-domain magnetic particles which show original spin-dependent transport properties and coherently strained semiconductor aggregates, the so-called "quantum dots", which exhibit remarkable opto-electronic properties. A strong promise of novel device applications merges up provided that nanoparticles could be purposely tailored to specific uses. The properties of these particles depend to a great extent on their internal atomic structure, their strain, their shape, size, size distribution and ordering, which in turn rely on the growth mechanisms. In this context, a challenging issue is to control the growth of large collections of particles by monitoring the relevant parameters in situ and in real time. A unique technique to probe collections of very small objects is Grazing Incidence Small Angle X-ray Scattering (GISAXS). However, to date, due to technical limitations, GISAXS has never been used during growth. In this report, we demonstrate this possibility using two prototypical cases. The first is the growth of metals (Ag, Pd, Pt) on MgO(001) at different temperatures, which are models of Volmer-Weber 3D growth of metal on oxide surfaces, and is thoroughly studied to investigate the elementary processes of heterogeneous catalysis. The second is the growth of cobalt on the herringbone reconstructed Au(111) surface, which is a model of self-organized cluster growth. We show that a complete description of the islands can be obtained by supplementing GISAXS measurements by grazing incidence wide angle xray scattering measurements performed in situ during growth, at the same time.

2:40pm SS2-WeA3 Structural Analysis of Quasicrystalline Al-Pd-Mn using Angle-Resolved Low Energy Ion Scattering, *C.J. Jenks*, *P.A. Thiel, A.R. Ross, T.A. Lograsso,* Iowa State University, Ames Laboratory, *J.A. Whaley, B. Bastasz,* Sandia National Laboratories

We have used angle-resolved low-energy ion scattering to examine the clean surface structure and composition under ultra-high vacuum conditions of a single grain of icosahedral $Al_{71}Pd_{20}Mn_9$ oriented with a five-fold axis perpendicular to the surface. Our results are consistent with the surface maintaining five-fold symmetry after sputtering followed by annealing at 800 K. We find that the topmost surface layer is > 85 atomic % aluminum. A predominant neighbor atom distance of 7.6 ű 0.5 Å and a nearest neighbor distance of 3.0 ű 0.1 Å is calculated from our results. Our results are consistent with previous low energy electron diffraction intensity versus voltage (LEED-IV) calculations, recently published scanning tunneling microscopy results and a bulk model of Al-Pd-Mn quasicrystals.

3:00pm **SS2-WeA4 Structural Studies of Ti/Pt(111) Surfaces**, *S. Hsieh*, *T. Matsumoto, J. Kim, B.E. Koel*, University of Southern California

Alloys of platinum and a second metal component are of increasing interest for a number of applications. Structural studies have been carried out for bimetallic surfaces with Pt alloyed with many transition metals and main group metals. In this work, we have used He +-ion scattering (He+-ISS), Xray photoelectron spectroscopy (XPS), and low energy diffraction (LEED) to determine the structure of ordered Ti/Pt(111) surface alloys formed by depositing ultrathin Ti films on Pt(111) and annealing to different temperatures up to 1100 K. The Ti film coverage was determined by He⁺-ISS. No LEED pattern was observed at room temperature immediately after Ti deposition. At 800 K, Ti started to alloy with Pt and formed a ($6x \sqrt{43}$) structure in LEED that grew sharper as the temperature was increased to 1000 K. A weak (2 x 2) pattern was observed for Ti coverages larger than 1 monolayer, but this structure was less stable and disappeared at high temperature leaving only the (6x $\sqrt{43}$) pattern. XPS showed that the Ti core level spectra shifted by 2.0 eV upon alloying compared to that from a thick Ti film. Observation and further characterization of the new Ti/Pt(111)-(6x $\sqrt{43}$) surface structure should aid in understanding and tailoring chemical properties of practical catalysts.

3:20pm **SS2-WeA5 Thermal Stability of Thin Ti Films on Al Single Crystal Surfaces¹**, *C.V. Ramana*, *R.J. Smith*, Montana State University, *B.S. Choi*, Jeonju University, Korea, *B.S. Park*, *A. Saleh*, Charles Evans & Associates, *D. Jeon*, Myongji University, Korea

Chemical roughness and alloy formation at metallic interfaces can significantly degrade the performance of multilayer thin film magnetic device structures. We have investigated the use of metal interlayers, one or two atoms thick, to stabilize the interface for ordered growth of metal films with minimal intermixing. Specifically, thin Ti interlayers have been used to stabilize the Fe-Al(100) interface, a system characterized by considerable interdiffusion at room temperature. The benefits of the interlayer concept are strongly coupled to the stability of the interlayer at elevated temperatures. In this investigation we have characterized the structure of thin Ti layers on Al single crystal surfaces as a function of temperature using Rutherford backscattering and channeling (RBS/c) and low-energy ion scattering (LEIS). The Ti layers are shown to be stable up to temperatures of about 400° C, at which point diffusion of Ti into the Al lattice occurs. LEIS measurements, combined with RBS show clearly that the Ti atoms move into the surface at these temperatures. Channeling measurements show that the Ti atoms sit on Al lattice sites as a substitutional impurity. The stability of the Ti film appears to increase with the packing density of the Al surface, being slightly more stable for the close-packed Al(111) surface, and diffusing into the more open Al(110) surface at a lower temperature.

¹ Work supported by NSF Grant DMR-0077534.

3:40pm SS2-WeA6 Nucleation and Growth of Ag Films on a Quasicrystalline AlPdMn Surface, V. Fournée, T. Cai, A.R. Ross, T.A. Lograsso, J.W. Evans, P.A. Thiel, Iowa State University

Nucleation and growth of thin films of Ag on the 5-fold surface of an Al72Pd19.5Mn8.5 icosahedral quasicrystal is studied with STM. For low coverages, flux-independent island nucleation is observed, likely involving adatom capture at "traps". With increas ing coverage, islands start growing vertically, but then spread, and ultimately form hexagonal nanocrystals. These have fcc symmetry and pyramid-like multilayer stacking along the <111> direction. The constituent hexagonal islands have five different orientations, rotated by 2p/5, thus remembering the symmetry of the substrate. These results are discussed in the context of strategies most likely to yield pseudomorphic growth.

4:00pm **SS2-WeA7 Helium Atom Scattering Studies of Si-Cu (001) and Sn-Cu (001) Surface Alloys, L.V. Goncharova**, D.V. Potapenko, B.J. Hinch, Rutgers University, X. Zhang, D.R. Strongin, Temple University, L. Wood, Dow Corning Corporation

Copper acts catalytically in the commercial "Direct Synthesis" of dimethyldichlorosilane; the later being a key component in the manufacturing of silicone materials. While Cu-Si systems have been studied intensively, the roles of other components, such as Sn, Zn and Al, which act as promoters in the "Direct Synthesis", are not well understood. We report on the growth and dynamics of silicon and thin tin films on Cu (001), as studied with high-resolution helium atom scattering (HAS), low energy electron diffraction (LEED) and Auger electron spectroscopy (AES). We have shown that the incommensurate "5x3" structure is formed when silicon is deposited on Cu (001) via saturation exposure to silane at 420K. 1 With Sn deposition temperatures above 200K a series of ordered reconstructions are observed on Cu (001) in the submonolayer regime.² Coadsorption of tin and silicon on Cu (001) is of a key importance as it enables a new low temperature desorption mechanism of methylsilanes. The relationships between structures in coadsorbed tin and silicon on the Cu (001) surface, and yields of different methylsilane products will be presented.

¹ A.P.Graham, B.J. Hinch, G.P.Kochanski, E.M. McCash, and W. Allison, Phys.Rev.B 50 (1994) 15304.

² E.McLoughlin, A.A. Cafolla, E. AlShamaileh, C.J. Barnes, Surf.Sci. 482-485 (2001) 1431.

4:20pm SS2-WeA8 Growth and O₂ Reactivity of the Cu/Si(5 5 12) System, P.H. Woodworth, J.C. Moore, A.A. Baski, Virginia Commonwealth University

Our group has extensively studied the growth behavior of Group IB metals such as Ag and Au on the row-like template provided by the clean Si(5 5 12) surface.¹ Here, this work is extended to the remaining IB metal of Cu. Our scanning tunneling microscopy studies show that Cu forms two distinct phases on Si(5 5 12): a lower temperature phase (< 600 °C) where Cu decorates the underlying (5 5 12) surface, and a higher temperature phase (> 600 °C) where it induces faceting to the nearby (113) plane. Similar to the Ag and Au systems, the lower temperature phase results in the formation of Cu "nanowires" with a spacing equal to the 5.4 nm periodicity of the (5 5 12) surface. When the annealing temperature is increased, however, the (5 5 12) surface to (113) faceting. At lower Cu coverages (< 0.5 ML), (113) planes appear to coexist with (5 5 12), but at higher

coverages (> 0.5 ML) these planes form sawtooths with opposing (111) faces. The occurrence of (113) planes has also been seen for the higher temperature growth of Au on Si(5 5 12), indicating the inherent stability of this plane. We have also studied the O_2 reactivity of the Cu-induced (113)/(111) sawtooths at exposures of 50 to 200 Langmuirs and temperatures of 600 to 800 °C. As expected, an amorphous oxide appears to grow on the surface at lower temperatures (<650 °C), and etching occurs at higher temperatures (>650 °C). For the case of etching, the sawtooths are gradually removed to produce trapezoidal (113)/(111) islands. The density of these islands decreases with increasing temperatures on the surface.¹ A.A. Baski, K.M. Saoud, K.M. Jones, Appl. Surf. Sci. 182, 216 (2001).

4:40pm SS2-WeA9 NIXSW Analysis of the Disorder Transition of Chlorine on Cu(111), A.G. Shard, University of Sheffield, UK, C. Ton-That, University of Cambridge, UK, P.A. Campbell, University of Dundee, UK

Chlorine adsorbs on Cu(111) primarily in threefold hollow sites, with a slight preference for the 'fcc' site (above a third layer copper atom) as opposed to the 'hcp' site. We have monitored the relative population of the two sites at a variety of coverages and temperatures using Normal Incidence X-ray Standing Waves (NIXSW). Disordered surfaces at low coverages or high temperatures have approximately equal populations of the two hollow sites, providing a measure of confirmation for the small energy difference recently calculated between them.¹ Adsorption of chlorine to a Cu(111) crystal at 180K results in an ordered root 3 surface, with equal populations of 'fcc' and 'hcp' sites, implying the prolonged existence of metastable 'hcp' domains at this temperature. The room temperature root 3 structure has a large 'fcc' population, which decreases close to the disorder transition at 350K. These data are discussed and compared with Monte Carlo simulations.

¹K. Doll and N. M. Harrison, Chem. Phys. Lett., 317, 282 (2000).

5:00pm SS2-WeA10 Vibrations of Water Adsorbed on Ru(0001)¹, *P.J. Feibelman*, Sandia National Laboratories

To see whether vibration spectroscopy confirms or contradicts the idea that the wetting layer of D₂O/Ru(0001) is half-dissociated,² vibration spectra have been computed from first principles for comparison to experiment. The calculations show that dissociation of the non-hydrogen-bonding O-D bonds of a heavy-water bilayer eliminates the highest-energy O-D stretch feature, and replaces it with a lower frequency mode. This behavior agrees with recent Sum Frequency Generation observations,³ lending credence to the argument that a half dissociated D₂O layer is needed both to explain why water wets Ru(0001) at all, and to account for the inference drawn from Low Energy Electron Diffraction data, that the O atoms of $\sqrt{3x}\sqrt{3}$ -D₂O/Ru(0001) are nearly coplanar. Beyond helping to clarify the nature of the wetting layer, the computed vibration spectra also permit an estimate of its zero-point energy relative to that of competing adsorption structures. Zero-point energy is found to favor half-dissociated adlayers because, of every four oxygen-hydrogen bonds in an intact-water-molecule structure, one is replaced by a softer metal-hydrogen bond in a half-dissociated arrangement. For $\sqrt{3x}\sqrt{3}$ -D₂O/Ru(0001), this zero-point stabilization amounts to about 30 meV per D₂O. In the case of H₂O adsorption, it would be ~50 meV/ad-molecule.

¹ Work supported by the U. S. Department of Energy under Contract No. DE-AC04-94AL85000. Sandia National Laboratories is a multi-program laboratory operated by Sandia Corporation, a Lockheed-Martin Company, for the U. S. DOE.

² P. J. Feibelman, Science 295, 99(2002).

³ D. N. Denzler, unpublished.

Thursday Morning, November 7, 2002

Biomaterials

Room: C-201 - Session BI+HS+SS-ThM

Biosensors and Biodiagnostics

Moderator: J. Hickman, Clemson University

8:20am BI+HS+SS-ThM1 Surface Functionalization for Self-Referencing and Multi-Channel Surface Plasmon Resonance (SPR) Biosensors, J. Ladd, C. Boozer, Q. Yu, J. Homola, S. Yee, S. Jiang, University of Washington

Recently, a novel SPR sensor with on-chip referencing has been realized. In this sensor, one half of the gold sensing surface is covered with a high refractive index overlayer of tantalum pentoxide (Ta2O5). When polychromatic beam illuminates the sensing surface, surface plasmon resonance in the areas with and without the overlayer occur at different wavelengths. Therefore, the reflected light exhibits two dips associated with SPRs in those two areas. When functionalized properly, one of the areas can be used as a specific sensing channel for detection of specific biointeractions and the other can act as a reference channel for compensation for background refractive index fluctuations. In this work we present a new functionalization approach for these mixed architecture chips. The gold side of the chip is functionalized with a mixed self-assembled monolaver of polyethylene oxide (PEO) and biotin terminated thiols whereas the Ta2O5 side is coated with PEO terminated silanes. The PEO terminated thiols and silanes serve as a protein resistant background, while the biotin-terminated thiols are used to bind streptavidin, which in turn immobilizes biotinylated antibodies. Hence, the gold side of the chip is used for the binding and detection of target analytes and the Ta2O5 side functions as a reference channel that monitors bulk refractive index changes and temperature drift. We have applied this functionalization to an SPR based biosensor and have studied two model systems: mouse IgG and human hCG. In addition, we have quantified and compared the protein resistance of the PEO thiols versus the PEO silanes. This information will help us better compensate for non-specific effects and improve robustness of SPR measurements.

8:40am BI+HS+SS-ThM2 Chemical Sensing Using Ultra-Fast Micro-Boiling, O. Thomas, R.E. Cavicchi, M.J. Tarlov, National Institute of Standards and Technology

We report a novel liquid sensing method that exploits micro-boiling phenomena on the surface of rapidly heated thin film heaters. The heaters are thin films of platinum and gold-plated platinum that are approximately tens of micrometers in width and hundreds in length. The micro-heaters are immersed in solutions where they are rapidly heated to high temperature with short, 5 - 40 microsecond, square voltage pulses. The temperature-time responses of the micro-heaters are obtained by measuring their resistance during the application of the heating pulse. The bubble nucleation event associated with boiling is signaled in the temperature-time transient by an inflection point that results from a change in heat transfer when a vapor film forms on the heater. Because of the extremely high heating rates, superheating is observed where nucleation temperatures approaching 300°C have been measured for aqueous solutions. The bubble nucleation temperature and average heater temperature during the micro-boiling process have been found to be highly dependent on the surface wettability of the heater, as well as the presence of surfactant molecules. We will report on the use of alkanethiol self-assembled monolayers to investigate the effect of surface wettability on micro-boiling. We will demonstrate that temperature-time transients of hydrophobic SAMs are distinct from those of hydrophilic SAMs and that information on SAM stability can be gleaned from transient data. We will also present preliminary results on using the micro-boiling phenomenon to detect surface binding events such as DNA hybridization and biotin-avidin coupling.

9:00am BI+HS+SS-ThM3 Nanofluidic and Biomimetic Bioanalytical Systems, G.P. Lopez, University of New Mexico INVITED

This talk will present recent progress on the development of hybrid nanomaterials containing synthetic and biosynthetic components for use in bioanalytical applications including separation and biosensing. Examples include the development of mesoporous s ilica microbeads that incorporate functional biomolecular components (e.g., transmembrane proteins in lipid bilayer systems) and stimuli-responsive polymers for the formation of "cell mimics" that preserve biological function in a robust, deterministic, n onliving system. Microscopic beads can be used in a variety of bioanalytical system formats including suspension assays in flow cytometry and microfluidic assays and separations in affinity microcolumns. Several aspects of these bioanalytical systems will be explored including

optimization of ligand-receptor pairs for direct transduction of biomolecular recognition, microfluidic considerations, and fluorescence detection principles.

9:40am BI+HS+SS-ThM5 A Gold Nanoparticle Sensor to Interrogate Biomolecular Interactions in Real-time on a Surface, N. Nath, A. Chilkoti, Duke University

We present a label-free optical technique to study biomolecular interactions in real time on a surface that is based on particle surface plasmon resonance (PSPR). We demonstrate that the absorbance spectrum of immobilized gold nanoparticles on glass exhibits a red shift as well as an increase in the absorbance at peak wavelength as a function of binding of biomolecules at the solid-water interface. The results obtained with the absorbance sensor were compared with those obtained using conventional SPR for fibrinogen adsorption onto a COOH-terminated surface and for the binding of streptavidin to a biotin-functionalized surface. We have also examined the sensitivity and dynamic range of the sensor as a function of nanoparticle size, and found a threefold improvement in sensitivity as the size of the nanoparticles is increased from 13 to 50 nm. This sensor is attractive because of its simplicity: gold nanoparticles are easily prepared with high reproducibility, they can be readily immobilized on glass, and their absorbance spectrum can be easily measured using widely available UV-vis spectrophotometers. Furthermore, this technique should be easily amenable to the design of chips in an array format for application in high-throughput immunoassays and proteomics.

10:00am BI+HS+SS-ThM6 Evaluation of Methodologies for Arraying a Porous Inorganic Bioassay Support¹, C. Cole, Nova Research, Inc., D.B. Chrisey, R.J. Colton, H. Kim, B.R. Ringeisen, Naval Research Laboratory, C.R. Tamanaha, Geo-Centers, Inc., L.J. Whitman, Naval Research Laboratory

A membrane-based immunosensor has been developed for the detection of eight biological agents with a response time of <15 minutes and a sensitivity ~3 orders of magnitude higher than conventional ELISAs. The Force Discrimination Biosensor² (FDB) uses generically functionalized 0.8 µm-diameter beads to label captured target; a magnetic field gradient removes nonspecifically bound beads, thus improving sensitivity by reducing both background and the incident of false positives. Already demonstrated for single analyte detection, methodologies to array the alumina ultrafiltration membrane for multiplexed detection have been evaluated. One of the biggest challenges is to array hydrophobic antibody conjugates onto porous hydrophilic PEG-biotin surfaces without losing pattern integrity due to lateral wicking. Patterning via a PDMS stamp or mask works reasonably well, but is too cumbersome for the patterning of the large number of membranes needed for practical applications. Instead, a pulsed laser transfer technique developed at NRL has been adapted to pattern antibody conjugates³ onto PEGylated membranes. With an average element dimension of $(100 \ \mu m)^2$ and 200 μm spacing between elements, a 10 x 10 array can be written in 3 mm². Such arrays can be patterned to give a single diagnostic for a variety of bacterial, viral, or protein agents without requiring the use of an additional membrane for positive/negative controls. Multiplexed assays for bacterial spores and cells, viruses, and protein toxins have been performed with these filters; results will be presented to demonstrate the application of pulsed laser writing to biosensor patterning.

¹ Supported by the Joint Service Technical Panel for Chemical and Biological Defense.

² Lee et al., Anal. Biochem. 287, 261 (2000). ³ Ringeisen et al., Biomaterials 23, 161 (2002).

10:20am BI+HS+SS-ThM7 DIOS-MS for Reaction Monitoring and Chemical Analysis, Z. Shen, University of California, San Diego, G. Siuzdak, M.G. Finn, The Scripps Research Institute, J.E. Crowell, University of California, San Diego

Desorption/Ionization On Silicon Mass Spectrometry (DIOS-MS) is a new mass spectrometry strategy based on pulsed laser desorption/ionization from a porous silicon surface. DIOS-MS is similar to matrix-assisted laserdesorption ionization mass spectrometry (MALDI-MS) in that it utilizes the same instrument; however, in DIOS-MS, porous silicon is used to trap analytes deposited on the surface and laser radiation is used to vaporize and ionize these molecules, without the presence of any matrix material. We have shown that DIOS-MS can be used for a wide range of small molecules as well as biomolecules at the femtomole and attomole level with little or no fragmentation. DIOS-MS offers many unique advantages including good sensitivity, low background ion interference, and high salt tolerance. We will demonstrate the application of DIOS-MS to small molecule quantitative analysis, high throughput screening, chemical reaction monitoring, enzyme-substrate reaction and inhibition characterization, drug metabolism studies, and protein identification. We will also discuss aspects of the desorption and ionization mechanisms of DIOS.

10:40am **BI+HS+SS-ThM8 ToF-SIMS Analysis of PNA/DNA Hybridization on Thiolated Biosensor Chips**, *M. Schröder*, Westfälische Wilhelms-Universität Münster; Germany, *J.C. Feldner, S. Sohn, H.F. Arlinghaus*, Westfälische Wilhelms-Universität, Germany

We have investigated a diagnostic method that uses peptide nucleic acid (PNA) biosensor chips to detect hybridization of unlabeled DNA. Using two different approaches, different PNAs were immobilized onto Au-coated spots with an approximate diameter of 100µm. One method was to immobilize thiolated PNA in a single-step reaction to the Au-surface via an Au-S-bond. The other method was to crosslink the N-terminal end of the PNA to a preformed layer of 11-mercaptoundecanoic acid (MUA) in a reaction consisting of two steps forming an amide bond. These layers were hybridized with complementary and non-complementary unlabeled singlestranded DNAs (ssDNA). Since the backbone of DNA, in contrast to PNA, contains phosphorous, it is possible to identify DNA-PNA-hybrids with time-of-flight mass spectrometry (ToF-SIMS) via DNA-specific phosphaterelated ions at the masses 63 amu (PO_2) and 79 amu (PO_3) . In addition to these signals, the deprotonated bases M-H were detected in both immobilization approaches. In the case of the two-step-immobilization, it was possible to independently control the different steps by measuring characteristic peaks of MUA-fragments. Due to the manifold controlpossibilities, especially variation of surface-density of the immobilized PNA and saturation of the remaining active Au-binding-sites with different thioles, it is possible to optimize hybridization conditions and suppression of uncharacteristic bonding of the ssDNA to the Au-surface. From the obtained data it can be concluded that both PNA immobilization approaches are very promising for designing PNA biosensors and that ToF-SIMS is a useful tool for identifying DNA-PNA-hybrids on these biosensor chips with good discrimination.

11:00am BI+HS+SS-ThM9 Covalent Attachment and Hybridization of DNA Oligomers at Polycrystalline Diamond Thin Films, T. Knickerbocker, W. Yang, W. Cai, University of Wisconsin-Madison, J.N. Russell, Jr., J. Butler, Naval Research Laboratory, D.M. Gruen, J.A. Carlisle, Argonne National Laboratory, L.M. Smith, D. Van der Weide, **R.J.** Hamers, University of Wisconsin-Madison

Diamond has a number of unique properties, including a very wide range of electrochemical stability and very good electrical and thermal properties. These properties may make diamond a particularly attractive material to use as a substrate for biological sensors. We have explored the covalent bonding of DNA to several different types of diamond thin films, including free-standing polycrystalline films, thin films of microcrystalline diamond on silicon substrates, and ultrananocrystalline diamond thin films. Starting with H-terminated diamond, we prepared a homogeneous amine-terminated surface using a photochemical attachment processes, optimized using corelevel photoemission spectroscopy. These amine-terminated diamond surfaces are then used as a starting point for subsequent attachment of DNA oligomers. The efficiency and selectivity of hybridization have been determined using conventional fluorescence measurements after the surface-bound oligomers are hybridized with fluorescently-tagged complementary and non-complementary oligomers. Our studies show that DNA-modified diamond surfaces show good hybridization properties and good selectivity. More importantly, the DNA-modified diamond surfaces show extremely good stability with repeated hybridizations, and retain this selectivity even after being dried and later reconstituted. This talk will discuss the fabrication of DNA-modified diamond surfaces for biosensor applications, and the differences and similarities between the various forms of DNA-modified diamond thin films.

11:20am **BI+HS+SS-ThM10 Direct Electronic Detection of DNA Hybridization at Surfaces**, *W. Cai*, *J. Peck*, *D. Van der Weide*, *R.J. Hamers*, University of Wisconsin-Madison

We have explored the use of electrical measurements to detect DNA hybridization in a label-free manner at surfaces. Our work has emphasized materials that are compatible with microelectronics, including DNA-modified surfaces of silicon, gold, and diamond. While most previous studies have focused on detection via low-frequency measurements, our work has focused on measurements at high frequencies, from ~10 kHz up to 10 GHz. The use of radio- and microwave-frequencies brings with it reduction in 1/f noise, the possibility of constructing electrically resonant devices for enhanced sensitivity, and the ability to perform single-ended measurements based on reflection instead of transmission. At these high frequencies, the electrical properties are controlled by the capacitance of the electrical double-layer, with some possible contributions from the space-charge region of semiconducting substrates. Using electrochemical impedance spectroscopy, we find a small, but reproducible change in

capacitance at the interface when DNA oligomers are hybridized with the complements. By comparing the responses generated when the surfacebound oligos are exposed to matched and mismatched sequences in solution, we can separate the changes in dielectric properties arising from hybridization from other possible sources of systematic error. To enable measurements to be performed with high sensitivity on very small areas, we have constructed a novel heterodyne reflectometer that allows us to measure the dielectric properties of very small interfaces in a manner that is essentially zero-background. To do this, we take advantage of the fact that the electric double-layer is intrinsically nonlinear, and that hybrization and other biological binding processes modify the dielectric properties of the double-layer region. This talk will discuss different schemes for direct electronic detection of DNA hybridization, with particular emphasis on the use of RF and microwave methods.

11:40am **BI+HS+SS-ThM11 Engineered Biointerfaces for Protein Biochip Applications**, *H.B. Lu*, *M. Mariano, S. Schweizer, H.M. Tran, L.A. Ruiz-Taylor, H. Hong, H.H.J. Persson, R.L. Cicero, P. Kernen, P. Wagner, Zyomyx, Inc.*

Protein biochip technology promises breakthroughs in large-scale protein analysis. Measuring and analyzing protein activities in a highly efficient, miniaturized and parallel fashion requires advanced surface chemistries for reproducible protein immobilization and minimized non-specific adsorption. Controlling the solid-liquid interface of a miniaturized biochip becomes a key step for maintaining protein activity and integrating highly sensitive detection techniques. We present several reactive surfaces engineered for protein biochip applications at Zyomyx. Systematic efforts on designing organic layers on different substrates have been carried out to improve packing density, orientation, and functionality of immobilized capture reagents, as well as to minimize non-specific biomolecule adsorption in complex biological samples. The latter is particularly important for improving detection limits and obtaining meaningful results in multiplex protein assays. To reduce non-specific adsorption and optimize chip performance, we incorporated oligo- and poly-ethylene glycol (EG) molecules in our organic layers that are well known to reduce non-specific protein adsorption. Effects of substrate type, surface coverage, and molecular structure of the assembled organic layers on specific and nonspecific interaction of biomolecules with the surfaces are presented. Specificity, loading capacity and detection sensitivity of protein immunoassays using high-density protein arrays configured with these surfaces are demonstrated and discussed.

Magnetic Interfaces and Nanostructures Room: C-205 - Session MI+SS-ThM

Magnetic Spectroscopies

Moderator: D.A. Hite, NIST

8:20am MI+SS-ThM1 Photoemission and X-Ray Absorption Measurements on the CMR Materials La_{1-x}Ca_xMnO₃ and La_{1-x}Sr_xMnO₃, *N. Mannella*, University of California at Davis, *A. Rosenhahn*, Lawrence Berkeley National Laborarory, *S. Mun*, Intel Corporation, *S.-H.* Yang, IBM Almaden Research Center, *Y. Tomioka*, *Y. Tokura*, Joint Research Center for Atom Technology, Japan, *C.S. Fadley*, Lawrence Berkeley National Laboratory

We report core and valence photoemission results obtained with synchrotron radiation for a set of high quality single-crystal CMR samples, namely $La_{1-x}Ca_xMnO_3$ and $La_{1-x}Sr_xMnO_3$ with x ranging from 0 to 0.4. The measurements were performed after cleaving the crystals in situ in UHV, yielding very clean and stoichiometric surfaces. X-ray absorption spectroscopy (XAS) and high-resolution valence band measurements at temperatures above and below the Curie temperature will also be discussed. The Mn 3s core level spectra show the expected multiplet splitting in binding energy, an effect which can sensitively probe the spin state of magnetic atoms. Our data reveal a non-linear dependence of the multiplet splitting on the hole concentration x, contrary to what one would expect in the simplest picture according to which hole doping causes a corresponding number of Mn^{3+} ions to become Mn^{4+} . These results may indicate an inadequacy of the conventional model based on the nominal Mn^{3+} - Mn^{4+} valence states. We have also measured Mn 3s spectra as a function of temperature. Our data suggest a short-range-order magnetic transition above the bulk Curie temperature, yielding a quantitative estimate of temperatures higher than T_c at which the material shows magnetic order of local character. This work was supported by the U.S. Department of Energy, Office of Science, Office of Basic Energy Sciences, Materials Sciences Division, under Contract No. DE-AC03-76SF00098.

8:40am MI+SS-ThM2 MOKE Studies of Magnetic Coupling in Co/Cr₂O₃/CrO₂, *R. Cheng*, *A.N. Caruso*, *L. Yuan*, *S.-H. Liou*, *P.A. Dowben*, University of Nebraska-Lincoln

 $\rm CrO_2$ is an attractive material for spin-polarized electron tunneling because of the high electron polarization and is among the predicted half metallic ferromagnets (metallic for one spin direction while insulating for the other spin direction, i.e. 100% spin polarization). Because the native surface layer of $\rm CrO_2$ is $\rm Cr_2O_3$, by evaporating Co thin films (5–20 nm) on top of epitaxial CrO_2 films on TiO_2 (100) substrates, a Co/Cr_2O_3/CrO_2 trilayer can be readily fabricated. >From in situ MOKE studies and ex situ SQUID measurements for the magnetic Co/Cr_2O_3/CrO_2 trilayers, the characteristic behavior of ferromagnetic-paramagnetic-ferromagnetic coupling above room temperature was observed. The thickness of Co and the temperature dependence of the magnetic hysteresis loops, obtained from MOKE, indicate different shapes, and the coercive fields show strong but not monotonic temperature dependence. These results indicate that there are changes in magnetic coupling and magnetization orientation particularly apparent as the temperature approaches the T_c of CrO₂.

9:00am MI+SS-ThM3 Polarized X-Rays and Magnetic Interfaces, H. Ohldag, Stanford Synchrotron Radiation Laboratory, A. Scholl, E. Arenholz, Advanced Light Source, F. Nolting, Swiss Light Source, Y. Acremann, J. Stohr, Stanford Synchrotron Radiation Laboratory, F.U. Hillebrecht, Forschungszentrum Karlsruhe, Germany, S. Maat, M.J. Carey, IBM Almaden Research Center INVITED

While interfaces are supposed to dominate the behavior of magnetic multilayer their identification and characterization remains an experimental challenge. A prominent example is the loop shift (exchange bias) and the coercivity increase found if a ferromagnet (FM) is coupled to an antiferromagnet (AFM). Although exchange bias was discovered over 40 years ago our understanding of its origin is still poor. We use dichroism xray absorption spectromicroscopy in a photoemission electron microscope to study the magnetic coupling between AFM NiO(001) and FM Co. We observe large (1-20mm) AFM domains at the surface of bare NiO(001) single crystals. Upon in situ deposition of thin FM Co layers (1.5nm) a reorientation of the AFM axes takes place. The uniaxial anisotropy axes of the FM and the AFM are then aligned parallel domain by domain. Spectroscopy data show that the Co deposition causes a chemical reaction and formation of an interfacial CoNiOx layer. Microscopy images reveal its polarization to be aligned parallel to the Co layer. Upon annealing both, the uniaxial anisotropy and the amount of interfacial spins increases indicating the direct link between interfacial polarization and parallel exchange coupling. A small fraction of interfacial spins does not follow the external field. These so called pinned moments lead to an additional vertical shift in the hysteresis loop of the interfacial spins. The number of pinned spins can be diretly correlated to the size of the exchange bias field. Our findings clearly show that a proper description of magnetic coupling in Co/NiO as well as in other AFM/FM systems needs to consider the properties of a distinct interfacial layer that can deviate significantly from the bulk properties of each material.

¹H. Ohldag, A. Scholl et al., PRL 86(13), pp. 2878, 2001.

²F. U. Hillebrecht, H. Ohldag et al., PRL 86(15), pp. 3419, 2001.

³H. Ohldag, A. Scholl et al., PRL 87 art. no 247201, 2001.

9:40am MI+SS-ThM5 A Compact Angle Resolving Spin-Polarized Photoemission Spectrometer for "Double Polarization" X-ray Diffraction Spectroscopy of Magnetic Nanostructures, S.A. Morton, University of Missouri-Rolla, J.G. Tobin, Lawrence Livermore National Laboratory, G.D. Waddill, University of Missouri-Rolla

Recent studies of spin dependent x-ray photoelectron diffraction from magnetic nanostructures excited with circularly polarized photons have demonstrated that the technique can provide a powerful probe of element specific atomic scale magnetic structure; however, the asymmetries involved are low, typically 1-2%. Calculations suggest that combining excitation via circularly polarized photons with spin polarized photoelectron detection in a "double polarization" experiment should lead to a 5-10 fold increase in asymmetry. However combining high angular resolution XPD with spin resolving capability poses significant experimental challenges. The authors describe a unique new compact angle resolving spin spectrometer currently being developed at the Advanced Light Source, Lawrence Berkeley National Laboratory. This combines a large (11 inch) diameter fixed hemispherical analyzer with a novel rotatable input lens system allowing data with +-1 degree angular resolution to be acquired for any combination of incident and emission angles, including normal incidence/ normal emission: a geometry critical for certain magnetic measurements. The analyzer is equipped with both multichannel detection for spin integrated spectroscopies, such as magnetic linear or circular dichroism, and a Mott detector capable of resolving the photoelectron spin polarization along the two perpendicular axis of the rotational plane. Rapid switching between spin integrated and spin resolved modes is achieved by

focusing the photoelectrons through a small hole in the detector of the hemispherical analyzer and into the compact mini-Mott detector situated immediately behind the channelplates. The spectrometer system also incorporates additional sample growth and characterization facilities such as co-evaporation from multiple deposition sources, LEED and Auger together with sample heating and cooling to provide a comprehensive system for the preparation and analysis of magnetic nanostructures.

10:00am MI+SS-ThM6 In-plane Vector Magnetometry on Rectangular Co Dots using Polarized Neutron Reflectivity, K. Temst, M.J. Van Bael, J. Swerts, D. Buntinx, C. Van Haesendonck, Y. Bruynseraede, K.U. Leuven, Belgium, H. Fritzsche, Hahn-Meitner-Institut Berlin, Germany, R. Jonckheere, IMEC vzw, Belgium

We have measured the off-specular polarized neutron reflectivity of a periodic array of rectangular magnetic polycrystalline Co-dots, which were prepared by a combination of electron beam lithography and molecular beam deposition. The dots have a strong shape anisotropy, imposed by a length-to-width ratio of 4:1. The intensity of the off-specular satellite reflection was monitored as function of the magnetic field parallel to the rows of dots and in the plane of the film, allowing us to analyze the magnetization reversal process using the four spin-polarized cross-sections. Analysis of the neutron reflectivity provides in-plane vector magnetometry during magnetization reversal. The neutron reflectivity data are complemented by micromagnetic simulations.

10:20am MI+SS-ThM7 Magnetism of Adatoms and Clusters, P. Gambardella, Ecole Polytechnique Fédérale de Lausanne, Switzerland INVITED

In the last ten years, x-ray magnetic circular dichroism (XMCD) has found widespread application as an element-specific magnetometry tool in the study of magnetic thin films. Here we show that x-ray absorption spectroscopy (XAS) and XMCD can be successfully employed to probe diluted transition-metal systems with surface impurity concentration as low as 3 x 10^{12} atoms cm⁻², thus leading to the direct characterization of the electronic and magnetic configuration of impurity systems as well as supported nanostructures. Combined XAS-XMCD provide simultaneous information about the the d-valence state and related spin and orbital moment of transition-metal atoms that is not accessible by traditional techniques such as, e.g., magnetic susceptibility, resistivity, and electron paramagnetic resonance measurements. A first fundamental issue is how the magnetic moment of surface adatoms depends on the interaction with the host conduction electrons. We show that Fe, Co, and Ni, owing to delectron localization, display large spin and orbital moments on low electron density simple-metal substrates which are progressively quenched as the surface electron densitiy increases.¹ A second fundamental issue is how the interaction with the substrate and adjacent adatoms influnces the magnetic anisotropy of the system. We report giant magnetic anisotropy values up to 3.3 meV/atom for Co clusters and atomic wires on Pt surfaces. A clear correlation is established between the atomic coordination, the magnitude of the orbital moment and the anisotropy energy, with implications for magnetic ordering phenomena.²

¹ P. Gambardella et al., Phys. Rev. Lett. 88, 047202 (2002).

² P. Gambardella et al., Nature 416, 301 (2002).

11:00am MI+SS-ThM9 Probing Buried Interfaces with Soft X-ray Standing Wave Spectroscopy: Application to the Fe/Cr Interface, S.-H. Yang, B.S. Mun, Lawrence Berkeley National Laboratory, N. Mannella, University of California, Davis, S.K. Kim, J.B. Kortright, J. Underwood, F. Salmassi, E. Arenholz, A. Young, Z. Hussain, M.A. van Hove, Lawrence Berkeley National Laboratory, C.S. Fadley, University of California, Davis We will discuss a novel type of non-destructive method for spectroscopically studying buried nanometer-scale interfaces and other nanostructures with soft x-ray standing waves. Strong standing waves with a period of 4.0 nm and approximately 3:1 contrast ratios are created via Bragg reflection from a synthetic multilayer of form [B4C/W]40. By growing a wedge-shaped Fe/Cr bilayer on top of this multilayer, the mechanical translation of the sample exposed to a fixed and finely focussed synchrotron radiation beam is converted into a translation of the standing wave through the interface. Analyzing various core photoelectron intensities as a function of angle and beam position permits deriving layer thicknesses and interface mixing/roughness scales. Magnetic circular dichroism in photoemission from the 2p and 3p levels of Fe and Cr further permits deriving the positions and widths of regions with decreased (increased) ferromagnetic alignment for Fe (Cr), showing that normally antiferromagnetic Cr becomes ferromagnetic just below the center of the interface but with antiparallel alignment with respect to Fe, and that the equal-concentration region in the center of the interface strongly inhibits magnetic alignment for both species along the direction of net magnetizations that is probed. The magnetically-altered regions in both

metals are only 1-2 atomic layers in thickness. 3s spectra from Fe and Cr further indicate that the local spin moments on both atoms do not change on crossing the interface. This standing wave-plus-wedge method should have a range of applications for the characterization of magnetic and nonmagnetic nanostructures and their interfaces. Work supported by the U.S. Department of Energy, Office of Science, Office of Basic Energy Sciences, Materials Sciences Division, under Contract No. DE-AC03-76SF00098.

Processing at the Nanoscale Room: C-109 - Session PN+SS-ThM

Patterning and Functionalization

Moderator: W.N. Unertl, University of Maine

8:20am PN+SS-ThM1 Carbon Nanotube Synthesis and Non-Covalent Surface Chemistry, H. Dai, Stanford University INVITED

This presentation will cover our latest results on, (1) Patterned growth of carbon nanotubes architectures on surfaces. Strategies for assembling nanotubes at their synthesis stage by self-assembly or external forces to orient nanotubes will be shown. (2) (2) Charge transfer interactions between small molecules and polymers with nanotube surfaces and the influence to the physical properties of nanotubes will be discussed. Charge transfer and photochemical effects will be presented. (3) Various non-covalent functionalization schemes for nanotubes will be described. Molecular and metal species can be attached to nanotube sidewalls by pi-stacking, van der Waals and hydrophobic interactions, electroless deposition, metal coordination chemistry. Functionalization by biological molecules will also be presented. The implications of controlled chemical synthesis and functionalization to future nano-electronics for chemical and biological applications will be discussed.

9:00am **PN+SS-ThM3 Thiol Diffusion in Dip Pen Nanolithography**, **P.E. Sheehan**, S.E. Kooi, L.J. Whitman, Naval Research Laboratory

Interest in the properties of nanometer scale objects has greatly increased in recent years and with it the desire for tools to create these objects. Dip Pen Nanolithography (DPN) is one promising tool because it is widely accessible, flexible in choice of materials, and capable of creating structures as small as 10 nm. Our research has expanded the range of molecules used in DPN and has calibrated the rate of their deposition and spread. Calibration of the deposition was performed by developing a model of the diffusive spread of thiols from an AFM tip.¹ To our knowledge, this model allowed the first direct determination of a diffusion coefficient for an alkanethiol on gold. The effect of alkane chain length and terminal on the diffusion coefficient was also studied, and we find that the length of the alkane chain significantly affects deposition. For instance, hexadecanethiol (16 carbons) deposits much more rapidly than the slightly longer octadecanethiol (18 carbons), indicating that chain-chain interactions strongly influence the deposition rate. A fundamental insight into the DPN deposition mechanism was also gained during these studies. It had been proposed that the water meniscus that naturally forms between an AFM tip and the scanned surface enables deposition. When we examined the effect of humidity on thiol diffusion, no correlation was found. Moreover, we find that deposition persists even after two days under dry nitrogen. For this reason, we propose that ODT is deposited directly onto the surface and does not require water as a medium.

¹ P. E. Sheehan and L. J. Whitman, Phys. Rev. Lett. 88 (2002) 156104.

9:20am PN+SS-ThM4 Reversible Layer Phase Transition Controlled by the Scanning Tunneling Microscope Tip, S. Berner, M. de Wild, L. Ramoino, S. Schintke, University of Basel, Switzerland, H. Suzuki, Kansai Adv. Res. Center, Japan, A. Baratoff, H.-J. Guentherodt, University of Basel, Switzerland, T.A. Jung, Paul Scherrer Institute, Switzerland

Sub-phthalocyanine (SubPc) on Ag(111) shows a complex phase behaviour of the growing first molecular monolayer. With increasing layer coverage, 2D lattice gas, condensed honeycomb superstructure and hexagonal close packed layers are observed. A previous study of SubPc on Ag(111) dealt with the coexistence of the honeycomb superstructure and the 2D lattice gas and showed the high mobility of individual SubPc molecules at room temperature.¹ The complex phase behaviour is a general consequence of the repulsive nearest neighbour interaction between individual molecules and the diffusion at room temperature. In this work we studied SubPc layers with a coverage in the order of 0.7 monolayers on Ag(111) with room temperature scanning tunneling microscopy (STM). On large terraces the SubPc molecules form a hexagonal close packed (hcp) superstructure. However, experimental sequences on confined terrace areas (vacancy islands with diameters of 30-80 nm introduced by sputter defects) reveal

interesting details about the condensation and evaporation of molecular islands on a nanometer scale. In such vacancy islands reversible phase transitions between 2D mobile and 2D condensed (hcp) phases could be controlled by the STM tip. In addition, rotational flipping of the orientation of condensed islands between two different substrate lattice registries occurred. Different microscopic mechanisms are discussed in the context of this newly observed complex behaviour.

¹ S. Berner, M. Brunner, L. Ramoino, H. Suzuki, H.-J. Guentherodt, and T.A. Jung, Chem. Phys. Lett. 348 (2001) 175.

9:40am PN+SS-ThM5 Covalent Nanopatterning of Liquid Phase Organic Molecules to Silicon Surfaces using Conductive Atomic Force Microscopy, M.W. Such, C.R. Kinser, M.C. Hersam, Northwestern University

Electron stimulated desorption (ESD) with ultra-high vacuum (UHV) scanning tunneling microscopy (STM) is a well-established technique for creating reactive patterns of dangling bonds on predominantly hydrogen passivated silicon surfaces. Gas phase surface chemistry occurs selectively with these nanopatterns, allowing for controlled deposition of materials down to the single molecule level. Although this approach is effective in UHV, it has not yet been utilized for the patterning of non-UHV-compatible materials. This paper describes an analogous means of creating reactive nanopatterns on hydrogen passivated Si(111) surfaces using conductive atomic force microscopy (cAFM) in liquid environments. Unlike cAFM patterning in air that induces oxidation on silicon surfaces, this approach suppresses oxidation through encapsulation of the tip-sample junction in an anhydrous organic solvent (e.g., toluene or dimethyl sulfoxide). Following ESD induced with cAFM, olefinic organic molecules suspended in the organic solvent environment spontaneously bind to the dangling bond patterns. To demonstrate this technique, exo-5-norbornene-2-ol has been patterned with 50 nm resolution on Si(111):H. Lateral force microscopy and force-distance spectroscopy confirm the hydrophilic nature of this molecule compared to the hydrophobic Si(111):H surface. Following deposition, these nanopatterned molecules have been subjected to a subsequent nucleophilic acyl substitution reaction with Lauroyl Chloride at 50°C for 24 hours. Consistent with the expected dodecyl ester modification of the adsorbed norbornene molecule, the resulting nanopattern appears hydrophobic in LFM analysis. The stability of these nanopatterns to subsequent chemistry suggests that the adsorbed molecules are covalently bonded to the silicon substrate. Further applications of this lithography for covalently nanopatterning polymers and biological molecules to silicon surfaces will also be discussed.

10:00am PN+SS-ThM6 High Resolution Chemo-Mechanical Functionalization of Silicon Surfaces by Atomic Force Microscope, R.C. Davis, B.A. Wacaser, T.L. Niederhauser, Brigham Young University, I.A. Mowat, Charles Evans & Associates, M.R. Linford, Brigham Young University

We describe a versatile high-resolution method for chemical functionalization of silicon surfaces. An atomic force microscope (AFM) probe is used to mechanically induce chemical functionalization thereby simultaneously patterning and functionalizing the hydrogen-terminated silicon. A 20 nm radius of curvature probe is used to scribe the hydrogen-terminated silicon. When the Si-H and Si-Si bonds are broken in the presence of unsaturated hydrocarbons a reaction occurs in which the hydrocarbon chain is covalently bonded to the Si surface. Using this technique we have produced patches and patterned lines of alkene molecules on a Si (111) substrate with line widths down to 100 nm. Time of flight secondary ion mass spectroscopy measurements verifying the high-resolution chemical functionalization will be presented.

10:20am PN+SS-ThM7 Fabrication of Si Nanostructures by Scanning Probe Oxidation and Tetra-Methyl Ammonium Hydroxide Etching, F.S.-S. Chien, Center for Measurement Standards, Taiwan, W.-F. Hsieh, National Chiao-Tung University, Taiwan, S. Gwo, National Tsing-Hua University, Taiwan, A.E. Vladar, J.A. Dagata, National Institute of Standards and Technology

We demonstrated that the process of scanning probe microscope (SPM) oxidation and anisotropic tetra-methyl ammonium hydroxide (TMAH) etching is a low-cost and reliable method to produce smooth and uniform silicon nanostructures on a variety of silicon substrates. Etched structures with a pitch of 100 nm, positive- and negative-contrast structures, and features height greater than 100 nm have been produced on bare silicon, Si_3N_4 -coated and silicon-on-insulator wafers. Evolution of hexagonal pits on two-dimensional grid structures were shown to depend on the pattern spacing and orientation with respect to Si(110) crystal directions. We successfully combined SPM oxidation with traditional optical lithography in a mixed, multilevel patterning method for realizing micrometer- and nanometer-scale feature sizes, as required for photonic device designs. The

combination of SPM oxidation and TMAH etching is a promising approach to rapid prototyping of functional nano-photonic devices.

10:40am PN+SS-ThM8 Charge Trapping in Oxide-Nitride-Oxide-Silicon Structures Studied by Electrostatic Force Microscopy, S.-D. Tzeng, Y.-C. You, S. Gwo, National Tsing-Hua University, Taiwan, ROC

A novel approach of fabricating oxide-nitride-oxide-silicon (ONOS) charge storage structures is demonstrated by using the scanning-probe-induced oxidation process under ambient conditions. During the probe oxidation process, both positive and negative charges are injected and trapped inside the ONOS cell. By means of quantitative electrical force microscopy (EFM) measurements, we have investigated the trapping behavior of the probeoxidation-induced charges. We found that the retention time of the negative charge is much shorter than the positive one. By measuring the decay lifetimes of these trapped charges after annealing at different temperatures, we have determined the trapping energies of both types of charges. We also found that, after high-temperature annealing, these trapped charges can be detrapped. The resulting ONOS cell can be used as a nonvolatile memory element with write/erase capability locally controlled by a biased scanning probe tip.

11:20am PN+SS-ThM10 Ferroelectric Lithography for Multicomponent Nanofabrication, D.A. Bonnell, S.V. Kalinin, R.A. Alvarez, X. Lei, R. Shao, Z. Hu, J.H. Ferris, University of Pennsylvania

In spite of the variety of approaches to the assembly of nanowires, nanoparticles, and organic/biological molecules, device functionality has been achieved in only a few select systems. The organization of dissimilar molecular or nanostructural constituents into predefined structures necessary to yield functionality remains a challenge. We report here a novel approach that controls atomic polarization of ferroelectric substrates to vary local electronic structure. It will be demonstrated that chemical reactivity involving electron transfer is domain specific due to surface band bending. The minimum feature size is on the order of 3 nm and resolution positioning 10-20 nm. When combined with chemistry associated with self assembly, nanostructure composites consisting of oxide substrates, metal nanoparticles, and organic/biological molecules can be fabricated in predefined configurations. This leads to the potential to make electronic or opto-electronic devices on the 10 nm size scale. The approach will be demonstrated with simple devices.

11:40am PN+SS-ThM11 Size-Induced Ferroelectric Phase Transitions in PbTiO₃ and PbZrO₃ Nanotubes Formed by Sol-Gel Template Synthesis, *B.A. Hernandez*, *K.-S. Chang, E.R. Fisher, P.K. Dorhout*, Colorado State University

Nanotubes of the perovskite ABO3 (A = Pb, B = Ti,Zr) have been prepared by sol-gel template synthesis. A size-induced ferroelectric phase transition for PbTiO3 and PbZrO3 nanotubes was observed by thermal analysis. The nanotubes were prepared within Whatman Anodisc templates (200 nm pore size) with a sol-gel method using titanium and zirconium alkoxides and lead acetate. Scanning electron microscopy demonstrated that the structures formed within the template were 50 14m long tubes with 200 nm outer diameters. Transmission electron microscopy and electron diffraction revealed that the tubes were polycrystalline. Comparison of the d-spacing between electron and bulk powder X-ray diffraction patterns allowed assignment of the crystalline phase of the nanotubes as tetragonal for PbTiO3. Differential scanning calorimetery was used to monitor the ferroelectric phase transition temperature (Tc). Comparison between the bulk powders and nanotubes showed an anomalous decrease Tc. Values for PbTiO3 Tc were determined to be between 496.5°- 489.7°C for bulk powders with grain sizes of 75 and 35 nm respectively and 234.4°C for the nanotubes having a grain size of 11.2 nm. Preliminary results for PbZrO3 shows that the Tc decreases from 229.9 for bulk powder to 123.6 for nantRoom temperature Raman spectra also indicated structural size effects by monitoring the energies of the E1(TO) soft mode and relative intensities of the E2(TO) mode.

Surface Science Room: C-112 - Session SS+EL+OF-ThM

Reactions and Patterning of Organics on Silicon Moderator: S.F. Bent, Stanford University

8:20am SS+EL+OF-ThM1 Fixation of Alkyl Groups on Si(111) Surface through C-Si Single Covalent Bond formed by Reaction of Grignard Reagent and H:Si(111), T. Yamada, T. Inoue, K. Yamada, N. Takano, T. Osaka, Waseda University, Japan, H. Harada, K. Nishiyama, I. Taniguchi, Kumamoto University, Japan

Alkyl adsorbates that are directly bonded to the outermost atoms of silicon wafer surfaces have prospective properties for application in nanometerscale fabrication and surface functionalization.¹ Several methods have been proposed to deposit alkyl groups on hydrogen-terminated H:Si(111).² The conversion of the HSi bonds in H:Si(111) into C-Si bonds caused by chemical processes is an important issue in preparing the organic adlayers. In this work, high-resolution electron energy loss spectroscopy (HREELS) was utilized to prove the formation of single covalent bonds between Si(111) surface atoms and alkyl groups by the chemical reaction of a Grignard reagent and hydrogen-terminated H:Si(111)(1x1).² The reaction was performed by heating a piece of H:Si(111) in 1M tetrahydrofuran (at 65°C) or diethylether solution (at 30°C) of desired alkylmagnesium halide for 18 hours under Ar atmosphere. By this reaction condition, somewhat 20% of the product surface were still covered with residual hydrogen. The bending vibration mode of the residual hydrogen (630 cm⁻¹) obscured the alkyl signals in the range of 600 - 700 cm⁻¹. By using deuterium-terminated D:Si(111), the vibration at 680 cm⁻¹, assigned to the C-Si bond, was isolated within the spectrum of CH₃-. The CH₃ groups were thermally stable at temperatures below 600 K. Similar features were observed for C_2H_{5} -, phenyl- and so on. The C-Si bonds are essential for enhancing the stability and lowering the mobility of alkyl moieties. Such properties of alkyl moieties of will lead to a new prospective science and technology in nanometer-scale fabrication.

¹T. Yamada, N. Takano, K. Yamada, S. Yoshitomi, T. Inoue, and T. Osaka, Jpn. J. Appl. Phys. 40 (2001) 4845.

²R. Boukherroub, S. Morin, F. Bensebaa and D. D. M. Wayner, Langmuir 15 (1999) 3831.

8:40am SS+EL+OF-ThM2 Chemomechanical Production of Sub-Micron Edge Width, Functionalized, ~20 Micron Features on Silicon, *M.R. Linford*, Y.-Y. Lua, T.L. Niederhauser, B.A. Wacaser, Brigham Young University, I.A. Mowat, Charles Evans & Associates, A.T. Woolley, R.C. Davis, Brigham Young University, H.A. Fishman, Stanford University Medical School

We have recently reported that monolayers on silicon can be formed, and silicon substrates concomitantly patterned, when native oxide-terminated silicon is scribed with a diamond-tipped instrument in the presence of 1alkenes,^{1,2} 1-alkynes,^{1,2} alkyl halides (chlorides, bromides, and iodides),^{2,3} and alcohols.^{3,4} Monolayers were prepared in the open laboratory with reagents that had not been degassed.¹⁻⁴ However, while this method is particularly facile, the features produced using a diamond scribe are coarse and irregular.¹ The high degree of edge and surface roughness in these features will no doubt limit the utility of our earlier work in some circumstances. Here we describe a substantial improvement in our earlier method by showing the production of sharp, well-defined, functionalized features on silicon that are invisible to the naked eye and very shallow. In contrast to the earlier procedure that used oxide-terminated silicon and a diamond-tipped scribe,¹⁻⁴ this new method consists of 1) cleaning and drying a silicon shard, 2) immersing the silicon in a fluoride ion etch to remove its native oxide and produce hydrogen-terminated silicon, 3) wetting the dry, H-terminated silicon surface with a reactive liquid, and 4) scribing the surface with a small tungsten carbide ball. Both Si(100) and Si(111) were successfully patterned and functionalized with this new method.

¹ Niederhauser, T. L.; Jiang, G.; Lua, Y.-Y.; Dorff, M. J.; Woolley, A. T.; Asplund, M. C.; Berges, D. A.; Linford, M. R. Langmuir 2001, 19, 5889-5900.

² Lua, Y.-Y.; Niederhauser, T. L.; Matheson, R.; Bristol, C.; Mowat, I. A.; Asplund, M. C.; Linford, M. R. In Press Langmuir 2002.

³ Niederhauser, T. L.; Lua, Y.-Y.; Sun, Y.; Jiang, G.; Strossman, G. S.; Pianetta, P.; Linford, M. R. Chem.Mater. 2002, 14, 27-29.

⁴ Niederhauser, T. L.; Lua, Y.-Y.; Jiang, G.; Davis, S. D.; Matheson, R.; Hess, D. A.; Mowat, I. A.; Linford, M. R. In press Angewandte Chemie 2002.

9:00am SS+EL+OF-ThM3 Formation of Nanoscale Organic and Inorganic Features on Semiconductor Surfaces, J.M. Buriak, Purdue University INVITED

Integration of molecular devices and nanoscale materials with semiconductors, including silicon and germanium, is an area of intense interest, due to the potential for interfacing nanomaterials with the macroworld. We have developed a number of wet chemical routes which allow for covalent attachment of both organic functionalities, including molecular wires, and inorganic nanoparticles. For instance, a cathodic electrografting reaction between alkynes and hydride-terminated silicon surfaces results in alkynyl moieties bound directly through Si-C bonds, with no intervening oxide layer. The surfaces are air and water stable, and can withstand boiling pH 12 solutions. In order to pattern these alkynyl groups on the silicon surface in nanoscale regions, conducting probe lithography has been utilized to write the organic monolayers, with feature sizes as small as 30 nm. For inorganic structure patterning, electroless deposition has been combined with microcontact printing, dip pen nanolithography (DPN), and UV-mediated hydrometallation to produce nano- and micronscale features. These approaches and others will be described.

9:40am SS+EL+OF-ThM5 Structures, Dynamics, and Chemical Reactivity of Si (001) at Finite Temperatures: A First Principles Study, D. Pillay, Y. Wang, G.S. Hwang, The University of Texas at Austin

Imparting organic functions onto a well-defined functionality of semiconductor surfaces with atomic-scale precision provides an enormous opportunity to develop new molecular devices including chemical and biological sensors and molecular electronic devices. For semiconductor systems, the rates and pathways of chemical reactions are strongly influenced by local electronic structures determined by surface reconstructions and defects. Due to such complex structural effects, chemical dynamics on semiconductor surfaces has not been fully understood. To gain molecular-level control, therefore, first we must develop a detailed understanding of structures, dynamics, and chemical reactivity of clean, defective, or modified (with various adsorbates) surfaces at finite temperatures, along with the structures and bonding of organic compounds onto the surfaces. In this talk we will present first principles quantum mechanics [Density Functional Theory with plane-wave basis sets and pseudopotentials] simulations for structures, dynamics, and chemical reactivity (towards organic species) of (001)-faced Si and Ge surfaces at finite temperatures. This includes the dynamics of buckled dimers on clean and defective surfaces and their effects on adsorption dynamics of various organic molecules.

10:00am **SS+EL+OF-ThM6 Superexchange Interactions in STM-Organic-Semiconductor Systems**, *L.C. Teague*, *J.J. Boland*, University of North Carolina at Chapel Hill

The incorporation of organic layers and individual molecules into existing semiconductor technologies requires a thorough understanding of surface/molecule reactions. Although numerous studies have focused on the reaction of individual molecules with the Si(100) surface, the specific reaction mechanisms remain poorly understood. The similarity of the Si(100)-2 x 1 surface chemistry with that of C=C systems opens up the possibility of a wide range of organic chemistry reactions. Here, a combination of Scanning Tunneling Microscopy (STM) and Density Functional Theory (DFT) calculations are used to study and interpret the reaction of 1,3-cyclohexadiene (1,3-CHD) with the bare Si(100)-2 x 1 surface. Because STM probes the local density of states (LDOS), the local bonding geometry of 1,3-CHD can be inferred from the location of the π bond in the adsorbed molecule. Other groups have reported similar observations.^{1,2} However, DFT calculations indicate the π^* orbital is located several eV above the Fermi Energy and should be energetically inaccessible under typical bias conditions. Here, we show that these images can be understood by considering the interaction between the STM tip and the molecule-surface system. The superexchange mixing of the tip dangling bond state with the filled π state on the molecule produces a new state within the tunneling window. This state is responsible for the observed image contrast and suggests superexchange effects of this type may be important in understanding the charge transfer that occurs through these molecular systems.

 ¹ Hamaguchi, K.; Machida, S.; Nagao, M.; Yasui, F.; Mukai, K.; Yamashita, Y.; Yoshinobu, J.; Kato, H. S.; Okuyama, H.; Kawai, M.; Sato, T.; Iwatsuki, M. J. Phys. Chem. B 2001, 105, 3718.
² Hovis, J. S.; Liu, H.; Hamers, R. J. J. Phys. Chem. B, 1998, 102, 6873.

10:20am SS+EL+OF-ThM7 Modifying the Semiconductor Interface with Organonitriles, M.A. Filler, C. Mui, C.B. Musgrave, S.F. Bent, Stanford University

Organic functionalization of group-IV semiconductor surfaces has recently garnered considerable attention and applications in the areas of molecular electronics, biological recognition, and reagentless micropatterning have been proposed. If these and other concepts are to become technologically feasible, however, the creation of an ordered and selectively grown layer as well as the ability to successively attach additional organic monolayers will be necessary. Organonitrile compounds were studied as potential candidates for first and subsequent layer surface reactions on Si(100)-2x1 and Ge(100)-2x1. Bonding is investigated experimentally with infrared

spectroscopy and theoretically with density functional theory. We find that acetonitrile does not react on the Ge(100)-2x1 surface at room temperature and explain this result with kinetic and thermodynamic arguments. A [4+2] cycloaddition product through the conjugated π system and a [2+2] C=C cycloaddition product through the alkene are found to be the dominant surface adducts for the multifunctional molecule 2-propenenitrile. While the non-conjugated molecules 3-butenenitrile and 4-pentenenitrile are not expected to form a [4+2] cycloaddition product, both show vibrational modes characteristic of this adduct and we propose the possibility of a surface catalyzed reaction. Pathways directly involving only the nitrile functional group are thermodynamically unfavorable at room temperature on Ge(100)-2x1 and the conversion of the remaining nitrile functionality as well as its use in additional surface reactions will also be presented.

10:40am SS+EL+OF-ThM8 Adsorption and Reaction of Allyl- and Ethyl-amine on Germanium and Silicon Surfaces, P. Prayongpan, C.M. Greenlief, University of Missouri-Columbia

The adsorption and reaction of allyl- and ethyl-amine with the Ge(100) and Si(100) surfaces is examined. These processes are followed by a variety of surface sensitive techniques including ultraviolet photoelectron spectroscopy and temperature programmed desorption. Possible adsorption structures are also examined by theoretical methods. Density functional theory calculations are used to help interpret the photoelectron spectroscopy data. The calculated molecular orbital energies (within Koopmas' approximation) are used to help identify adsorbed molecular species, as well as, reaction intermediates. The interaction of these nitrogen-containing molecules with surface dimmer bonds and ordering of the resulting surface layers will be discussed.

11:00am **SS+EL+OF-ThM9** Adsorption Chemistry of Cyanogen **Bromide and Iodide on Silicon (100)**, *N.F. Materer*, *P. Rajasekar*, *E.B. Kadossov*, Oklahoma State University

The adsorption of cyanogen iodide (ICN) and bromide (BrCN)on a silicon (100) surface is studied by X-ray photoelectron spectroscopy (XPS), ultraviolet photoelectron spectroscopy (UPS) and thermal desorption spectroscopy (TPD). After submonolayer exposures, XPS indicates that the CN triple bond of both ICN and BrCN emains intact upon adsorption at 100K. The UPS spectrum of these molecules contains two peaks assigned to the pi electrons in the CN triple bond. The splitting of these levels, due to the interaction between the pi electrons on the cyanogen and the halide, show that some portion of the initially adsorbed cyanogens halide also remains intact upon low temperatures adsorption. In contrast, the UPS spectrum of ICN and BrCN adsorbed at room temperature on Si(100) contains only one peak due to the pi electrons in the carbon nitrogen triple bond. The lack of splitting in the room temperature UPS spectrum is a result of XC (X=Br, I) bond dissociation. Thus, the XC bonds breaks while the CN bond remains intact during room temperature adsorption on Si(100). Upon annealing the Si(100) surface to higher temperatures, the UPS spectra indicates that the C-N triple bond remains intact until approximately 700 K. Simultaneous changes in the C 1s photoelectron peak are consistent with the idea that C-N bond cleavage in the cyanogen halides is correlated with silicon carbide formation.

11:20am SS+EL+OF-ThM10 Theoretical Adsorption Studies of ICN on the Si(100) Surface, E.B. Kadossov, P. Rajasekar, N.F. Materer, Oklahoma State University

Ab initio quantum calculations have been used to study the adsorption and surface reactions of ICN on the Si(100) surface represented by Si₂H₁₂ single-dimer cluster. At low temperatures, experiments show that some faction of the initially exposed ICN is molecularly absorbed to the surface. Calculations of the molecularly absorbed species support the formation of end-on configuration with the N forming a dative bond with the lone pair on the Si(100) surface. Upon annealing, experiments reveal that the remaining molecular adsorbed ICN species dissociate to produce I and CN species on the surface. Calculations show that this process can take place directly or through a stable side-on adsorption intermediate. The transition barrier to form the side-on intermediate species is slightly lower than for the direct reaction (12.82 vs. 17.26 kJ/mol). After dissociation, the CN is bound to the silicon surface through either the C or the N ends. The C bound species possesses the lowest energy and is consistent with experimental XPS results. In addition, these two possible structures are separated by an activation barrier of 107.39 kJ/mol, easily overcome by the excess adsorption energy. An alternate pathway for the ICN side-on species is to isomerize into an INC structure through a 212.26 kJ/mol activation barrier. However, the activation barrier between this new species and the dissociated state is 5.53 kJ/mol. This transition barrier is even lower than the 84.05 kJ/mol barrier between side-on ICN surface species and the dissociated state.

11:40am SS+EL+OF-ThM11 Infrared Study of Adsorption of C₆H₆ onto Si(100)(2x1), M. Shinohara, H. Watanabe, Y. Kimura, H. Ishii, M. Niwano, Tohoku University, Japan

The interaction of benzene with the (100) and (111) surfaces of silicon has proven to be an interesting model system for molecular adsorption on semiconductor surfaces. The adsorption of benzene on the Si(100)(2x1) surface has been expensively studied in recent years both experimentally and theoretically. Previous elaborate theoretical calculations predicted that adsorption of benzene onto the Si(100)(2x1) surface leads to two different adsorption structures: One corresponds to benzene adsorbed on top of a dimer row between two adjacent Si dimers. This structure has four C atoms of benzene bonded to four Si atoms from two adjacent dimers. The other corresponds to the benzene molecule that sticks on top of the dimer row and has two of its C atoms bonded to two Si atoms of a single surface dimer. However, there still is a controversy regarding which structure is more favored. In this study, we have investigated the adsorption of benzene C2H6 on the Si(100)(2x1) surface using infrared absorption spectroscopy (IRAS) in the multiple internal reflection geometry (MIR) and the so-called hybrid density-functional theory (DFT) to determine the most preferred adsorption structure of benzene on Si(100)(2x1) at room temperature. IRAS-MIR provides us with valuable information about the hydrogen bonding configurations on semiconductor surfaces. We analyzed IRAS spectra in the C-H stretching vibration region to determine the detailed adsorption structure of benzene. The central result is that benzene adsorbs in different manners depending on the surface coverage of benzene: at low coverage the molecule adsorb on the surface to favor the formation of benzene adsorbed on two adjacent dimers. On the other hand, at high coverage the molecule adsorb on the Si surface to generate benzene adsorbed on a single dimer. We also discuss the reason why the adsorption structure depends on surface coverage.

Surface Science Room: C-110 - Session SS+EL-ThM

Structure of Semiconductor Surfaces & Interfaces Moderator: C.J. Palmstrom, University of Minnesota

8:20am **SS+EL-ThM1 Strain Control of the Ge(105) Surface via Hydrogen Adsorption**, *Y. Fujikawa*, *M. Kawashima*, *T. Nagao*, *T. Sakurai*, Tohoku University, Japan, *M.G. Lagally*, University of Wisconsin-Madison

Controlling the size and shape of Ge quantum dots formed on the Si(001) substrate is of great technological importance for their potential application in future semiconductor devices. Surfactant effects on this system are regarded as a promising method to achieve the controlled growth of quantum dots. Among them, hydrogen adsorption, which has been studied intensively, is known to suppress the formation of Ge "huts", pyramidal nanocrystals bounded by four Ge{105} facets.¹ We have investigated hydrogen adsorption on a Ge(105) surface formed on a Si(105) substrate using STM to elucidate the role of surface strain on the stability of Ge(105) under hydrogen-adsorption conditions. The STM images of Ge(105) surfaces with adsorbed hydrogen atoms are understood based on the newlyestablished atomic structure of Ge(105).² We observe the stability of hydrogen-covered Ge(105) for different amounts of Ge initially deposited on the Si(105) surface. We find that hydrogen adsorption on Ge(105) surfaces formed from deposited amounts of Ge less than 1.5 ML makes the surface remarkably unstable and results in the formation of local defects. This fact indicates that hydrogen adsorption on Ge(105) increases the surface strain by arresting the strain-relief mechanism that would ordinarily occur on clean Ge(105) with the formation of sp²-hybridized dimers. Thus, the formation of Ge(105) will be unfavorable and suppressed in the presence of adsorbed hydrogen. This work is supported by $\bar{\text{NSF}}.$

¹ Kahng et al., Phys. Rev. Lett. 80, 4931 (1998).

² Fujikawa et al., Phys. Rev. Lett. 88, 176101 (2001).

8:40am SS+EL-ThM2 A LEEM Study of the Ge(001)-(2x1)-(1x1) Phase Transition; Domain Wall Proliferation and Dimer Break-up, *E. van Vroonhoven, H.J.W. Zandvliet, B. Poelsema*, University of Twente, The Netherlands

The Ge(001) surface exhibits two phase transitions. At low temperatures it is c(4x2) reconstructed, evolving with increasing temperature into (2x1). The origin of the reconstruction is dimerization of the surface: the number of dangling bonds is reduced from two per surface atom, for a bulk terminated surface, to only one. In the c(4x2) phase the dimers are buckled in an anti-symmetric way; in the (2x1) phase the dimers rapidly switch between the two buckled orientations and appear symmetric. Due to the diamond structure of Ge, the dimer rows on neighboring terraces are rotated

by 90°. At high temperature the (2x1) phase disappears and the (1x1) phase emerges. Two conflicting models have been proposed in literature. One model suggests that this phase transition is driven by vacancy pair creation and dimer break-up on the Ge(001) surface. The other claims that the phase transition involves (2x1) domain wall (step) proliferation rather than dimer break-up. Our results demonstrate that domain wall proliferation sets in around 950 K, leading to a complete loss of contrast in LEEM around 1050 K. The dimers, however, remain clearly visible up to about 1130 K. The dimer concentration is a strong function of the substrate temperature between 1030 and 1130 K. Our combined microscopy and diffraction data are only consistent with the first model. It is even possible for the first time to directly extract the free energy gain of dimerization, being 1.6 eV per pair. This value compares perfectly with calculations performed for silicon after scaling with the melting temperature. We estimate the temperature to be accurate with \pm 25 K and thus the dimerization energy with \pm 5%.

9:00am SS+EL-ThM3 Encapsulation of SiGe Quantum Wells and Quantum Dots, G.G. Jernigan, P.E. Thompson, US Naval Research Laboratory

Semiconductor device characteristics are dependent on the chemical and structural properties of the electrical interface. As such, we are interested in SiGe quantum wells and quantum dots grown in Si. Heterojunctions between Si / SiGe / Si are chemically smeared due to Ge segregation, but little is known about the structural nature of the heterojunctions. We will present an STM study of the encapsulation of a Si_{0.8}Ge_{0.2} alloy grown in Si at 500, 650, and 800 °C. Alloy deposition induces a rougher morphology than the inital Si surface. Intermixing of Ge from the alloy with the Si substrate is observed to happen immediately to produce a rough surface. The amount of intermixing increases with increasing growth temperature, and at 800 °C the surface roughness exceeds the thickness of deposited alloy. After intermixing, Ge segregates out from the alloy, and the surface Ge leads to an island growth mechanism, which further increases the surface roughness. At 500, 650, and 800 °C the alloy surfaces obtain a steady-state value for surface roughness, which has been characterized as 2D planar, rippled, and hutted, respectively. Encapsulation of the alloy layer with Si attempts to restore a smooth morphology. At 800 °C where the height of the huts are ~40 nm, a 5 nm Si layer reduced the hut height to ~10 nm, and after 20 nm of Si, the huts are gone. Remnants of the underlying alloy morphology can still be seen on the surface in the form of square pits where material did not fill in between the huts. For lower growth temperatures, less Si is needed to reduce the surface roughness, and square pits are still observed from the underlying alloy. The square pits arise from Ge segregation modifying the SA and SB step-edge sticking coefficient of Si to produce equal sized S_A and S_B terraces. A structural model for the heterointerfaces based on the STM observations will be presented.

9:20am SS+EL-ThM4 First Atomic-Resolution Ultrahigh Vacuum Scanning Tunneling Microscopy Study of GaSe/Si(111) Ultrathin Films, T. Ohta, A. Klust, J.A. Adams, Q. Yu, M.A. Olmstead, F.S. Ohuchi, University of Washington

Gallium-selenide thin films deposited on Si(111) are of increasing interest for applications, both in their own right as optoelectronic structures, and as non-reactive, low surface energy, high band gap buffer layers for subsequent nanostructure formation. Gallium selenide crystallizes into two crystal structures, layered GaSe and cubic Ga2Se3 with bandgaps of 2.0 and 2.6eV, respectively. Crystal structure and stoichiometry of the deposited Ga_xSe_v can be controlled by the substrate temperature during deposition. We present the first atomic-resolution ultrahigh vacuum scanning probe microscopy study of GaSe/Si(111) ultrathin films. When GaSe thin films are deposited at substrate temperature 520°C, atomically flat surfaces consisting of a single molecular layer of GaSe with altered step structures of 7*7-Si(111) were observed. These surfaces have no dangling bonds to react with residual gases, or to provide nucleation sites for subsequent growth. We also observed occasional point defects causing long-range alterations of the local band bending, but no sharp states revealed by the tunneling spectroscopy. At lower substrate temperatures, Ga_xSe_y multilayers with flat surface and triangle features with 3-4nm sides were formed. Height difference of the atomic steps suggests that the multilayers have a cubic structure. These triangles are likely associated with Ga or Se vacancies in the Ga₂Se₃.

This work was partially supported by the M. J. Murdock Charitable Trust and NSF Grant DMR 0102427.

9:40am SS+EL-ThM5 Electronic and Structural Properties of Aluminum Selenide Ultrathin Film on Si(111), J.A. Adams, A.A. Bostwick, T. Ohta, A. Klust, University of Washington, E. Rotenberg, Advanced Light Source, F.S. Ohuchi, M.A. Olmstead, University of Washington

The wide band gaps of aluminum selenide and gallium selenide make them appealing candidates for blue-green opto-electronics, and they are closely lattice matched to silicon making them compatible in silicon-based structures and devices. However, very little is known about the properties of aluminum selenide heteroepitaxial films. Bulk aluminum selenide, a defected wurtzite structure, has a 3.1 eV band gap, and its hexagonal lattice constant is about 1.3% larger than Si(111). Unlike gallium selenide, which is stable in both layered GaSe and defected zincblende Ga₂Se₃ structures, layered AlSe has not been reported in either bulk or thin film form. We investigated varying thicknesses of ultrathin films of aluminum selenide grown epitaxially on Si(111) including sub-monolayer growth, a single bilayer, and the subsequent initial stages of growth on the bilayer. The AlSe/Si interface forms a bilayer structure similar to GaSe-terminated Si, although the temperatures for bilayer formation and for Se-evaporation from the film are higher for AlSe than for GaSe. The reactivity of the AlSe terminated Si(111) surface with both residual gases and for subsequent film growth is much higher than that of GaSe. Further deposition of aluminum selenide produces films that resemble the bulk stochiometry Al₂Se₃. Electronic band-structure for AlSe/Si was investigated using angle resolved photoelectron spectroscopy (ARPES). Unlike GaSe/Si, the AlSe bilayer appears to have a true surface state. Si-Al bond lengths and Al-Se bond lengths were measured by energy dependent photoelectron diffraction (EDPD). Initial results indicate that the Al-Si bond is 8% larger that in Al/Si(111)-($\sqrt{3}x\sqrt{3}$). Heterostructures of AlSe/GaSe on Si(111) will also be discussed. Funded by NSF Grant DMR-0102427.

10:00am **SS+EL-ThM6 Ga Surface Segregation in ErAs (100)/GaAs (100)**, *H.K. Jeong*, *T. Komesu, C.-S. Yang, P.A. Dowben*, University of Nebraska-Lincoln, *B.D. Schultz, C.J. Palmstrom*, University of Minnesota Surface segregation has now been characterized by angle resolved x-ray photoemission for NiMnSb, a variety of perovskites, and a number of binary alloys. Using angle-resolved x-ray photoemission spectroscopy (ARXPS), the surface composition of the sample can be roughly established since the effective probing depth is shorter at large emission angles with respect to the surface normal. Epitaxial thin films of the rare earth pnictide ErAs(100) can be grown on GaAs(100), but at elevated temperatures the ErAs film degrades. Ga segregation through the ErAs to the surface has been identified by angle-resolved X-ray photoemission spectroscopy, following extensive annealing. The angle-resolved XPS data indicates that the segregation of Ga is extensive throughout the ErAs thin film and is not restricted just to the surface layer.

10:20am SS+EL-ThM7 Absolute Orientation-Dependent TiN(001) Step Energies from Two-Dimensional Equilibrium Island Shape and Coarsening Measurements on Epitaxial TiN(001) Layers, S. Kodambaka, S.V. Khare, V. Petrova, University of Illinois, A. Vailionis, Stanford University, I. Petrov, J.E. Greene, University of Illinois

In situ high-temperature (1030-1185 K) scanning tunneling microscopy was used to determine the equilibrium shapes of two-dimensional TiN vacancy islands on atomically-smooth terraces of epitaxial TiN(001) layers. Inverse Legendre transformations of the equilibrium island shapes yield relative step energies as a function of step orientation within an orientation-independent scale factor λ , the equilibrium chemical potential of the island per unit TiN molecular area. We then use quantitative TiN(001) adatom island coarsening measurements to determine λ and, hence, absolute orientation-dependent step energies β and step stiffnesses beta. For <110> and <100> steps on TiN(001), we obtain: $\beta_{110} = 0.21\pm0.05 \text{ eV/Å}, \ \beta_{100} = 0.25\pm0.05 \text{ eV/Å}, \ beta_{110} = 0.9\pm0.2 \text{ eV/Å}, \ and \ beta_{100} = 0.07\pm0.02 \text{ eV/Å}. From the beta values, we calculate kink formation energies <math display="inline">\epsilon_{110} = 0.40\pm0.2 \text{ eV}$ and $\epsilon_{100} = 0.11\pm0.1 \text{ eV}$ based on the unrestricted terrace-step-kink model.

10:40am SS+EL-ThM8 Scanning Force Microscopy Measurements on Ionic Crystals at Low Temperatures and Comparison to Atomistic Simulations, *R. Hoffmann*, *M.A. Lantz*, University of Basel, Switzerland, *L.N. Kantorovich*, University College London, UK, *A. Baratoff, H.J. Hug*, University of Basel, Switzerland, *A.L. Shluger*, University College London, UK, *H.-J. Güntherodt*, University of Basel, Switzerland

Alkali halide surfaces were the first insulating materials to be imaged by scanning force microscopy (SFM) with true atomic resolution. Although atomic resolution images on alkali halides have been obtained by several groups, the tip-sample interaction above specific sites has so far been studied only theoretically.¹ Knowing this interaction force provides insight into atomic resolution image mechanisms and allows to study bonding

interactions on a surface on the atomic scale. Recently, site-specific forcedistance experiments have been performed for the first time at low temperatures on the Si(111) 7x7 surface.² Here we report similar measurements on the KBr (001) and the NaCl (001) surface in which we study the interaction forces and the imaging mechanism. The short-range forces have been calculated using atomistic simulations. The magnitude of the calculated forces agrees well with the experimental data, although for KBr the calculated corrugation is larger than the measured one even when the long-range forces are included. For NaCl also the corrugation is in good agreement to the experiment.

¹ L. N. Kantorovich et al. Surf. Sci. 445, 283 (2000)

² M. A. Lantz et al. Science 291, 2580 (2001)

11:00am SS+EL-ThM9 Core-level Spectroscopy Study of the Clean c(4x2) and the Hydrogenated 2x1-H Phases on the 3C-SiC(001) Surface, L.S.O. Johansson, S.M. Widstrand, K.O. Magnusson, M.I. Larsson, Karlstad University, Sweden, H.W. Yeom, Yonsei University, Korea, S. Hara, S. Yoshida, AIST, Japan

We report a core-level spectroscopy investigation of the clean Si-terminated 3C-SiC(001)-c(4x2) surface and the hydrogenated 3C-SiC(001)2x1-H surface. The 2x1-H surface was formed by exposing the clean c(4x2) surface to excited hydrogen gas. Desorption of the hydrogen at 900° C led to the restoration of the c(4x2) periodicity. Higher hydrogen exposures led to the formation of diffuse 1x1 and mixed 3x1/2x1 phases, as observed by low-energy electron diffraction (LEED). This behaviour is remarkably similar to hydrogen adsorption on the Si(001)2x1 surface. Si 2p core-level spectra from the clean c(4x2) surface displayed the characteristic surface peak shifted by 1.4 eV to lower binding energy, which in previous studies has been attributed to Si adatoms on top of a Si-terminated surface.^{1,} ² The formation of the 2x1-H surface lead to dramatic changes in the Si 2p lineshape, where the main surface components now appeared closer to the bulk peak. Detailed decompositions of the spectra are presented and are discussed in relation to the suggested structural models for the c(4x2)surface^{3,4} and to previous core-level studies.^{1,5}

- 1 M.L. Shek, Surf. Sci. 349, 317 (1996).
- ² A. Catellani, G. Galli, and F. Gygi, Appl. Phys. Lett. 72, 1902 (1998).
- ³ P. Soukiassian, F. Semond, L. Douillard, A. Mayne, G. Dujardin, L. Pizzagalli, and C. Joachim, Phys. Rev. Lett. 78, 907 (1997).
- ⁴ W. Lu, P. Krüger, J. Pollmann, Phys. Rev. Lett. 81, 2292 (1998).

⁵ V. Yu. Aristov, H. Enriquez, V. Derycke, P. Soukiassian, G. Le Lay, C. Grupp, and A. Taleb-Ibrahimi, Phys. Rev. B 60, 16553 (1999).

11:20am SS+EL-ThM10 The Anomalous Effective Surface Debye Temperature of ErAs(100), T. Komesu, H.K. Jeong, P.A. Dowben, University of Nebraska-Lincoln, B.D. Schultz, C.J. Palmstrom, University of Minnesota

We have recently explored the surface electronic structure of ErAs(100), as well as the compositionally stability, but the vibrational modes are a key contribution to both electronic structure and compositional stability. Consistent with a surface electronic structure different from the bulk, here we show that the surface vibrational modes are different from the bulk from our estimates of surface and bulk Debye temperature using LEED (low energy electron diffraction) and XPS (X-ray photoemission spectroscopy). This could contribute to the very large temperatures dependence of transport effects across ErAs interfaces.

11:40am SS+EL-ThM11 CRN Models of Covalent Amorphous Materials and Their Interfaces, D. Yu, G.S. Hwang, The University of Texas at Austin

Understanding the structural properties of covalent amorphous (semiconductor and dielectric) materials and their interfaces as well as defect-dopant dynamics in the disordered systems is an outstanding problem of great importance for microelectronic and optoelectronic applications. Significant advances in Continuous Random Network (CRN) models have made it possible to generate the amorphous and interface structures that are in good agreement with experiments. This further allows us to address the behaviors of defects and dopants in the disordered structures. In this talk we will present our newly developed CRN models and some recent results on i) the diffusion and clustering dynamics of vacancies and self-interstitials in a-Si and the amorphous-crystalline interface, ii) the structures of a very thin amorphous SiO₂ layer and its interfaces with Si, and iii) thermal stability of Si/Ge nanoclusters in SiO₂.

Surface Science Room: C-108 - Session SS-ThM

Electronic Structure and Stimulated Processes

Moderator: R. Bartynski, Rutgers University

8:20am SS-ThM1 Electronic Structure of Atomic Chains on Vicinal Silicon, J.N. Crain*, University of Wisconsin - Madison, K.N. Altmann, Synchrotron Radiation Center, Ch. Bromberger, Philipps - University, Germany, A. Kirakosian, J.-L. Lin, J.L. McChesney, F.J. Himpsel, University of Wisconsin - Madison

Surface states on semiconductors provide a unique opportunity to study low-dimensional electron systems. States at the Fermi level are in the band gap and thus do not couple to the bulk states. Thereby, truly two- and onedimensional metals can be achieved. An example of a 2D metal is Si(111)- $\sqrt{21x}\sqrt{21}(Ag + Au)$ which exhibits two distinct Fermi surfaces associated with Ag and Au.¹ By growing chains of gold atoms on Si(111), Si(557), Si(335), and Si(337) we demonstrate the capability of engineering onedimensional metallic states with varying inter-chain spacings and electron count. In addition, we find a new Si(111)-5x2 Gadolinium reconstruction akin to a lattice of 1D spin chains. Using a combination of STM and angle resolved photoemission we map the real-space and momentum-space electronic structures for these atomic chains. By locking the atoms to the silicon lattice the Peierls transition is overcome. The resulting metallic bands exhibit novel properties including the formation of two half-filled metallic bands in place of a single semiconducting band and a continuous 1D to 2D transition within a single band.^{2,3,4} The engineering of 1D metals is instrumental in the search for exotic electron behavior like the Luttinger $liquid.^{5}$

¹ J. N. Crain, K. N. Altmann, C. Bromberger, and F. J. Himpsel, Submitted to Phys. Rev. B.

² R. Losio, K. N. Altmann, and F. J. Himpsel, Phys. Rev. Lett. 85, 808 (2000)

³ R. Losio, K. N. Altmann, A. Kirakosian, J.-L. Lin, D. Y. Petrovykh, and F. J. Himpsel, Phys. Rev. Lett. 86, 4632 (2001).

⁴ K. N. Altmann, J. N. Crain, A. Kirakosian, J.-L. Lin, D. Y. Petrovykh, F. J. Himpsel, and R. Losio, Phys. Rev. B 64, 035406 (2001).

⁵ J. Voit, Rep. Prog. Phys. 58, 977 (1995).

8:40am SS-ThM2 Origin of the Negative Shift Observed in the XPS Spectra of Cu and Ag Cations having d⁰ Electronic Configuration, D.A. Kukuruznyak, J.G. Moyer, A.L. Ankudinov, J.J. Rehr, F.S. Ohuchi, University of Washington

We discuss the phenomenon of the negative chemical shift in the XPS spectra, where an oxidized ion appears to be chemically reduced. The effect is illustrated in the the Cu^{1+} cation within a spinel crystal structure and in Ag1+ in silver fluorides, AgF and AgF2. We have found that the negative chemical shift of the core levels is caused by similar shifts of the ions 3-d and 4-d Valence Bands. We therefore modeled the experimental valence band photoemission spectra by theoretical DOS of the d-levels using an ab initio FEFF8 code. This code is based on a relativistic Greens function real space full multiple scattering formalism and allows accurate determination of the position of the levels with respect to the Fermi energy. We have determined that the negative shift of the d-levels is not caused by a longrange electrostatic interaction (Madelung potential). The amount of the total charge on the Cu¹⁺ cation in the spinel structure was similar to that of copper in Cu₂O, thus charging is not the cause of negative shift either. It was also found that only Cu 4s and 4p electrons participate in the chemical bonding. Completely filled d¹⁰ shells of the copper in spinel structure do not form a band, but were localized, having an atomic-like character. The 3dlevel therefore appeared as a false valence band edge in the spectrum. A similar effect was observed for the silver compounds. We claim that the negative chemical shift is not due to charging or splitting effects, but occurs when a completely occupied non-bonding d10 shell appears on the XPS spectra as a false valence band edge.

9:20am **SS-ThM4 Electronic Band Structure of Sn/Si(111)**, *J. Lobo*, *A. Tejeda*, Universidad Autonoma de Madrid, Spain, *A. Mugarza*, Universidad del Paés Vasco, Spain, *E.G. Michel*, Universidad Autonoma de Madrid, Spain

We report an investigation on the electronic band structure of the Sn/Si(111)-($\sqrt{3x}\sqrt{3}$)R30° phase using angle-resolved photoemission, in the coverage range between 1/6 and 1/3 ML, both at room and at low temperature, with special emphasis in the analysis of its metallic character and in the evolution of the surface states as a function of temperature and coverage. The photoemission experiments have been performed at HASYLAB (Hamburg, Germany). This phase has deserved widespread

attention since the discovery of a temperature induced phase transition to a low temperature (3x3) phase. Several different models have been put forward to explain the nature of the phase transition, that is observed only in the case of Ge(111): formation of a surface charge density wave, stabilized by correlation effects or defects; dynamical fluctuations, that destroy the (3x3) phase at RT; or existence of a soft phonon. There is no indication of a (3x3) pattern at low temperature for Sn/Si(111), but several features of the (3x3) phase are found in the valence band. We present also an analysis on the influence of the defect density in the surface state behavior and metallic character. The results found for the ideal $(\sqrt[3]3x\sqrt{3})R30^\circ$ phase at 1/3 ML coverage support the dynamical fluctuations model for the phase transition. While a (3x3) phase is not observed in the temperature range accessible, the system exhibits a behavior similar to the one found in Sn/Ge(111) (split surface state band that survives at RT). The existence of a semiconductor to metal transition has been investigated in detail.

9:40am SS-ThM5 Electron Confinement in Metallic Ultrathin Films, Z.Q. Qiu University of California at Berkeley INVITED

Electron confinement or quantum well (QW) state manifests in metallic thin films as the film thickness is reduced to nanometer scale. Photoemission provides the most direct observation of QW states in k-space. The unique capabilities now available at the Advanced Light Source (ALS) at Berkeley make it possible to image QW states on the atomic scale. The photoemission results from ALS on Cu thin films grown on fcc Co(100) are presented using single- and double-wedge samples. First, we will discuss how the QW states are formed in the Cu film and how to describe it using the phase accumulation model. Second, we will show how the QW states result in the oscillatory interlayer coupling between two ferromagnetic Co layers across a thin Cu layer.

10:20am SS-ThM7 Dominance of the Final State in Photoemission Mapping of the Fermi Surface of Co Thin Films, *R.L. Kurtz, X. Gao,* Louisiana State University, *A.N. Koveshnikov,* Simon Fraser University, Canada, *R.L. Stockbauer,* Louisiana State University

The Fermi surface of tetragonally-distorted fcc Co grown on Cu(001) has been investigated with angle-resolved photoemission and compared with first-principles calculations. Photoelectron angular distributions were obtained with a display-type ellipsoidal-mirror analyzer at the LSU CAMD synchrotron light source for electrons emitted from E_F using photons in the energy range of 20-80 eV. These angular distributions show distinct patterns that vary with photon energy as different regions of the Brillouin zone are sampled. In order to evaluate the correspondence to Fermi surface contours, we have computed the band structure of tetragonally-distorted Co. We have used WIEN97.9 to perform a spin-polarized gga FLAPW calculation including spin-orbit interactions for a pseudomorphic fcc structure with an in-plane lattice constant that of Cu while the vertical lattice parameter is reduced by 5%. From this, the resulting Fermi surfaces have been extracted and cross-sectional contours were produced corresponding to the various photon energies used in the measurements. We find that there is rather poor agreement between these contours and the structures seen in photoemission. To investigate this further, we have computed the momentum matrix elements using the final states produced in the band calculation. In the case of Co, the resulting angular distributions that we predict are in much better agreement with our data, and even reproduce the photon polarization effects that are observed. These observations suggest that comparison with first principles calculations are extremely important, particularly in the case of flat-band materials such as the d-bands of Co seen here. The slow dispersion of the occupied states, when coupled with the rapid dispersion of the final state, produces angular distributions whose contours are heavily influenced by the final state.

10:40am SS-ThM8 Spin-Resolved Photoemission of Surface States in H on W(110), E. Rotenberg, Lawrence Berkeley National Laboratory, M. Hochstrasser, J.G. Tobin, Lawrence Livermore National Laboratory, S.D. Kevan, University of Oregon

Surface states of metals can be split due to the spin-orbit-coupling (SOC) interaction, as first shown experimentally by LaShell et al for Au(111) surface states.¹ Their conjecture was that the surface states could be split by SOC when the bulk inversion symmetry was broken at the vacuum/metal interface. Later we found a similar splitting for W(110) and Mb(110) surfaces and furthermore that this splitting could be enhanced with hydrogen or alkali metal adsorption.² In the present work, the hydrogenated surface electronic states on W(110) have been measured using spin-resolved photoemission. The origin of the splitting is confirmed to be spin-orbit-coupling. In confirmation of the conjecture by LaShell et al, we observe 100% polarization of these states in local regions of momentum space. The spins are aligned in the plane of the surface, perpendicular to the electronic momentum relative to the S-bar symmetry point.

* Morton S. Traum Award Finalist

¹ S. LaShell, B. A. McDougall, and E. Jensen, Phys. Rev. Lett. 77, 3419 (1996).

11:00am SS-ThM9 Ultraviolet Laser Interactions with Single Crystal Sodium Nitrate: Wavelength Dependence of Photodesorbed Products, *L. Cramer, J.T. Dickinson,* Washington State University, *W.P. Hess,* Pacific Northwest National Laboratory

Sodium nitrate is a wide bandgap ionic material containing an oxyanion. Single crystals show a strong absorption band in the ultraviolet due to a π to π^* transition in the nitrate. Previous work has suggested that a number of neutral emission products are due to direct excitation of this band. In this study we compare the laser induced ion and neutral atom/molecule emissions from single crystal NaNO₃ at three wavelengths: at the band maximum (193 nm) and two minima on either side of the maximum (248 nm and 157 nm). Surprisingly, little correlation with the π to π^* absorption is observed, including molecular species derived from the nitrate. Our results are better explained by defect mediated processes attributed to anion vacancies. These results are corroborated by simultaneous laser induced photoelectron emission measurements that are very sensitive to low densities of electron trap defects at insulating surfaces.

11:20am SS-ThM10 Low Dimensional Metallic States in Heavily Irradiated CaF₂ Thin Films on Si(111), A.A. Bostwick, J.A. Adams, A. Klust, University of Washington, E. Rotenberg, Advanced Light Source, M.A. Olmstead, University of Washington

Calcium fluoride is a wide band gap ionic insulator that undergoes photosimulated desorption of fluorine. It has been previously reported by Karlsson et al.1 that heavily irradiated thin (2.5 – 4 triple layers) CaF2/Si(111) films show a sharp metallic defect state associated with an ordered array of surface fluorine vacancies. We find two additional states in thicker, irradiated films (5-10 triple layer), one at higher binding energy and one at lower energy than the surface state. These states also cross the Fermi level dispersing upwards from normal emission. The zone-center energies of these states depend on the thickness of the initial CaF2 film, hinting that the electrons are confined in the growth direction. The upper state could lie within the band gap of the silicon substrate, but the lower state, which is more than 1.5 eV below the Fermi level at the zone-center, does not. These states are observed after prolonged irradiation, much longer than that necessary to produce the surface state. We postulate that these new states are due to the formation of fluorine vacancy clusters (Ca metal quantum dots) within the CaF2. Funded by DOE grant DE-FG03-97ER45646/A0003.

¹ Karlsson et al., Phys. Rev. Lett. 57,1247 (1986).

11:40am SS-ThM11 Ion Emission from Ultrathin Resists during Exposure to Metastable Atom Beams, Y. Yamauchi, X. Ju, T. Suzuki, M. Kurahashi, National Institute for Materials Science, Japan

The combination of ultrathin resists and slow metastable atom beams has attracted attention because of its potential for downscaling the semiconductor lithography beyond the diffraction limit, proximity effect, or transmission of conventional exposure radiations, i.e., ultraviolet light, electron beam, and soft x-ray. Slow metastable atoms carrying fairly large excitation energy in their electronic system interact only with topmost atoms at surfaces because the kinetic energies of the atoms are so low that they are reflected above surfaces. These extreme surface sensitivity and damage-free feature to under layers are desirable for an exposure radiation in lithography. Since Berggren et al.¹ had suggested the atom lithography, several groups have reported their success on pattern transfer employing metastable atom beams for ultrathin resists (self-assembled monolayer (SAM) of alkanethiolate,1 hydrogen passivation on silicon surface2 followed by wet chemical etching. As to the fundamental phenomena of resists caused by the irradiation of metastable atoms, however, are not well understood. Recently metastable-atom-stimulated desorption (MSD) was discovered for water and alkali coadsorbed surfaces.3 We have investigated MSD of positive ions from alkanethiolate-SAMs and from hydrogenpassivated Si(111) surfaces. The MSD data show H⁺ and CH_x⁺ desorption from of the alkanethiolate-SAMs and H desorption from the hydrogenpassivated Si(111) surfaces, which provide direct evidence for the dissociation of alkanethiolate-SAMs and of silicon hydrides by metastable helium atom beams at the initial stage of the pattern transfer.

¹ K. K. Berggren, et al., Science 269 (1995) 1255.

² S. B. Hill, et al., Appl. Phys. Lett. 74 (1999) 2239.

³ M. Kurahashi and Y. Yamauchi, Phys. Rev. Lett. 84 (2000) 4725; T. Suzuki, et al., Phys. Rev. Lett. 86 (2001) 3654.

Thursday Afternoon, November 7, 2002

Surface Science

Room: C-112 - Session SS+EL-ThA

Growth & Etching on Semiconductor Surfaces

Moderator: A.C. Kummel, University of California, San Diego

2:00pm SS+EL-ThA1 Epitaxial Growth Dynamics of Semiconductor Quantum Dot Structures, S.R. Leone, University of California and Lawrence Berkeley National Laboratory INVITED

The formation of Ge nanodots on Si(100) occurs by strain-induced mechanisms (Ge is 4% larger than Si) and obeys the Stranski-Krastanov (SK) growth mode: a wetting layer (3-5 layers) is followed by the formation of three-dimensional (3D) Ge structures. Quantitative studies of Ge island size distributions and their shape transformations, including huts, pyramids, domes, and superdomes, and shape changes due to annealing of the islands under the influence of surfactants, such as arsenic, are studied by molecular beam epitaxial growth and atomic force microscopy (AFM) post-analysis. For device applications, it is important to attain control over the size and spatial distributions of self-assembled nanostructures. The Ge growth experiments are also carried out on patterned silicon substrates (mesas formed by electron beam lithography followed by etching), for specific positioning of the dots. A 'one island on one mesa' relationship is achieved. The density of islands is higher than can normally be produced on unpatterned silicon, where island coalescence would usually occur well before this density is possible. Preferential growth on the tops of the mesas most likely occurs because the Si mesa tops are deformable, fulfilling a strain relaxation condition. In this work, pyramid-type islands as small as 25 nm are also aligned on the mesa tops, and no limit to the size reduction of the islands is apparent, being controlled mainly by the size of the etched features that can be introduced.

2:40pm **SS+EL-ThA3 Si Deposition on H-terminated Si(100) Surfaces**^{*}, *J.-Y. Ji*, *T.T. Barus, T.-C. Shen*, Utah State University, *G. Qian*, University of Illinois at Urbana-Champaign, *X. Luo*, National Renewable Energy Laboratory, *S. Ren*, Illinois State University, *S. Zhang*, National Renewable Energy Laboratory, *Y.C. Chang*, University of Illinois at Urbana-Champaign

The presence of H has long been considered adverse to Si homoepitaxy. Copel and Tromp¹ reported that while no apparent effect on epitaxy was observed at H coverage <1 ML and H segregates at growth temperature >400 K, a drastic epitaxial temperature increase was required at H coverage >1 ML. We will present the results of our STM, and first principle molecular dynamics studies on Si monohydride and dihydride effect in Si epitaxy. We confirmed that at growth temperatures ~ 500 K, H stays on the growth front on monohydride surfaces and epitaxy can be achieved but the domain sizes are much smaller than those grown on the bare Si. Continuous rebonding apparently is responsible for the epitaxial growth on Si monohydride surfaces. The diffusion barrier for the Si adatom along the Si monohydride dimer rows is calculated to be 1.1 eV which is significantly higher than the corresponding 0.6 eV barrier on the bare Si(100)-2x1 surface. To account for the H segregation, a mechanism to exchange H atoms between a surface Si atom and the incident Si atom is proposed. The experimental and theoretical result on the dihydride effect will be discussed. *This work is supported by NSF-DMR9875129, ARDA/ARO DAAD 19-00-1-0407 and DARPA-QuIST DAAD 19-01-1-0324

¹M. Copel and R. M. Tromp, Phys. Rev. Lett. 72, 1236 (1994).

3:00pm SS+EL-ThA4 An Atom-Resolved Study of Vacancy Dynamics and Surface Roughening on Bromine-Etched Si(100) Surfaces, C.F. Herrmann*, J.J. Boland, University of North Carolina, Chapel Hill

Halogen etching of Si(100) surfaces has long been considered to involve the selective removal of atoms from an essentially static surface. However, our high temperature scanning tunneling microscopy (STM) study reveals that halogen-covered surfaces are highly unstable. This instability stems from the inherent steric repulsions between halogen adatoms on the surface. At high temperatures, repulsive interactions are relieved by vacancy formation, diffusion and surface roughening, each of which is directly observed in real-time by STM. Together, these dynamical processes result in surface features identical to those found after high temperature etching. These results demonstrate that diffusion and roughening must be considered in any model of halogen etching. Moreover, steric repulsions and the instability they

create place fundamental limits on the ability to achieve atomically smooth morphologies using halogen etching.

3:20pm **SS+EL-ThA5 Dynamics of Si(100)-(2x1) Surface Modification** with Cl, G. Xu, E. Graugnard, V. Petrova, K.S. Nakayama, J.H. Weaver, University of Illinois at Urbana-Champaign

The etching dynamics of Cl-Si(100)-(2x1) at elevated temperature have been studied with variable temperature scanning tunneling microscopy. Clean samples were exposed to Cl₂ at room temperature to near saturation and then heated to 700 K for over 20 hours. By scanning the same area of the sample, we observed pit creation, diffusion, incorporation and annihilation. Pit annihilation has not been reported previously under conditions of steady state etching and surface saturation. We also observed regrowth islands creation, growth and decay. Surface reactions at 700 K produced single Si adatoms, which were bonded to Cl-free Si dimers. Single Si adatoms diffused through these Cl-free Si dimer sites, but adatom diffusion was restricted by the high Cl concentration. The adatoms could form regrowth dimers when they met or they could be accommodated at the ends of regrowth structures. The adatoms could also be released from the regrowth dimer rows with the assistance of bare dimers. We have also observed (3x2) and (5x2) surface structures and, for the first time, the phase transition between (3x2) and (5x2) structures and dimer vacancy lines.

3:40pm SS+EL-ThA6 Surface Modification without Desorption: Recycling of Cl on Si(100)-(2x1), K.S. Nakayama, E. Graugnard, J.H. Weaver, University of Illinois at Urbana-Champaign

We demonstrate the structural consequences of thermally activated reactions of Cl on Si(100)-(2x1). We used scanning tunneling microscopy at room temperature to obtain atomic-resolution images of the surface before and after thermal processing. We show surface modification under conditions where Cl is recycled rather than desorbed as SiCl₂. In this unexpected reaction, the surface roughens as dimer vacancies are produced. First, a dimer with 2 Cl atoms, 2SiCl, converts to SiCl₂ + Si. This allows the destabilized, bare Si atom to escape onto the terrace. At temperatures where the desorption is negligible, the SiCl₂ unit decays as the Cl atoms can move to other active sites of the Si surface, allowing the second Si atom to escape. The result is a dimer vacancy, Si atoms on the terrace that can form self-organized regrowth structures, and Cl that is able to participate in another pitting event. Access to this unexpected roughening pathway is controlled by the Cl concentration and temperature. This previously overlooked process represents an important component of Si(100) surface processing.

4:00pm SS+EL-ThA7 Spontaneous Roughening -- Fundamental Limits in Si(100) Halogen Etch Processing, D. Chen, J.J. Boland, University of North Carolina at Chapel Hill

A dynamical Scanning Tunneling Microscopy and Density Functional Theory study of the thermodynamic stability of halogen-terminated Si(100) surfaces is presented. Defects-free halogen-covered Si(100) surfaces are shown to be intrinsically unstable and prone to spontaneous roughening. This instability is the result of steric effects and is observed for all halogens except fluorine (which is already known to yield rough surfaces). These results demonstrate that an atomically smooth Si(100) morphology cannot be realized using halogen etch processing which sets a lower bound on the atomic scale perfection that can be achieved using such processing.

4:20pm **SS+EL-ThA8 Preparation of Atomically Flat Si(100) Surface by Ion Etching**, *J. Kim*, *J.-Y. Ji*, *T.-C. Shen*, Utah State University, *J.S. Kline*, *J.R. Tucker*, University of Illinois

Preparation of atomically flat Si(100) surface under limited thermal budget has been one of the challenging processes in the research of atom-scale electronic device fabrication. While atomically flat monohydride surfaces can be obtained by aqueous $\mathrm{NH}_4\mathrm{F}$ etching on Si(111) surfaces,¹ wetchemical process has yet to produce an atomically flat Si(100) hydride surface at a scale of more than a few nanometers. Ion irradiation effects on Si surfaces have been investigated extensively from mid-70s to early 90s as a surface cleaning process prior to Si epitaxy. Recent atomistic studies of ion sputtering on pristine Si and metal surfaces were more focused on the dynamics of ion-induced defects.² We are currently using STM to investigate the surface morphologies during ion etching of oxide or wetchemically prepared Si(100) surfaces by 0.4 - 1.5 keV Ar and Xe ions. We will delineate the effects of ion energy, ion fluence and substrate temperature, and assess the possibility of achieving atomically flat Si(100) surfaces by optimizing these parameters. This work is supported by NSF-DMR9875129, ARDA/ARO DAAD 19-00-1-0407 and DARPA-QuIST DAAD 19-01-1-0324.

* Morton S. Traum Award Finalist

¹ G. S. Higashi et al., Appl. Phys. Lett. 56, 656 (1990).

4:40pm SS+EL-ThA9 Probing the Chemistry of Impurities with STM: The Profound Effect of Dissolved Oxygen on Silicon Etching, S.P. Garcia, H. Bao, M.A. Hines, Cornell University

A new technique has been developed to quantify the surface reactivity of impurities, which combines the exquisite defect sensitivity of scanning tunneling microscopy (STM) and the analytical capabilities of atomistic kinetic Monte Carlo (KMC) simulations. This technique exploits kinetic competition between the impurity and a reference etchant to produce impurity-concentration-dependent changes in nanoscale etch morphology. These changes are then quantified using STM measurements and KMC simulations. We used this technique to measure the site-specific reactivity of dissolved O2 -- a ubiquitous impurity in aqueous solutions -- with Hterminated Si(111) surfaces. The site-specific reactivity of $O_2(aq)$ is surprisingly anisotropic. Oxidation of the highly strained dihydride step site is four times faster than oxidation of the relatively unstrained monohydride step site. Both steps are 10⁴ times more reactive than terrace sites. FTIR measurements of the Si-H stretch vibration showed that dissolved O2 inserts O atoms into surface Si-Si backbonds without removing the H-termination. Dissolved O2 does not attack Si-H bonds, since neither Si-H consumption nor silanol production is observed.

Surface Science Room: C-110 - Session SS-ThA

Tribology at Surfaces

Moderator: D.W. Brenner, North Carolina State University

2:00pm SS-ThA1 QCM-STM Studies of the Nanoscale Dynamics of "Model-System" and "Real-World" Lubricants, J. Krim, North Carolina State University INVITED

In order to gain a fundamental understanding of friction, and the closely related phenomenon of lubrication, one must understand, at the molecular level, how the energy associated with the work to overcome friction is converted to heat.¹ Such knowledge is key to understanding the rate at which an interface will heat, and in addition how chemical reactions and other physical processes triggered by heat will be affected by friction. One of the simplest possible geometries in which friction can occur, and thus be studied, is that of a fluid or crystalline monolayer adsorbed on an atomically flat surface. This geometry is experimentally accessible to experiments with a Quartz Crystal Microbalance (QCM), to numerical simulation techniques, and to analytic theory. Measurements of the tribological properties of "model system" and "real world" lubricants have been performed for rare gases, octane and TCP adsorbed on lead, iron and/or copper surfaces in open geometries (with QCM) and also in confined geometries (by bringing a STM tip into tunneling contact with the QCM electrode). Lead substrates are of particular interest on account the recent observation of superconductivity-dependent sliding friction. Iron and copper substrates are of interest for a variety of practical applications. Interaction potentials for adsorbed rare gases are known to a high degree of accuracy, allowing highly reliable comparisons of theory to experiment. TCP is meanwhile a "real-world" lubricant known for its demonstrated anti-wear properties for macroscopic systems. Although this lubricant has been the subject of much research for over 40 years, the atomic-scale details of its lubrication mechanisms are far from being satisfactorily understood.

¹"Surface science and the atomic-scale origins of friction: what once was old is new again.", J. Krim, Surf. Sci. 500, 741 (2002)

2:40pm SS-ThA3 A Quantitative Study of the Mechanical and Adhesive Origin of Molecular-Level Friction, J.E. Houston, Sandia National Laboratories, H.I. Kim Aerospace Corporation

In earlier work, we explored the origins of molecular-level friction using the interfacial force microscope and Au tips and substrates terminated by selfassembled monolayer films having various functional end groups. Here we continue that effort by applying contact-mechanics models to quantitatively analyze the mechanical properties of the films, their interfacial energies and the friction shear-stress values for each functional-group combination. Methyl end-group combinations represent only van der Waals bonding and purely mechanical friction, whereas carboxylic acid groups show significant hydrogen bonding. The results indicate that both the composite elastic modulus and the mechanical portion of the friction shear stress scale inversely with the total molecular length of the tip/substrate films. The adhesive energy shows an odd/even effect changing from inter-film for an even number of methylene units to purely intra-film bonding for oddnumbered films--the intra-film adhesion only appears in the lateral friction force. Very short methyl-terminated combinations indicate a significant non-contact component to the friction force. These results will be discussed in terms of the possible use of these films as molecular-level lubricants. Sandia is a multi-program laboratory operated by Sandia Corporation, a Lockheed Martin company, for the DOE under Contract DE-AC04-94AL85000.

3:00pm **SS-ThA4 Frictional Anisotropy at Crystalline Interfaces**, *C.M. Mancinelli*, *A.J. Gellman*, Carnegie Mellon University, *J.S. Ko*, Merck & Co., Inc.

Fundamental tribological studies in an ultra-high vacuum environment have been performed to probe the effect of anisotropy on the friction between two single crystalline metal surfaces. The study of frictional anisotropy, or the effects of lattice orientation at crystal interfaces, has been conducted to address two main questions: whether slip between sliding surfaces occurs more easily along certain crystallographic directions, and whether the observed orientation effect on friction is a result of surface lattice commensurability. The results of a study of the frictional anisotropy between single crystalline Cu(100) surfaces will be presented. Tribological investigations were conducted on surfaces prepared to be either truly clean or modified by adsorption of molecular ethanol in the boundary lubrication regime. A detailed comparison will be made between these results and those previously obtained for the frictional anisotropy between single crystalline Ni(100) surfaces.

3:20pm SS-ThA5 Nanopormorphism of C60 and Hydrocarbons on Metal Surfaces, T.S. Coffey, M. Abdelmaksoud, J. Krim, North Carolina State University

We report investigations of the validity of beliefs that nanoscale objects might have the same properties as macroscale objects, termed nanopormorphism. Since C60 molecules to rapidly rotate within their lattice position, tribologists envisioned nano-sized ball bearings. C60 is not an effective lubricant.¹ But differences in interfacial friction between rigid vs. rotating C60 remains an interesting topic. C60 forms close packed hexagonal films on both Ag(111) and Cu(111). However, on Ag(111), C60 spins in its lattice position, while it is rigid on Cu(111).² To determine if the spinning of C60 affects interfacial friction, we are employing QCM and AFM to compare the friction of methanol on C60/Ag(111) vs. methanol on C60/Cu(111). We examine whether the rolling nature of the C60 layer impacts the sliding friction as probed by QCM and AFM. Adsorbates at a surface can cause changes in the phonon dispersion curves, creating new modes that can be related to the sliding friction of the adsorbate. Among these new vibrational modes are three Frustrated Translational (FT) modes which probe the curvature of the molecule/surface potential along different spatial directions. For hydrocarbons adsorbed on many metals, the FT modes parallel to the surface (FTx, FTy) have energies much smaller than that perpendicular to the surface (FTz).³ The stiffness or high "spring constant" of the FTz mode compared to the low "spring constant" of the FTx and FTy modes brings to mind molecular scale shock absorbers. We are using QCM to study octane and acetylene sliding on Cu(111) and Pb(111) to determine how energy and damping of the FTz mode affects sliding friction.

¹ T. Coffey et al., J. Phys. Condensed Matter, 13 (2001) 4991-4999.

² T. Sakurai et al., App. Surf. Sci., 87/88 (1995) 405.

³ B.N.J. Persson and E. Tosatti, Eds, Physics of Sliding Friction, Ch. Woll, Kluwer Academic Publishers, Dorcdrecht, 1996.

4:00pm SS-ThA7 Tribochemical Wear of Silicon Nitride on Oxide Surfaces Studied by Atomic Force Microscopy, J.T. Dickinson, W. Maw, F. Stevens, S.C. Langford, Washington State University

Nanometer scale tribochemical wear of silicon nitride AFM tips was characterized on a variety of substrates in aquous solutions using atomic force microscopy. Wear at this small scale contrasts markedly with the macroscopic wear of silicon nitride. For aquous mediated wear, a chemically active substrate (one with the appropriate surface metal-hydroxide bonds) is required. These results are generally consistent with wear due to the formation and breaking of chemical bonds between the tip and the substrate. The wear rates are shown to be nonlinear in the applied normal force. We propose that stress-induced intermediate states involving hydroxyl groups form on both the AFM tip and the substrate. Chemical reactions subsequently form transient bridging chemical bonds that are responsible for tip wear.

4:20pm SS-ThA8 Adhesion Sensor: Non-Contact AFM for Quantitative Adhesion Measurements, *A. Schirmeisen*, *D. Weiner*, *H. Fuchs*, University of Muenster, Germany

The adhesion characteristics of metal coatings on Polycarbonate are of high technological interest. For example, Aluminum is used to coat plastic surfaces, with a wide range of applications. However, adhesion failure of metal coatings on polycarbonat is often observed. Methods such as flame

annealing¹ or plasma treatment² are typically employed to improve adhesion characteristics. Yet little is known of the microscopic processes leading to the modified surface properties. We can quantify the adhesion properties of Al on differently treated polymers using dynamic AFM. Conventionally, adhesion tests are performed using a tape puller or similar device. The sample is usually destroyed after the test and no lateral resolution of the adhesion properties is achieved. In a novel approach using NC-AFM we can quantify the adhesion characteristics of the polymer-metal interface with nm-resolution. We measure frequency shift versus distance curves of a functionalised NC-AFM cantilever on the polymer surface. A specially designed UHV apparatus allows the in-situ preparation of tip and sample and the investigation of the interfacial force interactions with a UHV-AFM. The tip is functionalised by evaporation of a thin Al film on the cantilever. The adhesion properties of the polymer are modified by plasma treatment. Measurements of frequency shift versus tip-sample distance reveal the influence of the sample treatment on the adhesion properties. Following the approach of Durig,³ we calculate force curves from the frequency shift data,⁴ and extract quantitative values for the interfacial adhesion energy.

¹ A.P.Pijpers, R.J. Meier, J. Electron Spectr. 121 (2001) 299

² C. Seidel, H. Kopf, B.Gotsmann, T. Vieth, H. Fuchs, K. Reihs, Appl. Surf. Sci. 150 (1999) 19

³ U. Durig, Appl. Phys. Lett. 75 (1999) 433

⁴ Calculation based on programm from H. Holscher, CAESAR Institute, Germany.

4:40pm SS-ThA9 The Frictional Behavior of a Hertzian Contact Analyzed using a New Contact Mechanical Model, U.D. Schwarz, Lawrence Berkeley National Laboratory, University of California

The study of the friction occurring at a Hertzian contact (i.e., the contact between a sphere and a flat surface or between two spheres) has always been a central issue in nanotribology, since realistic interfaces may be approximated by numerous individual Hertzian contacts that are within certain boundaries statistically distributed in all three dimensions. However, the theoretical description of the mechanical behavior of such contacts under load considering adhesion has been difficult in the past. Generally applicable models (i.e., models covering the "intermediate regime" between small, hard and large, soft contacts, as they might be most frequent in actual interfaces) required always numerical approaches. In this talk, I will present a new theory that covers the full parameter range for an adhesive Hertzian contact, but results in a simple equation describing the effective load acting on the surface that consists of adhesive and external contributions. The theory is based on a model interaction force that includes both short-range and long-range components. Comparison with numerical results obtained from the Maugis-Dugdale model as well as with experimental friction force microscopy data demonstrates the validity of the new approach.

Friday Morning, November 8, 2002

Surface Science Room: C-110 - Session SS-FrM

Self-Assembly at Surfaces

Moderator: D.H. Fairbrother, The Johns Hopkins University

8:20am SS-FrM1 Structure of Nitrile-functionalized Alkanethiolate Monolayers on Gold and Silver, A. Shaporenko, S. Frey, Universität Heidelberg, Germany, Ph. Harder, D.L. Allara, Pennsylvania State University, M. Zharnikov, M. Grunze, Universität Heidelberg, Germany Self-assembled monolavers (SAMs) formed from nitrile-functionalized alkanethiols (AT) are perspective candidates for SAM-based lithography and the fabrication of surfaces with low protein affinity. In addition, the polar nitrile group with a relatively large dipole moment is well-suitable to explore to what extent the structure of a non-substituted AT SAM can be affected by strongly interacting tail groups. We used several complementary experimental techniques, such as Xray photoelectron spectroscopy and near-edge X-ray absorption fine structure spectroscopy at the C1s and N1s absorption edges to get an information on the chemical identity, packing density, and orientational order in SAMs formed from CN(CH₂)₁₆SH (CN-C16) on (111) gold and silver substrates. The results imply that the substitution of the weakly interacting methyl groups by the nitrile entities has a strong influence on the molecular orientation, packing, and the structure of AT SAMs on both gold and silver. A strong dipole-dipole interaction between the polar nitrile groups is assumed to disturb a balance between the headgroup-substrate and interchain interactions, which is responsible for the SAM structure and packing density. In contrast to the methyl-functionalized AT SAMs, only a slight difference in the orientation of the alkyl chains in CN-C16/Au and CN-C16/Ag is observed. The nitrile groups in both CN-C16/Au and CN-C16/Ag are oriented almost parallel to the film surface, which is beneficial to minimize the dipole-dipole interaction between these moieties, but different from the "standard" orientation of the functional groups in ω -functionalized AT SAMs of the same chain length.

8:40am SS-FrM2 Self-assembled Monolayers on Aluminium: The Role of Oxide Surface Chemistry, T.A. Lewington, I. Liakos, G.E. Thompson, R.C. Newman, UMIST, UK, E. McAlpine, Alcan International, UK, M.R. Alexander, UMIST, UK

Application of self-assembling organics molecules on oxide-covered, metal surfaces is of growing interest in areas ranging from medical implants¹ to adhesion promotion pre-treatments.² In the latter application area, legislation is driving industry to explore environmentally friendly petreatments for aluminium. Corrosion protection has been obtained using difunctional alkyl-phosphonic acids assembled on aluminium as a paint pretreatment. It has been shown that one of the phosphonic acid head-groups form a phosphonate bond with the hydroxylated oxide film at the surface of the aluminium.³ In addition to coupling of the resin and surface, it has been proposed that hydration is inhibited at the phosphonate-aluminium interface.⁴ In contrast to the stable gold surface utilised in the assembly of alkane-thiols, the oxide at the aluminium surface is readily hydrated on exposure to ambient conditions.⁵ It is proposed that this instability causes the inconsistent self-assembly often obtained on the aluminium surface. Thus, the oxide surface chemistry of magnetron sputtered aluminium has been controlled using solution and atmospheric conditioning; the effect on self-assembly of alkane-phosphonic acids is reported. XPS has been used to provide oxide thickness and surface hydroxyl concentration while contact angle and FTIR measurements have been used to probe the SAM coverage and order. Evidence for hydration inhibition by phosphonic acids SAMs is presented.

¹ G. L. KENAUSIS et al. J Phys Chem B 104 (2000) 3298.

² I. MAEGE et al Prog Org Coatings 34 (1998) 1.

³ R. D. RAMSIER et al. Surf Sci 203 (1988) 72.

⁴ A. DAVIS et al. J Mater Sci 20 (1985) 975.

⁵ M. R. ALEXANDER et al. Surf Int Anal 29 (2000) 468.

9:00am SS-FrM3 A Thermodynamic Perspective on Self-Assembled Monolayer Growth, D.K. Schwartz, J. Mellott, University of Colorado, I. Doudevski, University of California, Santa Barbara, W. Hayes, Crompton Corp., C. Messerschmidt, Infinion Corp. INVITED

Self-assembled monolayers form spontaneously at the solution/solid interface as a consequence of molecular adsorption and two-dimensional self-organization. The self-organization process can be viewed from the perspective of the nucleation and growth of a dense 2D phase (solid) from a

less dense phase. In particular, the nucleation and growth kinetics of solid clusters in coexistence with a 2D "vapor" phase agree quantitatively with models of vapor phase epitaxial growth that predict growth regimes and scaling exponents. Other growth mechanisms are found, however, when the adsorbate/substrate interaction is varied. In fact, one can observe a qualitative change in the growth mechanism for a single system as a function of temperature. These mechanisms can be classified into three classes which can be viewed in a 2D thermodynamic context as occurring (1) below the liquid-vapor triple point, (2) above the liquid-vapor triple point, and (3) above the liquid-"solid" critical point, respectively.

9:40am SS-FrM5 pH-Dependence of the Interaction Between Functionalized Probes and Tri(Ethylene Glycol)-Terminated Self-Assembled Monolayers on Gold Studied with Force Spectroscopy, C. Dicke, G. Haehner, University of St Andrews, UK

The understanding of protein adsorption on ultrathin synthetic surfaces has attracted considerable interest in recent years. In particular, the understanding of non-specific interactions is one of the major concerns. Functionalized self-assembled monolayers (SAMs) represent a class of ultrathin model surfaces that allow it to study the resistance to protein adsorption. Several recent investigations demonstrated the outstanding protein repelling properties of SAMs formed by oligo(ethylene glycol) (OEG) terminated alkanethiols on gold. Different suggestions have been made in order to explain this observation. Due to the strong hydration of the EG units in aqueous solutions an extended net-like structured water layer has been proposed to be responsible for the observed behaviour. The possibility of a specific incorporation of ions from solution into the selfassembled structure has also been suggested. Furthermore, it has been speculated that interactions of hydroxyl and/or hydronium ions with the synthetic interface play a major role. In order to elucidate the nature of the forces underlying the protein resistance in more detail, SAMs of methoxytri(ethylene glycol)-terminated undecanethiolates (EG3-OMe) adsorbed on polycrystalline gold were investigated by chemical force spectroscopy under liquids. Measurements with differently functionalised probes were performed under aqueous solutions with various ionic strengths and pHvalues

10:00am **SS-FrM6 Extraordinary Properties of the C 1s Photoemission Line of n-alkanethiolates on Gold and Silver**, *K. Heister*, *M. Zharnikov*, University Heidelberg, Germany, *L.S.O. Johansson*, University Karlstad, Sweden, *M. Grunze*, University Heidelberg, Germany

The investigation of the C 1s photoemission line for n-alkanethiolate SAMs by synchrotron-based high resolution xray photoelectron spectroscopy (HRXPS) shows surprising properties. The energetic position of the C 1s emission line varies significantly by changing the substrate from Au to Ag. The analysis of this effect suggests that the observed shift of about 0.3-0.4 eV is only indirectly related to the substrate. Instead it seems to resemble the details of the film structure which change with the substrate. Besides we have observed that the C 1s peak shape alters with increasing alkyl chain length. The course of the peak shape evolution suggest a deconvolution of the C 1s emission line in several constituents. They can be attributed partly to intrinsic energy losses and partly to the influence of the close SAM-substrate interface on the innermost carbon atoms.

10:20am SS-FrM7 Temperature-Programmed Desorption and Scanning Tunneling Microscopy Studies of nAlkane Derivatives on Graphite: Desorption Energetics and the Influence of Functional Groups on Adsorbate Self-Assembly, T. Müller, K.T. Rim, G.W. Flynn, Columbia University, A.V. Teplyakov, University of Delaware

While carbon materials have found many practical applications ranging from sorption and catalyst support to the protection of magnetic storage media, numerous further uses may follow from the more recently discovered allotropes, fullerenes and carbon nanotubes. Alkane derivatives on the inert support provided by graphite can serve as model systems to study organic thin films and two-dimensional self-assembly. In the present study, Temperature Programmed Desorption (TPD) and Scanning Tunneling Microscopy (STM) are utilized to examine the influence of functionalization on the adsorption energetics and self-assembly of nalkanes on Highly-Oriented Pyrolytic Graphite (HOPG). For adsorption of 1-bromoalkanes, alkanoic acids, and 2-bromoalkanoic acids, full activation of the substrate surface required annealing temperatures of approximately 700 K. Molecular desorption from physisorbed mono- and multilayers was found to exhibit first and zeroth-order kinetics, respectively. A Redhead analysis of monolayer desorption signals uncovered a profound influence of alkane functional groups. As compared with unfunctionalized n-alkanes, the desorption energies of all derivative species studied here exhibit a reduced

chain length dependence in conjunction with an increased adsorption energy in the limit of zero chain length. Both effects reach their maximum for 2bromoalkanoic acids, where (up to 2-bromooctanoic acid) the adsorption energy is nearly independent of the number of methylene units. The presence of functional groups is seen to introduce additional interactions, causing added configurational constraints and a competition with alkyl chain interactions in determining self-assembly patterns. These trends will be discussed in the context of molecular self-assembly information provided by ambient (liquid/solid) and UHV STM studies.

10:40am SS-FrM8 Nanomolecular Motion Induced by Molecular Rectificator in the Self-Assembled Monolayers, T. Ishida, National Institute of Advanced Industrial Science and Technology (AIST), Japan, H. Fukushima, JRCHMM -JCII and TPRC, SEIKO EPSON Corporation, Japan, T. Tamaki, H. Tokumoto, National Institute of Advanced Industrial Science and Technology (AIST), Japan

Nanoscale molecular motion induced by polarity change of the electric field was observed by scanning tunneling microscopy (STM), when small amounts of asymmetrical disulfides containing terphenyl moieties were embedded into pre-assembled dodecanethiol self-assembled monolayers (SAMs). The class of disulfide was specifically designed to perform the large dielectric anisotropy in the terphenyl moiety. At the positive tip bias, few of protrusions were observed. When the STM tip bias turned to negative, many protrusions appeared on the binary monolayer surface. Scanning tunneling spectroscopy (STS) revealed the higher rectification property at the area of the terphenyl terminated monolayer where also showed the higher electrical conduction at the negative tip bias compared to positive one. The higher electrical conduction at the negative tip bias was likely to retract the STM tip, showing the apparent nanomolecular motion by the polarity change. Our observed nanomotion (about 1 min) is much faster than previously observed switching time (at least 20 min).¹ Also, the apparent molecular motion can be observed in the case of nanometer scale domains as well as single molecule.

¹Z.J. Donhauser et al., Science 292 (2001) 2303-2307.

11:00am SS-FrM9 Conductance Switching in Single Molecules, Z.J. Donhauser*, T.P. Pearl, P.S. Weiss, The Pennsylvania State University

We have studied functionalized phenylene ethynylene oligomers as candidate molecular electronic devices using scanning tunneling microscopy (STM). A simple self-assembly strategy has been demonstrated that allows us to control monolayer structure, placement of individual molecules, and switching activity of individual molecules. Alkanethiolate self-assembled monolayers (SAMs) were used as host matrices to isolate and to insulate individual candidate molecular electronic devices. The isolated molecules were individually addressed and electrically probed using STM imaging and spectroscopy. The guest molecules exhibit reversible conductance switching, manifested as a change in the topographic height in STM images. High and low conductance states are visible when the molecules are inserted in dodecanethiolate SAMs, but the low conductance states are of the same height or lower than the host matrix. Using thin alkanethiolate matrices (as low as octanethiolate) reveals that the molecules can occupy at least three discrete conductance states. The amount and rate of active switching can be mediated by the structure of the host matrix. Poorly ordered SAMs were produced using a short deposition time; molecules inserted in these monolayers have a high switching activity. Well-ordered SAMs were produced using a vapor annealing procedure, which has been demonstrated with mixed alkanethiolate monolayers. Guest molecules inserted in vapor annealed SAMs have a low switching activity.

11:20am SS-FrM10 Metastable Nanopattern Formation during Pb/Cu(111) Self-Assembly, R. van Gastel, R. Plass, Sandia National Laboratories, Albuquerque, N.C. Bartelt, Sandia National Laboratories, Livermore, G.L. Kellogg, Sandia National Laboratories, Albuquerque

Competing inter-atomic interactions on surfaces can lead to the spontaneous formation of ordered 2-D domain patterns in widely varying systems. The potential use of such patterns as templates for the fabrication of nanostuctures has fostered considerable interest in the underlying selfassembly process. Recently, it has been discovered that two phases of Pb on Cu(111) (a surface alloy and a Pb overlayer) self-assemble into nanoscale domain patters.¹ As the Pb coverage increases, the equilibrium patterns progress from islands of the overlayer (droplets) to stripes to islands of the alloy (inverted droplets). These equilibrium patterns are not the only patterns that can be constructed, however. Here, we use low energy electron microscopy to investigate metastable patterns that can be created by varying the temperature and deposition sequence. These include a stripe phase formed at low Pb coverages, and metastable droplet and inverted droplet

phases, in which the island sizes are larger than those of the equilibrium structures. Both the droplet and inverted droplet metastable structures can develop into "froth" patterns -- the 2-D analog of soap bubbles. These patterns evolve in a deterministic manner. If the droplet phase from which a froth phase is created is ordered, a stable array of ordered hexagonal domains results. If the initial droplet phase is not ordered, the froth phase coarsens by a well-defined set of rules.² Thus, Pb on Cu(111) provides a model system both to explore the type of metastable patterns that can be formed for nano-template applications and to determine the laws that govern the formation, evolution and stability of nanometer-scale, 2-D patterns. Work supported by the U. S. DOE under Contract DE-AC04-94AL85000.

R. Plass, J. A. Last, N. C. Bartelt, and G. L. Kellogg, Nature 412, 875 (2001)
D. Weaire and N. Rivier, Contemp. Phys. 25, 59 (1984)

11:40am SS-FrM11 Buffer-Layer-Assisted Nanostructure Growth Via Two-Dimensional Cluster-Cluster Aggregation, C.L. Haley, V.N. Antonov, J.H. Weaver, University of Illinois at Urbana-Champaign

Physical vapor deposition of metals onto Xe multilayers at 20 K produces three-dimensional clusters. Warming to room temperature desorbs the Xe and causes coalescence. The net motion, and hence the extent of coalescence, depends on the buffer layer thickness. Using transmission electron microscopy, we determined the spatial distribution of these nanostructures as a function of Xe thickness. Using the scaling concepts of cluster-cluster aggregation, we found a fractal dimension ranging from 1.42 to 1.72 for initial fractional coverages of 0.04 to 0.20, consistent with Monte Carlo simulations of two-dimensional diffusion-limited cluster aggregation (DLCA). Both the number density and the weighted average nanostructure size show a power law dependence on the Xe layer thickness, where the latter plays the role of time in DCLA modeling. These relationships facilitate the design of nanostructure arrays generated by desorption-assisted coalescence.

^{*} Morton S. Traum Award Finalist

Authors Index

Bold page numbers indicate the presenter

— A — Abdelmaksoud, M.: SS-ThA5, 58 Abramov, M.A.: BI+SS-TuA7, 20 Abriou, D.: SS3-TuA7, 26 Achete, C.A.: OF+EL+SS+SC-WeM6, 32 Acremann, Y.: MI+SS-ThM3, 49 Adams, J.A.: SS+EL-ThM4, 53; SS+EL-ThM5, 54; SS-ThM10, 56 Adib, K.: SS2-MoM1, 6; SS2-MoM2, 6 Ahn, S.J.: BI+SS-TuA4, 20 Aizawa, M.: SS3-TuM1, 18 Al-Abadleh, H.A.: SS-TuP18, 29 Al-Bataineh, S.: BI+SS-TuA10, 21 Alexander, M.R.: NS+SE+SS+MM-TuM5, 14; SS-FrM2, 60 Allara, D.L.: OF+EL+SS+SC-WeM5, 32; SS-FrM1, 60 Allred, D.D.: SS-TuP27, 31 Altman, E.I.: SS+EL-WeM2, 33; SS2-MoA9, 11 Altman, M.S.: SS2 -MoA4, 10 Altmann, K.N.: SS-ThM1, 55 Alvarez, R.A.: PN+SS-ThM10, 51 Amar. F.G.: SS2-MoM4. 6 Amberntsson, A.: SS1-MoA5, 9 Amonette, J.E.: EC+SS-MoA6, 8 An. T.: SS1-MoA1. 9 Anderson, M.L.: SS2-TuM7, 17; SS-WeP22, 39 Anderson, S.L.: SS3-TuM1, 18 Andersson, M.P.: SS1 -TuM10, 16; SS-WeM1, 34 Ankudinov, A.L.: SS-ThM2, 55 Antonov, V.N.: SS-FrM11, 61 Aoki, A.: EL+SS+SC-WeA10, 42; SS1 -MoM3, 4 Arenholz, E.: MI+SS-ThM3, 49; MI+SS-ThM9, 49 Arlinghaus, H.F.: BI+HS+SS-ThM8, 48; SS-WeP10. 37 Arredondo, M.G.: SS2 -TuA8, 25 Arvindan, N.: EC+SS-MoM9, 2 Asplund, M.C.: OF+SS+EL+SC -TuA5, 22; SS-WeP2, 36 Asscher, M.: SS1-WeA9, 44 Asthagiri, A.: SS1-MoM10. 5 Ayotte, P.: EC+SS-MoA8, 9 Azad, S.: SS1-MoA8, 10; SS3-TuM11, 19 – B – Baer, D.R.: EC+SS-MoA6, 8 Bai, M.: OF+SS+EL+SC -TuA7, 22 Baker, L.A.: SS2-MoA1, 10 Bao, H.: SS+EL-ThA9, 58 Baratoff, A.: PN+SS-ThM4, 50; SS+EL-ThM8, 54 Bartels, L.: SS-WeP11, 37 Bartelt, N.C.: SS-FrM10, 61; SS-WeP19, 38 Bartlett, B.: OF+SS+EL+SC-TuA3, 21 Barus, T.T.: SS+EL-ThA3, 57 Baski, A.A.: SS2-WeA8, 45; SS-TuP5, 27 Bastasz, B.: SS2-WeA3, 45 Batzill, M.: SS1-MoA9, 10: SS3-TuA10, 26: SS3-TuM5, 18; SS3-TuM8, 18 Beck, D.: SS3-TuA10, 26 Beck, K.M.: SS1-TuA4, 23 Bedzyk, M.J.: EC+SS-MoA4, 8 Behrendt, F.: SS1-TuM4, 15 Bellitto, V.J.: OF+SS+EL+SC -TuA3, 21 Benndorf, C.: EC+SS-MoA7, 8 Bent, S.F.: SS+EL+OF-ThM7, 52 Bera, S.: SS-WeP16, 38 Bermudez, V.M.: SS-TuP13, 29 Berner, S.: PN+SS-ThM4, 50 Bernstein, G.H.: SS-WeP1, 36 Bertness, K .: SS-TuP4, 27 Besenbacher, F.: OF+EL+SS+SC-WeM7, 32; SS1-MoA1, 9; SS1-MoM9, 5; SS1-TuM2, 14; SS2-

TuM1, 16; SS3-TuM3, 18; SS3-TuM6, 18; SS3-TuM7. 18 Block, J.: SS2-TuM8, 17 Bluhm, H.: SS1-TuM9, 16 Boesmans, M.: BI+SS-TuA7, 20 Boland, J.J.: SS+EL+OF-ThM6, 52; SS+EL-ThA4, 57; SS+EL-ThA7, 57 Bonn, M.: EC+SS-MoA1, 8 Bonnell, D.A.: PN+SS-ThM10, 51 Bonroy, K.: BI+SS-TuA7, 20 Boozer, C .: BI+HS+SS-ThM1, 47 Bostedt, C.: OF+SS+EL+SC-TuA6, 22 Bostwick, A.A.: SS+EL-ThM5, 54; SS-ThM10, 56 Bouchet, J.: SS-WeP26, 39 Boxer, S.G.: BI+SS-TuM10, 13 Bromberger, Ch.: SS-ThM1, 55 Brooks, MJ: OF+SS+EL+SC -TuA3, 21 Broqvist, P.: SS1-MoA5, 9 Brown, G.W.: SS+EL-WeM8, 34 Bruynseraede, Y .: MI+SS-ThM6. 49 Bukhtiyarov, V.I.: SS1-TuM9, 16 Bulkin, P.: MS+SE-MoM9, 3 Buntinx, D.: MI+SS-ThM6, 49 Burghaus, U.: SS2-MoM11, 7; SS-TuP24, 30 Buriak, J.M.: SS+EL+OF-ThM3, 51 Burnett, D.J.: SS1-TuM7, 15 Burst, J.M.: SS-TuP17, 29 Butler, J.: BI+HS+SS-ThM9, 48 – C — Cabarcos, O.: OF+EL+SS+SC -WeM5, 32 Cahill, D.G.: SS+EL-WeM7, 34 Cai, T.: EC+SS-MoM8, 1; SS2-TuM6, 17; SS2-WeA6, 45 Cai, W.: BI+HS+SS-ThM10, 48; BI+HS+SS-ThM9.48 Camargo, Jr., S.S.: OF+EL+SS+SC-WeM6, 32 Camillone III, N.: SS2-MoM2, 6 Campbell, C.T.: SS1-MoM6, 5; SS2-MoA8, 11 Campbell, P.A.: SS2-WeA9, 46 Campitelli, A.: BI+SS-TuA7, 20; EC+SS-MoM10, 2 Cantalini, C.: HS+SS+BI-WeA10, 43 Carey, M.J.: MI+SS-ThM3, 49 Carlisle, J.A.: BI+HS+SS-ThM9, 48

Carlos-Cuellar, S.: SS2-TuA7, 24 Carlson, D.L.: SS2 -MoM3, 6 Carman, A.J.: SS-TuP9, 28; SS-WeP3, 36 Caruso, A.N.: MI+SS-ThM2, 49; OF+SS+EL+SC-TuA7.22 Casey, S.M.: SS-TuP9, 28; SS-WeP3, 36 Castellarin-Cudia, C.: SS2-MoM8, 7 Castner, D.G.: BI+SS-TuM9, 12 Cavicchi, R.E.: BI+HS+SS-ThM2, 47 Chambers, S.A.: SS3-TuA1, 25 Chan, C.: OF+EL+SS+SC-WeM1, 32 Chan, Y.L.: SS1-TuM3, 15 Chang, K.-S.: PN+SS-ThM11, 51 Chang, Y.C.: SS+EL-ThA3, 57 Chang, Z.: EC+SS-MoM8, 1; SS2-TuM6, 17; SS3-TuM4, 18 Chapman, S.: SS-TuP23, 30 Chatterjee, B.: SS1-MoM5, 4 Chen, D.: SS+EL-ThA7, 57; SS2-MoA2, 10 Chen, D.A.: SS2-MoA6, 11; SS-WeP5, 36; SS-WeP6_36 Chen. G.: EL+SS+SC-WeA2. 41 Chen, J.G.: EC+SS-MoM7, 1; SS1-MoM11, 5 Chen, W.: SS-WeP8, 37 Cheng, G.: HS+SS+BI-WeA9, 43 Cheng, L.: EC+SS-MoA4, 8

Cheng, R.: MI+SS-ThM2, 49 Chi, P.: SS-TuP4, 27

Chien, F.S.-S.: PN+SS-ThM7, 50 Chien, S.-H.: SS1-TuM3, 15 Chilkoti, A.: BI+HS+SS-ThM5, 47; BI+SS-TuA4, 20 Chiu, H.-T.: EL+SS+SC-WeA5, 41 Cho, S.H.: SS-TuP15, 29 Choi, B.S.: SS2-WeA5, 45; SS-WeP20, 39 Choi, K.-H.: EC+SS-MoM10, 2 Chou, T.-B.: SS2-MoA3, 10 Chrisey, D.B.: BI+HS+SS-ThM6, 47 Chu, Y.W.: SS-WeP21, 39 Chuang, P.: SS1-TuM3, 15 Chuang, T.J.: SS1-TuM3, 15 Cicero, R.L.: BI+HS+SS-ThM11, 48 Clausen, B.S.: SS1-TuM2, 14 Coffey, T.S.: SS-ThA5, 58 Cohen, H.: SS-WeM8, 35 Cohen, P.I.: SS+EL-WeM1, 33 Cole, C.: BI+HS+SS-ThM6, 47 Colton, N.G.: EC+SS-MoA6. 8 Colton, R.J.: BI+HS+SS-ThM6, 47 Crain, J.N.: SS-ThM1, 55 Cramer, L.: SS-ThM9, 56 Cremer, P.S.: BI+SS-TuM7, 12 Cremona, M.: OF+EL+SS+SC-WeM6, 32 Crowder, M.: NS+SE+SS+MM-TuM6, 14 Crowell, J.E.: BI+HS+SS-ThM7, 47 Cui, B.: SS+EL-WeM1, 33 – D -Dagata, J.A.: PN+SS-ThM7, 50 Dai, H.: PN+SS-ThM1, 50 Daineka, D.: MS+SE-MoM9, 3 Dalsin, J.L.: BI+SS-TuM4, 12 Dalton, A.S.: SS+EL-WeM5, 34 D'Amato, M.J.: SS2-TuM7, 17 Darling, S.B.: SS-TuP28, 31 Daschbach, J.L.: EC+SS-MoM2, 1 Datskos, P.G.: HS+SS+BI-WeA8, 43 Davis, R.C.: PN+SS-ThM6, 50; SS+EL+OF-ThM2, 51 Davis, S.D.: SS-TuP3, 27 Dawody, J.: SS1-MoA5, 9 De Barros, M.I.: SS-WeP26, 39 de Jonge, W.I.M.: OF+EL+SS+SC-WeM4, 32 de Wild, M.: PN+SS-ThM4, 50 Dehaen, W.: BI+SS-TuA7, 20 Dhanak, V.R.: SS3-TuM9, 19 Diaz, S.F.: SS1-MoM6, 5 Dicke, C.: SS-FrM5, 60 Dickey, E.C.: SS3-TuA6, 26 Dickinson, J.T.: SS1-TuA4, 23; SS-ThA7, 58; SS-ThM9, 56 Diebold, U.: SS2 -MoM10, 7; SS3 -TuM8, 18; SS-TuP17.29 Dienel, T.: OF+SS+EL+SC-TuA10, 22 Djanarthany, S.: SS3-TuA7, 26 Doby, D.: SS2-TuA8, 25 Dohnálek, Z.: EC+SS-MoA8, 9; SS1-TuA10, 23 Donhauser, Z.J.: SS-FrM9, 61 Dorhout, P.K.: PN+SS-ThM11, 51 Doudevski, I.: SS-FrM3, 60 Doudin, B.: OF+SS+EL+SC-TuA7, 22 Dougherty, D.B.: SS2-TuM9, 17 Douillard, L.: SS2-TuM10, 17 Dowben, P.A.: MI+SS-ThM2, 49; OF+SS+EL+SC-TuA7. 22: SS+EL-ThM10. 54; SS+EL-ThM6, 54 Drévillon, B.: MS+SE-MoM9, 3 Droubay, T.: SS3-TuA1, 25 Drummer, C.: SS1-MoM4, 4 Ducharme, S.: OF+SS+EL+SC-TuA7, 22

Dugger, M.T.: NS+SE+SS+MM-TuM9, 14

Dulub, O.: SS2-MoM10, 7 Dvorak, J.: SS3-TuM4, 18 Dziura, T.: MS+SE-MoM2, 2 — E — Eapen, K.C.: NS+SE+SS+MM-TuM7, 14 Eck, S.: SS2-MoM8, 7; SS3-TuA8, 26 Eck, W.: BI+SS-TuM3, 12 Ecke, G.: SS-TuP8, 28 Emmison, N.: BI+SS-TuM11, 13 Engelhard, M.H.: SS1 -MoA8, 10; SS2 -MoM7, 7; SS3-TuM11, 19 Ermakov, A.V.: SS1-MoM1, 4 Ermanoski, I.: SS-WeP8, 37 Ernst, H.-J.: SS2-TuM10, 17 Evans, J.W.: SS1-MoA2, 9; SS2-WeA6, 45 - F -Fadley, C.S.: MI+SS-ThM1, 48; MI+SS-ThM9, 49; OF+SS+EL+SC -TuA6, 22 Fahey, A.: SS-TuP4, 27 Fain, Jr., S.C.: SS2-MoA8, 11 Fairborther, D.H.: SS2-TuA4, 24 Fairbrother, D.H.: OF+SS+EL+SC-TuA1, 21 Fairbrother, H.: SS2 -MoM3, 6 Faradzhev, N.S.: SS1-WeA6, 44; SS2-TuA4, 24 Fauster, T.: SS1-TuA1, 23 Feibelman, P.J.: SS+EL-WeM4, 33; SS2-TuM7, 17; SS2-WeA10, 46 Feldman, Y.: SS-WeM8, 35 Feldner, J.C.: BI+HS+SS-ThM8, 48; SS-WeP10, 37 Fenter, P.: EC+SS-MoA4, 8 Fernandez-Torres, L.C.: NS+SE+SS+MM-TuM3, 13 Ferris, J.H.: PN+SS-ThM10, 51 Ferris, K.F.: SS3-TuM11, 19 Filler, M.A.: SS+EL+OF-ThM7, 52 Finn, M.G.: BI+HS+SS-ThM7, 47 Finnis, M.: SS3-TuA3, 25 Fischer, D.A.: SS1-TuM7, 15; SS1-TuM8, 15 Fisher, E.R.: PN+SS-ThM11, 51 Fishman, H.A.: SS+EL+OF-ThM2, 51 Fitts, J.P.: SS2 -MoM1, 6; SS2 -MoM2, 6 Flavell, W.R.: SS3-TuM10, 19 Flipse, C.F.J.: OF+EL+SS+SC-WeM4, 32 Flynn, G.W.: SS2-MoM1, 6; SS2-MoM2, 6; SS-FrM7, 60; SS-WeP27, 40 Fomin, E.: SS2-TuM5, 17; SS-WeP17, 38 Foster, T.T.: NS+SE+SS+MM-TuM5, 14 Fournée, V.: SS2-WeA6, 45 France, C.B.: OF+EL+SS+SC-WeM3, 32 Francis, A.J.: SS1-MoM10, 5 Francis, L.: EC+SS-MoM10, 2 Frechette, J.: EC+SS-MoA3, 8 Frederick, B.G.: SS2-MoM4, 6; SS-WeM2, 34 Frederix, F.: BI+SS-TuA7, 20 Freeland, J.: SS-TuP25, 30 Frey, S.: SS-FrM1, 60 Fridell, E.: SS1-MoA5, 9 Friedt, J.-M.: EC+SS-MoM10, 2 Fritz, T.: OF+SS+EL+SC -TuA10, 22 Fritzsche, H.: MI+SS-ThM6, 49 Fu, J.: MS+SE-MoM6, 3 Fu, T.-Y.: SS-WeP18, 38 Fuchs, H.: SS-ThA8, 58 Fujikawa, Y.: SS+EL-ThM1, 53; SS-TuP16, 29 Fukidome, H.: SS-WeM5, 35 Fukuda, T.: SS-TuP10, 28 Fukushima, H.: SS-FrM8, 61 – G – Gabelnick, A.M.: SS1-TuM7, 15 Gadzuk, J.W.: SS1 -TuA5, 23 Gambardella, P.: MI+SS-ThM7, 49 Gao, J.: SS-WeP5, 36

Gao, L.: EC+SS-MoM5, 1

Gao, W.: OF+SS+EL+SC-TuA8, 22

Ghijsen, J.: OF+EL+SS+SC-WeM1, 32 Gil Girol, St.: SS2 -MoM11, 7 Gillen, G.: SS-TuP4, 27 Gimzewski, J.: EC+SS-MoA9, 9 Gladys, M.J.: SS-WeP8, 37 Gland, J.L.: SS1-MoA7, 9; SS1-TuM7, 15; SS1 -TuM8, 15 Godin, M.: SS-WeP9, 37 Goldsmith, J.: NS+SE+SS+MM-TuM6, 14 Goncharova, L.V.: SS2-WeA7, 45 Gong, X.: SS2-TuM3, 16 Goodman, D.W.: SS1-MoA4, 9; SS2-MoA7, 11; SS2-MoM9, 7; SS3-TuA9, 26; SS-TuP29, 31; SS-WeP14, 38 Gorostiza, P.: SS2-TuA10, 25 Gorte, R.J.: EC+SS-MoM3, 1 Grant, A.W.: SS1-MoA5, 9 Grassian, V.H.: SS2-TuA7, 24; SS2-TuA9, 25; SS TuP18, 29; SS-TuP19, 29 Grassman, T.J.: SS1-WeA3, 43 Grätzel, M.: SS3-TuM10, 19 Graugnard, E.: SS+EL-ThA5, 57; SS+EL-ThA6, 57 Greene, J.E.: SS+EL-ThM7, 54 Greenlief, C.M.: SS+EL+OF-ThM8, 52 Griesser, H.J.: BI+SS-TuA10, 21 Griffith, L.V.: SS2-MoM6, 6 Grube, H.: SS+EL-WeM8, 34 Gruen, D.M.: BI+HS+SS-ThM9, 48 Grunze, M.: BI+SS-TuM3, 12; SS-FrM1, 60; SS-FrM6, 60 Grütter, P.: SS-WeP9, 37 Guentherodt, H.-J.: PN+SS-ThM4, 50 Guimarães, P.I.: OF+EL+SS+SC-WeM6, 32 Güntherodt, H.-J.: SS+EL-ThM8, 54 Guptasarma, P.: SS-WeP24, 39 Güttler, A.: SS1-MoM4, 4 Gwo, S.: PN+SS-ThM7, 50; PN+SS-ThM8, 51; SS2-MoA3, 10 H -Haehner, G.: BI+SS-TuM3, 12; SS-FrM5, 60 Hale, J.: MS+SE-MoM7, 3 Hale, M.J.: EL+SS+SC-WeA1, 41 Haley, C.L.: SS-FrM11, 61 Halter, M.W.: BI+SS-TuM9, 12 Hamers, R.J.: BI+HS+SS-ThM10, 48; BI+HS+SS-ThM9 48 Hammer, B.: SS1-MoA1, 9; SS1 -MoM9, 5 Hang, Q.: SS-WeP1, 36 Hansen, R.W.C.: SS-WeP24, 39 Hara, S.: SS+EL-ThM9, 54 Harada, H.: SS+EL+OF-ThM1, 51 Harder, Ph.: SS-FrM1, 60 Harrington, D.A.: EC+SS-MoM11, 2 Hasegawa, S.: SS2-MoA5, 11; SS-TuP7, 28 Hashimoto, E.: SS-WeP12, 37; SS-WeP7, 37 Hata, K.: SS-TuP2, 27 Hävecker, M.: SS1-TuM9, 16 Hawley, M.E.: SS+EL-WeM8, 34 Hayes, W.: SS-FrM3, 60 Haynie, B.C.: OF+EL+SS+SC-WeM5, 32 Hebenstreit, E.L.D.: SS3-TuM8, 18 Hebenstreit, W.: SS3-TuM8, 18 Heinisch, R.: SS1-TuM4, 15 Heinz, T.F.: SS1-TuA3, 23 Heister, K.: SS-FrM6, 60 Heller, E.R.: SS-WeP29, 40 Hemminger, J.C.: SS1-MoA10, 10; SS2-TuA2, 24; SS2-TuA3, 24; SS3-TuA2, 25 Henderson, M.A.: SS2 -MoM7, 7 63

Gao, X.: SS-ThM7, 55

ThA4, 58

Garcia, S.P.: SS+EL-ThA9, 58

Garcia-Manyes, S.: SS2 -TuA10, 25

Georgiadis, R.M.: BI+SS-TuA8, 20

Gellman, A.J.: SS1-MoM2, 4; SS1-MoM7, 5; SS-

Hengerer, R.: SS3-TuM10, 19 Henrickson, S.E.: BI+SS-TuA5, 20 Henzler, M.: SS-TuP7, 28 Hernandez, B.A.: PN+SS-ThM11, 51 Herrmann, C.F.: SS+EL-ThA4, 57 Herrwerth, S.: BI+SS-TuM3, 12 Hersam, M.C.: PN+SS-ThM5, 50 Hess, Ch.: SS1-MoA4, 9 Hess, W.P.: SS1-TuA4, 23; SS-ThM9, 56 Hicks, R.F.: EL+SS+SC-WeA2, 41 Higgins, K.K.: SS2-TuA1, 24 Hildebrandt, T.: SS-TuP7, 28 Hill, D.: SS-WeP1, 36 Hillebrecht, F.U.: MI+SS-ThM3, 49 Himpsel, F.J.: SS-ThM1, 55 Hinch, B.J.: SS1-MoM1, 4; SS2-WeA7, 45 Hines, M.A.: SS+EL-ThA9, 58 Hirashima, H.: SS-WeP4, 36 Hirschmugl, C.J.: SS-WeP24, 39 Hiruta, R.: SS-TuP12, 28 Ho, H.Y.: SS-WeP21, 39 Hochstrasser, M.: SS-ThM8, 55 Hoffman, A.S.: BI+SS-TuA3, 20 Hoffmann, R.: SS+EL-ThM8, 54 Homola, J.: BI+HS+SS-ThM1, 47 Hong, H.: BI+HS+SS-ThM11, 48 Horvath, J.: SS1-MoM7, 5 Hotovy, I.: SS-TuP8, 28 Houston, J.E.: EC+SS-MoA2, 8; SS-ThA3, 58 Hrbek, J.: EC+SS-MoM8, 1; SS2-TuM6, 17; SS3-TuM4, 18 Hsieh, S.: SS1-MoA9, 10; SS2-WeA4, 45; SS3-TuM5, 18 Hsieh, W.-F.: PN+SS-ThM7, 50 Hu, C.: BI+SS-TuA3, 20 Hu, J.: MS+SE-MoM5, 3 Hu, X.F.: SS-WeP24, 39 Hu, Z .: PN+SS-ThM10, 51 Huang, H.: SS2-MoA4, 10 Hug, H.J.: SS+EL-ThM8, 54 Hussain, Z.: MI+SS-ThM9, 49 Husseini, G.: OF+SS+EL+SC -TuA5, 22; SS-WeP2, 36 Hwang, C.C.: SS-TuP11, 28; SS-TuP6, 27 Hwang, G.S.: SS+EL+OF-ThM5, 52; SS+EL-ThM11.54 Hwang, Y.-J.: SS-WeP18, 38 Hwu, H.H.: EC+SS-MoM7, 1 Hyun, J.: BI+SS-TuA4, 20 - | -Ichimiya, A.: SS+EL-WeM6, 34 Ichimura, S.: EL+SS+SC-WeA8, 42 Ichinokawa, T.: SS-WeP31, 40 Ihm, K.W.: SS-TuP11, 28 Iijima, Y.: SS-WeP31, 40 Ikarashi, K.: SS-TuP26, 30 Ikenaga, E.: SS-WeP12, 37; SS-WeP7, 37 Inanaga, S.: EL+SS+SC-WeA10, 42 Inaoka, T.: SS-TuP7, 28 Inazu, K.: SS2-TuA3, 24 Inoue, T.: SS+EL+OF-ThM1, 51 Inoue, Y.: SS1-TuM11, 16; SS-TuP26, 30; SS-WeP15.38 Ishida, T.: SS-FrM8, 61 Ishii, H.: SS+EL+OF-ThM11, 53 Iwasaki, H.: SS-TuP12, 28 – J — Jackson, B.: SS1-MoM4, 4 Jackson, R.H.: SS-WeM2, 34 Jacobs, D.C.: SS1-WeA2, 43; SS1-WeA4, 44 Jedrecy, N.: SS3-TuA7, 26 Jeffrey, C.A.: EC+SS-MoM11, 2 Jenks, C.J.: SS2-WeA3, 45 Jennison, D.R.: SS3-TuA1, 25 Jeon, C.: SS-TuP11, 28; SS-TuP6, 27 Jeon, D.: SS2-WeA5, 45

Jeong, H.K.: SS+EL-ThM10, 54; SS+EL-ThM6, 54 Jeong, J.: EL+SS+SC-WeA6, 41 Jergel, M.: SS-TuP8, 28 Jernigan, G.G.: SS+EL-ThM3, 53 Ji, J.-Y.: SS+EL-ThA3, 57; SS+EL-ThA8, 57 Jiang, G.: SS-TuP3, 27 Jiang, S.: BI+HS+SS-ThM1, 47 Jiang, Y .: SS1-MoA10, 10 Jirsak, T.: SS3-TuM4, 18 Johansson, L.S.O.: SS+EL-ThM9, 54; SS-FrM6, 60 Johs, B.: MS+SE-MoM7, 3 Joly, A.G.: SS1-TuA4, 23 Jonckheere, R.: MI+SS-ThM6, 49 Joyce, S.A.: SS2-MoM2, 6 Ju, X.: SS-ThM11, 56 Jung, T.A.: PN+SS-ThM4, 50 Jupille, J.: SS3-TuA7, 26 – K – Kadossov, E.B.: SS+EL+OF-ThM10, 52; SS+EL+OF-ThM9, 52 Kahn, A.: OF+EL+SS+SC-WeM1, 32; OF+SS+EL+SC-TuA8, 22 Kalinin, S.V.: PN+SS-ThM10, 51 Kam, L.: BI+SS-TuM10, 13 Kang, D.H.: SS1-MoM5, 4 Kang, J.: OF+SS+EL+SC -TuA2, 21 Kang, T.-H.: SS-TuP11, 28; SS-TuP6, 27 Kantorovich, L.N.: SS+EL-ThM8, 54 Kao, C.-L.: SS1-TuM5, 15 Kasianowicz, J.J.: BI+SS-TuA5, 20 Katsiev, B.: SS3 -TuM8, 18 Kawai, M.: SS-WeM5, 35; SS-WeM7, 35 Kawashima, M.: SS+EL-ThM1, 53 Kay, B.D.: EC+SS-MoA8, 9; EC+SS-MoM2, 1; SS1-TuA10, 23 Keister, J.W.: SS2 -TuM8, 17 Kellogg, G.L.: SS-FrM10, 61; SS-WeP19, 38 Kernen, P.: BI+HS+SS-ThM11, 48 Kevan, S.D.: SS-ThM8, 55 Khan, N.A.: SS1-MoM11, 5 Khanom, F.: EL+SS+SC-WeA10, 42; SS1-MoM3, 4 Khare, S.V.: SS+EL-ThM7, 54 Kim, B.: SS-TuP11, 28; SS-TuP6, 27 Kim, B.-I.: NS+SE+SS+MM-TuM3, 13 Kim, C.M.: SS-WeP14, 38 Kim, H.: BI+HS+SS-ThM6, 47 Kim, H.I.: SS-ThA3, 58 Kim, J.: SS+EL-ThA8, 57; SS1-WeA1, 43; SS2-WeA4, 45; SS3-TuA10, 26 Kim, K.-J.: SS-TuP11, 28; SS-TuP6, 27 Kim, S.K.: MI+SS-ThM9, 49 Kim, T.S.: SS1 - TuA6, 23 Kim, Y.: SS-WeM5, 35; SS-WeM7, 35 Kim, Y.D.: SS2-MoM9, 7 Kimmel, G.A.: EC+SS-MoA8, 9 Kimura, Y.: SS+EL+OF-ThM11, 53; SS-TuP1, 27 Kimura-Suda, H.: BI+SS-TuA9, 21 Kinsel, G.R.: BI+SS-TuM5, 12 Kinser, C.R.: PN+SS-ThM5, 50 Kirakosian, A.: SS-ThM1, 55 Klauser, R.: SS1-TuM3, 15 Kleban, P.: SS-WeM2, 34 Kleyn, A.W.: EC+SS-MoA1, 8 Kline, J.S.: SS+EL-ThA8, 57 Klust, A.: SS+EL-ThM4, 53; SS+EL-ThM5, 54; SS-ThM10, 56 Knickerbocker, T.: BI+HS+SS-ThM9, 48 Knop-Gericke, A.: SS1-TuM9, 16 Ko, J.S.: SS-ThA4, 58 Koch, N.: OF+EL+SS+SC-WeM1, 32 Kodambaka, S.: SS+EL-ThM7, 54 Koel, B.E.: SS1-MoA9, 10; SS2-WeA4, 45; SS3-TuA10, 26; SS3-TuM5, 18

Kogure, T.: SS2-MoA5, 11 Kohlhepp, J.T.: OF+EL+SS+SC-WeM4, 32 Kolmakov, A.: HS+SS+BI-WeA9, 43; SS2-MoA7, 11 Kolodziej, J.J.: SS2-TuM8, 17 Komeda, T.: SS-WeM5, 35; SS-WeM7, 35 Komesu, T.: SS+EL-ThM10, 54; SS+EL-ThM6, 54 Kooi, S.E.: OF+EL+SS+SC-WeM8, 33; PN+SS-ThM3, 50 Koopmans, B.: OF+EL+SS+SC-WeM4, 32 Korlahalli, R.: MS+SE-MoM5, 3 Kortright, J.B.: MI+SS-ThM9, 49 Korzeniewski, C.: EC+SS-MoM5, 1 Kosiba, R.: SS-TuP8, 28 Kota, G.P.: MS+SE-MoM2, 2 Koveshnikov, A.N.: SS-ThM7, 55 Kramar, J.A.: MS+SE-MoM6, 3 Krim, J.: SS-ThA1, 58; SS-ThA5, 58 Krueger, B.J.: SS2-TuA7, 24 Kuech, T.F.: EL+SS+SC-WeA3, 41 Kühnle, A.: SS1-MoM9, 5 Kukuruznyak, D.A.: SS-ThM2, 55 Kulkarni, S.: BI+SS-TuA3, 20 Kumarasinghe, A.R.: SS3-TuM10, 19 Kummel, A.C.: EL+SS+SC-WeA1, 41; SS1-TuA8, 23; SS1-WeA3, 43 Kunat, M.: SS2-MoM11, 7 Küppers, J.: SS1-MoM4, 4 Kurahashi, M.: SS-ThM11, 56 Kuribayashi, H.: SS-TuP12, 28 Kurnosikov, O.: OF+EL+SS+SC-WeM4, 32 Kurokawa, A.: EL+SS+SC-WeA8, 42 Kurtz, R.L.: SS-ThM7, 55 Kusmierek, D.O.: SS1-WeA6, 44 Kusunoki, I.: SS-TuP14, 29 Kuwano, S.: SS-TuP16, 29 - L -Lad, R.J.: NS+SE+SS+MM-TuM4, 13 Ladd. J.: BI+HS+SS-ThM1. 47 Laegsgaard, E.: SS2 -TuM1, 16; SS3 -TuM6, 18; SS3-TuM7, 18 Lagally, M.G.: SS+EL-ThM1, 53 Land, D.P.: SS-TuP21, 30 Langell, M.A.: SS2-MoM5, 6; SS-TuP23, 30 Langford, S.C.: SS-ThA7, 58 Langohr, J.: SS1-TuM4, 15 Lantz, M.A.: SS+EL-ThM8, 54 Laracuente, A.R.: SS2-MoA1, 10 Laroche, O.: SS-WeP9, 37 Larsson, M.I.: SS+EL-ThM9, 54 Laureyn, W.: BI+SS-TuA7, 20 Lauritsen, J.V.: SS1-TuM2, 14 Lavrik, N.V.: HS+SS+BI-WeA8, 43 Law, D.C.: EL+SS+SC-WeA2, 41 Lay, T.T.: SS3-TuA5, 25 Layman, K.A.: SS1-MoA10, 10; SS3-TuA2, 25 Lazzari, R.: SS3-TuA7, 26 Lea, A.S.: EC+SS-MoA6, 8 Leavitt, A.J.: SS2-TuA8, 25 Lee, C.: MS+SE-MoM2, 2 Lee, J.: SS1-WeA1, 43; SS3-TuM1, 18 Lee, S.: SS3-TuM1, 18 Lee, S.J.: SS1-WeA1, 43 Lee, W.: BI+SS-TuA4, 20 Leggett, G.J.: NS+SE+SS+MM-TuM5, 14 LeGore, L.J.: SS-WeM2, 34 Lei, X.: PN+SS-ThM10, 51 Le-Mogne, T.: SS-WeP25, 39; SS-WeP26, 39 Lennox, B.: SS-WeP9, 37 Leone, S.R.: SS+EL-ThA1, 57 Levi, D.H.: MS+SE-MoM10, 3 Levy, A.: MS+SE-MoM2, 2 Lewington, T.A.: SS-FrM2, 60 Lewis, H.D.: SS1-TuM7, 15 Lewis, J.S.: MS+SE-MoM11, 3

Li, M.: BI+SS-TuM5, 12; SS+EL-WeM2, 33; SS2-MoA9, 11 Liakos, I.: SS-FrM2, 60 Liday, J.: SS-TuP8, 28 Lilach, Y.: SS1-WeA9, 44 Lim, S.: EL+SS+SC-WeA6, 41 Lin, J.-L.: SS-ThM1, 55 Lin, M.-T.: SS2-MoA3, 10 Lin, W.-C.: SS2-MoA3, 10 Lin, Y.-F.: EL+SS+SC-WeA5, 41 Linderoth, T.R.: SS1-MoM9, 5; SS2-TuM1, 16 Linford, M.R.: OF+SS+EL+SC-TuA5, 22; PN+SS-ThM6, 50; SS+EL+OF-ThM2, 51; SS-TuP3, 27; SS-WeP2, 36; SS-WeP30, 40 Liou, S.-H.: MI+SS-ThM2, 49 Liu, D.-J.: SS1-MoA2, 9 Liu, G.: EC+SS-MoM8, 1; SS2-TuM6, 17; SS3 -TuM4, 18 Lobo. J.: SS-ThM4. 55 Lograsso, T.A.: SS2-WeA3, 45; SS2-WeA6, 45 Long, B.T.: SS2-MoA6, 11; SS-WeP5, 36 Lopez, G.P.: BI+HS+SS-ThM3, 47 Lopez, N.: SS3-TuM3, 18; SS3-TuM7, 18 Lormand, K.D.: SS-TuP21, 30 Lozzi, L.: HS+SS+BI-WeA10, 43 Lu, H.B.: BI+HS+SS-ThM11, 48 Lua, Y.-Y.: SS+EL+OF-ThM2, 51 Lunt, S.: SS-TuP27, 31 Luo, X.: SS+EL-ThA3, 57 – M – Ma, Q.: SS-TuP25, 30 Ma, S.: SS2-MoM4, 6 Maat, S.: MI+SS-ThM3, 49 Maazouz, M.: SS1-WeA2, 43 Maazouz, P.L.: SS1-WeA2, 43 Machesky, M.: EC+SS-MoA4, 8 Madey, T.E.: SS1 -WeA6, 44; SS2 -TuA4, 24; SS2 -TuM8, 17; SS-TuP22, 30; SS-WeP8, 37 Madix, R.J.: SS1-TuM5, 15 Maeda, S.: SS-TuP10, 28 Maes, G.: BI+SS-TuA7, 20 Magnusson, K.O.: SS+EL-ThM9, 54 Maithil, D.: SS1-MoM1, 4 Maiti, A.: SS3-TuM4, 18 Mallick, A.K.: SS3-TuM10, 19 Malmstadt, N.: BI+SS-TuA3, 20 Man, K.L.: SS2-MoA4, 10 Mancinelli, C.M.: SS-ThA4, 58 Mannella, N.: MI+SS-ThM1, 48; MI+SS-ThM9, 49 Mannsfeld, S.: OF+SS+EL+SC-TuA10, 22 Mao, Z.: SS3 - TuA6, 26 Mariano, M.: BI+HS+SS-ThM11, 48 Marmier, A.: SS3-TuA3, 25 Maroutian, T.: SS2-TuM10, 17 Marsh, A.L.: SS1-TuM8, 15 Martin, B.D.: OF+SS+EL+SC -TuA9, 22 Martin, J.M.: NS+SE+SS+MM-TuM1, 13; SS-WeP25, 39; SS-WeP26, 39 Materer, N.F.: SS+EL+OF-ThM10, 52; SS+EL+OF-ThM9, 52 Matsumoto, T.: SS1-MoA9, 10; SS2-WeA4, 45; SS3-TuM5, 18 Matsumura, Y.: SS-WeP12, 37; SS-WeP7, 37 Mattsson, T.R.: SS+EL-WeM4, 33; SS3-TuA1, 25 Mavrikakis, M.: EL+SS+SC-WeA3, 41 Maw, W.: SS-ThA7, 58 McAlpine, E.: NS+SE+SS+MM-TuM5, 14; SS-FrM2.60 McArthur, S.L.: BI+SS-TuM9, 12 McCarroll, W.H.: SS2-MoM5, 6 McChesney, J.L.: SS-ThM1, 55 McGuire, M.M.: SS2-MoM3, 6 Medvedev, V .: EC+SS-MoM1, 1 Meier, T.C.: SS2-MoM6, 6 Mellott, J.: SS-FrM3, 60

Messerschmidt, C.: SS-FrM3, 60 Messersmith, P.B.: BI+SS-TuM4, 12 Mewe, A.A.: SS2-TuM11, 17 Meyer, R.J.: SS1-TuA6, 23 Michel, A.E.: SS2-TuA9, 25; SS-TuP19, 29 Michel, E.G.: SS-ThM4, 55 Miletic, M.: SS1-MoA7, 9 Mills, P.: SS1 -MoM5, 4 Min, B.K.: SS3-TuA9, 26; SS-TuP29, 31 Misakian, M.: BI+SS-TuA5, 20 Mishra, B: NS+SE+SS+MM-TuM6, 14 Mitchell, G.E.: SS1-TuM8, 15 Mitchell, S.A.: BI+SS-TuM11, 13 Mitsui, T.: SS2-TuM5, 17; SS-WeP17, 38 Molina, L.: SS1-MoM9, 5 Moore, J.: NS+SE+SS+MM-TuM6, 14 Moore, J.C.: SS2-WeA8, 45; SS-TuP5, 27 Morin, S.: EC+SS-MoM11, 2 Morozov, A.N.: SS-TuP20, 29 Morton, S.A.: MI+SS-ThM5, 49 Moskovits, M.: HS+SS+BI-WeA9, 43 Mowat, I.A.: PN+SS-ThM6, 50; SS+EL+OF-ThM2, 51 Moyer, J.G.: SS-ThM2, 55 Mugarza, A.: SS-ThM4, 55 Mui, C.: SS+EL+OF-ThM7, 52 Muir, B.W.: BI+SS-TuA10, 21 Müller, T.: SS2-MoM2, 6; SS-FrM7, 60; SS-WeP27, 40 Mullins, C.B.: SS1 -TuA6, 23 Mun, B.S.: MI+SS-ThM9, 49 Mun, S.: MI+SS-ThM1, 48 Muralidharan, G.: HS+SS+BI-WeA8, 43 Murphy, C.: SS-WeP5, 36 Muryn, C.A.: SS3-TuM9, 19 Musgrave, C.B.: SS+EL+OF-ThM7, 52 — N – Nagao, T.: SS+EL-ThM1, 53; SS2-MoA5, 11; SS-TuP16, 29; SS-TuP7, 28 Nagy, K.L.: EC+SS-MoA4. 8 Naitoh, Y.: OF+EL+SS+SC-WeM7, 32 Nakakura, C.Y.: MS+SE-MoM1, 2 Nakamura, J.: SS-WeP4, 36 Nakamura, K.: EL+SS+SC-WeA8, 42 Nakano, H.: SS-WeP4, 36 Nakano, Y.: SS-WeP12, 37; SS-WeP7, 37 Nakayama, H.: SS-TuP10, 28 Nakayama, K.S.: SS+EL-ThA5, 57; SS+EL-ThA6, 57 Namiki, A.: EL+SS+SC -WeA10, 42; SS1 -MoM3, 4 Nanba, T.: SS-WeP13, 38 Nath, N.: BI+HS+SS-ThM5, 47 Nelson, A.J.: OF+SS+EL+SC-TuA6, 22; SS2-MoM6 6 Nelson, B.P.: MS+SE-MoM10, 3 Nelson, W.J.: BI+SS-TuM10, 13 Nemoto, J.: SS-TuP1, 27 Netzer, F.P.: SS2-MoM8, 7; SS3-TuA8, 26 Newberg, J.N.: SS2-TuA2, 24 Newberg, J.T.: SS2-TuA3, 24 Newman, R.C.: SS-FrM2, 60 Ngo, L.T.: SS2 -MoA8, 11 Niederberger, C.: SS1-MoM10, 5 Niederhauser, T.L.: PN+SS-ThM6, 50; SS+EL+OF-ThM2, 51; SS-TuP3, 27 Nielsen, C.: SS-WeP31, 40 Nikolov, N.: OF+SS+EL+SC -TuA9, 22 Nishiyama, H.: SS1-TuM11, 16; SS-TuP26, 30; SS-WeP15, 38 Nishiyama, K.: SS+EL+OF-ThM1, 51 Nitsche, R.: OF+SS+EL+SC-TuA10, 22 Niwano, M.: SS+EL+OF-ThM11, 53; SS-TuP1, 27 Nöel, N.: SS2-TuM10, 17 Nolting, F.: MI+SS-ThM3, 49 Nonaka, H.: EL+SS+SC-WeA8, 42

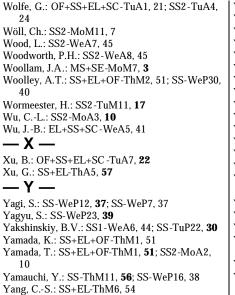
Norskov, J.K.: SS3-TuM3, 18; SS3-TuM7, 18 Novikova, T.: MS+SE-MoM9, 3 0 -Ogawa, J.: SS-WeP4, 36 Ogletree, D.F.: SS1-TuM9, 16; SS-WeP17, 38 Ogletree, F.: SS2-TuM5, 17 Ohashi, M.: SS1 -WeA7, 44 Ohldag, H.: MI+SS-ThM3, 49 Ohta, T.: SS+EL-ThM4, 53; SS+EL-ThM5, 54 Ohuchi, F.S.: SS+EL-ThM4, 53; SS+EL-ThM5, 54; SS-ThM2, 55 Okamoto, H.: SS2-MoA2, 10 Oliver, A.C.: EC+SS-MoA2, 8 Olmstead, M.A.: SS+EL-ThM4, 53; SS+EL-ThM5, 54; SS-ThM10, 56 Olsson, L.: SS1-MoA5, 9 Osaka, T.: SS+EL+OF-ThM1, 51 Osgood Jr., R.M.: EL+SS+SC -WeA7, 41 Osgood, Jr., R.M.: SS2-MoM1, 6; SS2-MoM2, 6 Ovchenkov, Y.: OF+SS+EL+SC -TuA7, 22 Ovsyanko, M.M.: SS2-TuM11, 17 Ozeki, M.: SS1-WeA7, 44 Ozenzoy, E.: SS1-MoA4, 9 - P – Pace, C.: MS+SE-MoM11, 3 Palmer, J.S.: SS+EL-WeM3, 33 Palmstrom, C.J.: SS+EL-ThM10, 54; SS+EL-ThM6, 54 Pang, C.L.: SS3-TuM9, 19 Paparazzo, E.: SS-WeP32, 40 Park, B.S.: SS2-WeA5, 45 Park, C.Y.: EC+SS-MoA4, 8 Park, C.-Y.: SS-TuP11, 28; SS-TuP6, 27 Parkinson, B.A.: OF+EL+SS+SC-WeM3, 32 Parsons, F.: SS-WeP5, 36 Paserba, K.R.: SS1-MoM2, 4 Patton, S.T.: NS+SE+SS+MM-TuM7, 14 Pearl, T.P.: SS-FrM9, 61 Peck, J.: BI+HS+SS-ThM10, 48 Peden, B.M.: EC+SS-MoM2, 1 Peden, C.H.F.: SS1-MoA8, 10; SS2-MoM7, 7 Pelz, J.P.: SS-WeP29, 40 Perez, T.D.: BI+SS-TuM10, 13 Perkins, C.L.: SS2-MoM7, 7 Perkins, J.D.: MS+SE-MoM10, 3 Perry, C.C.: SS2-TuA4, 24 Perry, S.S.: NS+SE+SS+MM-TuM3, 13 Persson, H.H.J.: BI+HS+SS-ThM11, 48 Peterson, A.W.: BI+SS-TuA8, 20 Petrov, I.: SS+EL-ThM7, 54 Petrova, V.: SS+EL-ThA5, 57; SS+EL-ThM7, 54 Petrovykh, D.Y.: BI+SS-TuA9, 21 Pillay, D.: SS+EL+OF-ThM5, 52 Pireaux, J.J.: OF+EL+SS+SC-WeM1, 32 Plass, R.: SS-FrM10, 61 Poelsema, B.: SS+EL-ThM2, 53; SS2-TuM11, 17 Poon, G.C.: SS1-WeA3, 43 Porter, L.M.: SS1-MoM10, 5 Potapenko, D.V.: SS1-MoM1, 4; SS2-WeA7, 45 Prasad, S.V.: NS+SE+SS+MM-TuM9, 14 Prayongpan, P.: SS+EL+OF-ThM8, 52 Proehl, H.: OF+SS+EL+SC-TuA10, 22 Pugmire, D.A.: SS2-MoM5, 6 Pyatt-Rudolph, E.L.: SS-TuP21, 30 - Q -Qian, G.: SS+EL-ThA3, 57 Qin, X.: SS1 -WeA4, 44 Qiu, Z.Q.: SS-ThM5, 55 Quan, W.X.: SS-TuP15, 29 Quinn, D.P.: SS1-TuA3, 23 Quinton, J.S.: SS-WeP8, 37 R — Rahman, F.: EL+SS+SC -WeA10, 42; SS1-MoM3, 4

Rajagopal, A.: OF+EL+SS+SC-WeM1, 32 Rajasekar, P.: SS+EL+OF-ThM10, 52; SS+EL+OF-ThM9, 52 Ramana, C.V.: SS2-WeA5, 45; SS-WeP20, 39 Ramoino, L.: PN+SS-ThM4, 50 Ramsey, M.G.: SS2-MoM8, 7; SS3-TuA8, 26 Rao, B.V.: SS-WeP11, 37 Ratner, B.D.: BI+SS-TuA1, 20 Raviswaran, A.: SS+EL-WeM7, 34 Reeves, C.T.: SS1-TuA6, 23 Rehr, J.J.: SS-ThM2, 55 Ren, S.: SS+EL-ThA3, 57 Renaud, G.: SS2-WeA1, 45; SS3-TuA7, 26 Reutt-Robey, J.: SS2-TuM9, 17 Reviakine, I.: SS-TuP20, 29 Reyes, R.: OF+EL+SS+SC-WeM6, 32 Rieder, K.H.: SS-WeM3, 34 Rim, K.T.: SS2-MoM1, 6; SS2-MoM2, 6; SS-FrM7. 60: SS-WeP27. 40 Ringeisen, B.R.: BI+HS+SS-ThM6, 47 Roberts, A.L.: SS2 -MoM3, 6 Roberts, J.T.: SS2-TuA1, 24 Robertson, B.: BI+SS-TuA5, 20 Robinson, M.C.: SS2-TuM2, 16 Rodriguez, J.A.: EC+SS-MoM8, 1; SS2-TuM6, 17; SS3-TuM4, 18 Roke, S.: EC+SS-MoA1, 8 Ronnau, A.: SS3-TuM3, 18; SS3-TuM6, 18 Rose, M.K.: SS2-TuM5, 17; SS-WeP17, 38 Rosei, F.: OF+EL+SS+SC-WeM7, 32; SS2-TuM1, 16 Rosenberg, R.A.: SS-TuP25, 30 Rosenhahn, A.: MI+SS-ThM1, 48 Roshko, A.: SS-TuP4, 27 Ross, A.R.: SS2-WeA3, 45; SS2-WeA6, 45 Rossetti, F.: SS-TuP20, 29 Rotenberg, E.: SS+EL-ThM5, 54; SS-ThM10, 56; SS-ThM8, 55 Rothfuss, C.: EC+SS-MoM1, 1 Rowe, J.E.: SS2-TuM8, 17; SS-WeP8, 37 Ruiz-Taylor, L.A.: BI+HS+SS-ThM11, 48 Russell, Jr., J.N.: BI+HS+SS-ThM9, 48; OF+SS+EL+SC-TuA3, 21 Ryan, P.: SS-TuP25, 30 - S – Saavedra, S.: BI+SS-TuM6, 12 Sadowski, J.T.: SS2-MoA5, 11; SS-TuP16, 29 Sailor, M.J.: HS+SS+BI-WeA1, 42 Sainoo, Y.: SS-WeM5, 35; SS-WeM7, 35 Saito, N.: SS1-TuM11, 16; SS-TuP26, 30; SS-WeP15, 38 Sakai, Y.: SS-WeP31, 40 Sakurai, M.: SS-WeP13, **38** Sakurai, T.: SS+EL-ThM1, 53; SS2-MoA5, 11; SS-TuP16. 29 Saleh, A.: SS2-WeA5, 45 Salmassi, F.: MI+SS-ThM9, 49 Salmeron, M.: SS1-TuM9, 16; SS2-TuM5, 17; SS-WeP17, 38 Salvador, P.: SS1-MoM10, 5 Santangelo, P.G.: OF+SS+EL+SC-TuA3, 21 Santra, A.K.: SS2 -MoM9, 7; SS3-TuA9, 26; SS-TuP29. 31 Santucci, S.: HS+SS+BI-WeA10, 43 Sanz, F.: SS2-TuA10, 25 Sardar, S.A.: SS-WeP12, 37; SS-WeP7, 37 Sasaki, N.: SS-WeM6, 35 Sato, J.: SS-TuP26, 30 Saw, C.K.: SS2-MoM6, 6 Schaub, R.: SS3-TuM3, 18; SS3-TuM6, 18; SS3-TuM7, 18 Schieke, J.: EL+SS+SC-WeA3, 41 Schintke, S.: PN+SS-ThM4, 50 Schirmeisen, A.: SS-ThA8, 58 Schlegel, M.L.: EC+SS-MoA4, 8 Schlögl, R.: SS1-TuM9, 16

Schmitz, P.J.: SS1 -MoA7, 9 Schneider, W.F.: SS1 -MoA7, 9 Schoiswohl, J.: SS3-TuA8, 26 Scholl, A.: MI+SS-ThM3, 49 Schroder, E.: SS2-TuM8, 17 Schröder, M.: BI+HS+SS-ThM8, 48; SS-WeP10, 37 Schroeder, P.G.: OF+EL+SS+SC-WeM3, 32 Schubert, U.S.: OF+EL+SS+SC-WeM4, 32 Schultz, B.D.: SS+EL-ThM10, 54; SS+EL-ThM6, 54 Schunack, M.: OF+EL+SS+SC-WeM7, 32; SS2-TuM1, 16 Schwartz, D.K.: SS-FrM3, 60 Schwartz, J.: OF+EL+SS+SC-WeM1, 32 Schwarz, U.D.: SS-ThA9, 59 Schweizer, S.: BI+HS+SS-ThM11, 48 Seebauer, E.G.: SS+EL-WeM5, 34; SS1-WeA8, 44 Seivewright, B.: SS-WeP9, 37 Sekiguchi, T.: SS2-MoA5, 11 Seo, J.M.: SS-TuP15, 29 Sevy, E.T.: OF+SS+EL+SC -TuA5, 22; SS-WeP2, 36 Sexton, J.Z.: EL+SS+SC -WeA1, 41; SS1-TuA8, 23 Sha, X .: SS1 -MoM4, 4 Shao, R.: PN+SS-ThM10, 51 Shaporenko, A.: SS-FrM1, 60 Shard, A.G.: BI+SS-TuM11, 13; SS2-WeA9, 46 Shashidhar, R.: OF+SS+EL+SC -TuA9, 22 Sheehan, P.E.: OF+EL+SS+SC -WeM8, 33; PN+SS-ThM3, 50 Shen, T.-C.: SS+EL-ThA3, 57; SS+EL-ThA8, 57 Shen, Z.: BI+HS+SS-ThM7, 47 Shern, C.S.: SS-WeP21, 39 Shigekawa, H.: SS-TuP2, 27; SS-WeM5, 35 Shimizu, R.: SS-TuP12, 28 Shinohara, M.: SS+EL+OF-ThM11, 53 Shivaprasad, D.: MS+SE-MoM5, 3 Shluger, A.L.: SS+EL-ThM8, 54 Sholl, D.S.: SS1-MoM10, 5 Sibener, S.J.: SS-TuP28, 31 Silver, R.: MS+SE-MoM6, 3 Sinnott, S.B.: SS3-TuA6, 26 Siuzdak, G.: BI+HS+SS-ThM7, 47 Skoglundh, M.: SS1-MoA5, 9 Skrobiszewski, J.L.: SS-TuP5, 27 Slavin, A.J.: SS2-TuM2, 16 Smallwood, S.A.: NS+SE+SS+MM-TuM4, 13; NS+SE+SS+MM-TuM7, 14 Smedh, M.H.: SS1-MoM6, 5 Smith, G.C.: SS3-TuM10, 19 Smith, L.M.: BI+HS+SS-ThM9, 48 Smith, R.J.: SS2-WeA5, 45; SS-WeP20, 39 Smith, R.S.: EC+SS-MoA8, 9; EC+SS-MoM2, 1; SS1-TuA10, 23 Snow, A.W.: OF+SS+EL+SC-TuA3, 21 Soda, K.: SS-WeP12, 37; SS-WeP7, 37 Sohn, S.: BI+HS+SS-ThM8, 48; SS-WeP10, 37 Song, W.: SS-WeP16, 38 Song, Z.: EC+SS-MoM8, 1; SS2-TuM6, 17 Srivastava, A.: EL+SS+SC-WeA7, 41 Stayton, P.S.: BI+SS-TuA3, 20 Steinke, I.P.: SS+EL-WeM1, 33 Stensgaard, I.: SS2-TuM1, 16; SS3-TuM6, 18; SS3-TuM7, 18 Stephan, J.: SS-TuP24, 30 Stevens, F.: SS-ThA7, 58 Stiehl, J.: SS1-TuA6, 23 Stockbauer, R.L.: SS3-TuM10, 19; SS-ThM7, 55 Stohr, J.: MI+SS-ThM3, 49 Stoian, G.: SS2-TuM11, 17 Stoner, B.: MS+SE-MoM11, 3 Strongin, D.R.: SS2-WeA7, 45 Stultz, J.: SS2-MoM9, 7 Stumpf, R.: SS+EL-WeM4, 33 Sturchio, N.C.: EC+SS-MoA4, 8

Stuve, E.M.: EC+SS-MoM1, 1; EC+SS-MoM9, 2 Su, C.W.: SS-WeP21, 39 Such, M.W.: PN+SS-ThM5, 50 Sudoh, K.: SS-TuP12, 28 Surnev, S.: SS2-MoM8, 7; SS3-TuA8, 26 Sutter, E.A.: NS+SE+SS+MM-TuM6, 14; SS+EL-WeM3, 33 Sutter, P.W.: SS+EL-WeM3, 33 Suzuki, H.: PN+SS-ThM4, 50 Suzuki, T.: SS-ThM11, 56 Swartzentruber, B.S.: SS+EL-WeM4, 33; SS2-TuM7, 17; SS-WeP22, 39 Swerts, J.: MI+SS-ThM6, 49 Syed, J.A.: SS-WeP12, 37; SS-WeP7, 37 Sysoev, S.E.: SS1-MoM1, 4 Szanyi, J.: SS1-MoA8, 10 — T — Tabard-Cossa, V.: SS-WeP9, 37 Tait, Jr., S.L.: SS2-MoA8, 11 Takami, T.: SS-TuP14, 29 Takano, N.: SS+EL+OF-ThM1, 51 Takeuchi, O.: SS-TuP2, 27 Talledo, A.: EC+SS-MoA7, 8 Tamaki, T.: SS-FrM8, 61 Tamanaha, C.R.: BI+HS+SS-ThM6, 47 Tanaka, K.: SS-WeP12, 37; SS-WeP7, 37 Tang, H.F.: EL+SS+SC-WeA3, 41 Tang, W.X.: SS2-MoA4, 10 Tangyunyong, P.: MS+SE-MoM1, 2 Taniguchi, I.: SS+EL+OF-ThM1, 51 Taniguchi, M.: SS-WeP12, 37; SS-WeP7, 37 Tarlov, M.J.: BI+HS+SS-ThM2, 47; BI+SS-TuA9, 21 Tazawa, T.: SS-WeP31, 40 Teague, L.C.: SS+EL+OF-ThM6, 52 Teeter, G.: EC+SS-MoA8, 9 Tejeda, A.: SS-ThM4, 55 Temst, K.: MI+SS-ThM6, 49 Tenne, R.: SS-WeM8, 35 Teplvakov, A.V.: SS-FrM7, 60: SS-WeP27, 40 Terminello, L.J.: OF+SS+EL+SC-TuA6, 22 Textor, M.: BI+SS-TuM1, 12 Thevuthasan, S.: SS2-MoM7, 7 Thiel, P.A.: SS2-WeA3, 45; SS2-WeA6, 45 Thissen, H.: BI+SS-TuA10, 21 Thomas, A.G.: SS3-TuM10, 19 Thomas, O.: BI+HS+SS-ThM2, 47 Thompson, G.E.: SS-FrM2, 60 Thompson, P.E.: SS+EL-ThM3, 53 Thornburg, S.N.: SS-TuP17, 29 Thornton, G.: SS3-TuM9, 19 Thostrup, P.: OF+EL+SS+SC-WeM7, 32; SS1-MoA1, 9; SS3-TuM7, 18 Thuermer, K.: SS2-TuM9, 17 Thundat, T.: HS+SS+BI-WeA8, 43 Tiba, M.V.: OF+EL+SS+SC-WeM4, 32 Tighe, T.B.: OF+EL+SS+SC-WeM5, 32 Timmons, R.B.: BI+SS-TuM5, 12 Tivarus, C.: SS-WeP29, 40 Tobin, J.G.: MI+SS-ThM5, 49; SS-ThM8, 55 Tobin, R.G.: SS1-TuM1, 14 Tokumoto, H.: SS-FrM8, 61 Tokura, Y.: MI+SS-ThM1, 48 Tolbert, M.A.: SS2-TuA5, 24 Tomioka, Y.: MI+SS-ThM1, 48 Ton-That, C .: SS2-WeA9, 46 Topsoe, H.: SS1-TuM2, 14 Totir, G.: SS2-MoM1, 6 Tran, H.M.: BI+HS+SS-ThM11, 48 Trenary, M.: SS1-MoM5, 4 Tsong, T.T.: SS-WeP18, 38 Tsoutsou, D.: SS3-TuM10, 19 Tsukada, M.: SS-WeM6, 35 Tsutsui, Y .: SS+EL-WeM6, 34 Tucker, J.R.: SS+EL-ThA8, 57 Tzeng, S.-D.: PN+SS-ThM8, 51

Tzvetkov, T.: SS1-WeA4, 44 – U -Uesugi-Saitow, Y .: EL+SS+SC-WeA9, 42 Ulrich, M.D.: SS-WeP8, 37 Underwood, J.: MI+SS-ThM9, 49 Unertl, W.N.: NS+SE+SS+MM-TuM4, 13 Usher, C.R.: SS2-TuA9, 25; SS-TuP19, 29 Uvdal, P.: SS1-TuM10, 16; SS-WeM1, 34 – V – Vaidyanathan, N.: SS1-MoM2, 4 Vailionis, A.: SS+EL-ThM7, 54 Valdivis, H.: EC+SS-MoA7, 8 Van Bael, M.J.: MI+SS-ThM6, 49 van Buuren, T.: OF+SS+EL+SC-TuA6, 22 Van der Weide, D.: BI+HS+SS-ThM10, 48; BI+HS+SS-ThM9, 48 van Gastel, R.: SS-FrM10, 61; SS-WeP19, 38 Van Haesendonck, C.: MI+SS-ThM6, 49 van Hove, M.A.: MI+SS-ThM9, 49 van Vroonhoven, E.: SS+EL-ThM2, 53 Vance, A.L.: OF+SS+EL+SC -TuA6, 22 Vanderlick, T.K.: EC+SS-MoA3, 8 Varazo, K.: SS-WeP6, 36 Vecitis, C.: SS2-TuA4, 24 Ventrice, Jr., C.A.: SS-TuP17, 29 Verdaguer, A.: SS2-TuA10, 25 Vestergaard, E.K.: SS1-MoA1, 9 Vijayaraghavan, G.: EC+SS-MoM5, 1 Visbeck, S.B.: EL+SS+SC-WeA2, 41 Vladar, A.E.: PN+SS-ThM7, 50 Vogel, V.: BI+SS-TuM9, 12 Vogrincic, P.: SS-TuP8, 28 - W -Wacaser, B.A.: PN+SS-ThM6, 50; SS+EL+OF-ThM2.51 Waddill, G.D.: MI+SS-ThM5, 49 Wagner, A.J.: OF+SS+EL+SC -TuA1, 21; SS2-TuA4, 24 Wagner, P.: BI+HS+SS-ThM11. 48 Wahlström, E.: SS3-TuM3, 18; SS3-TuM6, 18 Walker, A.V.: OF+EL+SS+SC-WeM5, 32 Wallace, W.T.: SS2-TuA8, 25 Walt, D.R.: HS+SS+BI-WeA5, 43 Wang, J.: BI+SS-TuA8, 20 Wang, L.-Q.: SS1-MoA8, 10; SS3-TuM11, 19 Wang, Y.: SS+EL+OF-ThM5, 52 Wang, Z.: SS1-WeA8, 44 Watanabe, H.: SS+EL+OF-ThM11, 53 Watanabe, S.: SS-WeM6, 35 Weaver, J.F.: SS1-TuM5, 15 Weaver, J.H.: SS+EL-ThA5, 57; SS+EL-ThA6, 57; SS-FrM11, 61 Weetall, H.H.: BI+SS-TuA5, 20 Wei, T.: SS2-MoM9, 7 Weiner, D.: SS-ThA8, 58 Weiss, P.S.: SS-FrM9, 61 Wells, J.C.: SS2-TuM3, 16 Wensmann, A.: SS2-TuA1, 24 Wesolowski, D.J.: EC+SS-MoA4, 8 Whaley, J.A.: SS2 -WeA3, 45 Whetten, R.L.: SS2-TuA8, 25 Whitman, L.J.: BI+HS+SS-ThM6, 47; BI+SS-TuA9, 21; HS+SS+BI-WeA3, 42; OF+EL+SS+SC-WeM8, 33; PN+SS-ThM3, 50; SS2-MoA1, 10 Whitney, U.: MS+SE-MoM3, 3 Widstrand, S.M.: SS+EL-ThM9, 54 Wight, S.A.: SS-TuP4, 27 Willcox, M.: BI+SS-TuA10, 21 Willey, T.M.: OF+SS+EL+SC-TuA6, 22 Williams, E.D.: SS2-TuM9, 17 Williams, P: SS-WeP9, 37 Winn, D.L.: EL+SS+SC-WeA1, 41 Winograd, N.: OF+EL+SS+SC-WeM5, 32 Wolf, L.K.: BI+SS-TuA8, 20



Yang, F.: MS+SE-MoM5, 3 Yang, S.-H.: MI+SS-ThM1, 48; MI+SS-ThM9, 49 Yang, W.: BI+HS+SS-ThM9, 48 Yang, Y.: SS1-WeA5, 44 Yang, Y.-W.: EL+SS+SC-WeA5, 41 Yang, Z.: SS-WeM2, 34 Yarmoff, J.A.: SS1-WeA5, 44 Yata, M.: EL+SS+SC-WeA9, 42 Yee, S.: BI+HS+SS-ThM1, 47 Yeom, H.W.: SS+EL-ThM9, 54 Yi, C.-W.: SS-WeP14, 38 Yi, S.I.: EL+SS+SC-WeA1, 41 Yong, K.: EL+SS+SC-WeA6, 41 Yoshida, S.: SS+EL-ThM9, 54; SS-TuP2, 27 Yoshitake, M.: SS3-TuA5, 25; SS-WeP16, 38; SS-WeP23, 39 You, Y.-C.: PN+SS-ThM8, 51 Young, A.: MI+SS-ThM9, 49 Yu, D.: SS+EL-ThM11, 54 Yu, Q.: BI+HS+SS-ThM1, 47; SS+EL-ThM4, 53; SS2-MoA8, 11 Yuan, L.: MI+SS-ThM2, 49 Yukawa, Y.: SS1-TuM11, 16; SS-WeP15, 38

- Z –

Zabinski, J.S.: NS+SE+SS+MM-TuM7, 14 Zachariah, M.R.: SS2-TuA1, 24 Zahl, P.: SS+EL-WeM3, 33 Zak, A.: SS-WeM8, 35 Zandvliet, H.J.W.: SS+EL-ThM2, 53 Zauscher, S.: BI+SS-TuA4, 20 Zecho, T.: SS1-MoM4, 4 Zhang, J.: BI+SS-TuM5, 12 Zhang, L.: EL+SS+SC-WeA3, 41; SS-TuP9, 28; SS-WeP3, 36 Zhang, Q.: SS2-TuM3, 16; SS-WeP11, 37 Zhang, S.: SS+EL-ThA3, 57 Zhang, X.: SS2-WeA7, 45 Zhang, Y.: HS+SS+BI-WeA9, 43 Zhang, Z.: EC+SS-MoA4, 8; SS2-TuM3, 16 Zharnikov, M.: SS-FrM1, 60; SS-FrM6, 60 Zhou, H.: MS+SE-MoM6, 3 Zhou, J.: SS2-MoA6, 11; SS-WeP6, 36 Zhu, X.-Y.: OF+SS+EL+SC-TuA2, 21 Zhu, Y.Z.: SS-TuP15, 29 Zhu, Z.: EL+SS+SC-WeA7, 41 Zilch, L.W.: SS-WeP30, 40 Zwahlen, M.: BI+SS-TuM3, 12